

AD625732

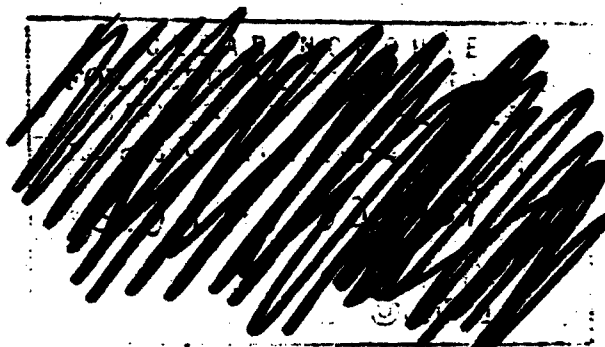
DASA 1718
URS 015-8

EFFECTS OF STRUCTURAL COMPRESSIBILITY
ON ACTIVE AND PASSIVE ARCHING IN
SOIL-STRUCTURE INTERACTION

Final Report
November 1965

Prepared for

DEFENSE ATOMIC SUPPORT AGENCY
Washington, D.C. 20301
Contract No. DA 39-146-AZ-288



URS
■
CORPORATION

Code 1

20050303263

DASA 1718
URS 645-8

**EFFECTS OF STRUCTURAL COMPRESSIBILITY
ON ACTIVE AND PASSIVE ARCHING IN
SOIL-STRUCTURE INTERACTION**

Final Report
November 1965

by

Harold C. Mason
URS CORPORATION
1811 Trousdale Drive
Burlingame, California

Prepared for

DEFENSE ATOMIC SUPPORT AGENCY
Washington, D.C. 20301
Contract No. DA-49-146-XZ-288

Reproduction, in whole or in part, subject
to DASA's approval, is permitted for any
purpose of the U.S. Government.

ABSTRACT

This report describes a theoretical and experimental study of the effects of structural length and compressibility on soil-structure interaction conducted for the Defense Atomic Support Agency. This study is based on the applications of basic concepts of active and passive arching involving development of shear planes in the soil, to soil-structure interaction.

The basic theory of static active and passive arching is reviewed, and theoretical relationships describing the effect that structural geometry (length to span) has on the load on the structure, are developed. Equations are developed for passive and active arching for deeply buried idealized compressible cylindrical structures vertically oriented. Linear and nonlinear soil conditions are investigated. The equations presented indicate that the effect of span, height (length), and compressibility of the structure, and of the ratio of lateral to axial stress, coefficient of internal friction, and compressibility of the soil are important in determining the load on the structure.

Equations are also derived to predict the load (on a trap door) resulting from differential strains occurring between the trap door and the bottom of the soil bin. Both active and passive arching cases and linear and nonlinear soil conditions are considered. The equations developed indicate the effect of span of the trap door and the ratio of lateral to axial stress, coefficient of internal friction and compressibility of the soil on the load on the trap door.

A limited experimental program was conducted to investigate the effects of the ratio of the soil to structural compressibility on the load on the structure. Good correlations are shown between the results of this study and the theoretical predictions employing soil parameters measured in normal laboratory soil tests. Similar correlations employing soil parameters as measured in normal laboratory tests are also shown between the results of a trap door experimental study conducted by another investigator and the theoretical predictions.

Also discussed are the effects of surface soil layers on tests conducted on model-sized structures in the shallow-depth-of-burial condition. The relationship between rate of loading and the rate of structural response was shown to be a controlling factor in determining whether the loading or unloading stress-strain relationship governs the arching behavior.

ACKNOWLEDGEMENTS

The author gratefully acknowledges the guidance and advice furnished by Majors Floyd Henk and Merrill Barnes of the Defense Atomic Support Agency during the conduct of the investigation. Also acknowledged is the assistance furnished by Messrs. C. K. Wiehle, J. V. Zaccor, and W. J. Stack of URS Corporation during the development of the analytical portion of the program and to Mr. R. L. Rhoda for support in conducting the experimental study.

CONTENTS

<u>Section</u>	<u>Page</u>
ABSTRACT	iii
ACKNOWLEDGEMENTS	v
NOTATION	xiii
1 INTRODUCTION	1
2 BACKGROUND	3
3 SOIL - STRUCTURE INTERACTION CONCEPTS	5
Active Arching	5
Passive Arching	9
Comparison of Active and Passive Arching	12
4 EFFECTS OF STRUCTURAL PARAMETERS	15
Effects of Structure Length and Span	15
Effects of Structural Compressibility	27
Passive Arching Case	27
Active Arching Case	32
Comparison of Active and Passive Arching	40
5 EFFECTS OF NONLINEAR SOIL CONDITIONS	43
Effects on Structural Length	43
Effects on Structural Compressibility	49
Passive Arching Case	49
Active Arching Case	54
6 EFFECTS OF DIFFERENTIAL DISPLACEMENT (TRAP DOOR EXPERIMENTS)	61
Effects of Linear Soil Conditions	61
Passive Arching Case	61
Active Arching Case	62
Effects of Nonlinear Soil Conditions	70
Passive Arching Case	70
Active Arching Case	71
7 COMPARISON OF THEORETICAL AND EXPERIMENTAL RESULTS	83
Structural Length	83
Structural Compressibility	85
Sidewall Friction	87
Results	89

CONTENTS (Cont.)

<u>Section</u>	<u>Page</u>
7 (Cont.)	
Differential Displacement (Trap Door Experiments)	92
Passive Arching Case	92
Active Arching Case	109
Application of Differential Displacement Data	117
8 EFFECTS OF SURFACE LAYERS	133
9 CONCLUSIONS AND RECOMMENDATIONS	135
Conclusions	135
Recommendations	136
10 REFERENCES	137
 <u>Appendix</u>	 <u>Page</u>
A URS EXPERIMENTAL PROGRAM	A-1

ILLUSTRATIONS

<u>Figure</u>		<u>Page</u>
1	Displacements Within a Soil Mass With an Inclusion More Compressible Than the Soil (Active Arching)	6
2a	Failure in Cohesionless Sand Caused by Downward Movement of a Long, Narrow Section of the Foundation	8
2b	Assumptions on Which Computation of Stress in Sand Between Two Vertical Surfaces of Sliding Is Based	8
3	Displacement Within a Soil Mass With an Inclusion Less Compressible Than the Soil (Passive Arching)	10
4	Assumptions Which Provide the Basis for Computations of Stress in the Soil Between the Two Vertical Surfaces of Sliding for the Case of the Rigid Inclusion in a Half Plane of Soil . . .	11
5	Examples of Active and Passive Soil-Structure Interaction As a Function of Depth	13
6	Zone of Influence of Rigid Structure	16
7	Deeply Buried Structure on Rigid Foundation	17
8	Zone of Influence Below a Rigid Structure	19
9	Zone of Influence Above a Rigid Structure	21
10	Relative Deformation Between the Soil and the Structure at the Bottom of the Structure (Passive Case)	24
11	Relationships Between NL and Y	29
12	Relationship Between Relative Stress (Y) and Length-to-Span Ratio (L/B) for a Range of NB Values for the Passive Case (Linear Soil Conditions)	30
13	Relationships Between C_r and Y for Various NL Values for the Passive Case (Linear Soil Conditions)	33
14	Relative Deformation Between the Soil and the Structure at the Bottom of the Structure (Active Case)	34
15	Relationship Between C_r and $1/Y'$ for Various NL Values for the Active Case (Linear Soil Conditions)	41
16	Relationship Between C_r and Y for an NL Value of 0.608 for the Conditions Ranging From the Active Through the Passive Case (Linear Soil Conditions)	42
17	Relationship Between NL and Y	45
18	Relationship Between Overstress (Y) and Length-to-Span Ratio (L/B) for Different NB Values for the Passive Case	47
19	Comparison Showing the Effect of Nonlinear Soil Conditions on the Relationship Between the Length-to-Span Ratio (L/B) and the Relative Stress (Y) for Constant NB for the Passive Case .	48

ILLUSTRATIONS (Cont.)

<u>Figure</u>		<u>Page</u>
20	Relationship Between C_r' and the Overstress Y for Various NL Values for the Passive Case (Nonlinear Soil Conditions)	52
21	Comparison Showing the Effect of Nonlinear Soil Conditions on the Relationship Between C_r' and the Relative Stress (Y) for NL = 0.608 for the Passive Case	53
22	Relationship Between C_r' and $1/Y'$ for Various NL Values for the Active Case (Nonlinear Soil)	57
23	Comparison Showing the Effect of Nonlinear Soil Conditions on the Relationship Between C_r' and Relative Stress $1/Y'$ for NL = 0.608	58
24	Comparison Showing the Effect of Nonlinear Soil Conditions on the Relationship Between C_r' and the Relative Stress Y for NL = 0.608 for the Passive and Active Cases	59
25	Relationship Between $J\Delta_B/B\epsilon_{s0}$ and Overstress $Y = (\sigma_o + \sigma_a/\sigma_o)$ for the Passive Case (Linear Soil Conditions)	63
26	Relationship of Differential Displacement per Unit Span Δ_B/B to the Overstress (Y) for a Range of $J/1000\epsilon_{s0}$ Values for the Passive Case (Linear Soil Conditions)	66
27	Relationship Between $J\Delta_B/B\epsilon_{s0}$ and Relative Stress $Y = (\sigma_o - \sigma_a/\sigma_o)$ for the Active Case (Linear Soil Conditions)	67
28	Relationship of Differential Displacement per Unit Span Δ_B/B to the Relative Stress (Y) for a Range of $J/1000\epsilon_{s0}$ for the Active Case (Linear Soil Conditions)	68
29	Relationship Between Differential Displacement per Unit Span (Δ_B/B) to the Relative Stress (Y) on Structure for $J/1000\epsilon_{s0} = 0.1465$ for the Range From the Active Through the Passive Cases (Linear Soil Conditions)	69
30	Relationship Between $M = (A/\sigma_o)^{2/3}(J\Delta_B/B)$ and Overstress Y for the Passive Case (Nonlinear Soil Conditions)	72
31	Relationship of Differential Displacement per Unit Span (Δ_B/B) to the Overstress (Y) for a Range of $(A/\sigma_o)^{2/3}(J\Delta_B/B)$ Values for the Passive Case (Nonlinear Soil Conditions)	74
32	Comparison Showing the Effect of Nonlinear Soil Conditions on the Relationship Between Δ_B/B and Overstress (Y) for $(A/\sigma_o)^{2/3}(J/1000) = 0.1465$ for the Passive Case	75
33	Relationship Between $M[(A/\sigma_o)^{2/3}(J\Delta_B/B)]$ and Understress Y for the Active Case (Nonlinear Soil Conditions)	77
34	Relationship of Differential Displacement per Unit Span (Δ_B/B) to the Understress (Y) for a Range of $(A/\sigma_o)^{2/3}(J/1000)$ Values for the Active Case (Nonlinear Soil Conditions)	79

ILLUSTRATIONS (Cont.)

<u>Figure</u>		<u>Page</u>
35	Comparison Showing the Effect of Nonlinear Soil Conditions on the Relationship Between Δ_B/B and Understress (Y) for $(A/\sigma_0)^{2/3}(J/1000) = 0.1465$ for the Active Case	80
36	Comparison Showing the Effect of Nonlinear Soil Conditions on the Relationship Between Δ_B/B and Relative Stress (Y) for Constant $(A/\sigma_0)^{2/3}(J/1000)$ for the Active and Passive Cases	81
37	Comparison of Experimental and Theoretical Results Indicating the Effect of Variations in Length-to-Span Ratio on the Load on the Structure	84
38	Comparison of Theoretical Results With the Experimental Results From Experimental Employing the Goldbeck Cell Showing the Effect of Length-to-Span Ratio	87
39	Comparison of the Theoretical and Experimental Results Showing the Effects of Structural Compressibility	91
40	Stress - Strain Curves for Granular Media	92
41	Structural Displacement - Time, On-Structure Stress - Time Histories	93
42	The Relation Between Angle of Internal Friction and Density for the Sands Tested	96
43	Comparison of One-Dimensional Loading Curves for Sand 1	97
44	Comparison of One-Dimensional Loading Curves for Sand 2	98
45	Dimensionless Plot of Pressure vs Deflection for Passive Arching Tests With Sand 2, $H/B = 1/3$, $P_s = 75$ psi	100
46	Dimensionless Plot of Pressure vs Deflection for Passive Arching Tests With Sand 2, $H/B = 2/3$, $P_s = 75$ psi	101
47	Dimensionless Plot of Pressure vs Deflection for Passive Arching Tests With Sand 2, $H/B = 1$, $P_s = 75$ psi	102
48	Dimensionless Plot of Pressure vs Deflection for Passive Arching Tests With Sand 2, $H/B = 1-1/3$, $P_s = 75$ psi	103
49	Dimensionless Plot of Pressure vs Deflection for Passive Arching Tests With Sand 2, $H/B = 1-2/3$, $P_s = 75$ psi	104
50	Dimensionless Plot of Pressure vs Deflection for Passive Arching Tests With Sand 2 $H/B = 2$, $P_s = 75$ psi	105
51	Dimensionless Plot of Pressure vs Deflection for Passive Arching Tests With Sand 2, $H/B = 2-1/3$, $P_s = 75$ psi	106
52	Dimensionless Plot of Pressure vs Deflection for Passive Arching Tests With Sand 2, $H/B = 2-2/3$, $P_s = 75$ psi	107
53	Small-Scale Dimensionless Plot of Pressure vs Deflection for Passive Arching Tests With Sand 2	109
54	One-Dimensional Compression Stress - Strain Curves for Sand 1	111

ILLUSTRATIONS (Cont.)

<u>Figure</u>		<u>Page</u>
55	One-Dimensional Compression Stress - Strain Curves for Sand 2 .	112
56	Dimensionless Plot of Pressure vs Deflection for Active Arching Tests With Sand 2, $H/B = 1/3$, $P_s = 75$ psi	113
57	Dimensionless Plot of Pressure vs Deflection for Active Arching Tests With Sand 2, $H/B = 2/3$, $P_s = 75$ psi	114
58	Dimensionless Plot of Pressure vs Deflection for Active Arching Tests With Sand 2, $H/B = 1$, $P_s = 75$ psi	115
59	Dimensionless Plot of Pressure vs Deflection for Active Arching Tests With Sand 2, $H/B = 2$, $P_s = 75$ psi	116
60	Dimensionless Plot of Pressure vs Deflection for Active Arching Tests With Sand 2, $H/B = 4$, $P_s = 75$ psi	117
61	Dimensionless Plot of Pressure vs Deflection for Active Arching Tests With Sand 2, $H/B = 1/3$, $P_s = 110$ psi	119
62	Dimensionless Plot of Pressure vs Deflection for Active Arching Tests With Sand 2, $H/B = 2/3$, $P_s = 110$ psi	120
63	Dimensionless Plot of Pressure vs Deflection for Active Arching Tests With Sand 2, $H/B = 1$, $P_s = 110$ psi	121
64	Dimensionless Plot of Pressure vs Deflection for Active Arching Tests With Sand 2, $H/B = 1/3$, $P_s = 40$ psi	122
65	Dimensionless Plot of Pressure vs Deflection for Active Arching Tests With Sand 2, $H/B = 2/3$, $P_s = 40$ psi	123
66	Dimensionless Plot of Pressure vs Deflection for Active Arching Tests With Sand 2, $H/B = 1$, $P_s = 40$ psi	124
67	Dimensionless Plot of Pressure vs Deflection for Active Arching Tests With Sand 1, $H/B = 1/3$, $P_s = 75$ psi	125
68	Dimensionless Plot of Pressure vs Deflection for Active Arching Tests with Sand 1, $H/B = 2/3$, $P_s = 75$ psi	126
69	Dimensionless Plot of Pressure vs Deflection for Active Arching Tests With Sand 1, $H/B = 1$, $P_s = 75$ psi	127
70	Dimensionless Plot of Pressure vs Deflection for Active Arching Tests With Sand 1, $H/B = 2$, $P_s = 75$ psi	128
71	Dimensionless Plot of Pressure vs Deflection for Active Arching Tests With Sand 1, $H/B = 4$, $P_s = 75$ psi	129
72	Dimensionless Plot of Pressure vs Deflection for Active Arching Tests With Sand 1, $H/B = 6$, $P_s = 75$ psi	130
73	Relationship Between Depth of Burial and Relative Stress for Various Δ_B/B Values	132
74	Relationship of Maximum Relative Stress vs Depth of Burial Showing the Effects of Surface Layers	134
75	Stress Gauge Pattern on Variable Compressibility Structure . .	A-2
76	Soil Displacement Measuring System	A-4
77	Variable Compressibility Structure	A-6

NOTATION

A = nonlinear soil modulus

B = one-half the span of the structure (movable section) or radius of the structure for a finite structure (in figures from Ref. 11, B is equivalent to $2B$ in the text)

c = cohesion

C_r = relative compressibility (linear case) E_{so}/E_{ST}

C_r' = relative compressibility (nonlinear case) $\frac{(A)^{2/3}}{E_{ST}}$

E_{so} = linear soil modulus

E_{ST} = effective modulus of the structure

$$H = \frac{\sigma_o + \sigma_a}{\sigma_o^{2/3}} = Y(\sigma^{1/3})$$

$$J = 2K \tan \phi$$

K = ratio of the horizontal (lateral) to the vertical (axial) stress

L = one-half the length of the structure

$\frac{L}{B}$ = length-to-span ratio

$$M = \left(\frac{A}{\sigma_o}\right)^{2/3} \frac{J\Delta}{B}$$

$$N = 2S_p = \frac{2K \tan \phi}{B}$$

q = surcharge per unit area

$$S_p = \frac{K \tan \phi}{B}$$

x = distance from reference plane to point of interest

Y = overstress or relative stress $\frac{\sigma_o + \sigma_a}{\sigma_o}$, $\frac{1}{Y'}$

Y' = understress or relative stress, $\frac{\sigma_o}{\sigma_o - \sigma_a} = \frac{1}{Y}$

Z = depth of the soil

Z_i = distance of influence

NOTATION (Cont.)

- γ = unit weight of the soil
- Δ_B = differential deformation between the soil and structure at the lower face
- Δ_{so} = soil deformation over 2L length under free-field stress σ_o
- Δ_{ST} = total deformation of the structure over and under $\sigma_o \pm \sigma_a$ stress
- Δ_{to} = net deformation $\Delta_{so} - \Delta_{ST}$
- Δ_x = total deformation of the column of the soil between the vertical surfaces of sliding below the structure
- Δ_y = deformation of the free-field soil below and adjacent to the structure
- δ = differential deformation between trap door and bottom of the bin in data taken from Ref. 11
- ϵ_{so} = soil strain related to the free-field stress σ_o
- ϵ_x = strain over a dx element at any point x within the vertical surfaces of sliding
- σ_a = arching stress
- σ_h = horizontal or lateral stress
- σ_o = free-field stress
- σ_v = vertical stress on a horizontal section at depth Z
- σ_x = vertical stress at any point x within the vertical surfaces of sliding
- σ_T = average stress due to sidewall friction
- τ = shear stress
- $\tan \phi$ = coefficient of internal friction of the soil
- ϕ' = angle of friction in sidewall friction calculations

Section 1
INTRODUCTION

Since February 1964, URS Corporation has been conducting a research program in the field of soil-structure interaction for the Defense Atomic Support Agency under Contract DA-49-146-XZ-288. The general objective of this research effort was to provide a better explanation of the soil-structure interaction phenomena that occur around a structure embedded in a soil medium subjected to nuclear-blast environments. Specifically, the research described herein was directed toward an understanding of the basic mechanism of soil behavior in soil-structure interaction.

This program was divided into two phases: (1) an experimental and theoretical study of the effects of structural compressibility on soil-structure interaction and (2) a systematic review and correlation of basic interaction research conducted in recent years. The results of the first part of the study, directed toward an understanding of the basic mechanism of static soil behavior in soil-structure interaction, are reported herein. The results of the second phase, directed toward establishing the present state of knowledge as well as furnishing background information for engineers concerned with protective construction research and design, are reported in the companion report, DASA 1711.

This report is organized into nine sections plus references and an appendix, the latter describing the details of the limited experimental program. Background presented in Section 2 is limited, since DASA 1711 covers this subject in detail. In section 3 the basic concepts of soil-structure interaction involving active and passive arching are reviewed. Section 4 covers the theoretical development of equations relating the total load on a buried structure, under linear soil conditions, to such structural parameters as length, span, and compressibility. Modifications to account for the effects of nonlinear soil conditions are considered in Section 5. Application of active and passive arching concepts to trap door experiments (differential displacement) are investigated theoretically in Section 6. The various theoretical results are compared in Section 7 with existing data, including trap door experiments, and those obtained in the present experimental program.

Section 8 covers a brief discussion of the effects of surface layers on model studies of arching, and Section 9 presents the conclusions and recommendations of the study.

Section 2 BACKGROUND

A considerable effort has been made by various research organizations to understand the response of soil and structural systems to nuclear explosions in order to provide protection for our retaliatory capabilities. This effort has generally been aimed at developing fundamental understanding of the effects, including those of the explosion, coupling of the explosive energy (both direct and air-induced), wave propagation through the media, soil-structure interaction, and response of the structure's contents to motion induced by the soil-structure interaction.

Since the explosion and air-blast phenomena are better understood, the real problems, then, are those of understanding the basic phenomena involved in the behavior under dynamic loading of soils and structures and the character of the soil-structure interaction resulting therefrom. Basic knowledge of this type could be used to help solve a specific design problem or to evaluate the strength of existing facilities.

The formidable problems of understanding the dynamic behavior of soil and the stress-wave propagation through soil are exemplified by the magnitude of the research effort already directed to this area. Recent URS studies aimed at gaining an understanding of the basic mechanisms of dynamic soil behavior and wave propagation in soil have shown that it is possible to establish relationships between particle velocity, wave velocity, and the secant modulus of the dynamic stress-strain relationship under shock stress-wave propagation (refs. 1-5). The establishment of these relationships completes the first steps in providing a prediction method based on an understanding of the mechanisms of soil behavior during loading.

Even though the design of underground structures subject to nuclear blast is an extension of conventional design problems, such as tunnels, culverts, and retaining walls, it has been a surprise to many in the protective construction field to discover the limitations of present knowledge regarding the response of soil-structure systems even to static loads. Although some basic concepts have been developed which have led to useful procedures for specific design

problems, there are not enough quantitative data regarding basic behavior to provide the necessary fundamental understanding for general design purposes. Even the conventional culvert problem is difficult if the parameters are changed beyond their usual limits. A review of recent studies in the soil-structure interaction area are discussed in the companion report for this work, DASA 1711. Brief reviews of some of the pertinent ones are also presented in Refs. 6 and 7.

Section 3
SOIL- STRUCTURE INTERACTION CONCEPTS

Since passive and active form the foundation for the further developments presented herein, this section is devoted to a brief review of the assumptions and resultant equations developed in Refs. 6 and 8. The two basic concepts of soil-structure interaction discussed in Ref. 6 show the applicability of active and passive arching. Since most real structures involve complex interrelations between these two types of arching, involving local flexibility and gross compressibility of the structure, the effort in Ref. 6 was confined to the use of idealized structures. Only extreme conditions of active and passive arching were developed in both the experimental and theoretical programs. This report deals with the conditions between these extremes as influenced by the compressibility and length of the structure. The effects of local flexibility is not treated in this study.

ACTIVE ARCHING

The active arching case investigated in Ref. 6 was the simplest possible and is one which arises when an idealized structure having a uniform compressibility across the entire face normal to the direction of loading is embedded in a soil of lesser compressibility. This difference in compressibility results in differential strain between the free-field soil and the structure as shown in Fig. 1. These differential strains result in a redistribution of stress by means of the shear strength of the soil.

Static active arching is treated in detail by Terzaghi in Refs. 8 and 9. The basic assumption of static arching is that the model is a two-dimensional half plane of soil resting at the depth Z on a rigid foundation having a movable finite section, the soil being subject to a uniform surface pressure. A second assumption is that the movable section deforms an amount sufficient to mobilize the shear forces to the surface. This is an extreme case of active arching and - for shallow-buried structures - exists when the structure compressibility is great enough to develop the entire shear force available. For deeply buried structures, the extreme exists when the shear forces are great enough to carry the weight of the soil above it and the surface load.

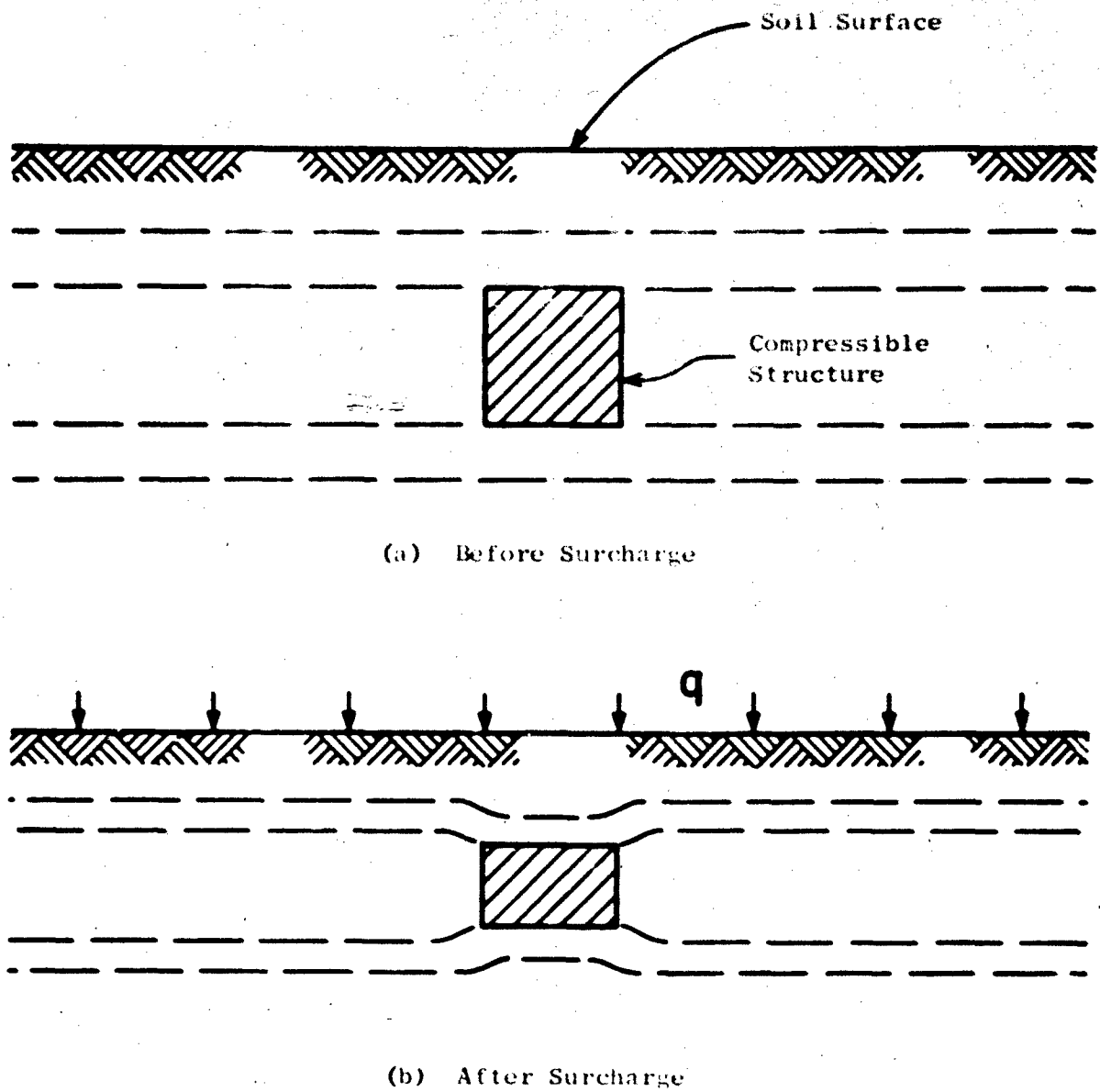


Fig. 1. Displacements Within a Soil Mass With an Inclusion More Compressible Than the Soil (Active Arching)

Figure 2 illustrates the assumptions that provide the basis for computation of stress in the soil between the two vertical surfaces of sliding in the active case. Solution of the equations resulting from a summation of the vertical forces at equilibrium results in the following equation for the stress at a given depth Z:

$$\sigma_v = \frac{B(\gamma - c/B)}{K \tan \phi} \left(1 - e^{-K \tan \phi Z/B} \right) + qe^{-K \tan \phi Z/B} \quad (1)$$

where

B = one-half the span of the structure (movable section)

γ = unit weight of the soil

c = cohesion

K = ratio of the horizontal (lateral) to the vertical (axial) stress

ϕ = coefficient of internal friction of the soil

Z = depth of the soil

σ_v = vertical stress on a horizontal section at depth Z

q = surcharge per unit area

This equation is for the solution of the two-dimensional condition and is representative of a movable section having a unit thickness, i.e., unit thickness perpendicular to the plane of the figure. For a section having a circular cross section of radius B, Eq. (1) becomes

$$\sigma_v = \frac{B}{2K \tan \phi} \left(\gamma - \frac{2c}{B} \right) \left(1 - e^{-2K \tan \phi Z/B} \right) + qe^{-2K \tan \phi Z/B} \quad (2)$$

where all the terms are the same as in Eq. (1), except B, which is the radius of the structure. If only the surcharge is considered, i.e., γ and c equal 0, these equations can be reduced to

$$\sigma_v = qe^{-K \tan \phi Z/B} \quad (1a)$$

$$\sigma_v = qe^{-2K \tan \phi Z/B} \quad (2a)$$

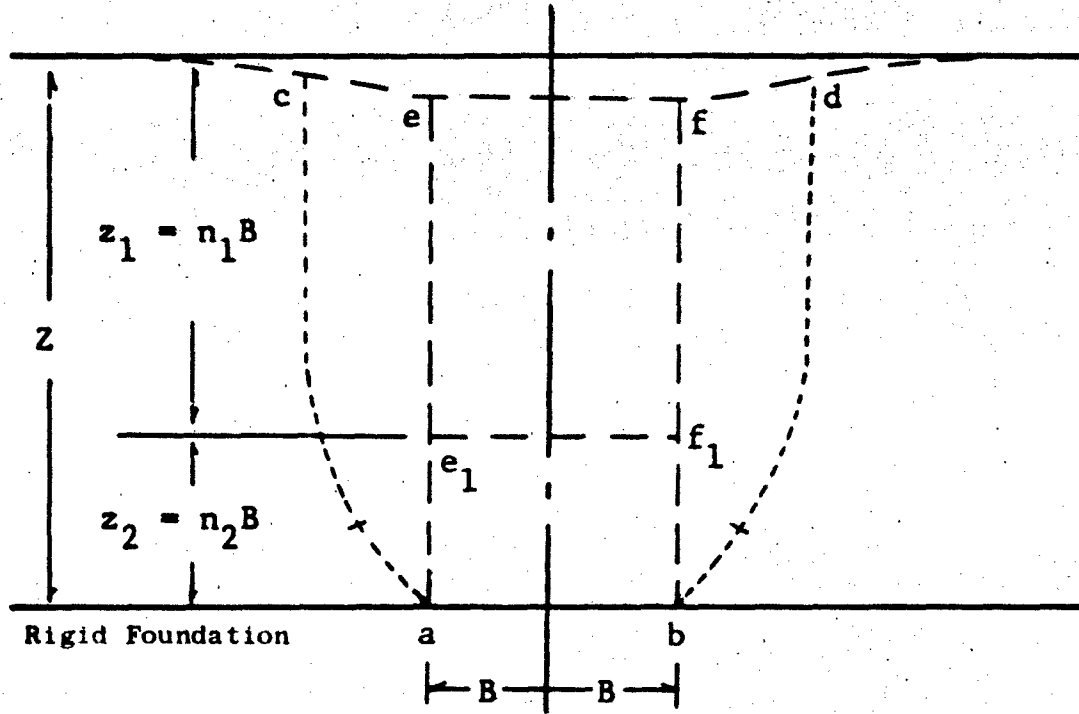


Fig. 2a. Failure in Cohesionless Sand Caused by Downward Movement of a Long, Narrow Section of the Foundation (from Ref. 8)

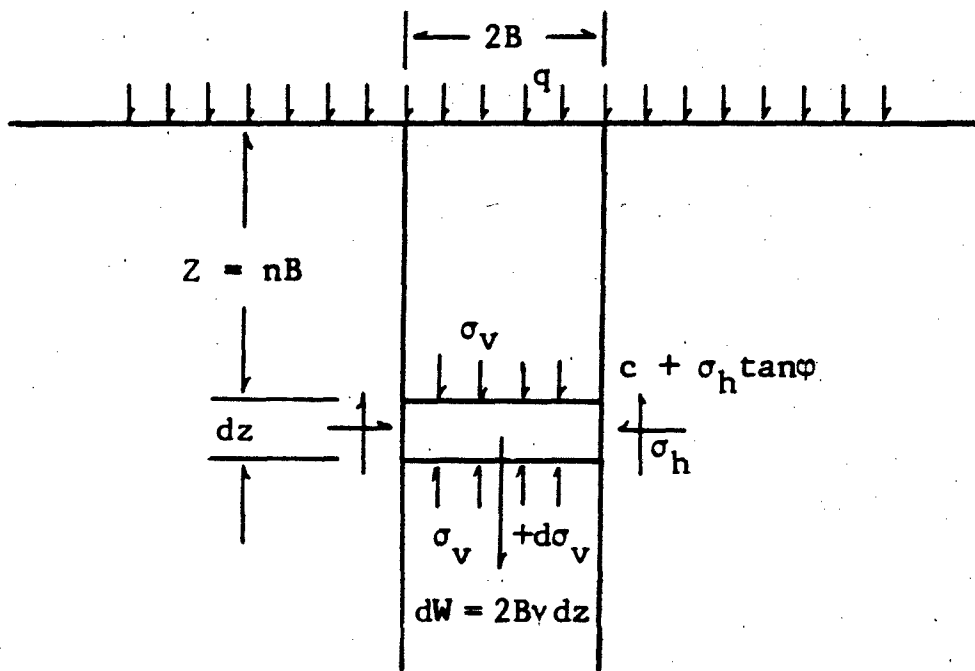


Fig. 2b. Assumptions on Which Computation of Stress in Sand Between Two Vertical Surfaces of Sliding Is Based (from Ref. 8)

PASSIVE ARCHING

The passive arching case investigated in Ref. 6 was also the simplest possible and is one which occurs when an idealized structure having a uniform compressibility across the entire face normal to the direction of loading is embedded in a soil of greater compressibility. This situation results in differential strain between the free-field soil and the structure similar to that shown in Fig. 3. These differential strains result, as in the active case, in a redistribution of stress by means of the shear strength of the soil.

In an attempt to find a solution to the static passive arching case, similar to that presented by Terzaghi for the static active arching case, Ref. 6 developed a similar analysis using the same mathematical principles. The basic assumption in this case is that the model is a two-dimensional half plane of soil subjected to a uniform surface pressure, with a rigid inclusion at a given depth. The second assumption is that the inclusion extends to infinity, so that a sufficient amount of differential displacement occurs to mobilize the shear forces to the surface, regardless of depth. This is the extreme case of passive arching for all depths of burial.

Figure 4 illustrates the assumptions that provide the basis for computation of stress in the soil between the two vertical surfaces of sliding in the passive case. Particular attention is drawn to the direction of the shear forces τ in Fig. 4 as compared with those in Fig. 2. Solution of the equations resulting from a summation of the vertical forces at equilibrium results in the following equation for the stress at a given depth Z:

$$c_v = \frac{B(\gamma + c/B)}{K \tan \phi} \left(e^{K \tan \phi Z/B} - 1 \right) + qe^{K \tan \phi Z/B} \quad (3)$$

The terms are as defined following Eq. (1).

Like Eq. (1), this equation is for the solution of the two-dimensional condition and is representative of a structure having a unit thickness. For a structure having a circular cross section of radius B, Eq. (3) becomes

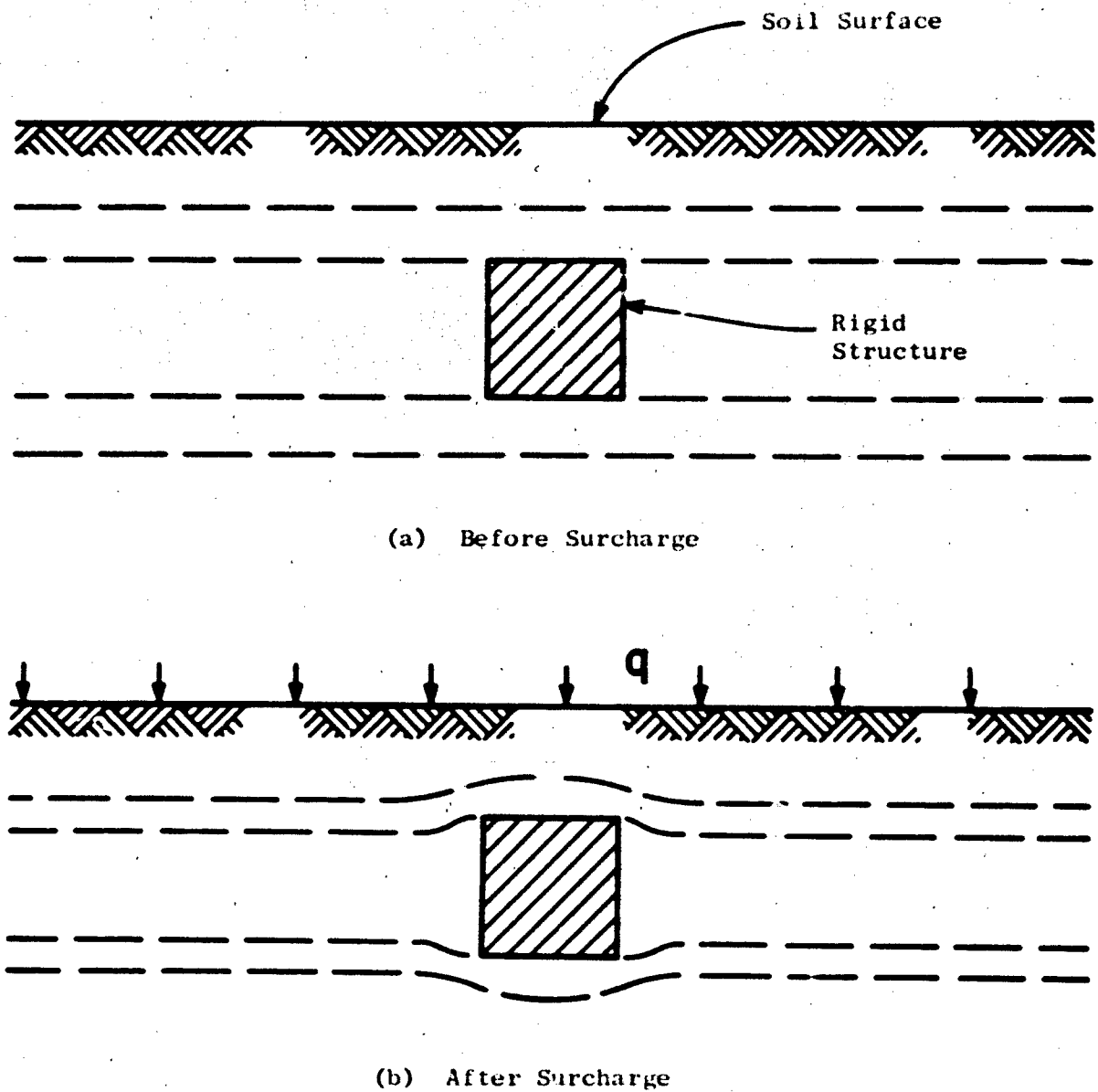


Fig. 3 Displacement Within a Soil Mass With an Inclusion Less Compressible Than the Soil (Passive Arching)

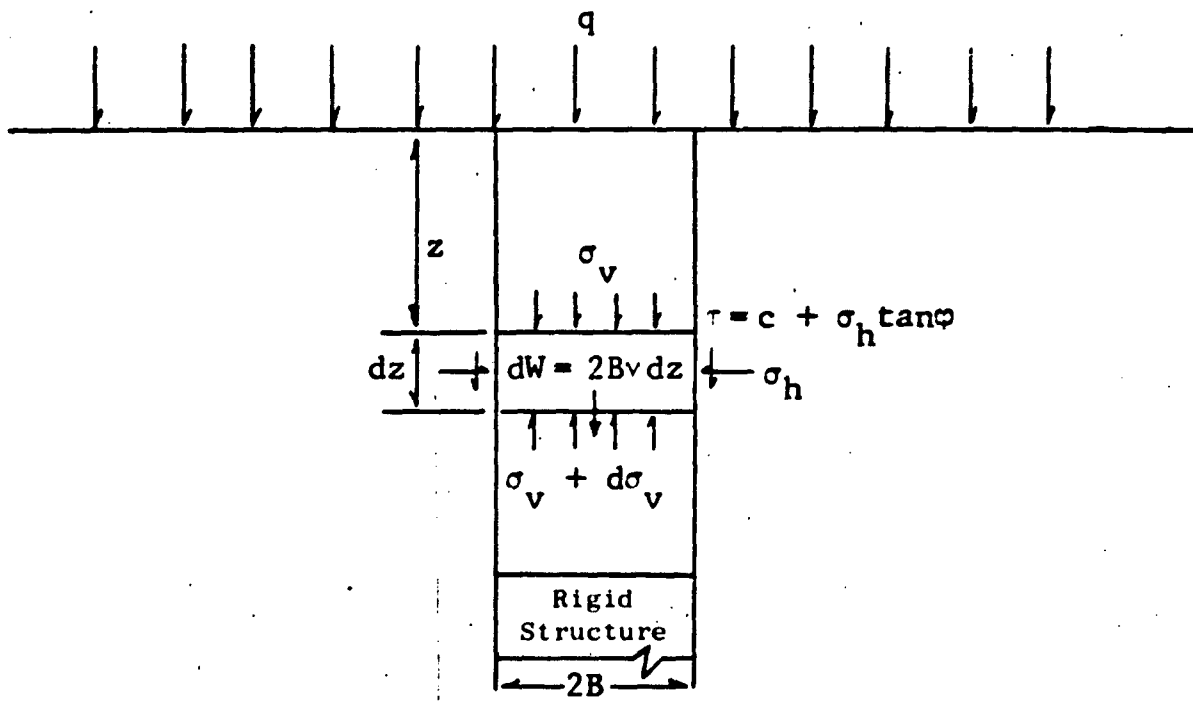


Fig. 4. Assumptions Which Provide the Basis for Computations of Stress in the Soil Between the Two Vertical Surfaces of Sliding for the Case of the Rigid Inclusion in a Half Plane of Soil

$$\sigma_v = \frac{B}{2K \tan \phi} \left(\gamma + \frac{2c}{B} \right) \left(e^{2K \tan \phi Z/B} - 1 \right) + qe^{2K \tan \phi Z/B} \quad (4)$$

If only the surcharge is considered, i.e., c and γ equal zero, these equations can be reduced to

$$\sigma_v = qe^{K \tan \phi Z/B} \quad (3a)$$

$$\sigma_v = qe^{2K \tan \phi Z/B} \quad (4a)$$

COMPARISON OF ACTIVE AND PASSIVE ARCHING

In the case of passive arching for structures of finite dimensions, the amount of differential deformation is dependent on the length of the structure and the relative compressibility between the structure and the soil. Therefore, a rigid structure of finite size will cause a given amount of differential deformation to occur between the soil and the structure regardless of the depth of burial. Since the amount of differential deformation required to develop all the shear forces between the structure and the surface is dependent upon depth, it is obvious that below the depth at which the amount of differential deformation required exceeds the amount developed between the soil and the structure, the load on the structure is controlled by the differential deformation developed.

It can be expected, then, that in the passive case the load on the rigid structure will increase exponentially as the structure burial is increased, following the form of Eq. (4) or (4a). For a structure of finite length, the load will increase until some critical depth is reached, below which point the load will be constant. In the case of active arching the load will decrease exponentially as the structural burial is increased, following the form of Eq. (2) or (2a). For a very compressible structure, the load on the structure will approach zero or, in the case of a structure of finite compressibility, the load will become constant below some critical depth. Figure 5 represents a plot of two of these conditions as a function of depth: for the maximum active arching (a very compressible structure) curve A, and for the passive arching on a rigid structure of finite length curve B. The data points shown are

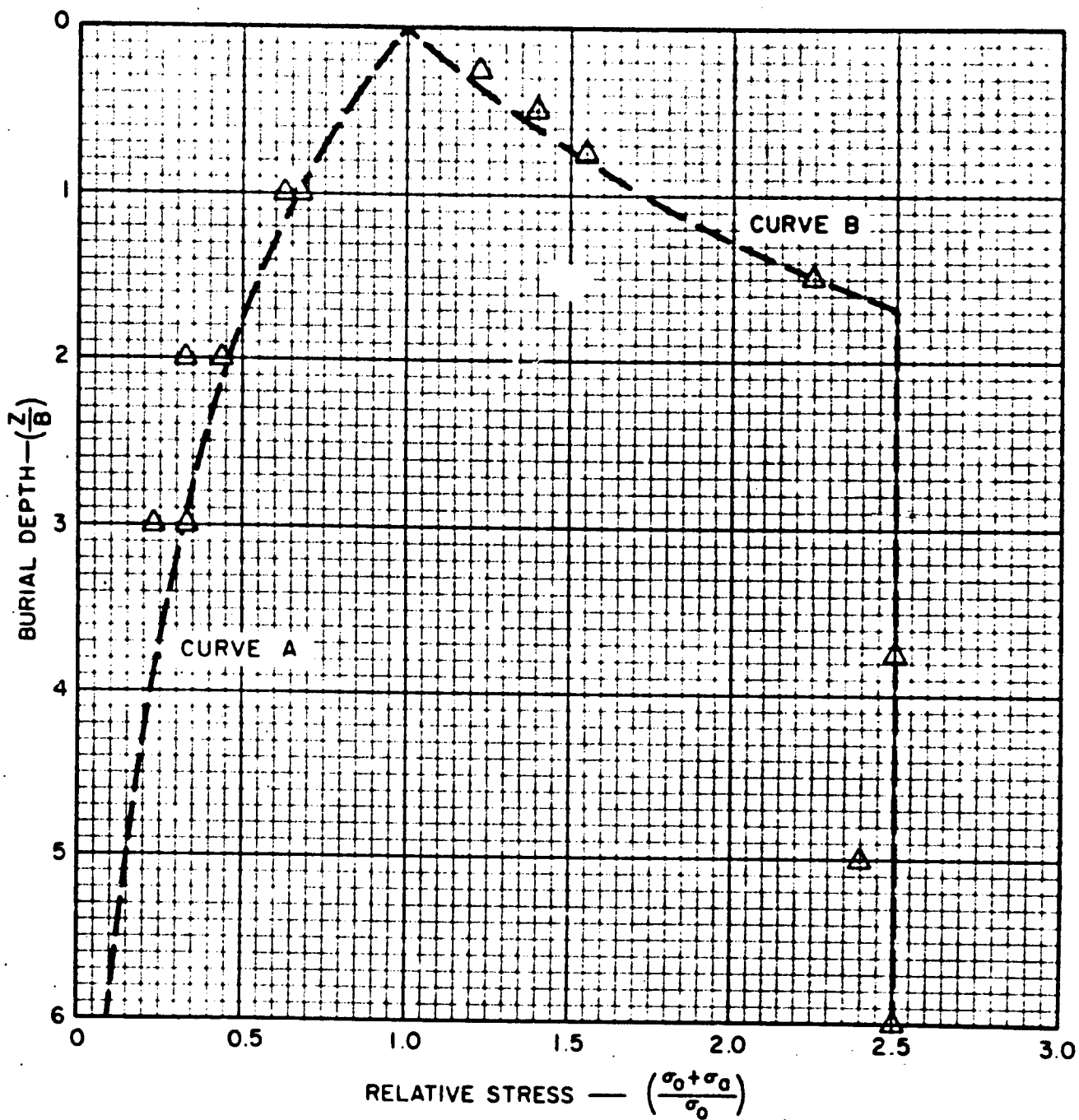


Fig. 5. Examples of Active and Passive Soil-Structure Interaction As a Function of Depth

for a URS* experimental structure in which only compressibility was varied (from rigid to very compressible). It is obvious that the point at which the break in Curve B occurs will vary as the length of the structure varies, and that the shape of Curve A and the upper portion of Curve B will vary with the span of the structure and the soil properties.

Since these two curves represent the extremes in relative compressibility, the area between them represents the various conditions of relative compressibilities between these two extremes. This report deals with research directed toward gaining an understanding of static soil-structure interaction in the area between these two limits and toward determining the influence of structural length on the load on a rigid structure in the deeply buried condition. One point between the two extremes is known; that is when the relative compressibility is one, i.e., when the soil and the structure have the same compressibility, the load on the structure is equal to the free-field stress.

* The data were reported in Ref. 6.

Section 4
EFFECTS OF STRUCTURAL PARAMETERS

As discussed earlier, a structure of finite length that is less compressible than the soil causes a differential deformation to occur, the influence of which extends some distance above and below the structure. In these influenced areas the stress will be greater than the free-field stress, while above and below the influenced areas the stress will be free-field. If the distance to the point where the influence ceases is defined as the distance of influence Z_1 , then any structure for which the depth of burial Z is greater than the distance of influence Z_1 can be said to be deeply buried. If Z is less than Z_1 , then the structure can be said to be shallow buried. Figure 6 illustrates these conditions. The active and passive arching relationship described previously and in Ref. 6 cover the shallow-buried condition. This report deals principally with the deeply buried conditions.

EFFECTS OF STRUCTURE LENGTH AND SPAN

Assume a right circular cylindrical structure* of $2B$ diameter and $2L$ length buried at a depth of Z such that Z_1 , the zone of influence, is less than Z , i.e., deeply buried. If the structure is considered to be rigid and sitting on a rigid foundation, then the greatest differential strain that can be developed is that due to the axial shortening of the soil laterally adjacent to the structure, i.e., free-field. In the case illustrated in Fig. 7, the soil element $2L$ in length is subjected to the free-field stress c_o , i.e., q ;** therefore it would shorten an amount equal to Δ_{so} where

$$\Delta_{so} = \frac{2Lc_o}{E_{so}} \quad (5)$$

* While the following relationships can be developed for a structure of unit thickness (two-dimensional), or even one of rectangular cross section, the shape chosen was a right cylinder having a circular cross section to conform to the shape of the structures to be used in an experimental program.

** It is assumed that for the static case there is no decay of stress with depth.

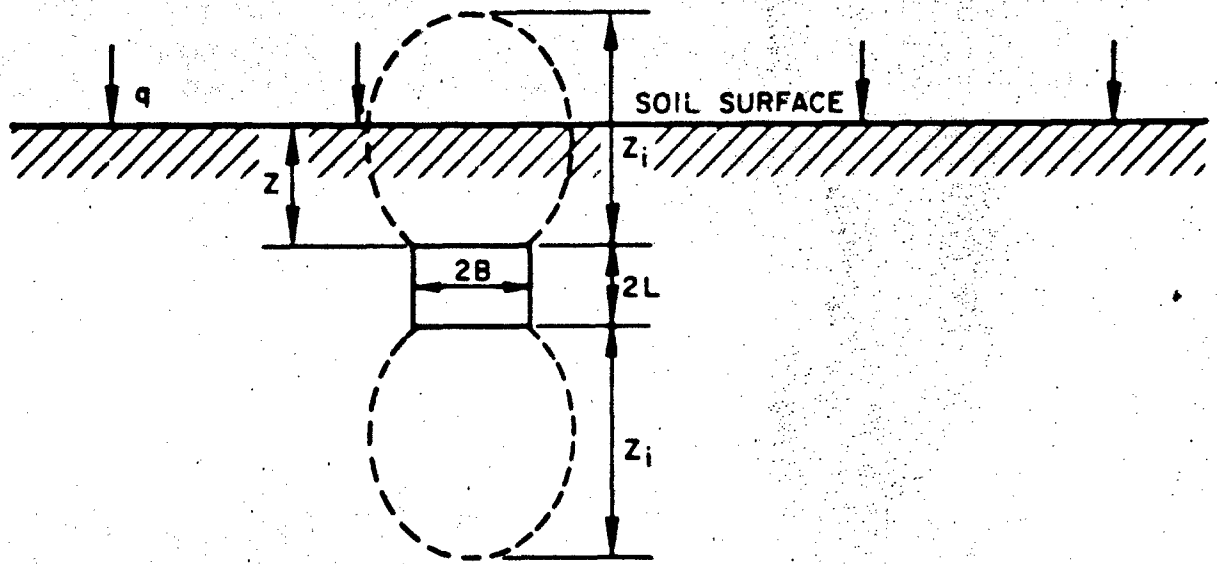
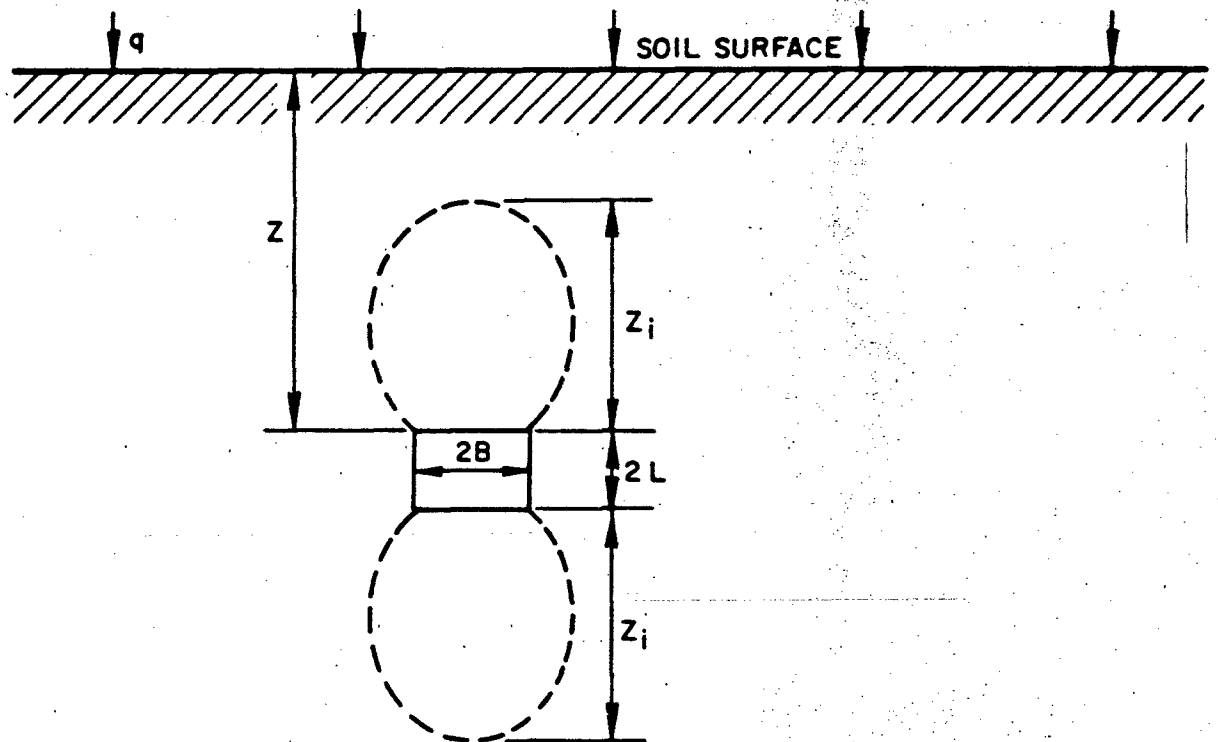
(a) SHALLOW DEPTH BURIAL $Z < Z_i$ (b) DEEPLY BURIED STRUCTURES $Z > Z_i$

Fig. 6. Zone of Influence of Rigid Structure

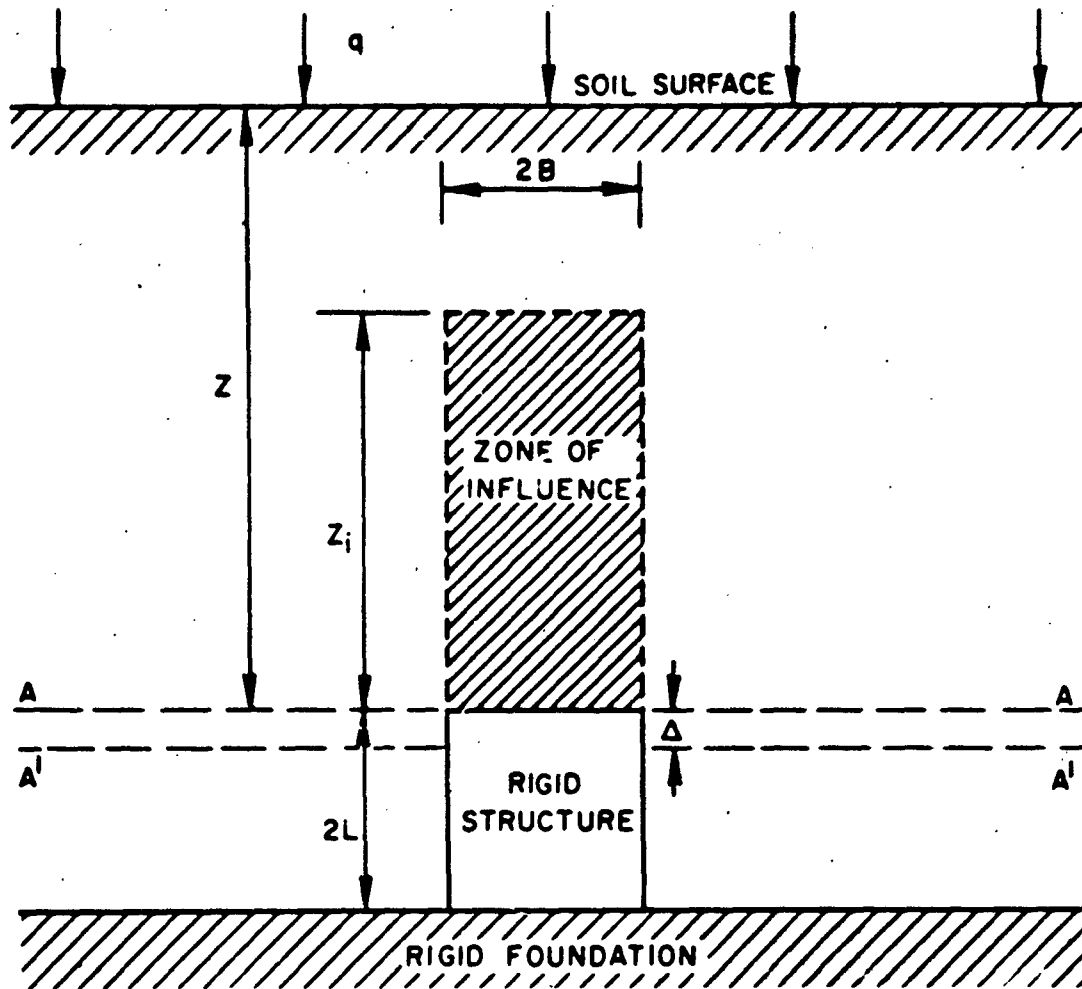


Fig. 7. Deeply Buried Structure on Rigid Foundation

where

σ_o = free-field stress

L = one-half the length of the structure

E_{so} = soil modulus (assumed to be linear)*

Since a rigid structure is being considered, Δ_{so} is the amount of differential deformation of the plane through the upper surface of the structure. As discussed earlier, this will result in downward shear forces on the element of soil above the structure, i.e., passing arching will result. If this passive arching force is denoted by σ_a , an average arching stress, then the total average stress on the structure can be expressed as $\sigma_o + \sigma_a$.

If in considering the stress distribution below a structure completely surrounded by soil, it is assumed that there is no sidewall friction on the sides of the structure, then the total average stress on the top surface of the structure is applied to the soil beneath the structure. At some distance Z_i below the structure, the point where there is no longer any influence, the stress in the soil will be reduced to the free-field stress σ_o . It can be assumed that the arching stress σ_a was redistributed to the surrounding soil by means of shear stresses. It is further assumed that this can be represented by the concepts of the vertical surfaces of sliding used in the development of Eqs. (1) and (4). A simple examination of the soil element abcd in Fig. 8 shows that in order to reduce the stress from $\sigma_o + \sigma_a$ at the point immediately below the structure to σ_o at the plane DD, the shear forces must be upward. This means that at any point x below the structure, the stress σ_x is described by Eq. (2a) [or Eq. (2) for the more general solution], which can be written

$$\sigma_x = (\sigma_o + \sigma_a) e^{-2K \tan \phi x/B} \quad (2b)$$

This relationship is only true while $\sigma_x \geq \sigma_o$, i.e., when $x < Z_i$; at x equal to or larger than Z_i , $\sigma_x = \sigma_o$.

* Relationships for the case of a nonlinear modulus are presented in Section 5.

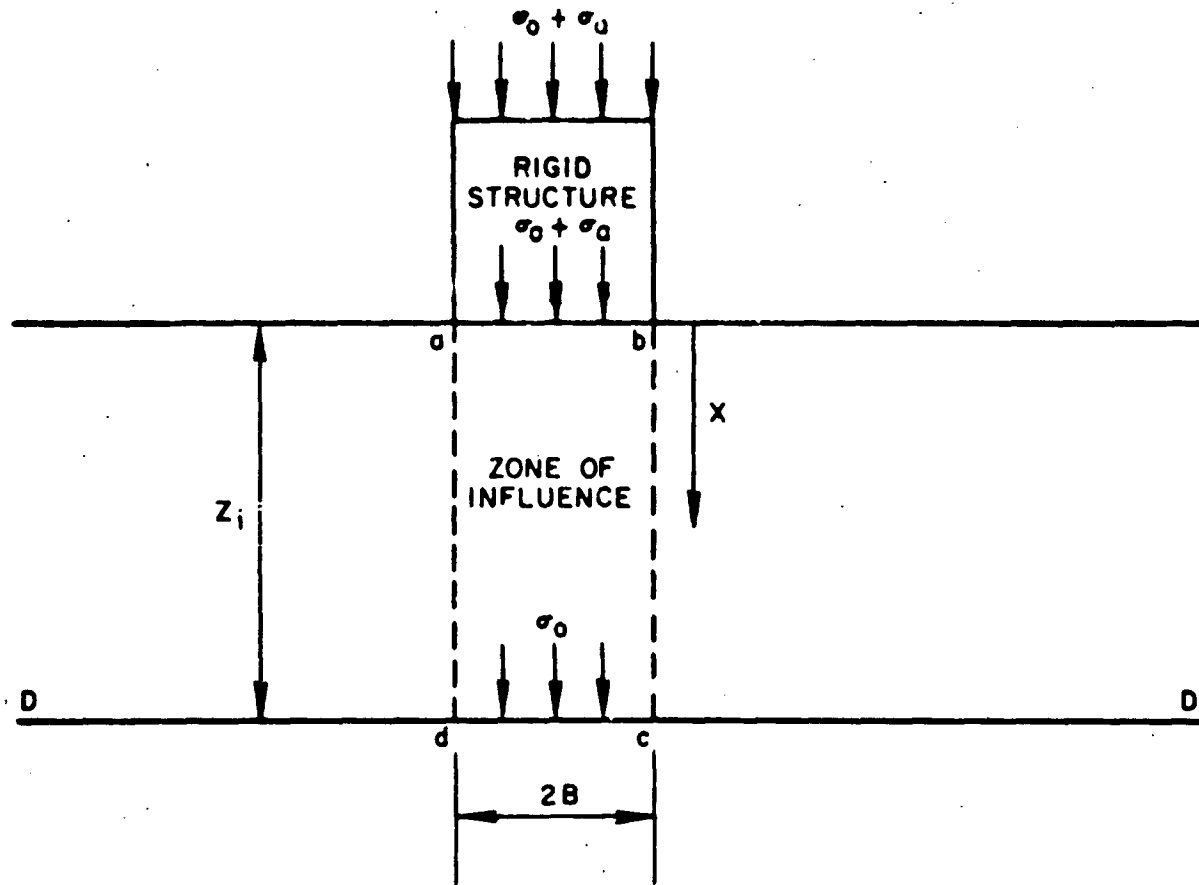


Fig. 8. Zone of Influence Below a Rigid Structure

Therefore

$$\sigma_o = (\sigma_o + \sigma_a) e^{-2K \tan \varphi Z_1/B} \quad (6)$$

solving for the zone of influence Z_1 gives

$$Z_1 = \frac{B}{2K \tan \varphi} \ln \left(\frac{\sigma_o + \sigma_a}{\sigma_o} \right) \quad (7)$$

A similar static analysis at the upper end of the structure can be made. At the point above the structure where the influence of the structure ends, i.e., at Z_1 , the stress in the soil element above the structure is equal to the free-field stress, σ_o . At this point there also is no differential strain* between the soil inside and outside the projected vertical surface of sliding, therefore the deformation of the column of soil above the structure has to be equal to the differential displacement between the soil and the structure at the top surface of the structure. Therefore, in Fig. 9 the plane AA can be used as a reference, since it moves the same amount over both the affected and unaffected areas. Further, since the soil outside the vertical surfaces of sliding move downward, the shear forces must be downward; hence, passive arching occurs, the stress σ_x at any point x within the affected area can be written as

$$\sigma_x = \sigma_o e^{2K \tan \varphi x/B} \quad (8)$$

As defined above σ_x at the surface of the structure is

$$\sigma_x = \sigma_o + \sigma_a \quad (9)$$

Therefore, by equating Eqs. (8) and (9) at $x = Z_1$,

$$\sigma_o + \sigma_a = \sigma_o e^{2K \tan \varphi Z_1/B} \quad (10)$$

* This means that all points on plane AA (Fig. 9) move uniformly, i.e., body motions of the free-field are not of concern.

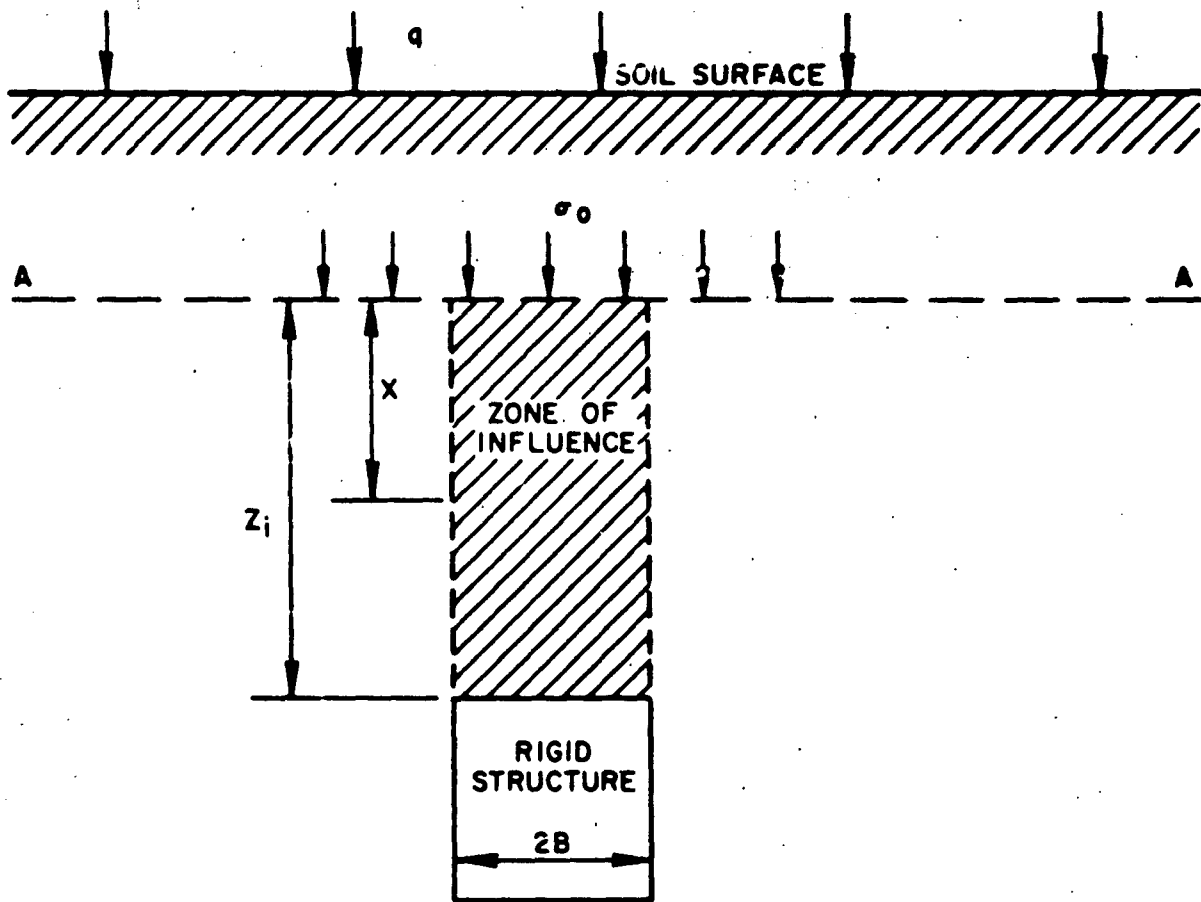


Fig. 9. Zone of Influence Above a Rigid Structure

If we solve Eq. (10) for Z_i ,

$$Z_i = \frac{B}{2K \tan \varphi} \ln \left(\frac{\sigma_o + \sigma_a}{\sigma_o} \right) \quad (11)$$

$$Z_i = \frac{B}{2K \tan \varphi} \ln \left(\frac{\sigma_o + \sigma_a}{\sigma_o} \right) \quad (7)$$

A comparison of Eqs. (7) and (11) shows that the zones of influence above and below the structure are the same and therefore must be the result of differential deformations at the top and bottom of the structure that are identical.

The strain of an incremental layer of soil within the soil element abcd below the structure (Fig. 8) can be written as

$$\epsilon_x = \frac{\sigma_x}{E_{so}} \quad (12)$$

and the total deformation of the entire element can be written as

$$\Delta_x = \int_0^{Z_i} \epsilon_x dx \quad (13)$$

Substituting Eqs. (12) and (2b) in Eq. (13) results in

$$\Delta_x = \int_0^{Z_i} \frac{\sigma_x}{E_{so}} dx = \int_0^{Z_i} \left(\frac{\sigma_o + \sigma_a}{E_{so}} \right) e^{-2K \tan \varphi x/B} dx \quad (14)$$

or

$$\Delta_x = (\sigma_o + \sigma_a) \left(\frac{B}{2E_{so} K \tan \varphi} \right) \left(1 - e^{-2K \tan \varphi Z_i/B} \right) \quad (15)$$

Letting

$$\frac{K \tan \varphi}{B} = S_p$$

and substituting in Eq. (15)

$$\Delta_x = \frac{\sigma_o + \sigma_a}{2E_{so} S_p} \left(1 - e^{-2S_p Z_i} \right) \quad (15a)$$

Substituting S_p in Eq. (11) gives

$$Z_i = \frac{1}{2S_p} \ln \left(\frac{\sigma_o + \sigma_a}{\sigma_o} \right) \quad (11a)$$

or

$$2S_p Z_i = \ln \left(\frac{\sigma_o + \sigma_a}{\sigma_o} \right) \quad (11b)$$

Further, substituting Eq. (11b) into Eq. (15a) gives for the deformation of the soil element abcd

$$\Delta_x = \frac{\sigma_o + \sigma_a}{2E_{so} S_p} \left[1 - e^{-\ln \left(\frac{\sigma_o + \sigma_a}{\sigma_o} \right)} \right] \quad (16)$$

Since the stress below the plane DD in Fig. 10 is σ_o , all points in the plane DD must move uniformly, and therefore it can serve as a reference. By examining the free-field portion of the soil element DDCC, i.e., excluding the element abcd, it can be seen that since it is compressed under an average stress of σ_o (free-field stress), the amount of deformation of the CC plane is to the C'C' position and is represented by

$$\Delta_y = \frac{\sigma_o Z_i}{E_{so}} \quad (17)$$

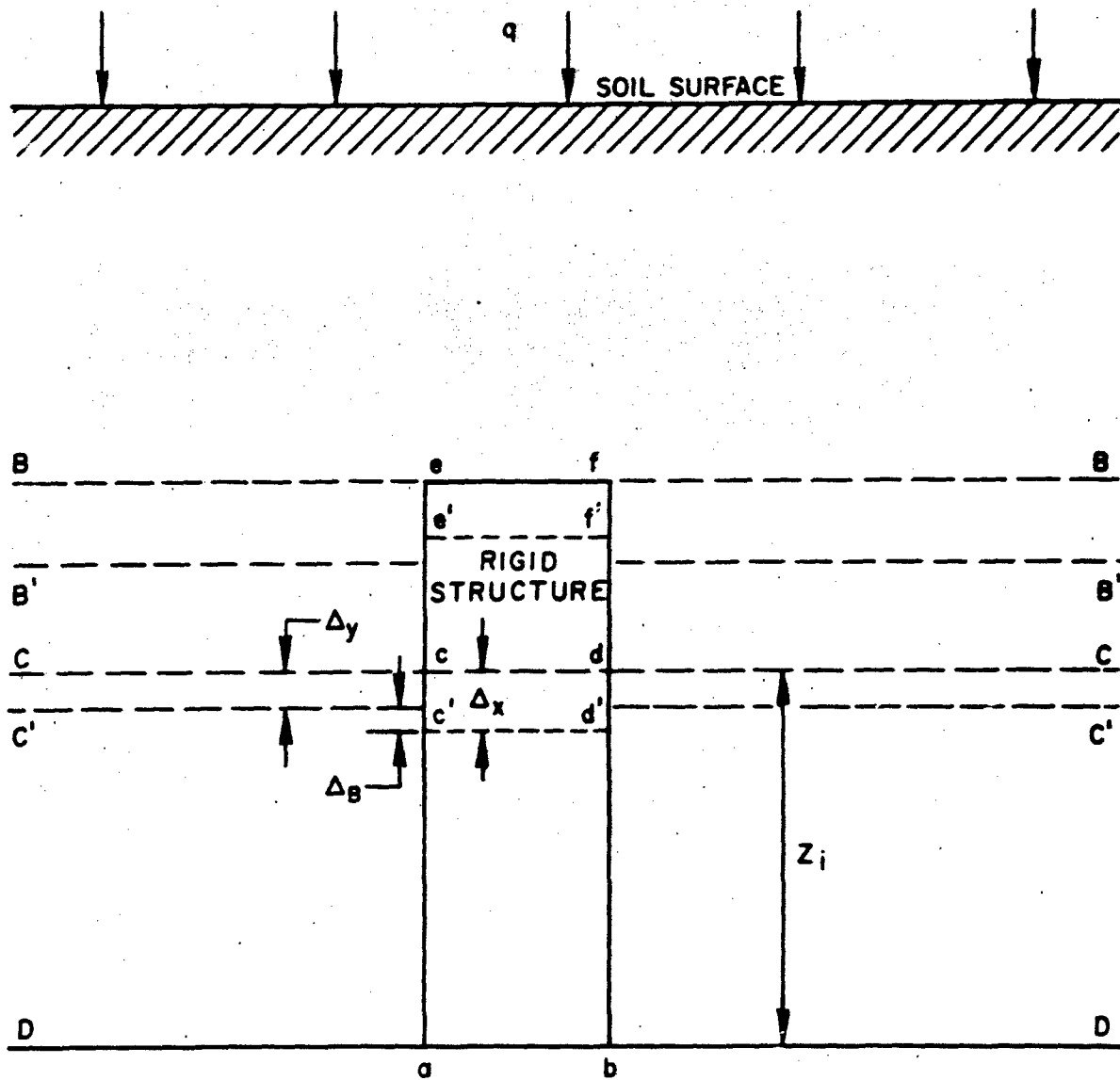


Fig. 10. Relative Deformation Between the Soil and the Structure at the Bottom of the Structure (Passive)

Substituting Eq. (11a) gives

$$\Delta_y = \frac{\sigma_o}{2E_{so} S_p} \ln \left(\frac{\sigma_o + \sigma_a}{\sigma_o} \right) \quad (18)$$

The differential deformation between the two elements C'C'DD and abc'd' is

$$\Delta_B = \Delta_x - \Delta_y \quad (19)$$

Substituting Eqs. (16) and (18) in (19) gives

$$\Delta_B = \left(\frac{\sigma_o + \sigma_a}{2E_{so} S_p} \right) \left[1 - e^{-\ln \left(\frac{\sigma_o + \sigma_a}{\sigma_o} \right)} \right] - \left(\frac{\sigma_o}{2E_{so} S_p} \right) \ln \left(\frac{\sigma_o + \sigma_a}{\sigma_o} \right) \quad (20)$$

and represents the differential motion between the soil directly under the structure and the free-field soil and, hence, the differential motion between the soil adjacent to the structure and that of the structure.

An examination of the soil element represented by BBCC shows that the plane CC is translated to the position of C'C', accounting for a portion of the motion of the plane BB toward the B'B' position. The remaining portion is the result of the compression of the soil in the BBCC element under the free-field stress of σ_o . The amount of motion may be represented by

$$\Delta_{so} = \frac{2L\sigma_o}{E_{so}} \quad [\text{see Eq. (5)}] \quad (21)$$

The mechanism for transferring additional load to the structure has been shown to be the same process as the one for redistributing that load below the structure - namely, shear stresses - developed by differential strain. It has also been shown from a comparison of Eqs. (7) and (11) that the deformations in the soil directly above and below the structure are equal since the zones of influence are equal.

Therefore the sum $2\Delta_B$ must be equal to Δ_{so} in Eq. (21); or

$$\Delta_B = \frac{\Delta_{so}}{2} \quad (22)$$

Or equating one-half of Eq. (21), i.e., Eq. (22), with Eq. (20)

$$\frac{\sigma_o L}{E_{so}} = \frac{\sigma_o + \sigma_a}{2E_{so} S_p} \left[1 - e^{-\ln\left(\frac{\sigma_o + \sigma_a}{\sigma_o}\right)} \right] - \frac{\sigma_o}{2E_{so} S_p} \ln\left(\frac{\sigma_o + \sigma_a}{\sigma_o}\right) \quad (23)$$

Multiplied by $2E_{so} S_p / \sigma_o$, Eq. (23) becomes

$$2S_p L = \frac{\sigma_o + \sigma_a}{\sigma_o} \left[1 - e^{-\ln\left(\frac{\sigma_o + \sigma_a}{\sigma_o}\right)} \right] - \ln\left(\frac{\sigma_o + \sigma_a}{\sigma_o}\right) \quad (24)$$

Let $2S_p L = N$ and

$$\frac{\sigma_o + \sigma_a}{\sigma_o} = Y$$

Then Eq. (24) becomes

$$NL = Y - Ye^{-\ln Y} - \ln Y \quad (25)$$

Since

$$e^{-\ln Y} = \frac{1}{Y}$$

Eq. (25) becomes

$$NL = Y - \frac{Y}{Y} - \ln Y \quad (25a)$$

or

$$NL = Y - 1 - \ln Y \quad (26)$$

xpanded into the original terms, this becomes

$$2K \tan \phi \frac{L}{B} = \frac{\sigma_o + \sigma_a}{\sigma_o} - \ln \left(\frac{\sigma_o + \sigma_a}{\sigma_o} \right) - 1 \quad (27)$$

Figure 11 is a plot computed from the relationship between $(\sigma_o + \sigma_a)/\sigma_o$, i.e., the overstress Y and $2K \tan \phi L/B$, i.e., NL, expressed in Eq. (27). Figure 12 is a plot of the relationship between overstress (relative stress) Y and the length-to-span ratio, L/B, for a range of $2K \tan \phi$, (NB), values.

EFFECTS OF STRUCTURAL COMPRESSIBILITY

Passive Arching Case

Since most soil structures are not rigid, but have some gross compressibility, this parameter must be incorporated into any theory to predict the load on the structure. An examination of Fig. 10 shows that any compressibility in the structure will tend to reduce the differential deformation between the soil and the structure. The deformation of the structure is dependent upon the load, the length, and the effective modulus of the structure, which are related by the following equation:

$$\Delta_{ST} = \frac{\sigma_o + \sigma_a}{E_{ST}} (2L) \quad (28)$$

where

Δ_{ST} = deformation of the structure

σ_o = free-field stress

σ_a = arching stress

$\sigma_o + \sigma_a$ = total average stress on the structure

L = 1/2 the length of the structure

E_{ST} = effective modulus of the structure

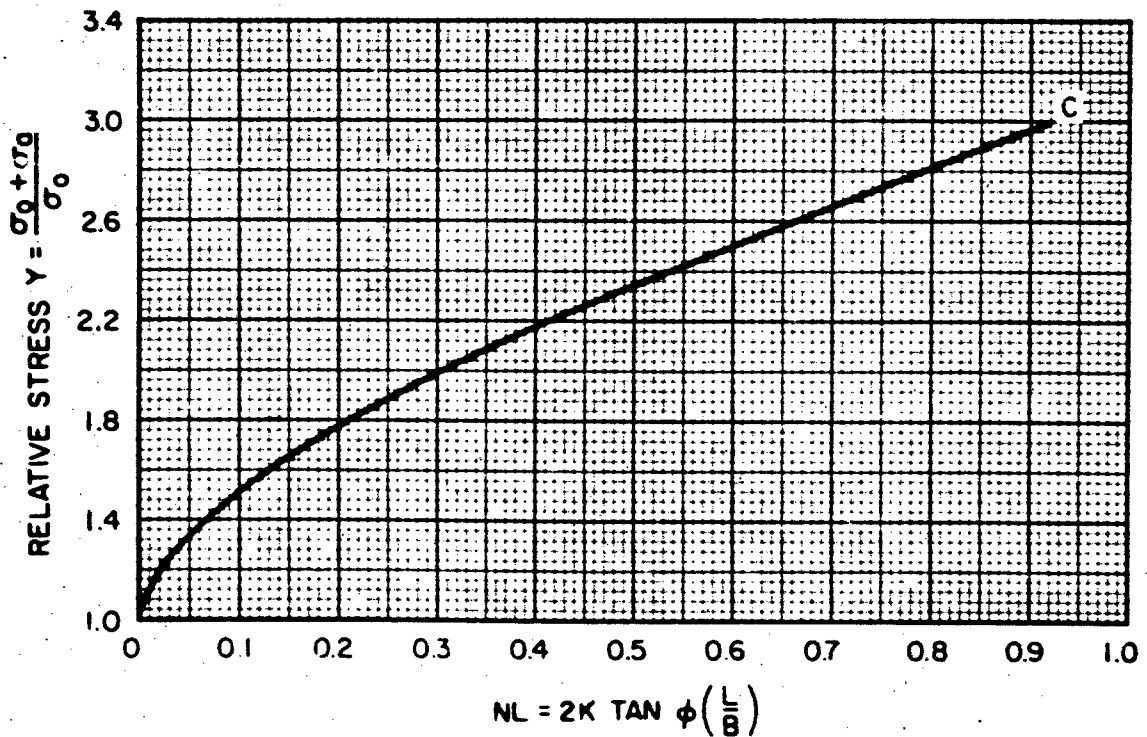
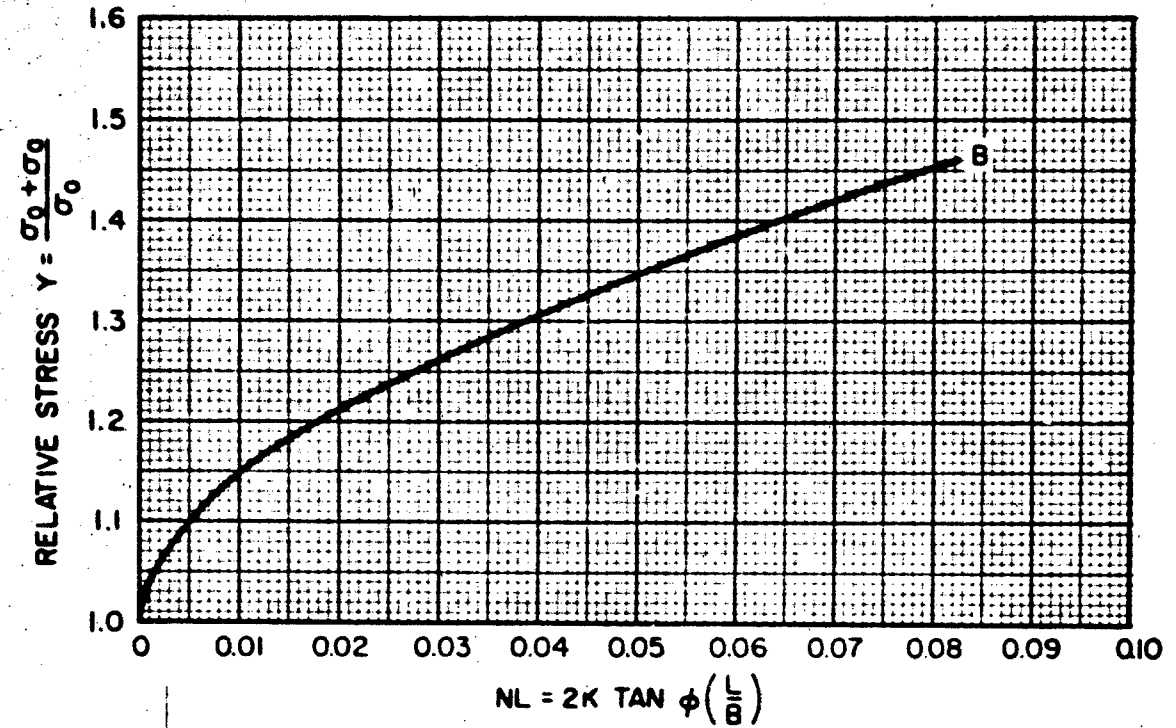


Fig. 11. Relationships Between NL and Y [Eq. (27)]

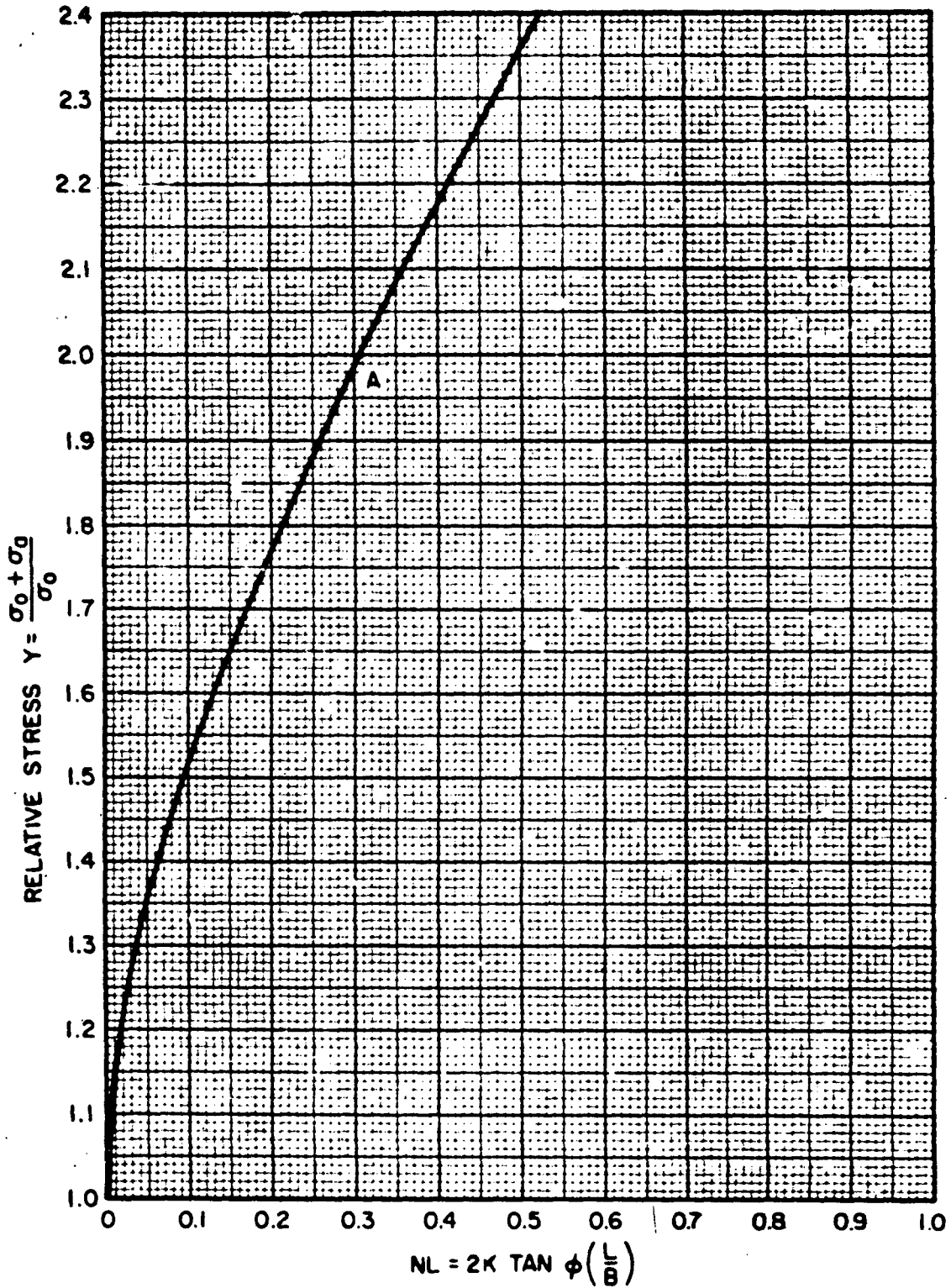


Fig. 11 (Cont.)

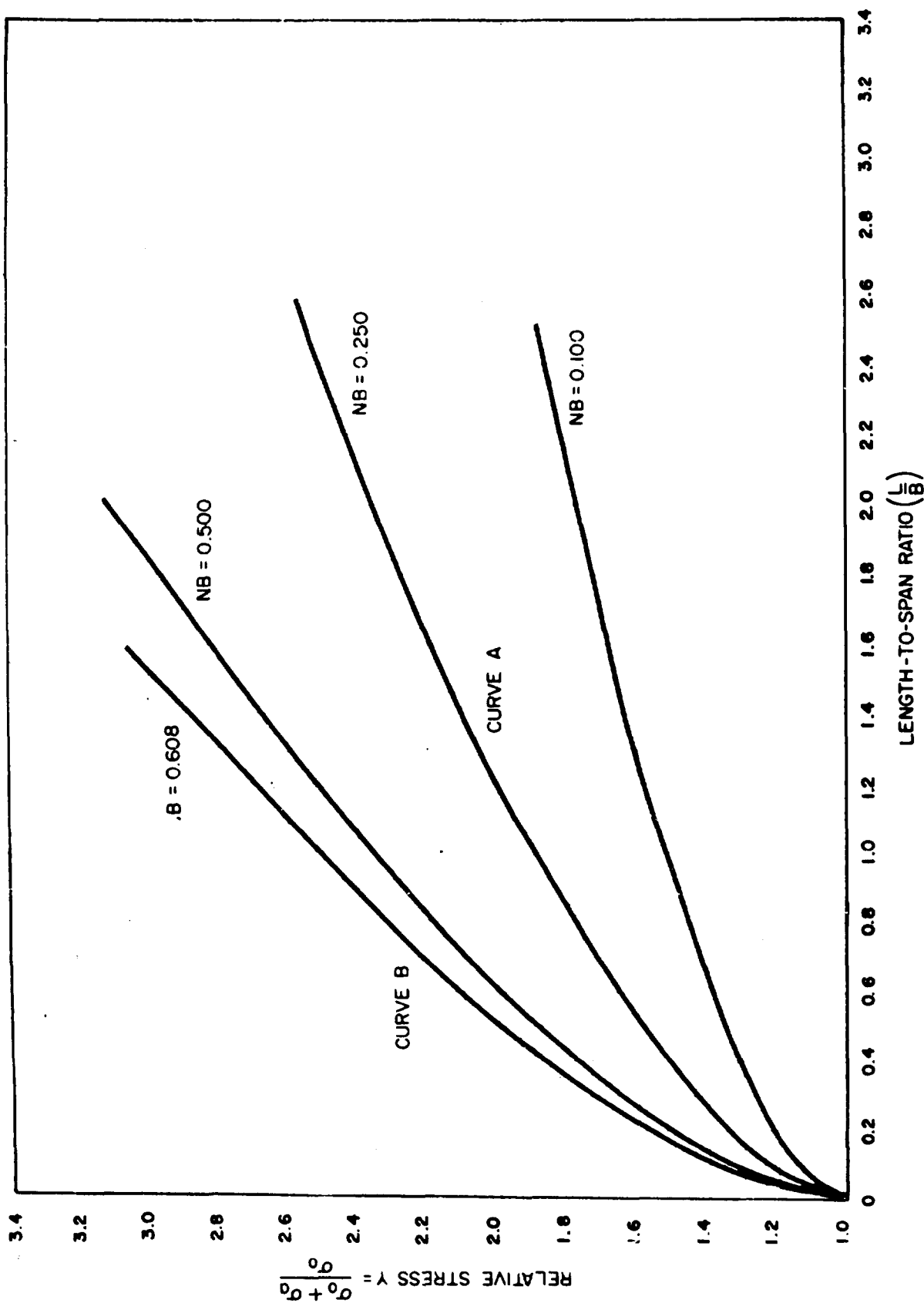


Fig. 12. Relationship Between Relative Stress (Y) and Length-to-Span Ratio (L/B) for A Range of NB Values for the Passive Case (Linear Soil Conditions)

As stated earlier for the rigid case, the maximum total deformation available is represented by Eq. (21), i.e., the shortening of the soil laterally adjacent to the structure. Therefore subtracting Eq. (28) from Eq. (21) gives

$$L_{to} = \frac{2L\sigma_o}{E_{so}} - \frac{2L}{E_{ST}} (\sigma_o + \sigma_a) \quad (29)$$

Further equating one-half of Eq. (29) with Eq. (20) yields

$$\frac{\sigma_o L}{E_{so}} - \frac{\sigma_o + \sigma_a}{E_{ST}} (L) = \frac{\sigma_o + \sigma_a}{2E_{so p}} \left[1 - e^{-\ln\left(\frac{\sigma_o + \sigma_a}{\sigma_o}\right)} \right] - \frac{\sigma_o}{2E_{so p}} \ln\left(\frac{\sigma_o + \sigma_a}{\sigma_o}\right) \quad (30)$$

Multiplied by $2E_{so p} \sigma_o$, Eq. (30) becomes

$$2S_p L - \left(\frac{\sigma_o + \sigma_a}{\sigma_o}\right) \left(\frac{E_{so}}{E_{ST}}\right) (L) (2S_p) = \frac{\sigma_o + \sigma_a}{\sigma_o} \left[1 - e^{-\ln\left(\frac{\sigma_o + \sigma_a}{\sigma_o}\right)} \right] - \ln\left(\frac{\sigma_o + \sigma_a}{\sigma_o}\right) \quad (31)$$

Let

$$2S_p = N \qquad \frac{E_{so}}{E_{ST}} = C_r$$

and

$$\frac{\sigma_o + \sigma_a}{\sigma_o} = Y$$

Eq. (31) then becomes

$$NL - YC_r NL = Y \left(1 - e^{-\ln Y} \right) - \ln Y \quad (32)$$

Since

$$e^{-\ln Y} = \frac{1}{Y}$$

Eq. (32) becomes

$$NL - Y C_r NL = Y \left(1 - \frac{1}{Y} \right) - \ln Y \quad (33)$$

or

$$-Y C_r NL = Y - 1 - \ln Y - NL \quad (33a)$$

or

$$C_r = \frac{1 - Y + \ln Y + NL}{NLY} \quad (34)$$

Expanded into the original terms this becomes

$$C_r = \frac{1 - \frac{\sigma_o + \sigma_a}{\sigma_o} + \ln \left(\frac{\sigma_o + \sigma_a}{\sigma_o} \right) + \frac{2K \tan \epsilon L}{B}}{\frac{2K \tan \epsilon L}{B} \left(\frac{\sigma_o + \sigma_a}{\sigma_o} \right)} \quad (35)$$

Figure 13 is a plot computed for four different NL values from the relationships between C_r (relative compressibility), i.e., E_{so}/E_{ST} , and Y (relative stress), i.e., $(\sigma_o + \sigma_a)/\sigma_o$, expressed in Eq. (35).

Active Arching Case

Equation (35) was developed for a compressible structure exhibiting passive arching, i.e., for a structure stiffer than the soil in which it was embedded.

Since it is possible and even desirable to design structure, which exhibit active arching, a similar analysis is made for these conditions. An examination of Fig. 14 shows that when the compressibility of the structure exceeds that of the soil, the differential strain will be in the opposite direction.

As in the previous case, the deformation of the structure is dependent upon the load and the length and effective modulus of the structure, which are related by the following equation:

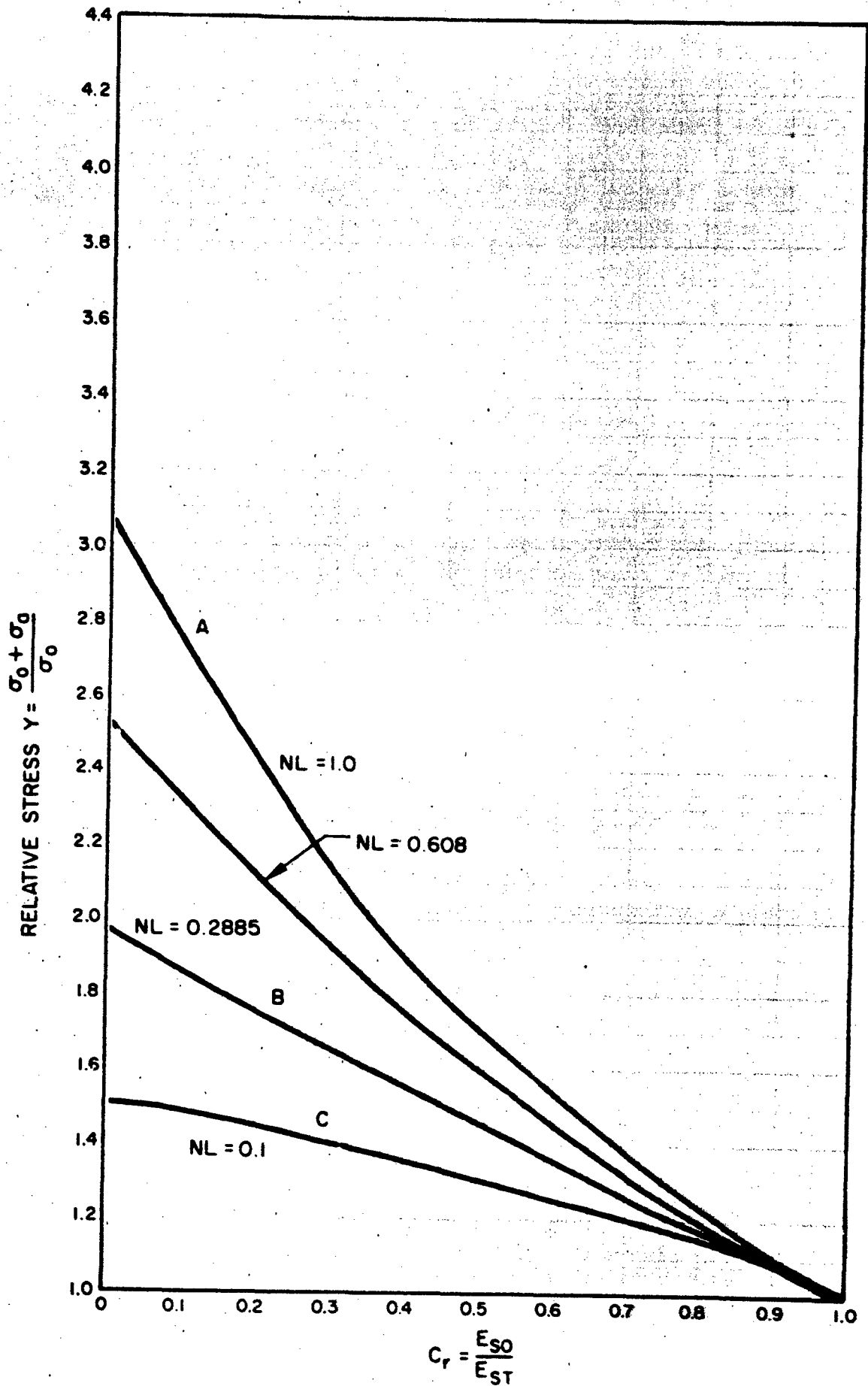


Fig. 13. Relationship Between C_r and Y [Eq. (35)] for Various NL Values for the Passive Case (Linear Soil Conditions)

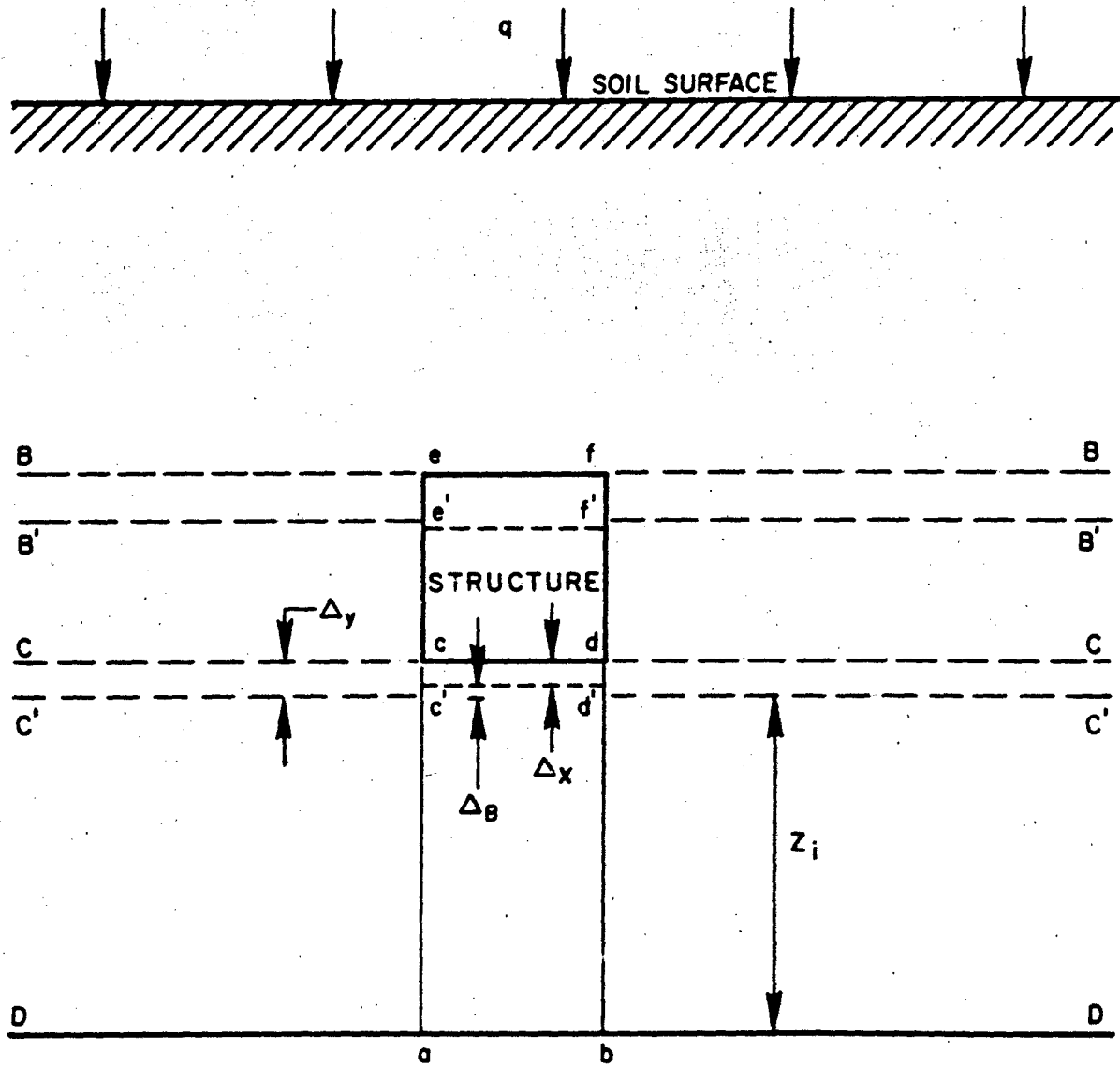


Fig. 14. Relative Deformation Between the Soil and the Structure at the Bottom of the Structure (Active Case)

$$\Delta_{ST} = \frac{(\sigma_o - \sigma_a)}{E_{ST}} (2L) \quad (36)$$

where

Δ_{ST} = deformation of the structure

σ_o = free field stress

σ_a = arching stress

$\sigma_o - \sigma_a$ = total average stress
on the structure

L = one-half the length of the structure

E_{ST} = effective modulus of the structure

From Fig. 1-1 it can be shown that the maximum total differential deformation, Δ_{to} , available is the difference between the deformation of the structure and that of the soil over a length equivalent to $2L$.

Therefore:

$$\Delta_{to} = \Delta_{ST} - \Delta_{so} \quad (37)$$

where

Δ_{so} = the deformation of the soil column laterally adjacent to the structure $2L$ in length

therefore

$$\Delta_{so} = \frac{\sigma_o 2L}{E_{so}} \quad [\text{see Eq. (5)}] \quad (38)$$

where

E_{so} = soil modulus (assumed to be linear)

substituting Eqs. (36) and (38) in Eq. (37)

$$\Delta_{to} = (\sigma_o - \sigma_a) \frac{2L}{E_{ST}} - \frac{\sigma_o 2L}{E_{so}} \quad (39)$$

If we assume that half of this takes place at each end,* the differential deformation, Δ_{to} , to cause arching is one half of Eq. (39), i.e.,

$$\Delta_{to} = \frac{(\sigma_o - \sigma_a)}{E_{ST}} (L) - \frac{\sigma_o L}{E_{so}} \quad (40)$$

The differential deformation below the structure can be seen to be the difference between Δ_x and Δ_y in Fig. 14. The strain at any point within the soil column below the structure is related to the stress within the soil column at that point, σ_x , and the modulus of the soil, E_{so} , in the following manner:

$$\epsilon_x = \frac{\sigma_x}{E_{so}} \quad (41)$$

If it is assumed that at some depth Z_i below the structure there is no influence from the structure, the total deformation Δ_x of that column of soil can be expressed as

$$\Delta_x = \int_0^{Z_i} \epsilon_x dx = \int_0^{Z_i} \frac{\sigma_x}{E_{so}} dx \quad (42)$$

If the stress applied by the structure to the soil is $(\sigma_o - \sigma_a)$, and the stress becomes σ_o again at some depth Z_i below the structure, then the soil mass must have gained additional load σ_a from shear stresses along the vertical shear planes. This behavior is expressed by the equation (of the general form shown in Eq. (4a)

$$\sigma_x = (\sigma_o - \sigma_a) e^{+2K \tan \phi x/B} \quad (43)$$

* A discussion of this assumption is presented in Section 4, p. 22.

substituting in Eq. (42)

$$\Delta_x = \int_0^{Z_i} \frac{(\sigma_o - \sigma_a)}{E_{so}} e^{+2K \tan \varphi x/B} dx \quad (44)$$

or

$$= \frac{(\sigma_o - \sigma_a) B}{(2K \tan \varphi) E_{so}} e^{+2K \tan \varphi Z_i/B} - \frac{(\sigma_o - \sigma_a) B}{(2K \tan \varphi) E_{so}} \quad (45)$$

$$= \frac{(\sigma_o - \sigma_a) B}{(2K \tan \varphi) E_{so}} \left(e^{+2K \tan \varphi Z_i/B} - 1 \right) \quad (46)$$

If the soil laterally adjacent to the soil column analyzed above is assumed to be subject to the free-field stress, then:

$$\Delta_y = \frac{\sigma_o Z_i}{E_{so}} \quad (47)$$

As stated above, the stress σ_x in the soil column below the structure is equal to the free-field stress, σ_o , at Z_i . Therefore, Eq. (43) can be written:

$$\sigma_x = \sigma_o = (\sigma_o - \sigma_a) e^{2K \tan \varphi Z_i/B} \quad (48)$$

solving for Z_i

$$\frac{2K \tan \varphi Z_i}{B} = \ln \left(\frac{\sigma_o}{\sigma_o - \sigma_a} \right)$$

or

$$Z_i = \frac{B}{2K \tan \varphi} \ln \left(\frac{\sigma_o}{\sigma_o - \sigma_a} \right) \quad (49)$$

substituting in Eq. (47)

$$\Delta_y = \frac{\sigma_o}{E_{so}} \left[\frac{B}{2K \tan \phi} \ln \left(\frac{\sigma_o}{\sigma_o - \sigma_a} \right) \right] \quad (50)$$

Since the differential deformation below the structure Δ_B is equal to the difference between Δ_y and Δ_x , i.e.,

$$\Delta_B = \Delta_y - \Delta_x \quad (51)$$

substituting Eqs. (46) and (50) in (51)

$$\Delta_B = \frac{\sigma_o}{E_{so}} \left[\frac{B}{2K \tan \phi} \ln \left(\frac{\sigma_o}{\sigma_o - \sigma_a} \right) \right] - \frac{(\sigma_o - \sigma_a) B}{2K \tan \phi E_{so}} \left(e^{+2K \tan \phi Z_1/B} - 1 \right) \quad (52)$$

substituting Eq. (49) for Z_1 in Eq. (52) gives

$$\Delta_B = \frac{\sigma_o B}{2K \tan \phi E_{so}} \left[\ln \left(\frac{\sigma_o}{\sigma_o - \sigma_a} \right) \right] - \frac{(\sigma_o - \sigma_a) B}{2K \tan \phi E_{so}} \left[e^{+\ln \left(\frac{\sigma_o}{\sigma_o - \sigma_a} \right)} - 1 \right] \quad (53)$$

Since it was assumed that Δ_B was equal to Δ_{to} , or that the total differential deformation available was divided equally at the top and bottom of the structure,* Eqs. (40) and (53) can be equated.

$$\frac{(\sigma_o - \sigma_a)}{E_{ST}} L - \frac{\sigma_o L}{E_{so}} = \frac{\sigma_o B}{2K \tan \phi E_{so}} \left[\ln \left(\frac{\sigma_o}{\sigma_o - \sigma_a} \right) \right] - \frac{(\sigma_o - \sigma_a) B}{2K \tan \phi E_{so}} \left[e^{+\ln \left(\frac{\sigma_o}{\sigma_o - \sigma_a} \right)} - 1 \right] \quad ($$

Let

$$\frac{2K \tan \phi}{B} = N$$

* This assumption was discussed in Section 4, p. 22 for the case where there was no sidewall friction along the side of the structure.

therefore

$$\frac{(\sigma_o - \sigma_a)}{E_{ST}} L - \frac{\sigma_o L}{E_{SO}} = \frac{\sigma_o}{NE_{SO}} \left[\ln \left(\frac{\sigma_o}{\sigma_o - \sigma_a} \right) \right] - \frac{\sigma_o - \sigma_a}{NE_{SO}} \left[e^{\ln \left(\frac{\sigma_o}{\sigma_o - \sigma_a} \right)} - 1 \right] \quad (55)$$

or

$$\frac{(\sigma_o - \sigma_a)}{E_{ST}} L - \frac{\sigma_o L}{E_{SO}} = \frac{\sigma_o}{NE_{SO}} \left\{ \ln \left(\frac{\sigma_o}{\sigma_o - \sigma_a} \right) - \left(\frac{\sigma_o - \sigma_a}{\sigma_o} \right) \left(e^{\ln \left(\frac{\sigma_o}{\sigma_o - \sigma_a} \right)} - 1 \right) \right\} \quad (56)$$

Multiplied by $\frac{E_{SO}}{L\sigma_o}$

$$\frac{(\sigma_o - \sigma_a)}{\sigma_o} \frac{E_{SO}}{E_{ST}} - 1 = \frac{1}{NL} \left[\ln \left(\frac{\sigma_o}{\sigma_o - \sigma_a} \right) - \left(\frac{\sigma_o - \sigma_a}{\sigma_o} \right) \left(e^{\ln \left(\frac{\sigma_o}{\sigma_o - \sigma_a} \right)} - 1 \right) \right] \quad (57)$$

letting $\frac{E_{SO}}{E_{ST}} = C_r$ and $\left(\frac{\sigma_o}{\sigma_o - \sigma_a} \right) = Y'$

$$\frac{C_r}{Y'} - 1 = \frac{1}{NL} \left[\ln Y' - \frac{1}{Y'} \left(e^{\ln Y'} - 1 \right) \right] \quad (58)$$

$$C_r = \frac{Y'}{NL} \left[\ln Y' - \frac{e^{\ln Y'} - 1}{Y'} + \frac{1}{Y'} \right] + Y' \quad (59)$$

Since $e^{\ln Y'} = Y'$, Eq. (59) becomes

$$C_r = \frac{Y'}{NL} \left[\ln Y' - 1 + \frac{1}{Y'} \right] + Y' \quad (60)$$

Expanding into the original terms, Eq. (60) becomes

$$C_r = \left(\frac{\sigma_o}{\sigma_o - \sigma_a} \right) \left(\frac{B}{2K \tan \phi L} \right) \left[\ln \left(\frac{\sigma_o}{\sigma_o - \sigma_a} \right) - 1 + \left(\frac{\sigma_o - \sigma_a}{\sigma_o} \right) \right] + \left(\frac{\sigma_o}{\sigma_o - \sigma_a} \right) \quad (61)$$

Figure 15 is a plot of C_r , the ratio of soil and structural compressibilities, vs $\frac{1}{Y'}$, relative stress (understress), for the range of NL values in the active arching case.

Comparison of Active and Passive Cases

In order to compare the active and passive cases, Eq. (34) for the passive case can be put in terms of Y' .

$$C_r = \frac{1}{NLY} \left[1 - Y + \ln Y \right] + \frac{1}{Y} \quad (34)$$

Since $Y = \frac{1}{Y'}$, Eq. (34) becomes

$$C_r = \frac{Y'}{NL} \left[1 - \frac{1}{Y'} + \ln \frac{1}{Y'} \right] + Y' \quad (34a)$$

This compares with Eq. (60) for the active case:

$$C_r = \frac{Y'}{NL} \left[\ln Y' - 1 + \frac{1}{Y'} \right] + Y' \quad (60)$$

The two equations are plotted in Fig. 16 for $NL = 0.608$, showing they are a smooth continuous function.

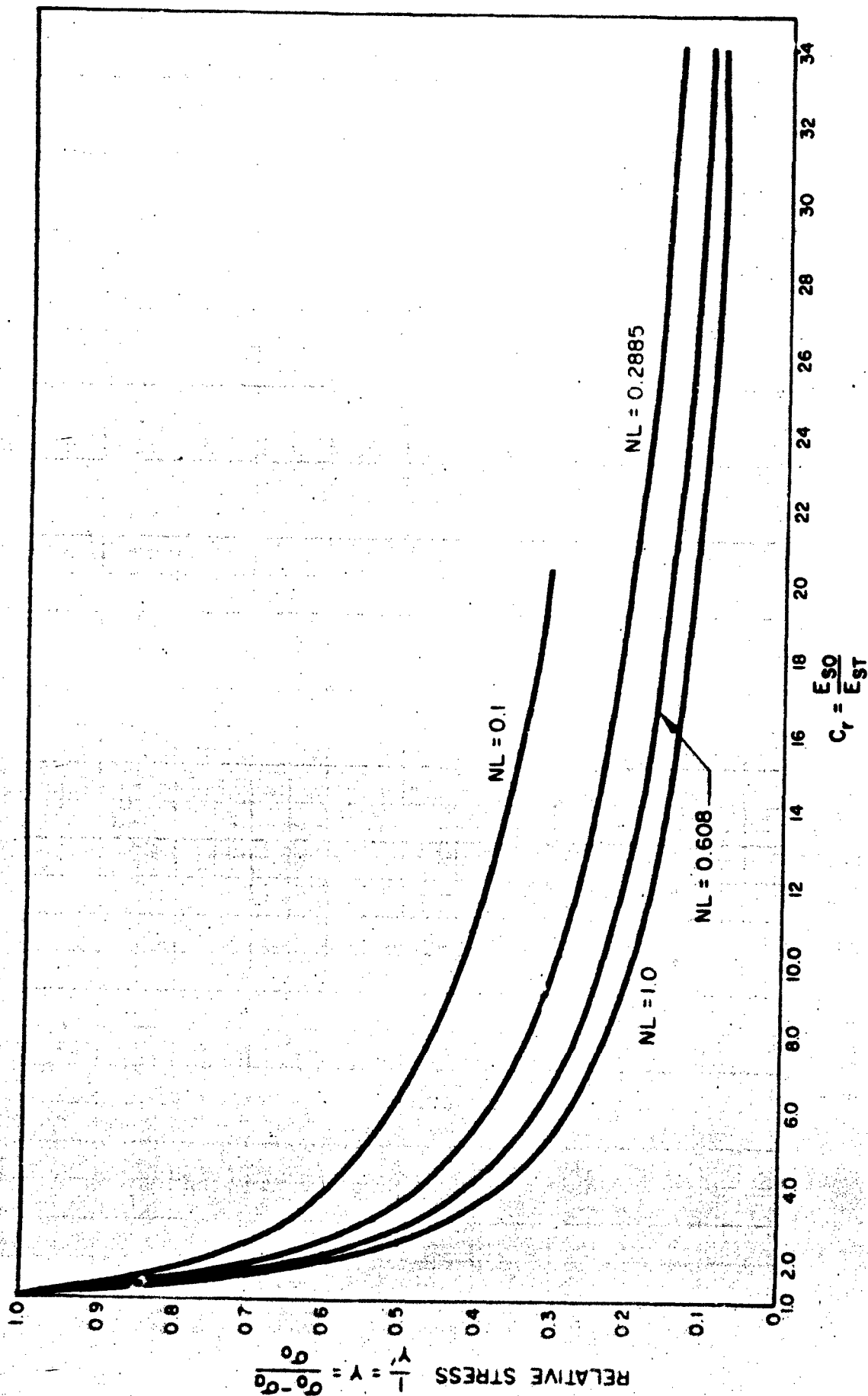
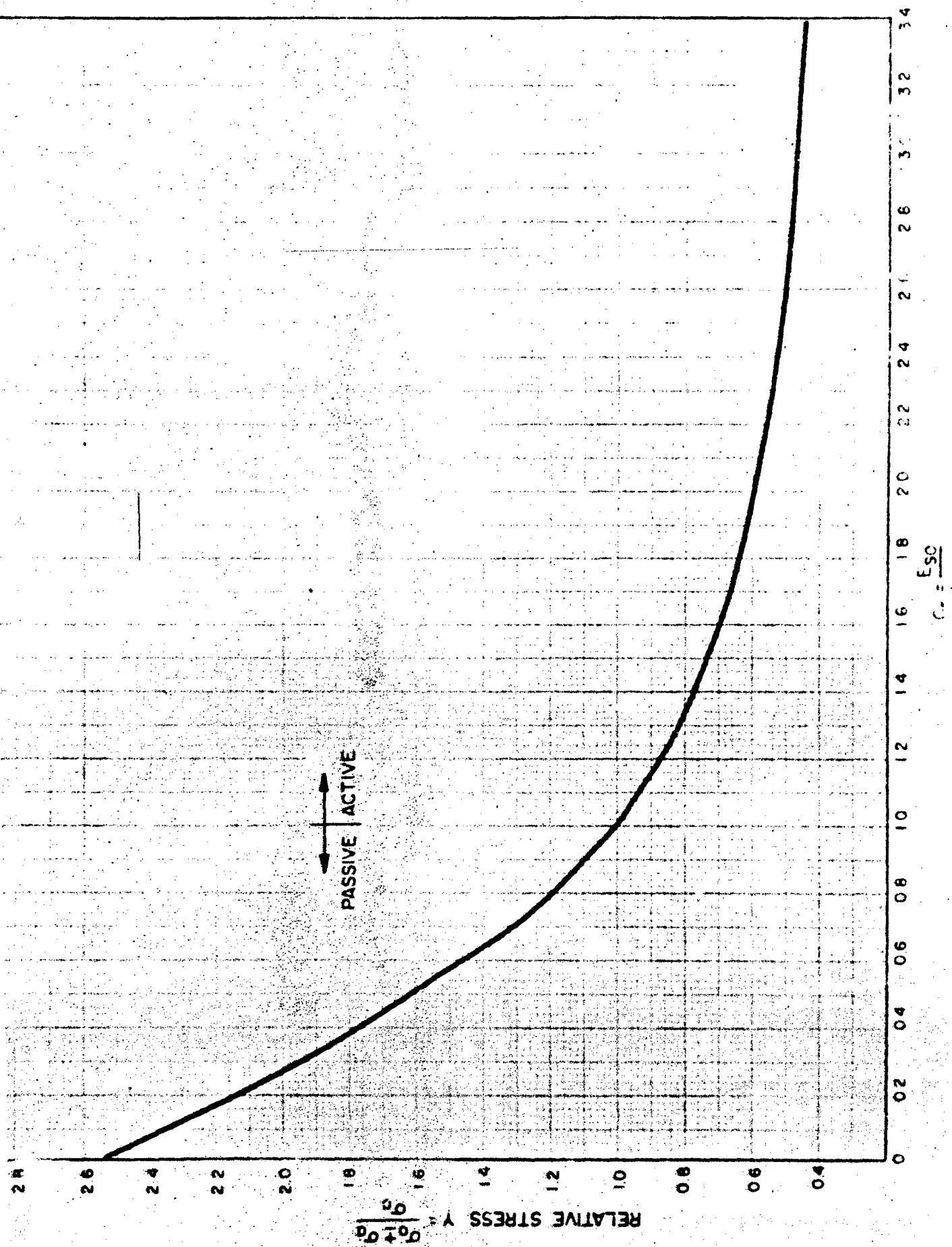


Fig. 15. Relationship Between C_r and $1/Y'$ [Eq. (60)] for Various NL Values for the Active Case (Linear Soil Conditions)



Section 5
EFFECTS OF NONLINEAR SOIL CONDITIONS

Since very few soils really exhibit linear stress-strain relationships, it is necessary to try and simulate the nonlinearity in order to develop reasonable prediction methods.

This section is devoted to investigating the influence nonlinear behavior, such as expressed by the following stress-strain relationship, will have on the basic responses discussed in the earlier sections.

$$\sigma_o = A\epsilon^{3/2} \quad (62)$$

EFFECTS ON STRUCTURAL LENGTH

To evaluate the effect of the interrelationships between the nonlinear soil conditions and structural length, it is convenient to redevelop Eq. (26). In order to do so, one must start with Eq. (15). Substituting Eq. (62) for Eq. (12) in Eq. (15) in Section 4, Eq. (15) then becomes

$$\Delta_x = \left(\frac{\sigma_o + \sigma_a}{A} \right)^{2/3} \left(\frac{B}{2K \tan \phi} \right) \left(1 - e^{-2K \tan \phi Z_1/B} \right) \quad (63)$$

continuing with the substitution Eq. (16) becomes:

$$\Delta_x = \left(\frac{\sigma_o + \sigma_a}{A} \right)^{2/3} \frac{1}{2S_p} \left[1 - e^{-\ln \left(\frac{\sigma_o + \sigma_a}{\sigma_o} \right)} \right] \quad (64)$$

carrying out the analysis and substitution, Δ_y in Eq. (18) becomes

$$\Delta_y = \left(\frac{\sigma_o}{A} \right)^{2/3} \left(\frac{1}{2S_p} \right) \left[\ln \left(\frac{\sigma_o + \sigma_a}{\sigma_o} \right) \right] \quad (65)$$

Subtracting Eq. (65) from Eq. (64) results in a new equation equivalent to Eq. (20):

$$\Delta_B = \left(\frac{\sigma_o + \sigma_a}{A}\right)^{2/3} \left(\frac{1}{2S_p}\right) \left[1 - e^{-\ln\left(\frac{\sigma_o + \sigma_a}{\sigma_o}\right)} \right] - \left(\frac{\sigma_o}{A}\right)^{2/3} \left(\frac{1}{2S_p}\right) \left[\ln\left(\frac{\sigma_o + \sigma_a}{\sigma_o}\right) \right] \quad (66)$$

By substituting Eq. (62) in Eq. (21), it becomes

$$\Delta_{so} = 2L \left(\frac{\sigma_o}{A}\right)^{2/3} \quad (67)$$

Combining Eq. (66) and one-half Δ_{so} of Eq. (67), as indicated in Eq. (22),

$$\left(\frac{\sigma_o}{A}\right)^{2/3} L = \left(\frac{\sigma_o + \sigma_a}{A}\right)^{2/3} \left(\frac{1}{2S_p}\right) \left[1 - e^{-\ln\left(\frac{\sigma_o + \sigma_a}{\sigma_o}\right)} \right] - \left(\frac{\sigma_o}{A}\right)^{2/3} \left(\frac{1}{2S_p}\right) \left[\ln\left(\frac{\sigma_o + \sigma_a}{\sigma_o}\right) \right] \quad (68)$$

Simplifying in the manner used to arrive at Eq. (26), Eq. (68) becomes

$$NL = Y^{2/3} - \frac{1}{Y^{1/3}} - \ln Y \quad (69)$$

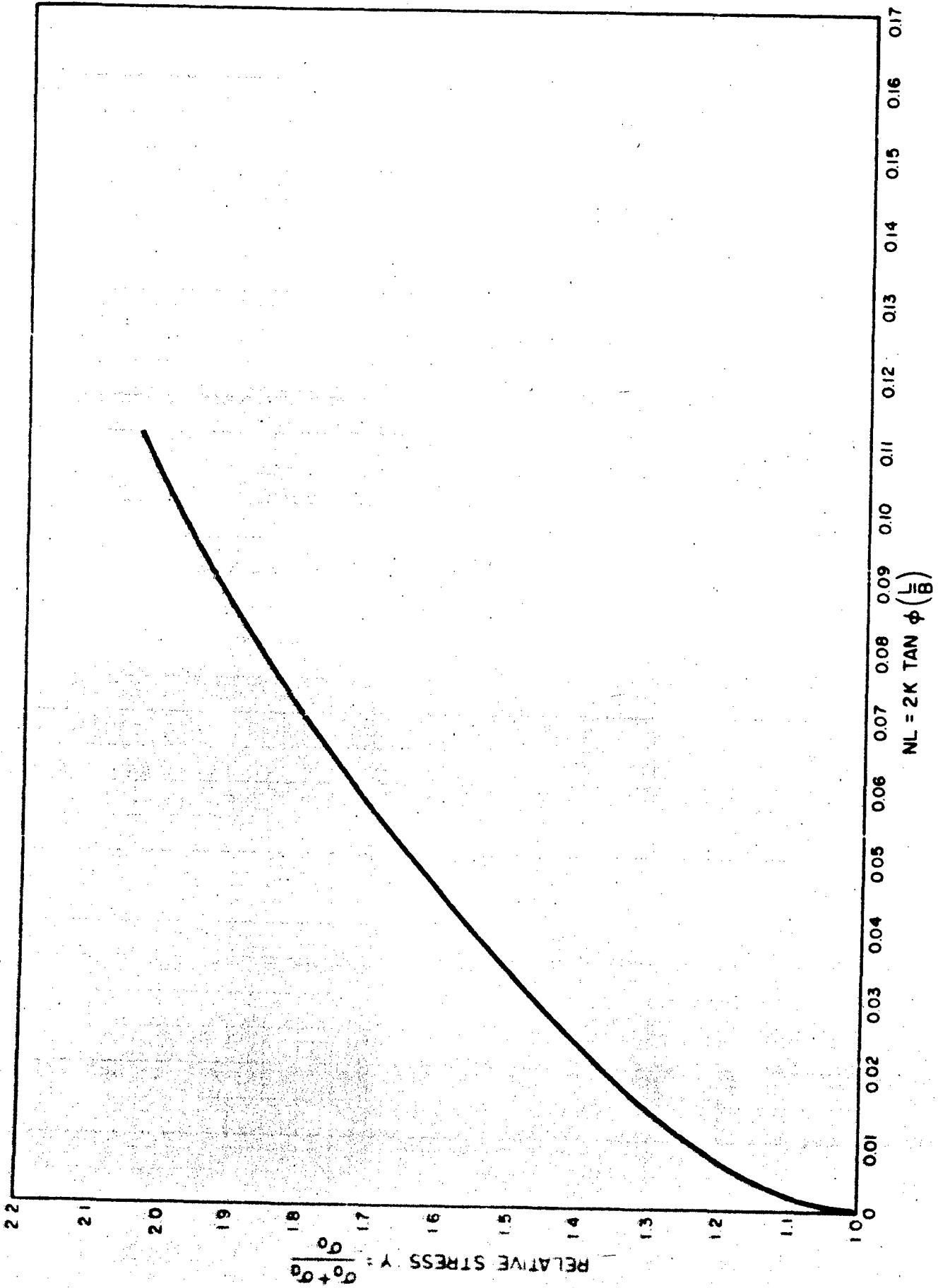
or expanding into original terms, this becomes

$$2K \tan \phi \left(\frac{L}{B}\right) = \left(\frac{\sigma_o + \sigma_a}{\sigma_o}\right)^{2/3} - \ln\left(\frac{\sigma_o + \sigma_a}{\sigma_o}\right) - \frac{1}{\left(\frac{\sigma_o + \sigma_a}{\sigma_o}\right)^{1/3}} \quad (70)$$

Figure 17 is a plot computed from the relationships between $2K \tan \phi L/B$ (i.e., NL) and $(\sigma_o + \sigma_a)/\sigma_o$ (i.e., Y) expressed in Eqs. (69) and (70).

Figure 18 is a plot of the relationship between overstress, Y , and the length-to-span ratio for a range of $2K \tan \phi$ (i.e., NB) values.

Figure 19 shows the comparison of the linear and nonlinear cases for a constant NB .



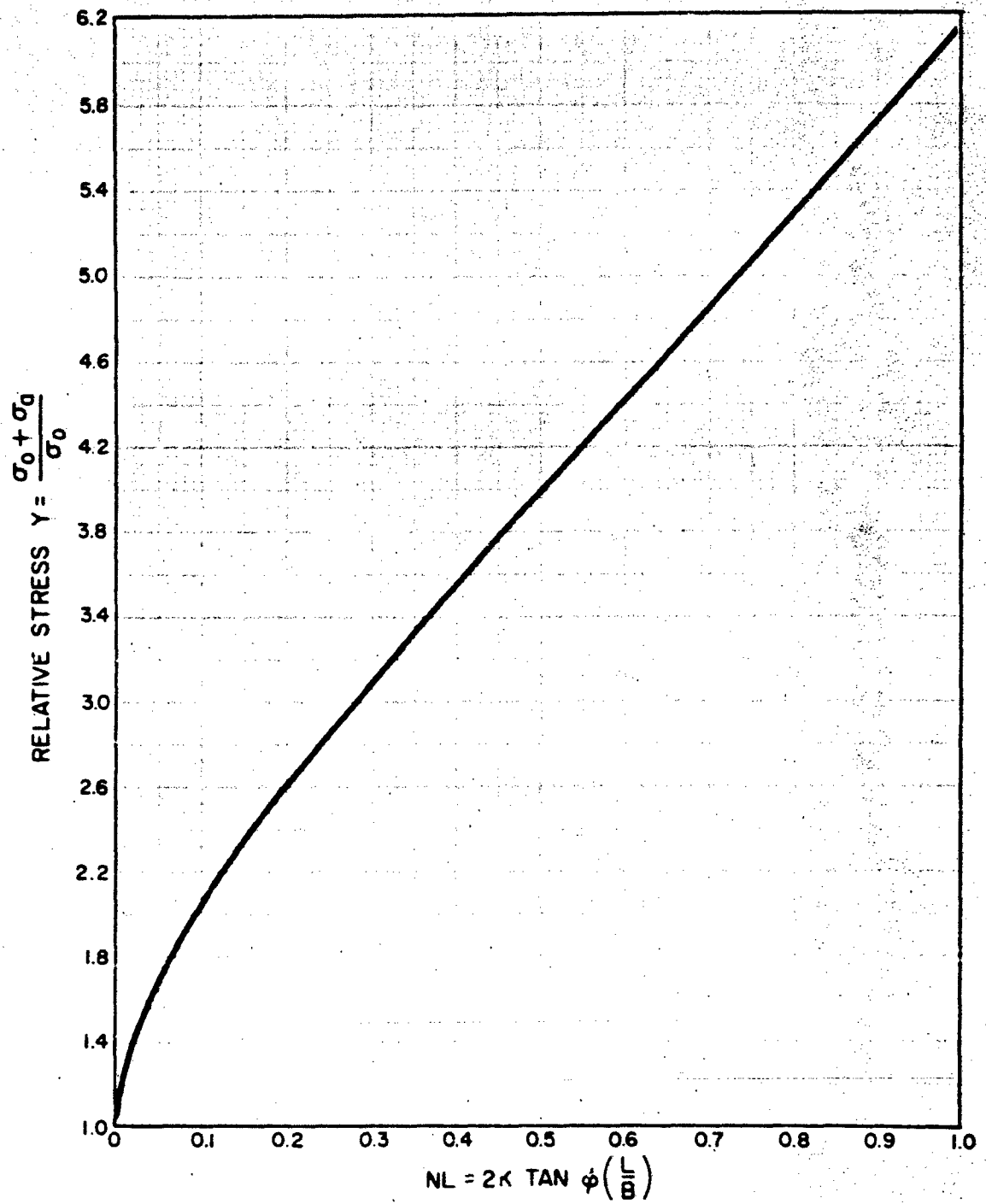


Fig. 17 (Cont.)

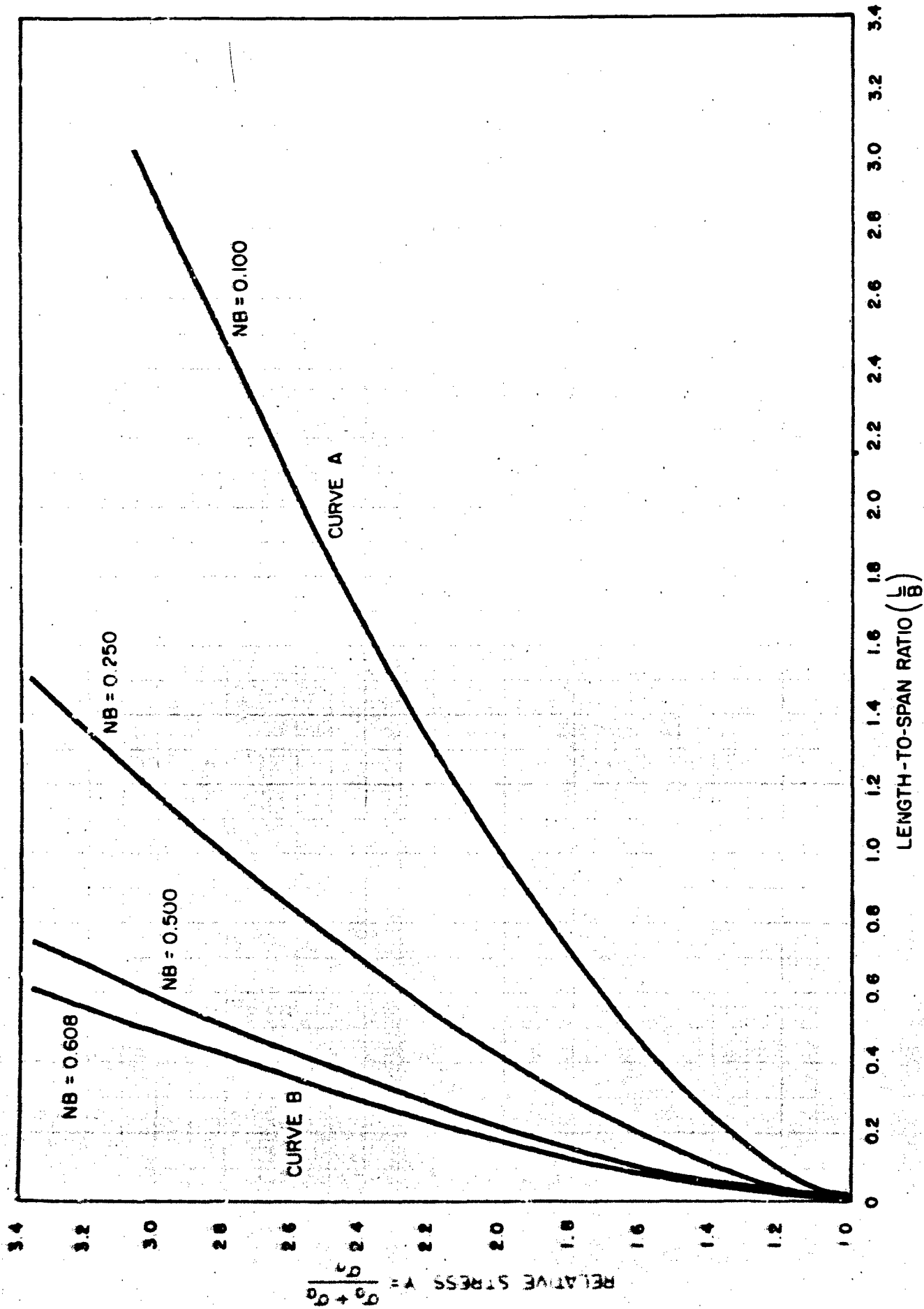


FIG. 18. Relationship Between Overstress (Y) and Length-to-Span Ratio (L/B) for Different NB Values for the Passive Case ($\sigma = A_p^{3/2}$ Nonlinear Soil Conditions)

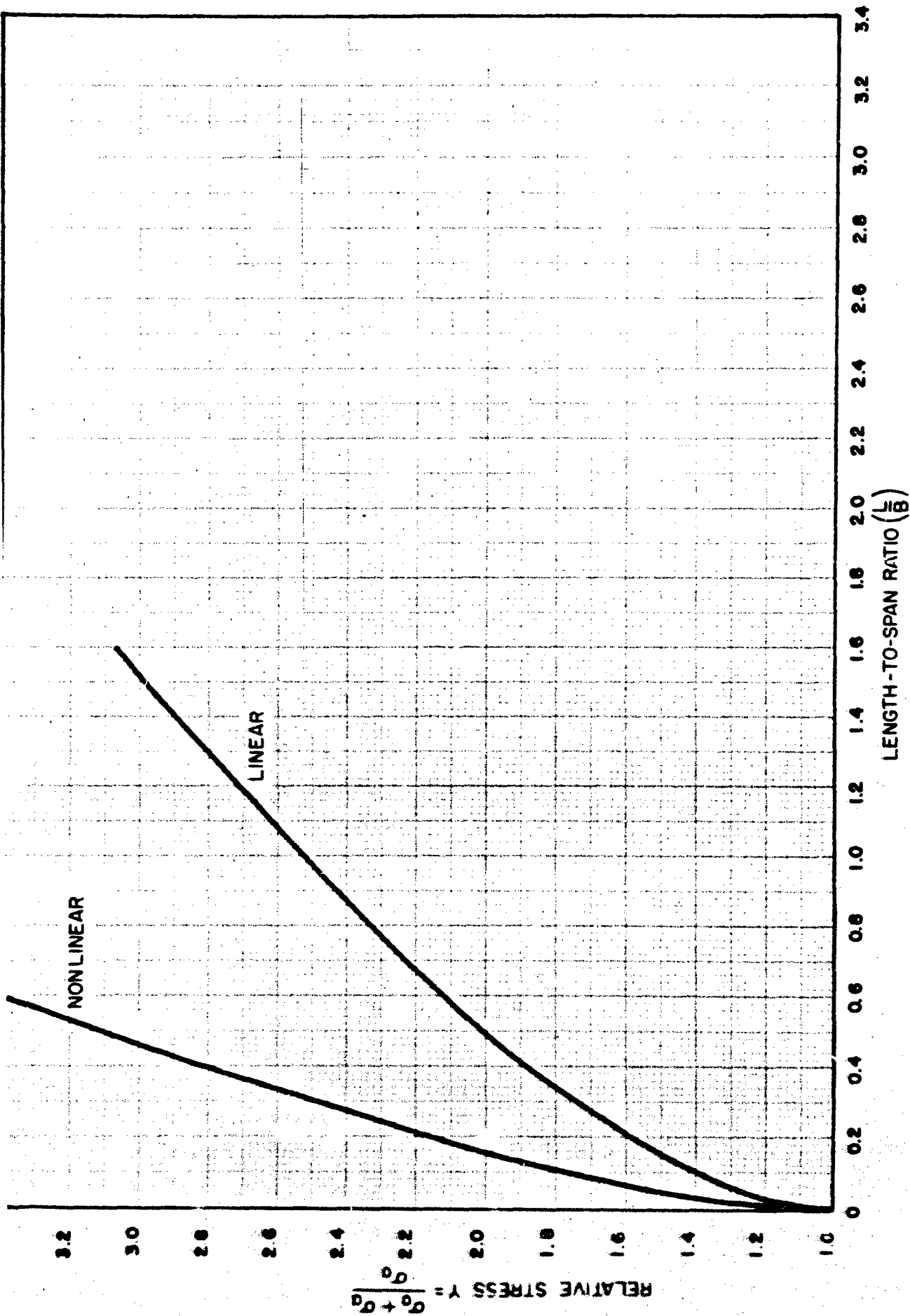


Fig. 19. Comparison Showing the Effect of Nonlinear Soil Conditions on the Relationship Between the Length-to-Span Ratio (L/B) and the Relative Stress (Y) for Constant NB for the Passive Case

EFFECTS ON STRUCTURAL COMPRESSIBILITY

Passive Arching Case

By substituting Eq. (62) for Eq. (12) in Eq. (29), it becomes

$$\Delta_{to} = 2L \left(\frac{\sigma_o}{A} \right)^{2/3} - \frac{2L}{E_{ST}} (\sigma_o + \sigma_a) \quad (71)$$

Equating one-half of Eq. (71) with Eq. (66) gives:

$$\left(\frac{\sigma_o}{A} \right)^{2/3} L - \left(\frac{\sigma_o + \sigma_a}{E_{ST}} \right) L = \left(\frac{\sigma_o + \sigma_a}{A} \right)^{2/3} \left(\frac{1}{2S_p} \right) \left[1 - e^{-\ln \left(\frac{\sigma_o + \sigma_a}{\sigma_o} \right)} \right] \quad (72)$$

$$-\left(\frac{\sigma_o}{A} \right)^{2/3} \left(\frac{1}{2S_p} \right) \ln \left(\frac{\sigma_o + \sigma_a}{\sigma_o} \right)$$

Multiplied by $2S_p \left(\frac{A}{\sigma_o} \right)^{2/3}$ Eq. (72) becomes

$$2S_p L - 2S_p \left(\frac{A}{\sigma_o} \right)^{2/3} \left(\frac{\sigma_o + \sigma_a}{E_{ST}} \right) L = \left(\frac{\sigma_o + \sigma_a}{\sigma_o} \right)^{2/3} \left[1 - e^{-\ln \left(\frac{\sigma_o + \sigma_a}{\sigma_o} \right)} \right] - \ln \left(\frac{\sigma_o + \sigma_a}{\sigma_o} \right) \quad (73)$$

Let $2S_p = N$; $\frac{(A)^{2/3}}{E_{ST}} = C'_r$

$$NL - NL C'_r \left(\frac{\sigma_o + \sigma_a}{\sigma_o} \right)^{2/3} = \left(\frac{\sigma_o + \sigma_a}{\sigma_o} \right)^{2/3} \left[1 - e^{-\ln \left(\frac{\sigma_o + \sigma_a}{\sigma_o} \right)} \right] - \ln \left(\frac{\sigma_o + \sigma_a}{\sigma_o} \right) \quad (74)$$

$$\text{let } \left(\frac{\sigma_o + \sigma_a}{\sigma_o} \right) = Y$$

$$\left(\frac{\sigma_o + \sigma_a}{\sigma_o} \right)^{2/3} = H$$

$$NL - NLC'_r H = Y^{2/3} \left(1 - e^{-\ln Y} \right) - \ln Y \quad (75)$$

Since $e^{-\ln Y} = \frac{1}{Y}$, Eq. (75) becomes

$$NL - HNL C'_r = Y^{2/3} \left(1 - \frac{1}{Y} \right) - \ln Y \quad (76)$$

or

$$- HNL C'_r = Y^{2/3} - \frac{Y^{2/3}}{Y} - \ln Y - NL \quad (77)$$

$$- HNL C'_r = Y^{2/3} - \frac{1}{Y^{1/3}} - \ln Y - NL \quad (78)$$

Since $H = \frac{\sigma_o + \sigma_a}{(\sigma_o)^{2/3}}$ multiplying by $\frac{(\sigma_o)^{1/3}}{(\sigma_o)^{1/3}}$ (80)

$$H = \left[\frac{\sigma_o + \sigma_a}{(\sigma_o)^{2/3}} \right] \left[\frac{(\sigma_o)^{1/3}}{(\sigma_o)^{1/3}} \right] = \left[\frac{\sigma_o + \sigma_a}{\sigma_o} \right] (\sigma_o)^{1/3} \quad (81)$$

Since $Y = \frac{\sigma_o + \sigma_a}{\sigma_o}$

$$H = Y(\sigma_o)^{1/3} \quad (82)$$

Substituting Eq. (82) into (78)

$$- (\sigma_o)^{1/3} Y NL C'_r = Y^{2/3} - \frac{1}{Y^{1/3}} - \ln Y - NL \quad (83)$$

Dividing by $-YNL$

$$(\sigma_o)^{1/3} C_r' = -\frac{1}{YNL} \left[Y^{2/3} - \frac{1}{Y^{1/3}} - \ln Y - NL \right] \quad (84)$$

or

$$(\sigma_o)^{1/3} C_r' = \frac{1}{YNL} \left[\frac{1}{Y^{1/3}} - Y^{2/3} + \ln Y + NL \right] \quad (85)$$

or

$$(\sigma_o)^{1/3} \frac{(A)^{2/3}}{E_{ST}} = (\sigma_o)^{1/3} C_r' = \frac{1}{NL} \left[\frac{1}{Y^{4/3}} - \frac{1}{Y^{1/3}} + \frac{1}{Y} \ln Y + \frac{NL}{Y} \right] \quad (86)$$

Expanding Eq. (86) into the original terms gives:

$$(\sigma_o)^{1/3} \frac{(A)^{2/3}}{E_{ST}} = \frac{1}{2K \tan \phi} \left(\frac{B}{L} \right) \left\{ \frac{1}{\left(\frac{\sigma_o + \sigma_a}{\sigma_o} \right)^{4/3}} - \frac{1}{\left(\frac{\sigma_o + \sigma_a}{\sigma_o} \right)^{1/3}} \right. \\ \left. + \frac{\sigma_o}{\sigma_o + \sigma_a} \left[\ln \left(\frac{\sigma_o + \sigma_a}{\sigma_o} \right) \right] + \frac{2K \tan \phi L}{B} \left(\frac{\sigma_o}{\sigma_o + \sigma_a} \right) \right\} \quad (87)$$

Figure 20 is a plot of the relationship, as shown in Eq. (86) of overstress (Y) and the product of stress level and the ratio of the nonlinear modulus of the soil to the effective modulus of the structure for a range of NL values for the passive case.

Figure 21 shows the comparison of the linear and nonlinear passive arching cases for a constant NL value.

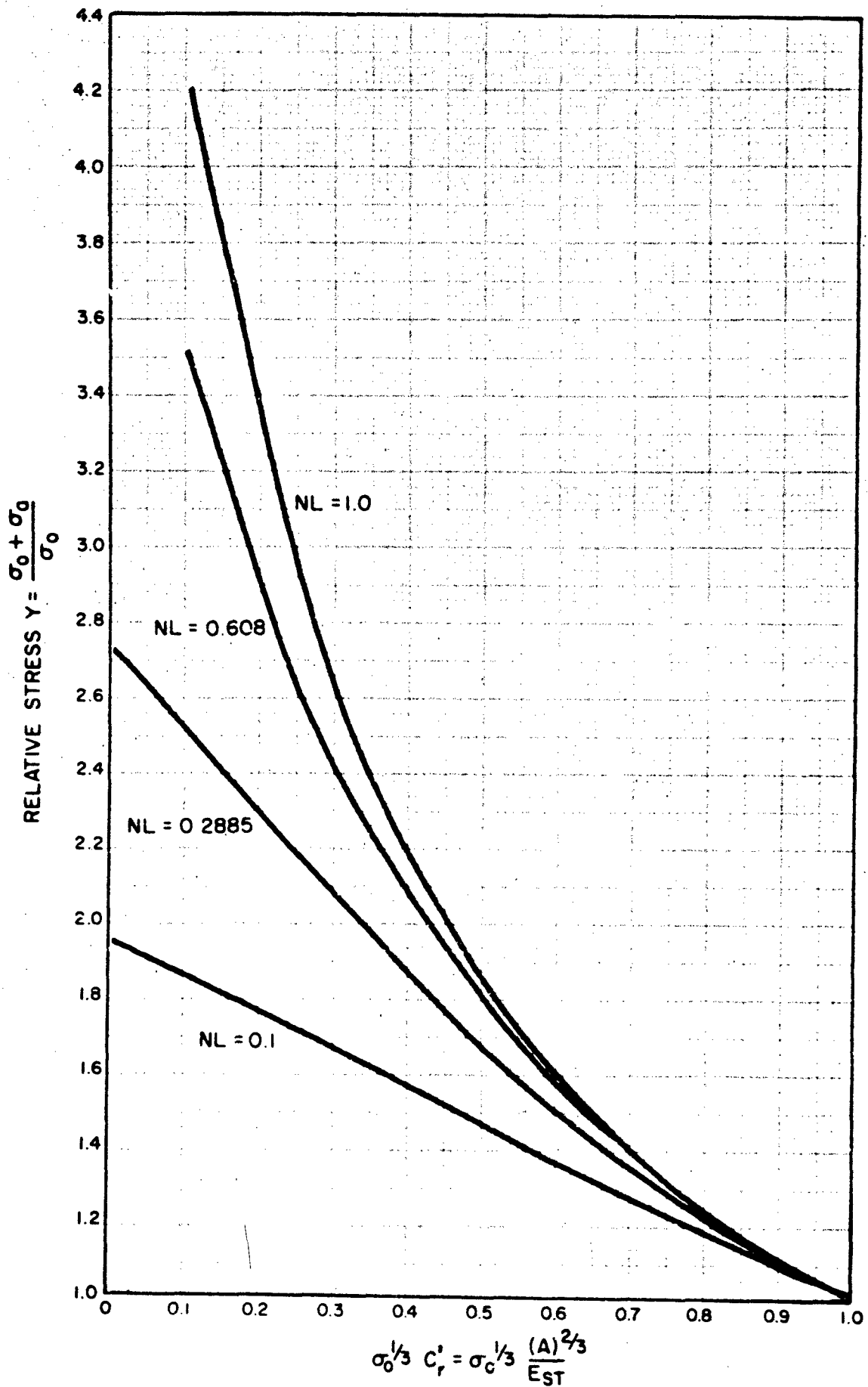


Fig. 20. Relationship Between C_r' and the Overstress Y for Various NL Values for the Passive Case (Nonlinear Soil Conditions)

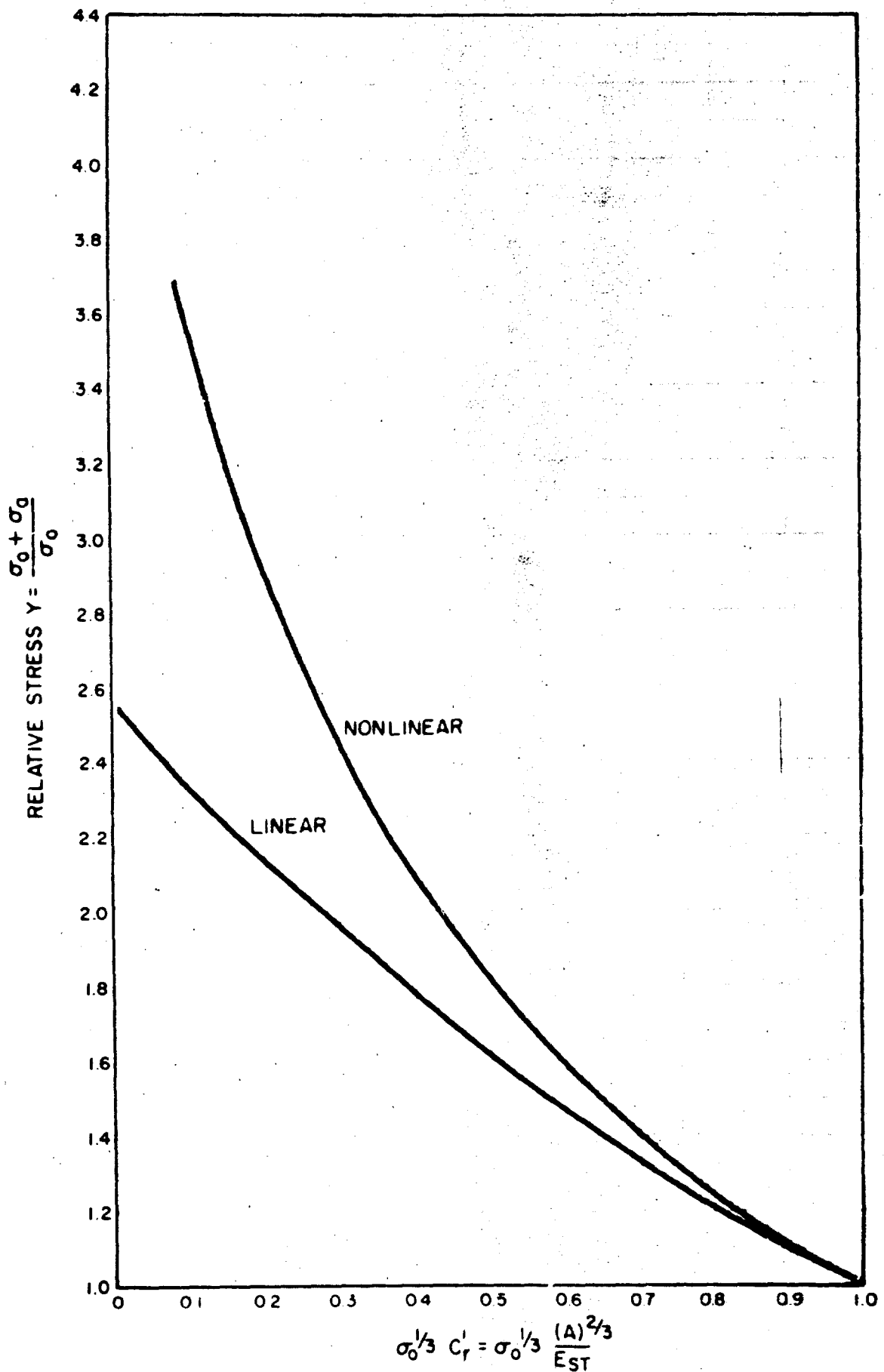


Fig. 21. Comparison Showing the Effect of Nonlinear Soil Conditions on the Relationship Between C_r' and the Relative Stress (Y) for $NL = 0.608$ for the Passive Case

Active Arching Case

As can be seen from the previous derivation for the passive case, $(\sigma_o/A)^{2/3}$ is substituted for σ_o/E_{so} and $[(\sigma_o + \sigma_a)/A]^{2/3}$ for $(\sigma_o + \sigma_a)/E_{so}$ in the linear case to obtain the nonlinear case.

By substituting the equivalent nonlinear terms in Eq. (55), we obtain the nonlinear active case. Equation (55) then becomes:

$$\left(\frac{\sigma_o - \sigma_a}{E_{ST}}\right) L - \left(\frac{\sigma_o}{A}\right)^{2/3} L = \left(\frac{\sigma_o}{A}\right)^{2/3} \frac{1}{N} \left[\ln\left(\frac{\sigma_o}{\sigma_o - \sigma_a}\right) \right] - \left(\frac{\sigma_o - \sigma_a}{A}\right)^{2/3} \frac{1}{N} \left[e^{\ln\left(\frac{\sigma_o}{\sigma_o - \sigma_a}\right)} - 1 \right] \quad (88)$$

or

$$\left(\frac{\sigma_o - \sigma_a}{E_{ST}}\right) L - \left(\frac{\sigma_o}{A}\right)^{2/3} L = \frac{1}{N} \left(\frac{\sigma_o}{A}\right)^{2/3} \left\{ \ln\left(\frac{\sigma_o}{\sigma_o - \sigma_a}\right) - \left(\frac{\sigma_o - \sigma_a}{\sigma_o}\right)^{2/3} \left[e^{\ln\left(\frac{\sigma_o}{\sigma_o - \sigma_a}\right)} - 1 \right] \right\} \quad (89)$$

Multiplied by $\left(\frac{A}{\sigma_o}\right)^{2/3} \frac{1}{L}$

$$\left(\frac{\sigma_o - \sigma_a}{\sigma_o^{2/3}}\right) \frac{(A)^{2/3}}{E_{ST}} - 1 = \frac{1}{NL} \left\{ \ln\left(\frac{\sigma_o}{\sigma_o - \sigma_a}\right) - \left(\frac{\sigma_o - \sigma_a}{\sigma_o}\right)^{2/3} \left[e^{\ln\left(\frac{\sigma_o}{\sigma_o - \sigma_a}\right)} - 1 \right] \right\} \quad (90)$$

Letting $\frac{(A)^{2/3}}{E_{ST}} = C'_r$ and $\left(\frac{\sigma_o}{\sigma_o - \sigma_a}\right) = Y'$

$$\left(\frac{\sigma_o - \sigma_a}{\sigma_o^{2/3}}\right) C'_r - 1 = \frac{1}{NL} \left[\ln Y' - \left(\frac{1}{(Y')^{2/3}} e^{\ln Y'}\right) + \frac{1}{(Y')^{2/3}} \right] \quad (91)$$

Since $e^{\ln Y'} = Y'$

$$\left(\frac{\sigma_o - \sigma_a}{\sigma_o^{2/3}} \right) C'_r - 1 = \frac{1}{NL} \left[\ln Y' - \frac{Y'}{(Y')^{2/3}} + \frac{1}{(Y')^{2/3}} \right] \quad (92)$$

or

$$\left(\frac{\sigma_o - \sigma_a}{\sigma_o^{2/3}} \right) C'_r - 1 = \frac{1}{NL} \left[\ln Y' - (Y')^{1/3} + \frac{1}{(Y')^{2/3}} \right] \quad (93)$$

as in the passive case

$$\frac{\sigma_o - \sigma_a}{\sigma_o^{2/3}} = \frac{\sigma_o^{1/3}}{Y'}$$

Eq. (93) then becomes

$$\frac{\sigma_o^{1/3}}{Y'} C'_r - 1 = \frac{1}{NL} \left[\ln Y' - (Y')^{1/3} + \frac{1}{(Y')^{2/3}} \right] \quad (94)$$

$$\sigma_o^{1/3} C'_r = \frac{Y'}{NL} \left[\ln Y' - (Y')^{1/3} + \frac{1}{(Y')^{2/3}} \right] + Y' \quad (95)$$

or

$$\sigma_o^{1/3} C'_r = \frac{1}{NL} \left[Y' \ln Y' - (Y')^{4/3} + (Y')^{1/3} + NLY' \right] \quad (96)$$

expanding into the original terms

$$\sigma_o^{1/3} C'_r = \frac{1}{2K \tan \phi} \left(\frac{B}{L} \right) \left[\left(\frac{\sigma_o}{\sigma_o - \sigma_a} \right) \ln \left(\frac{\sigma_o}{\sigma_o - \sigma_a} \right) - \left(\frac{\sigma_o}{\sigma_o - \sigma_a} \right)^{4/3} + \left(\frac{\sigma_o}{\sigma_o - \sigma_a} \right)^{1/3} \right] \quad (97)$$

$$+ \left(2K \tan \phi \right) \left(\frac{L}{B} \right) \left(\frac{\sigma_o}{\sigma_o - \sigma_a} \right)$$

Figure 22 is a plot of the relationship as shown in Eq. (96) of relative stress ($1/Y'$) and the product of stress level and the ratio of the nonlinear modulus of the soil to the effective modulus of the structure for a range of NL values for the active case.

Figure 23 shows the comparison of the linear and nonlinear active arching cases for a constant NL value.

Figure 24 shows the comparison for the linear and nonlinear arching cases for both the passive and active arching for the constant NL value.

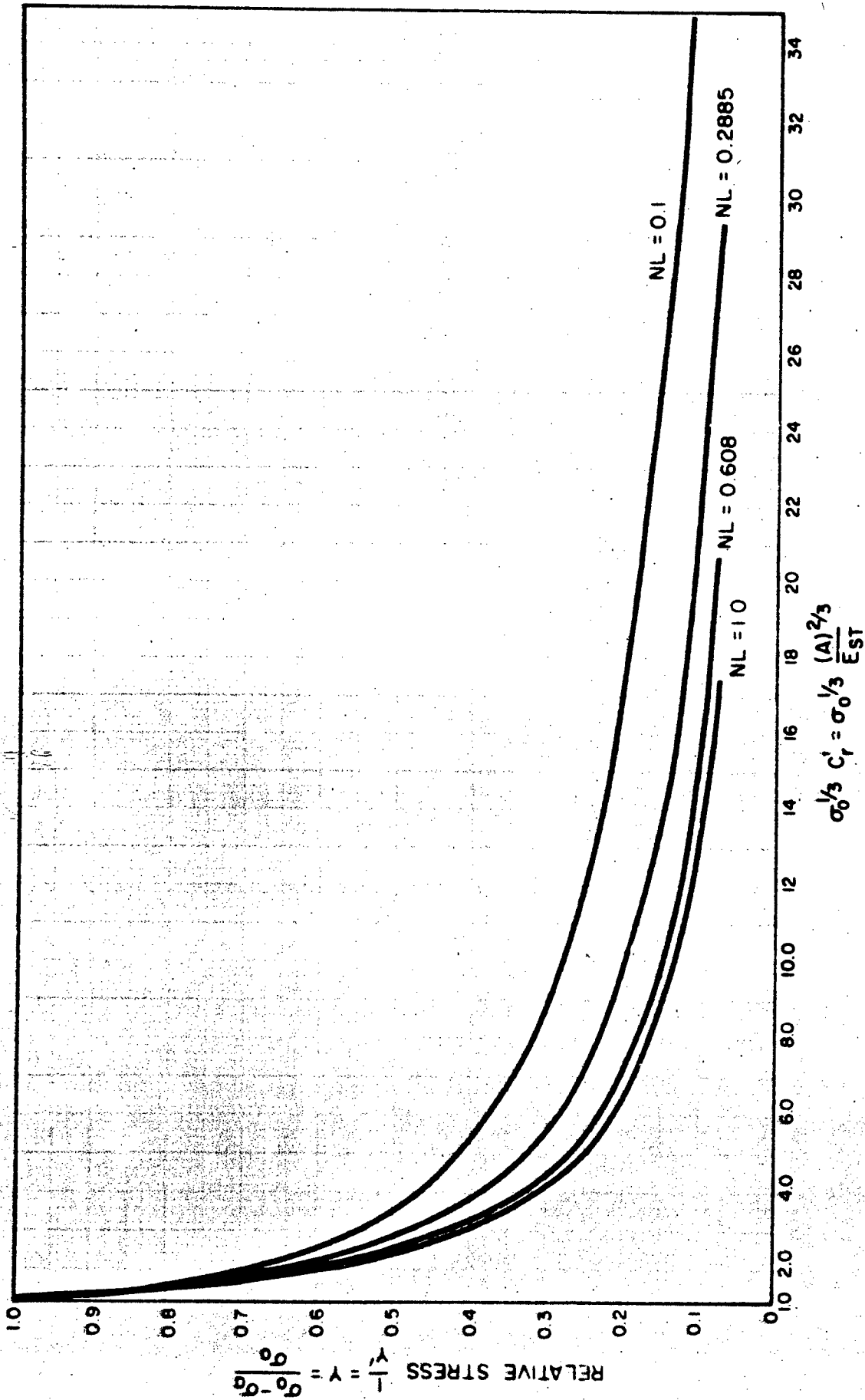


Fig. 22. Relationship Between C_r and $1/Y'$ [Eq. (96)] for Various NL Values for the Active Case (Nonlinear Soil)

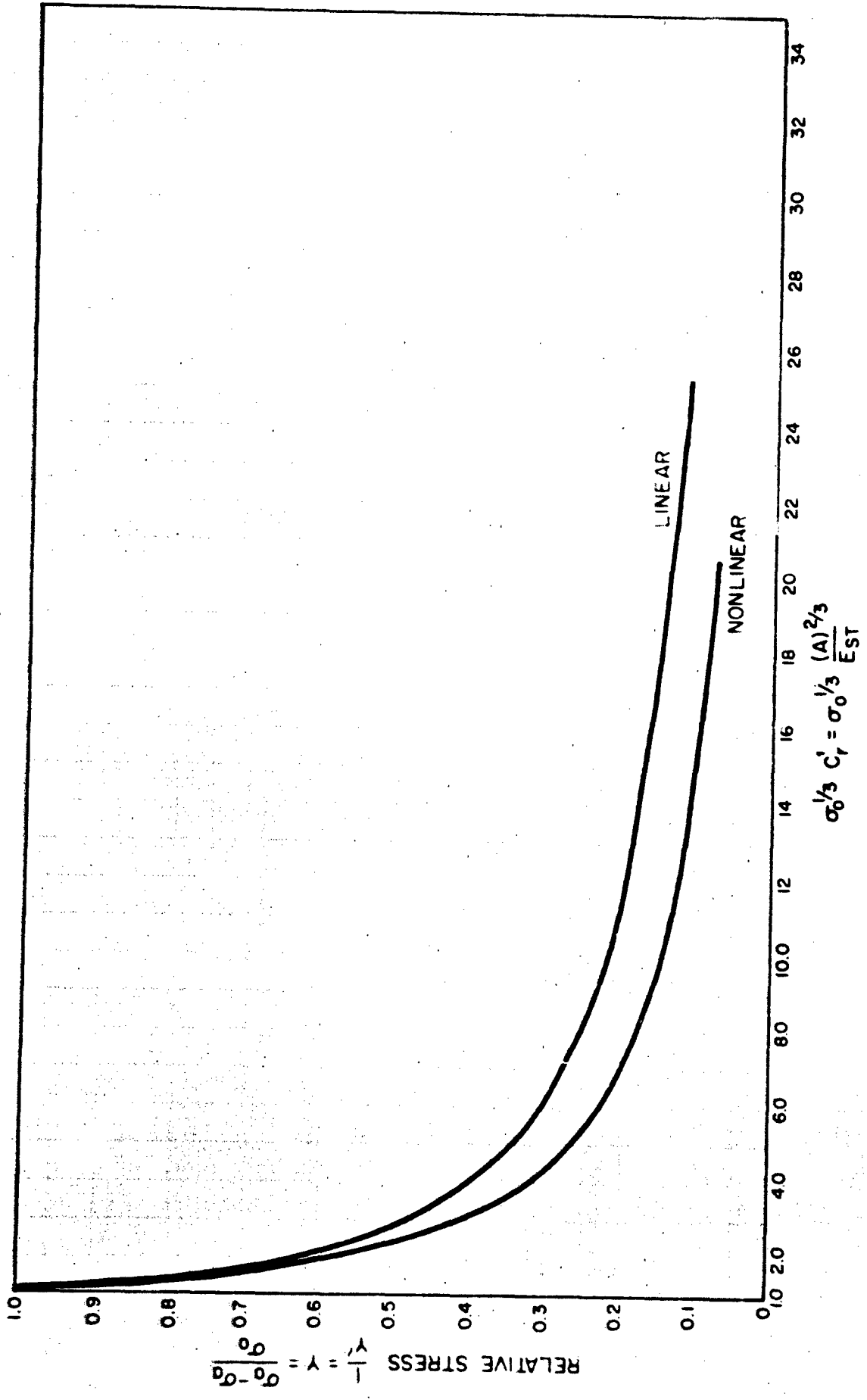


Fig. 23. Comparison Showing the Effect of Nonlinear Soil Conditions on the Relationship Between C_1 and Relative Stress $1 - \frac{\sigma_a - \sigma_b}{\sigma_a} = \gamma$

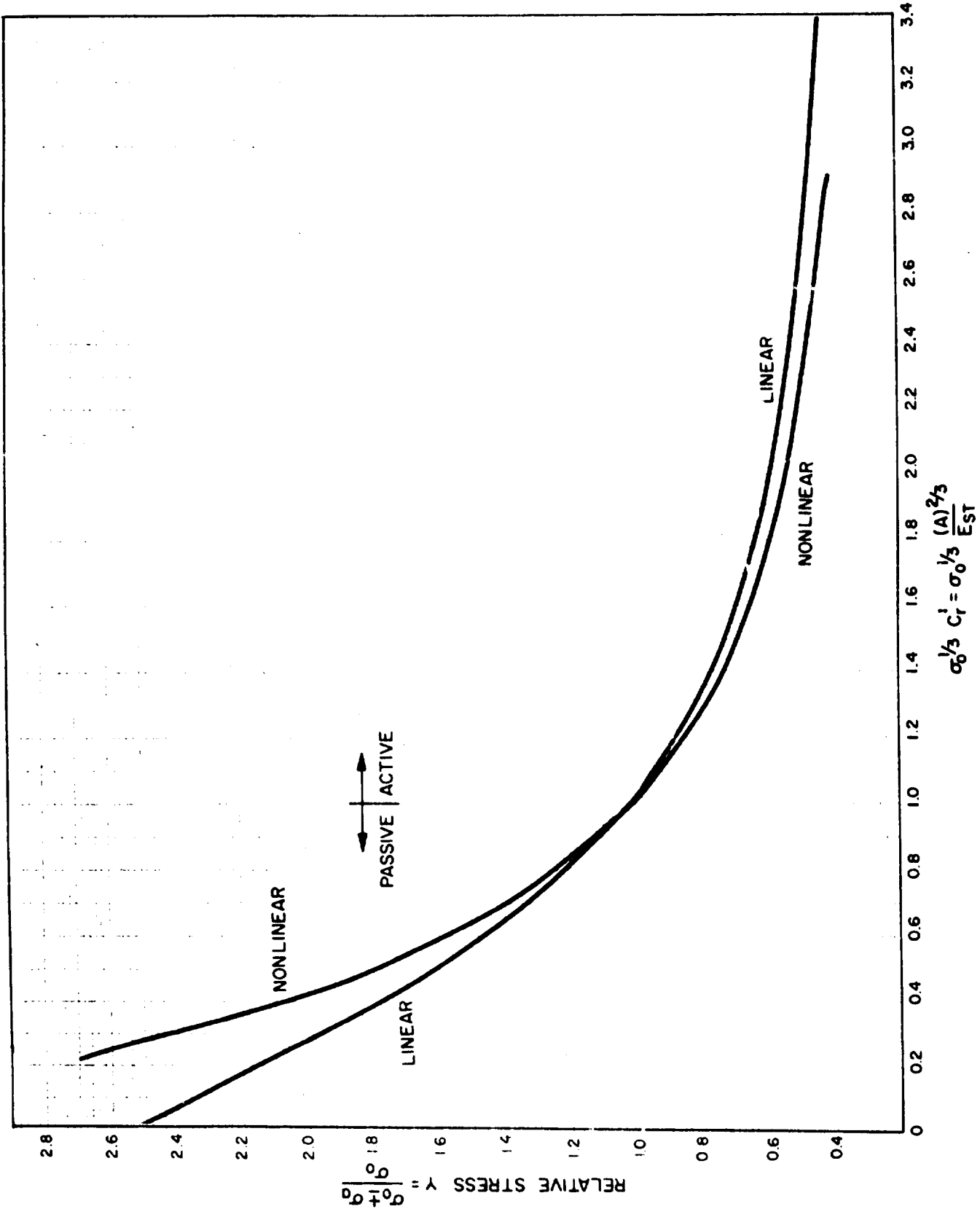


Fig. 24. Comparison Showing the Effect of Nonlinear Soil Conditions on the Relationship Between C_r^1 and the Relative Stress Y for $NL = 0.608$ for the Passive and Active Cases

Section 6

EFFECTS OF DIFFERENTIAL DISPLACEMENT (TRAP DOOR EXPERIMENTS)

Since the basic concepts of arching discussed in this report are founded on the concept of stress redistribution caused by differential strain occurring between the soil and the structure, an examination of the Terzaghi trap door concept is pertinent because that concept involves differential displacement.

EFFECTS OF LINEAR SOIL CONDITIONS

Passive Arching Case

An examination of the basic derivations shows that Eq. (20) is for the differential displacement in the passive arching case.

$$\Delta_B = \left(\frac{\sigma_o + \sigma_a}{2E_{so} S_p} \right) \left[1 - e^{-\ln \left(\frac{\sigma_o + \sigma_a}{\sigma_o} \right)} \right] - \left(\frac{\sigma_o}{2E_{so} S_p} \right) \ln \left(\frac{\sigma_o + \sigma_a}{\sigma_o} \right) \quad (20)$$

Since it is desirable, if possible, to normalize the overstress on the trap door to be independent of stress level, the first step is to put Eq. (20) in the form of Δ_B/B . Since $S_p = K \tan \varphi/B$ and $E_{so} = \sigma_o/\epsilon_{so}$, Eq. (20) becomes:

$$\Delta_B = (\sigma_o + \sigma_a) \left(\frac{\epsilon_{so}}{\sigma_o} \right) \left(\frac{B}{2K \tan \varphi} \right) \left[1 - e^{-\ln \left(\frac{\sigma_o + \sigma_a}{\sigma_o} \right)} \right] - (\sigma_o) \left(\frac{\epsilon_{so}}{\sigma_o} \right) \left(\frac{B}{2K \tan \varphi} \right) \ln \left(\frac{\sigma_o + \sigma_a}{\sigma_o} \right) \quad (98)$$

Letting $J = 2K \tan \varphi$, $Y = (\sigma_o + \sigma_a)/\sigma_o$, and dividing by B , Eq. (98) becomes:

$$\frac{\Delta_B}{B} = Y \frac{\epsilon_{so}}{J} \left(1 - e^{-\ln Y} \right) - \frac{\epsilon_{so}}{J} \ln Y \quad (99)$$

which reduces to:

$$\frac{J \Delta_B}{B \epsilon_{so}} = Y - 1 - \ln Y \quad (100)$$

Preceding Page Blank

Figure 25 is a plot computed from the relationship between overstress Y and the product of the ratio of the soil parameter J to the free-field strain ϵ_{so} times the ratio of the differential displacement Δ_B to one-half the span,

Expanding Eq. (100) into original terms, it becomes:

$$\frac{2K \tan \varphi}{\epsilon_{so}} \frac{\Delta_B}{B} = \left(\frac{\sigma_o + \sigma_a}{\sigma_o} \right) - 1 - \ln \left(\frac{\sigma_o + \sigma_a}{\sigma_o} \right) \quad (101)$$

or

$$\frac{\Delta_B}{B} = \frac{\epsilon_{so}}{2K \tan \varphi} \left[\left(\frac{\sigma_o + \sigma_a}{\sigma_o} \right) - 1 - \ln \left(\frac{\sigma_o + \sigma_a}{\sigma_o} \right) \right] \quad (101A)$$

Figure 26 is a plot of the relationship between overstress Y and the differential displacement-to-span ratio for a range of $\epsilon_{so} J$ values.

Active Arching Case

Making the same derivation for the active case, Eq. (53) becomes

$$\frac{J \Delta_B}{\epsilon_{so} B} = \ln Y' - 1 + \frac{1}{Y'} \quad (102)$$

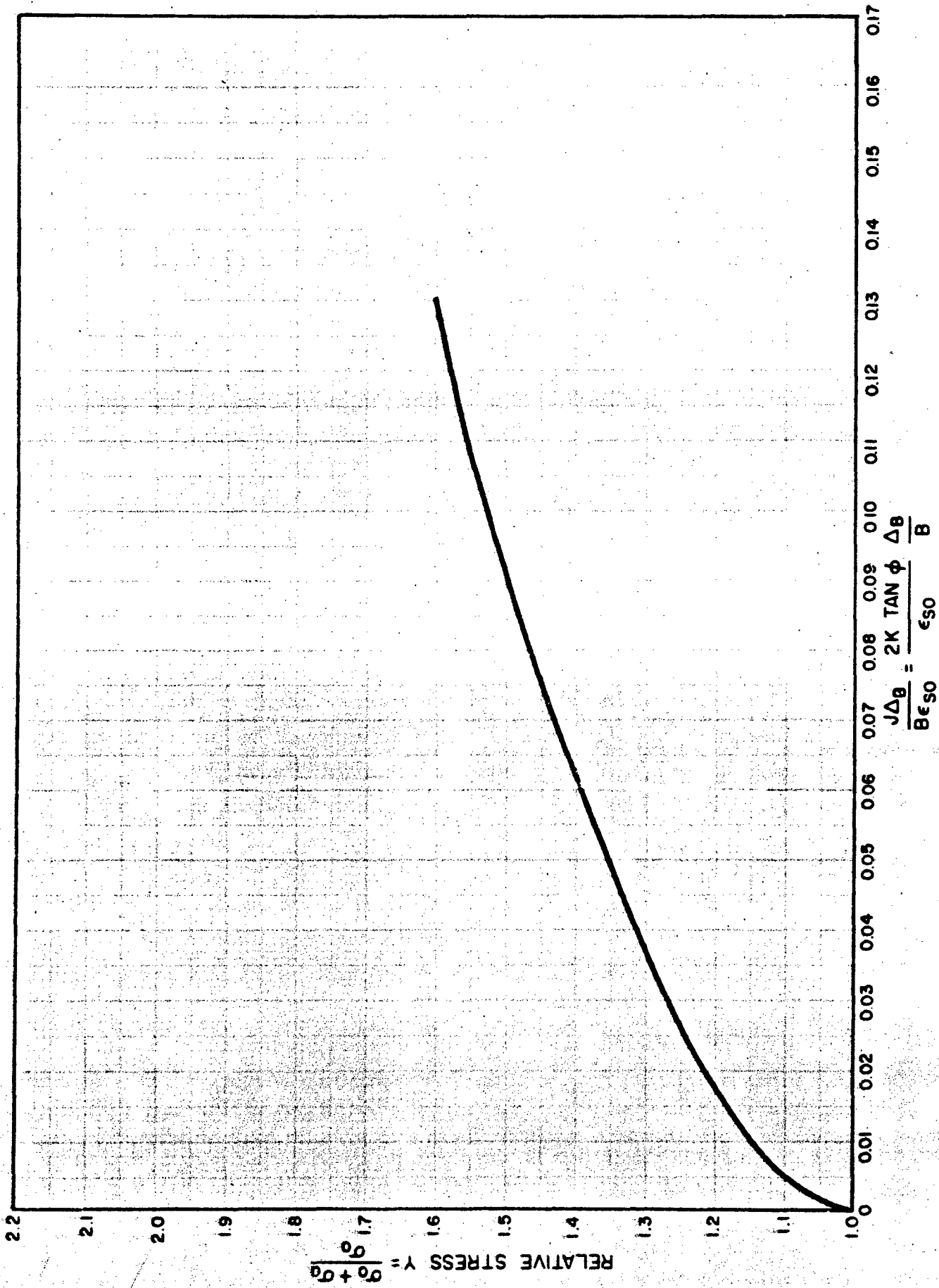
Figure 27 is a plot of the relationship between relative stress Y and the product of the ratio of the soil parameter J to the free-field strain ϵ_{so} times the ratio of the differential displacement Δ_B to one-half the span, B .

$$\frac{\Delta_B}{B} = \frac{\epsilon_{so}}{J} \left(\ln Y' - 1 + \frac{1}{Y'} \right) \quad (102A)$$

Figure 28 is a plot of the relationship between overstress Y and the differential displacement-to-span ratio for a range of J/ϵ_{so} values.

Figure 29 is a plot showing the relationship of the active and passive cases for a given J/ϵ_{so} value.

* It should be noted that ϵ_{so} is the free-field strain associated with the free-field stress level σ_o^{so} .



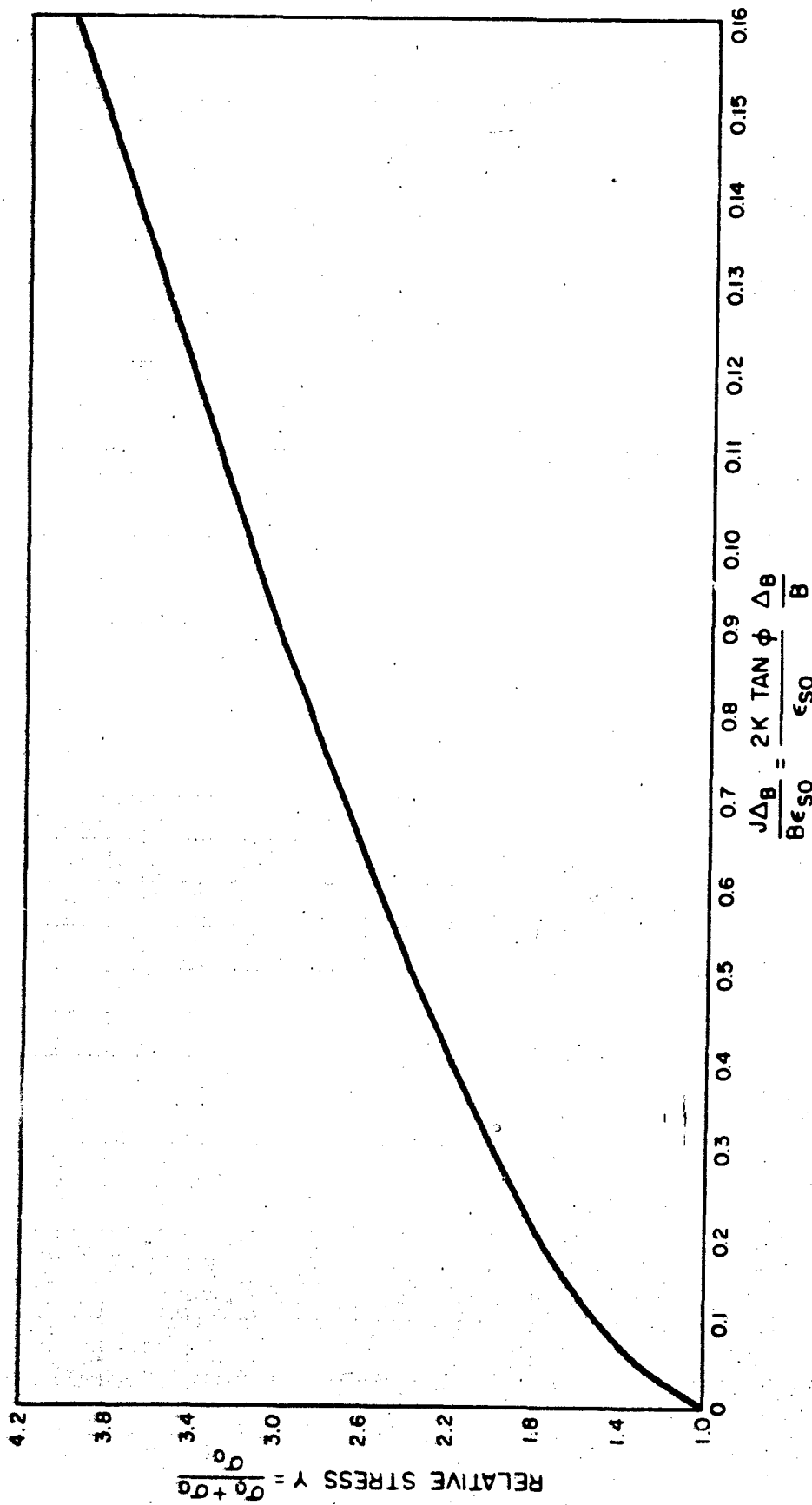


Fig. 25 (Cont.)

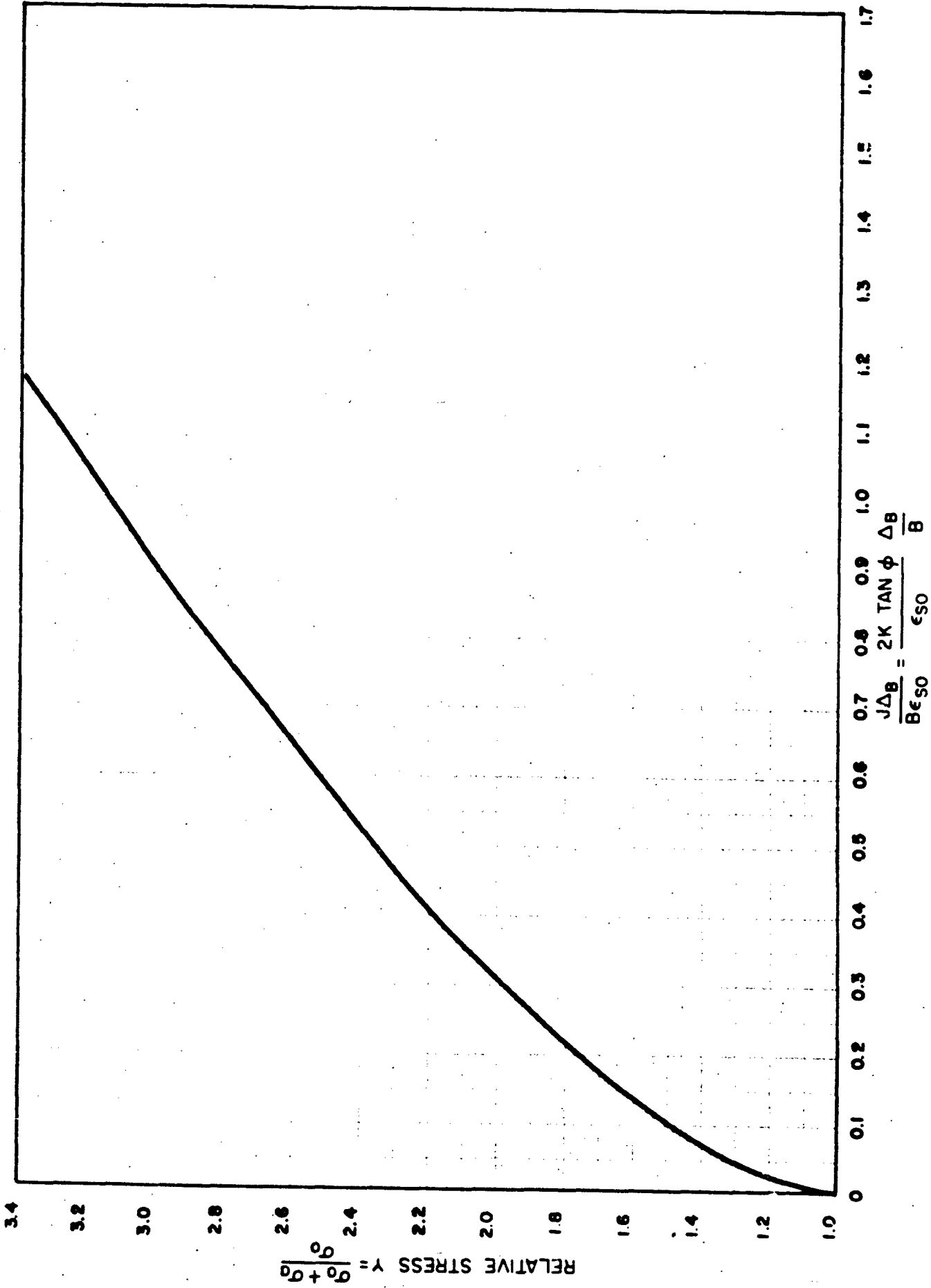


Fig. 25 (Cont.)

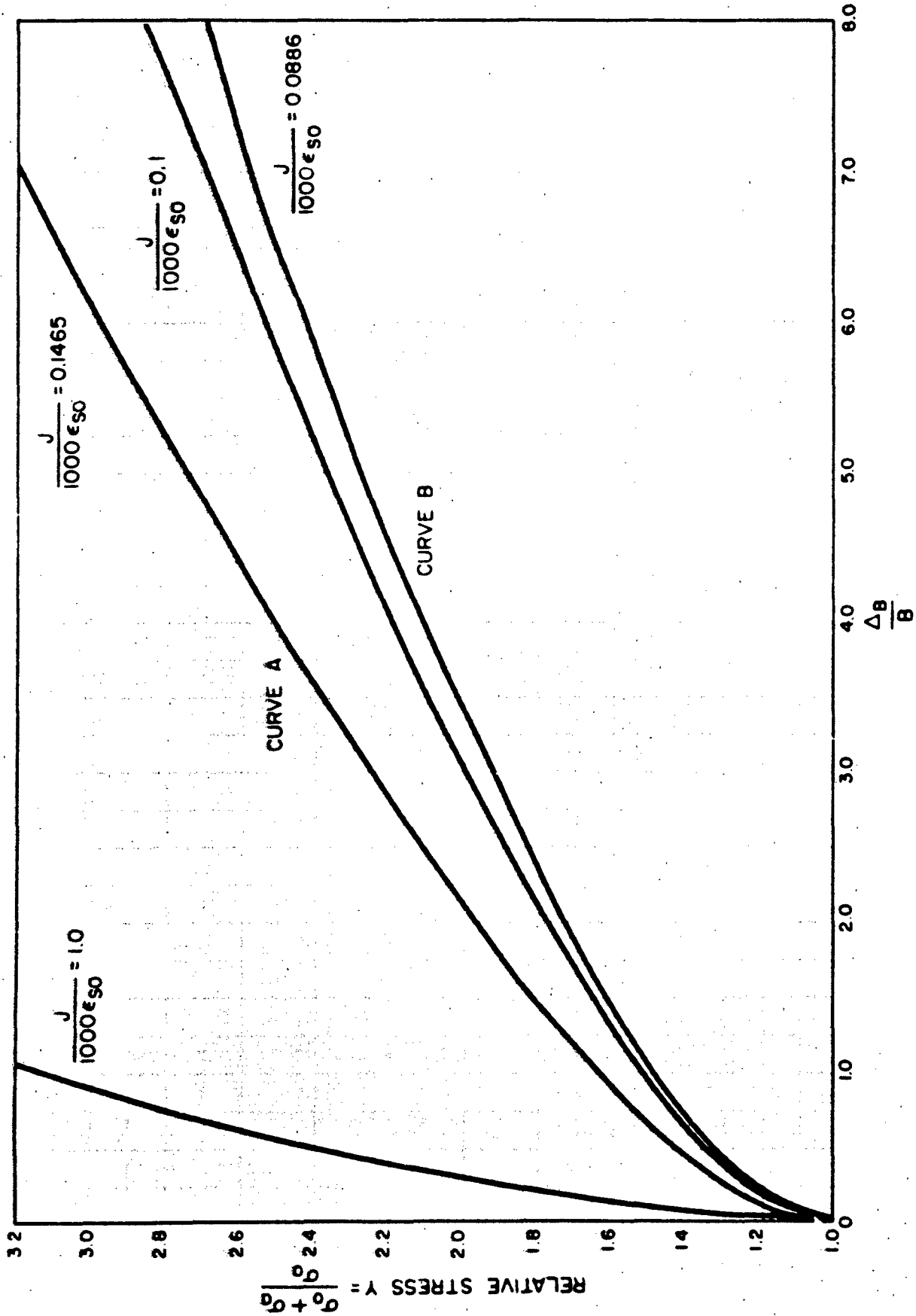


Fig. 26. Relationship of Differential Displacement per Unit Span $\Delta r/B$ to the Overstress (Y) for a Range

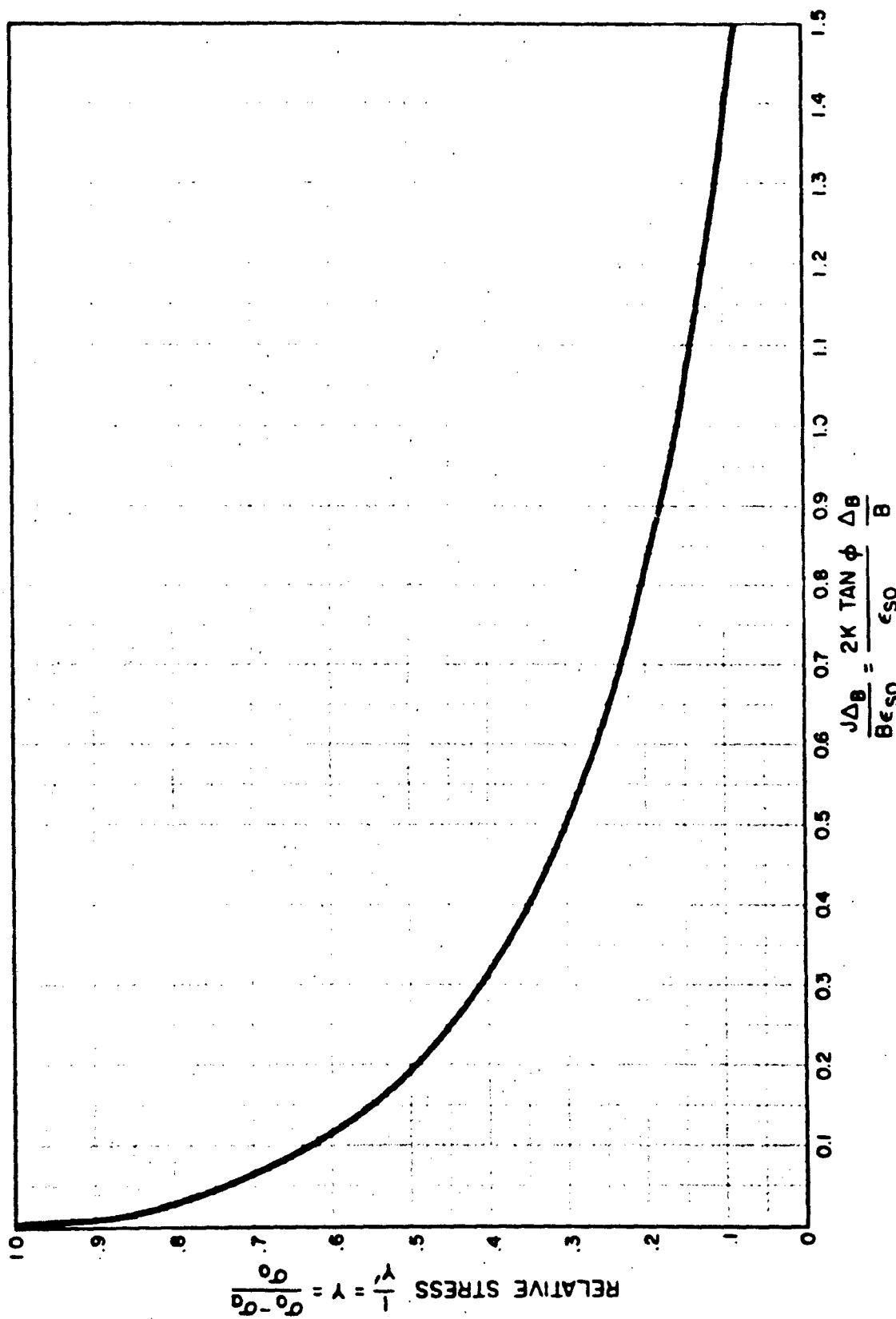


Fig. 27. Relationship Between $J\Delta B/B\epsilon_{SO}$ and Relative Stress $Y = (\sigma_0 - \sigma_a/\sigma_0)$ for [Eq. (102)] the Active Case (Linear Soil Conditions)

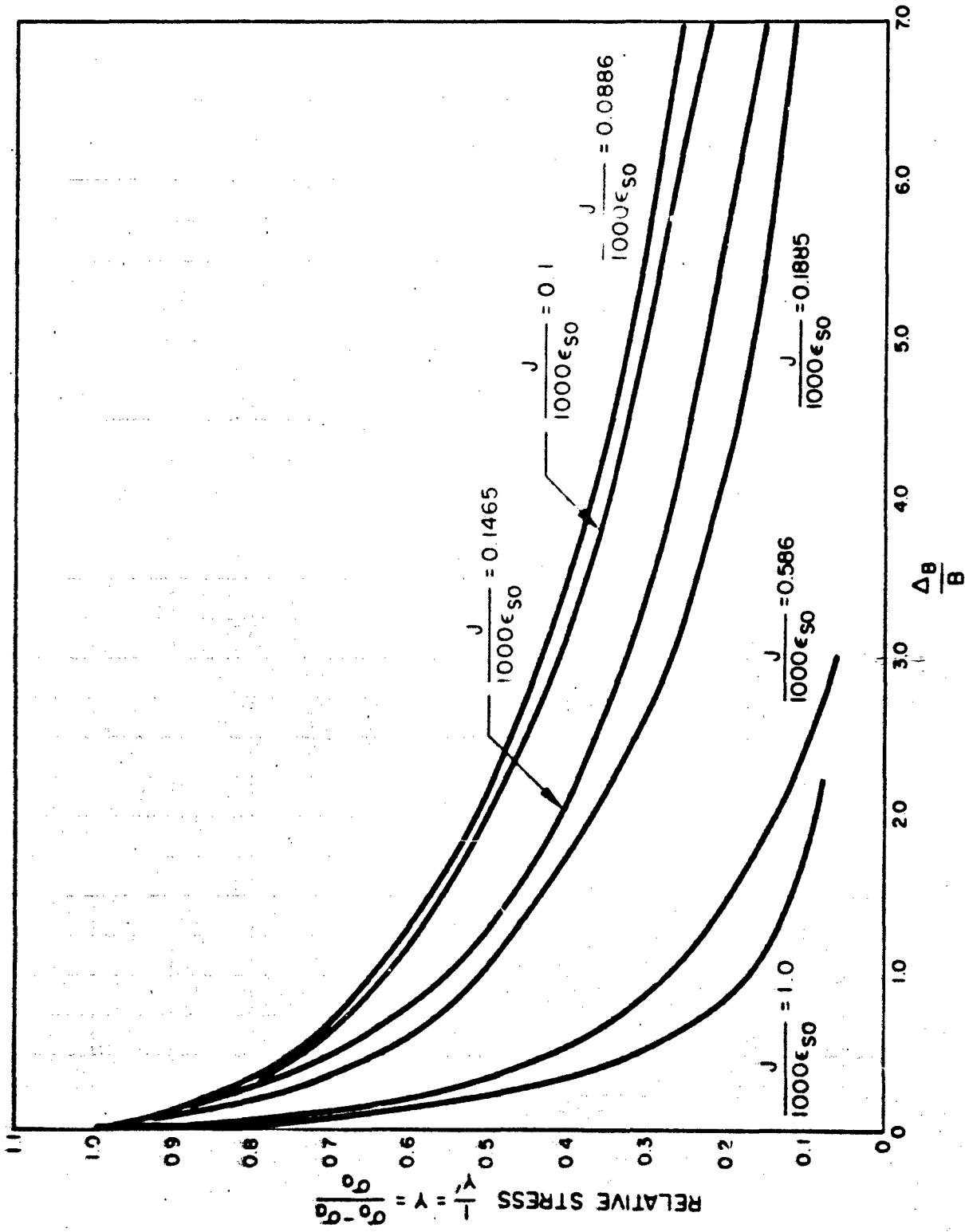


Fig. 28. Relationship of Differential Displacement per Unit Span $\Delta B/B$ to the Relative Stress (Y) for a Beam of $1/1000\epsilon_{50}$ for the Active Case (Linear Elastic Conditions)

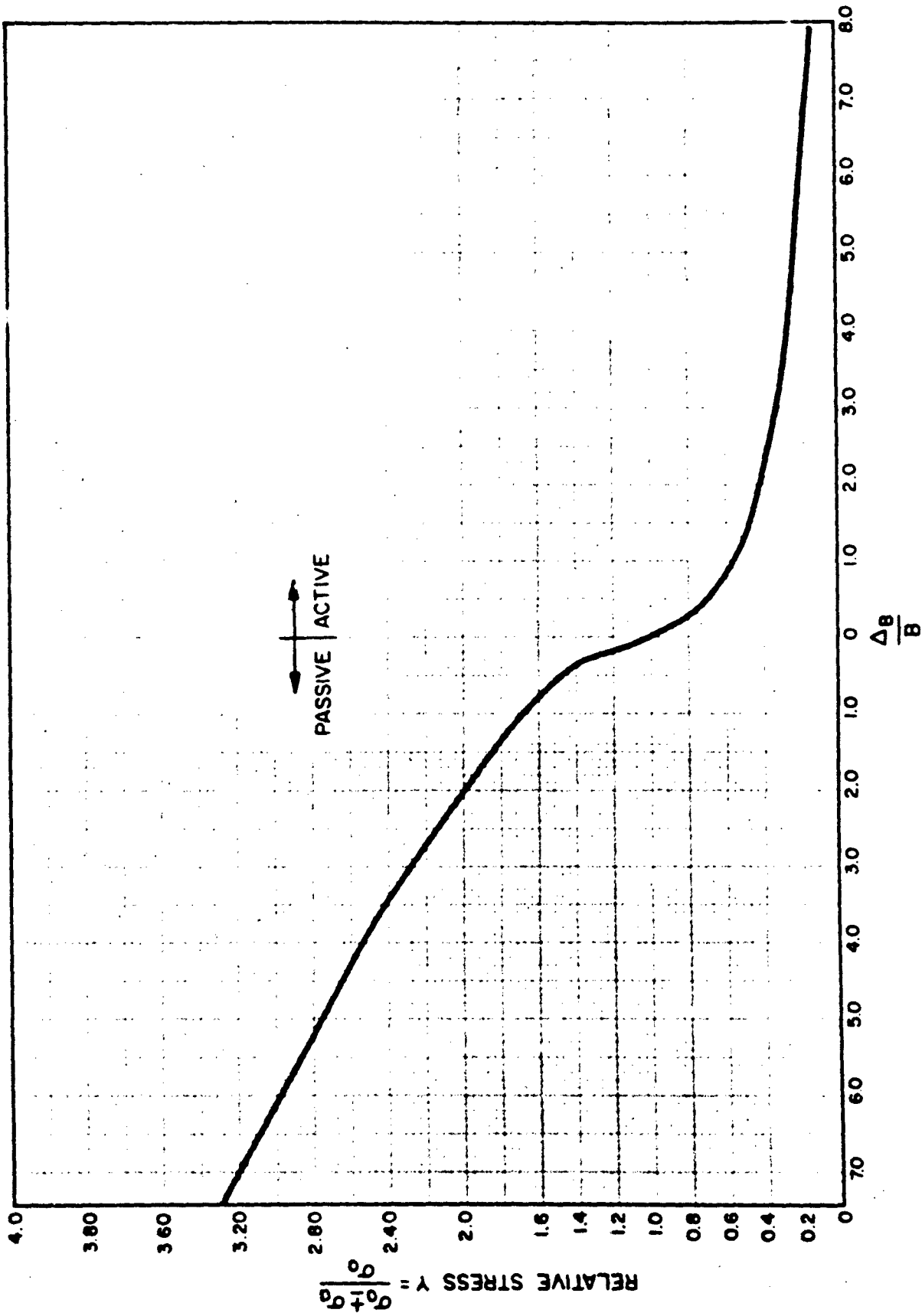


Fig. 29. Relationship Between Differential Displacement per Unit Span ($\Delta B/B$) to the Relative Stress (Y) on Structure for $J/1000c_{so} = 0.1465$ for the Range From the Active Through the Passive Case (Linear Soil Conditions)

EFFECTS OF NONLINEAR SOIL CONDITIONS

Again, since few soils exhibit a linear stress-strain behavior, it is well to examine the effect of the nonlinear nature of the behavior. As before, the nonlinear effect to be examined is expressed by Eq. (62):

$$\sigma_o = A\epsilon^{3/2} \quad (62)$$

Passive Arching Case

Examination of Section 5 shows that Eq. (66) expresses Δ_B in the nonlinear form for the passive case.

$$\Delta_B = \left(\frac{\sigma_o + \sigma_a}{A} \right)^{2/3} \left(\frac{1}{2S_p} \right) \left[1 - e^{-\ln \left(\frac{\sigma_o + \sigma_a}{\sigma_o} \right)} \right] - \left(\frac{\sigma_o}{A} \right)^{2/3} \left(\frac{1}{2S_p} \right) \left[\ln \left(\frac{\sigma_o + \sigma_a}{\sigma_o} \right) \right] \quad (66)$$

If we substitute $1/2S_p = B/J$, $J = 2K \tan \phi$, $Y = (\sigma_o + \sigma_a)/\sigma_o$ and divide by B, Eq. (66) becomes:

$$\frac{\Delta_B}{B} = \left(\frac{\sigma_o}{A} \right)^{2/3} Y^{2/3} \frac{1}{J} \left(1 - e^{-\ln Y} \right) - \left(\frac{\sigma_o}{A} \right)^{2/3} \frac{1}{J} \ln Y \quad (103)$$

which reduces to

$$\left(\frac{A}{\sigma_o} \right)^{2/3} \frac{J\Delta_B}{B} = Y^{2/3} \left(1 - e^{-\ln Y} \right) - \ln Y \quad (104)$$

Let

$$\left(\frac{A}{\sigma_o} \right)^{2/3} \frac{J\Delta_B}{B} = M$$

in Eq. (104). Then

$$M = Y^{2/3} - \frac{1}{Y^{1/3}} - \ln Y \quad (104A)$$

Figure 30 is a plot of the relationship for the passive case between overstress and M the product of the ratio of the soil parameter J to the free-field strain represented by $(A/\sigma_o)^{2/3}$ and the ratio of the different displacement Δ_B to one-half the span, B .

Expanding Eq. (104A) into the original terms, it becomes:

$$\frac{\Delta_B}{B} = \left(\frac{\sigma_o}{A}\right)^{2/3} \left(\frac{1}{2K \tan \phi}\right) \left[\left(\frac{\sigma_o + \sigma_a}{\sigma_o}\right)^{2/3} - \frac{1}{\left(\frac{\sigma_o + \sigma_a}{\sigma_o}\right)^{1/3}} - \ln \left(\frac{\sigma_o + \sigma_a}{\sigma_o}\right) \right] \quad (105)$$

Figure 31 is a plot of the relationship between overstress and the displacement-to-span ratio for a range of $[(A/\sigma_o)^{2/3}]$ ($J/1000$) values.

Figure 32 shows the comparison of the linear and nonlinear passive arching cases for a constant $[(A/\sigma_o)^{2/3}]$ ($J/1000$) value.

Active Arching Case

If $(\sigma_o/A)^{2/3}$ and $[(\sigma_o - \sigma_a)/A]^{2/3}$ are substituted for σ_o/E_{so} and $(\sigma_o - \sigma_a)/E_{so}$ respectively in Eq. (53), the following equation results:

$$\Delta_B = \left(\frac{\sigma_o}{A}\right)^{2/3} \left[\left(\frac{B}{2K \tan \phi}\right) \ln \left(\frac{\sigma_o}{\sigma_o - \sigma_a}\right) - \left(\frac{\sigma_o - \sigma_a}{A}\right)^{2/3} \left(\frac{B}{2K \tan \phi}\right) \left[e^{\ln \left(\frac{\sigma_o}{\sigma_o - \sigma_a}\right)} - 1 \right] \right] \quad (106)$$

Again, if we substitute, $J = 2K \tan \phi$, $Y' = \sigma_o/(\sigma_o - \sigma_a)$ and divide by B , Eq. (106) becomes:

$$\frac{\Delta_B}{B} = \left(\frac{\sigma_o}{A}\right)^{2/3} \left(\frac{1}{J}\right) \ln Y' - \left(\frac{\sigma_o}{A}\right)^{2/3} \left(\frac{1}{Y'}\right)^{2/3} \left(\frac{1}{J}\right) \left[e^{\ln Y'} - 1 \right] \quad (107)$$

Multiplying by $\left(\frac{A}{\sigma_o}\right)^{2/3} J$

$$\left(\frac{A}{\sigma_o}\right)^{2/3} \frac{J \Delta_B}{B} = \ln Y' - \frac{e^{\ln Y'}}{(Y')^{2/3}} + \frac{1}{(Y')^{2/3}} \quad (108)$$

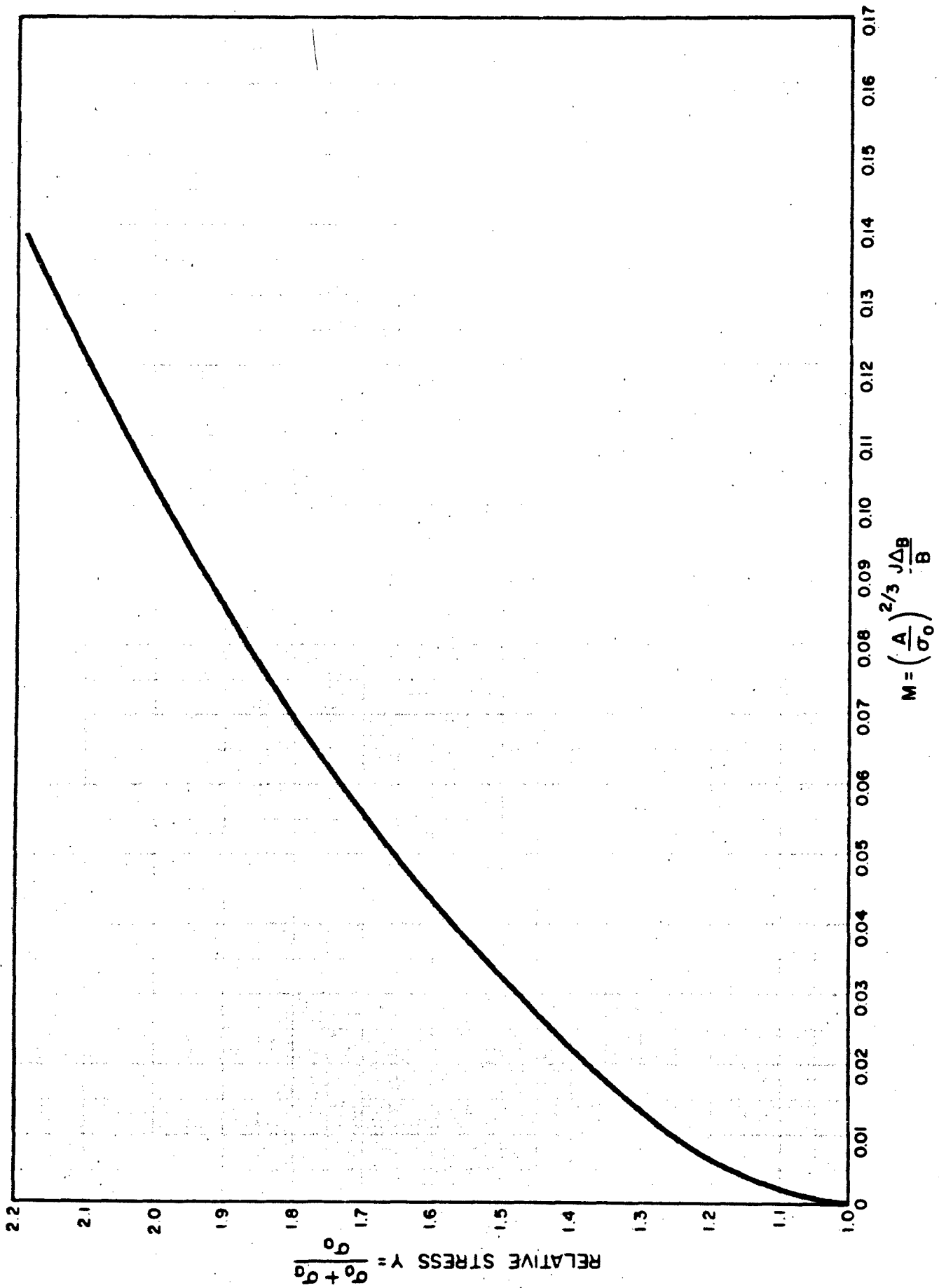
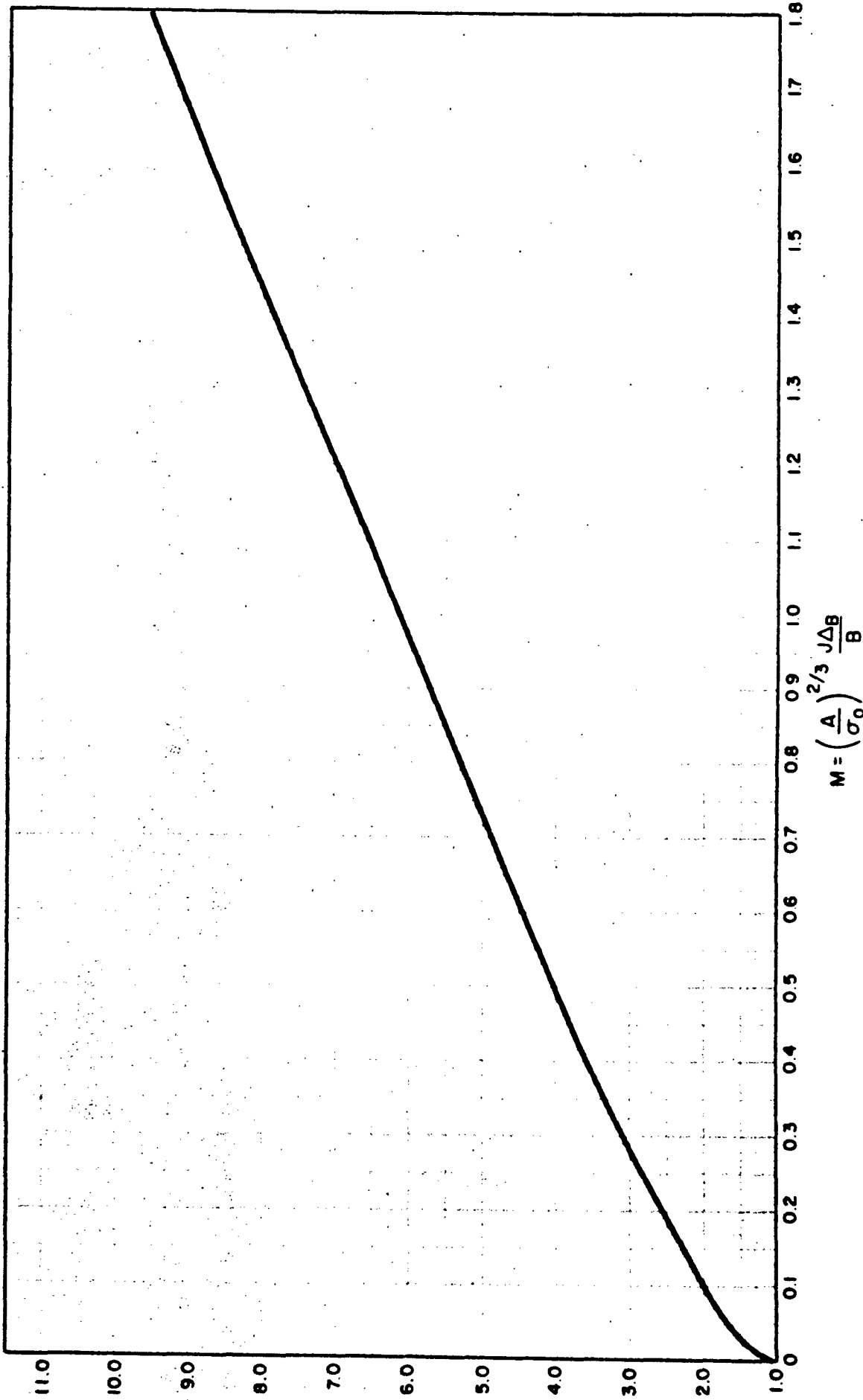


Fig. 20 Relationship Between $M = \left(\frac{A}{\sigma_0}\right)^{2/3} \frac{J\Delta B}{B}$ and Relative Stress



$$M = \left(\frac{A}{\sigma_0}\right)^{2/3} \frac{J\Delta B}{B}$$

FIG. 30 (Cont.)

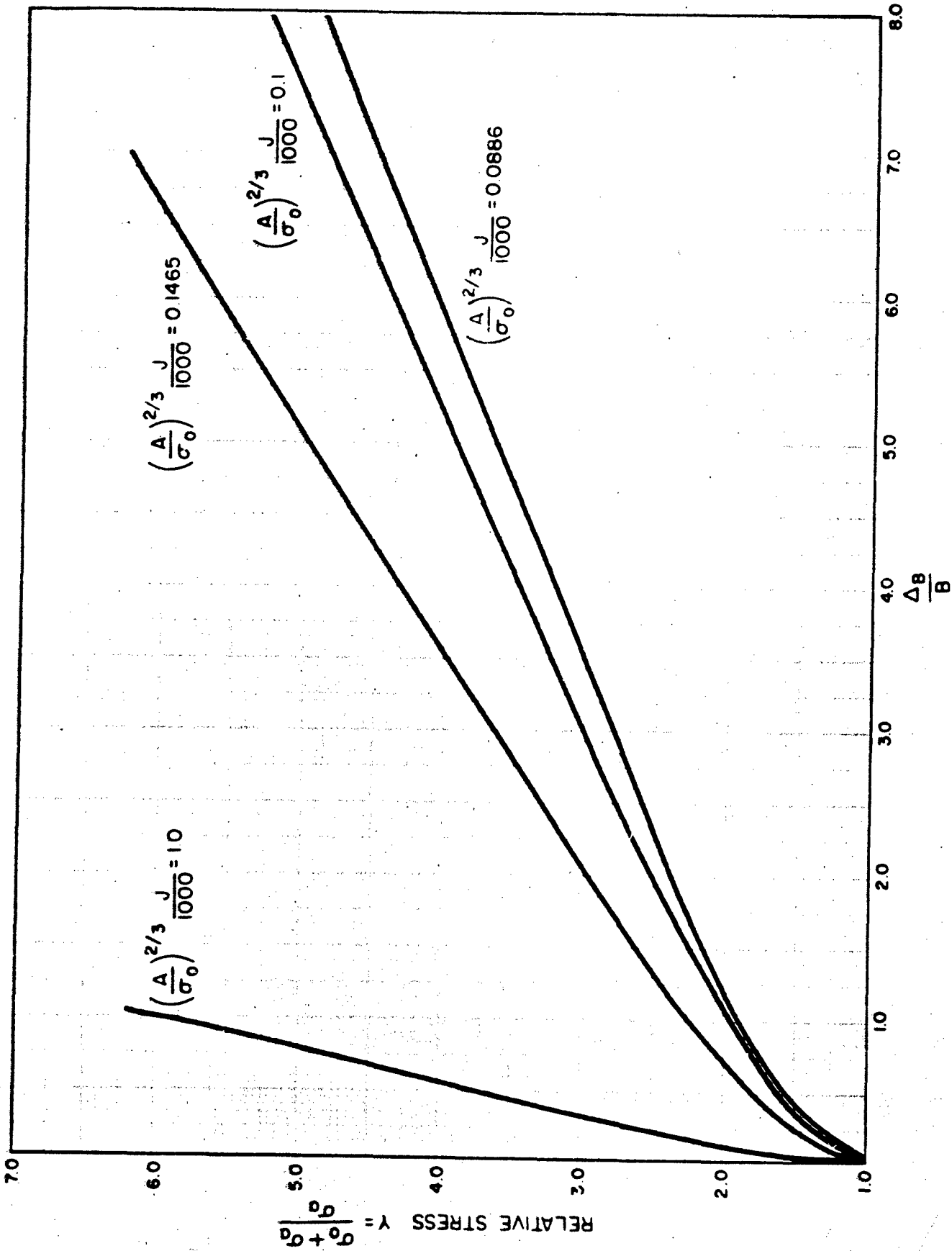


Fig. 31. Relationship of Differential Displacement per Unit Span ($\Delta B/B$) to the Overstress (Y) for a Range of $(A/\sigma_0)^{2/3}(J/\Delta B/B)$ Values for the Passive Case (Nonlinear Soil Conditions)

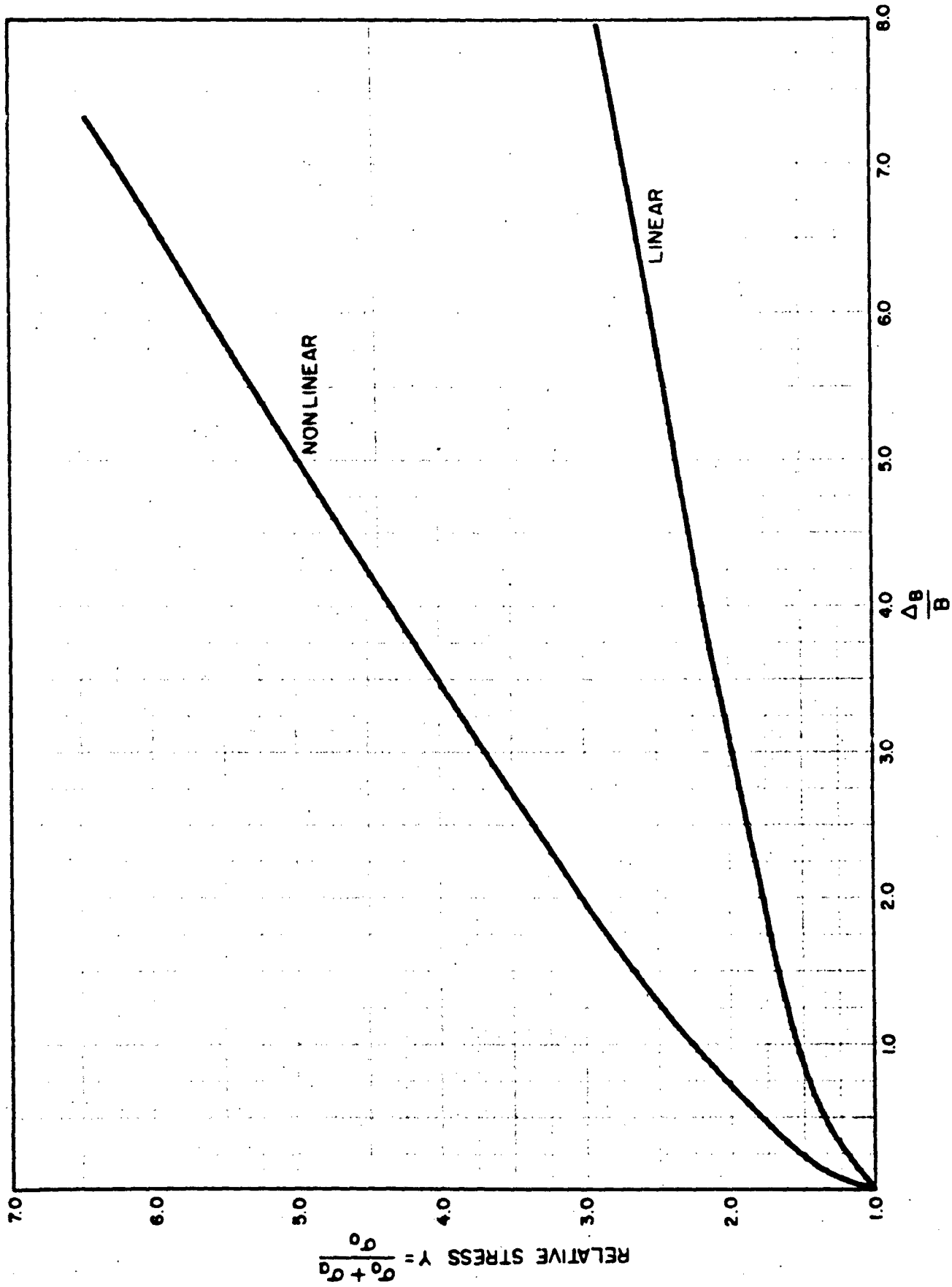


Fig. 32. Comparison Showing the Effect of Nonlinear Soil Conditions on the Relationship Between A_v/R and Overstress (V) for $(\Delta/\pi)^{2/3} (1/1000) - 0.145$

Since $(A/\sigma_o)^{2/3} J \Delta_B/B = M$ and $e^{\ln Y'} = Y'$, Eq. (108) becomes

$$M = \ln Y' + (Y')^{1/3} + \frac{1}{(Y')^{2/3}} \quad (109)$$

Figure 33 is a plot of the relationship for the active case between relative stress Y and of M , the product of the ratio of the soil parameter J to the free-field strain represented by $(A/\sigma_o)^{2/3}$ and the ratio of the differential displacement Δ_B to one-half the span B .

Expanding Eq. (109) into the original terms gives:

$$\frac{\Delta_B}{B} = \left(\frac{\sigma_o}{A}\right)^{2/3} \left(\frac{1}{2K \tan \alpha}\right) \left[\ln \left(\frac{\sigma_o}{\sigma_o - \sigma_a}\right) - \left(\frac{\sigma_o}{\sigma_o - \sigma_a}\right)^{1/3} + \frac{1}{\left(\frac{\sigma_o}{\sigma_o - \sigma_a}\right)^{2/3}} \right] \quad (110)$$

Figure 34 is a plot of the relationship between relative stress Y and the displacement-to-span ratio Δ_B/B for a range of $(A/\sigma_o)^{2/3} J/1000$ values.

Figure 35 shows the comparison of the linear and nonlinear active arching case for a constant $(A/\sigma_o)^{2/3} J/1000$ value.

Figure 36 is a plot showing the relationship of the active and passive, linear and nonlinear cases for a given $(A/\sigma_o)^{2/3} J/1000$ value.

It should be noted that in all cases the overburden and cohesion elements of the equations have been dropped for simplicity in developing the equations and because they were not relevant in comparison with the experimental results. It would be a relatively simple matter, after the development has gotten to the point of application to real structures, to include these terms.

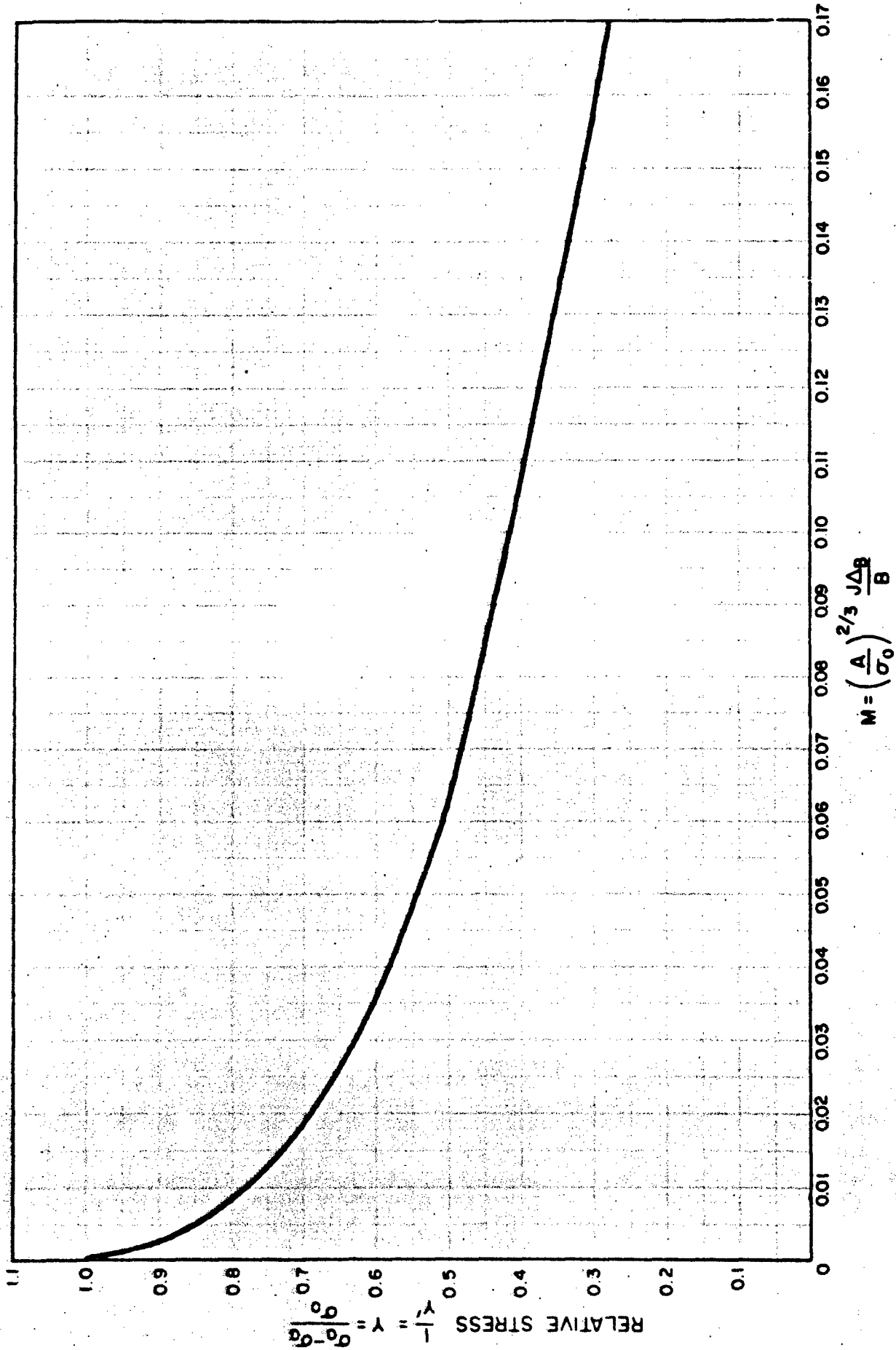


Fig. 33. Relationship Between M, i.e., $\left[\left(A/\sigma_0 \right)^{2/3} (J\Delta B/B) \right]$, and Understress Y for [Eq. (109)].

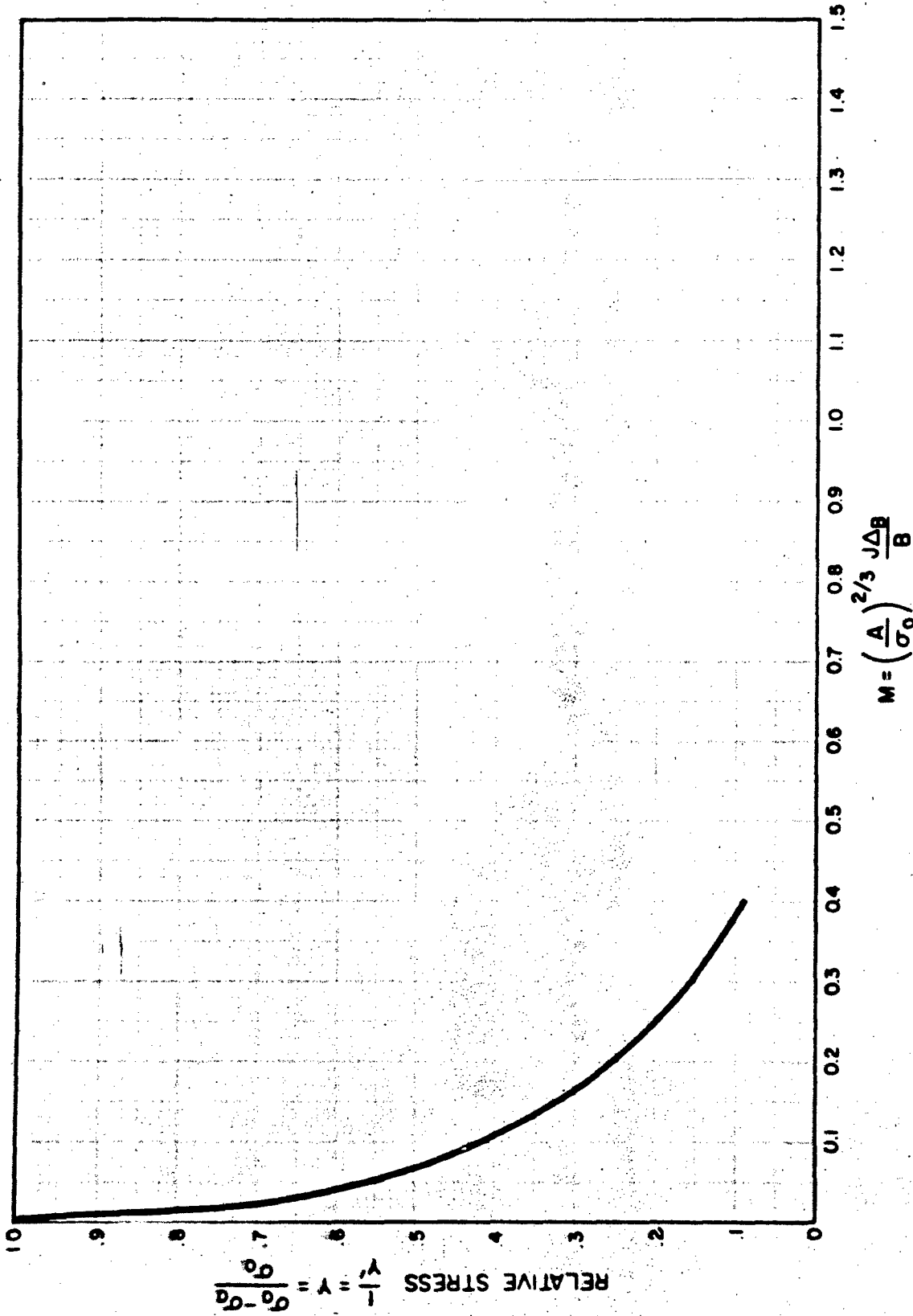


Fig. 33 (Cont.)

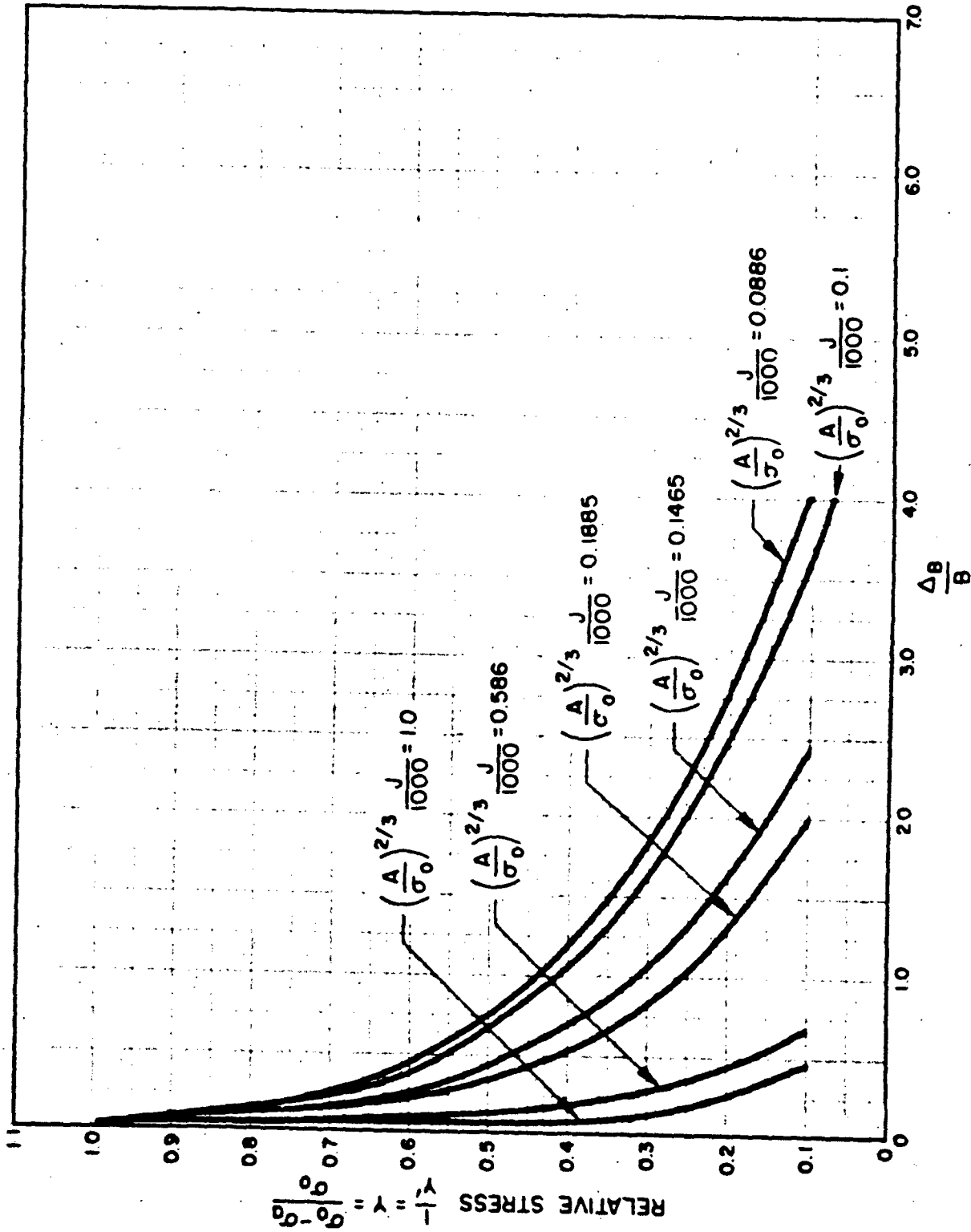


FIG. 34. Relationship of Differential Displacement per Unit Span ($\Delta B/B$) to the Understress (Y) for a Range of $(A/\sigma_0)^{2/3}(J/1000)$ Values for the Active Case (Nonlinear Soil Conditions)

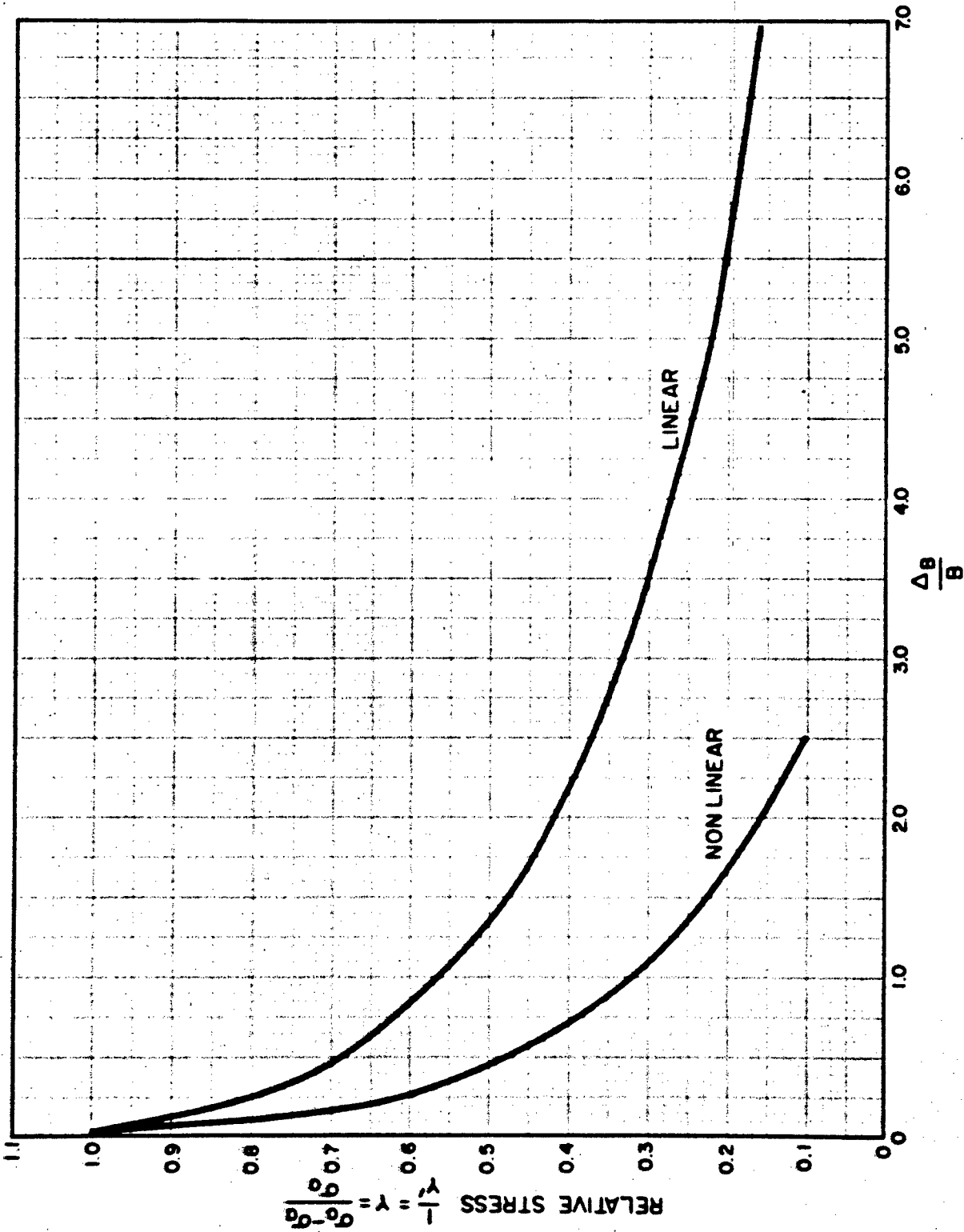


Fig. 35. Comparison Showing the Effect of Nonlinear Soil Conditions on the Relationship Between $\Delta B/B$ and Understress (Y) for $(A/\sigma_0)^{2/3} (J/1000) = 0.1465$ for the Active Case

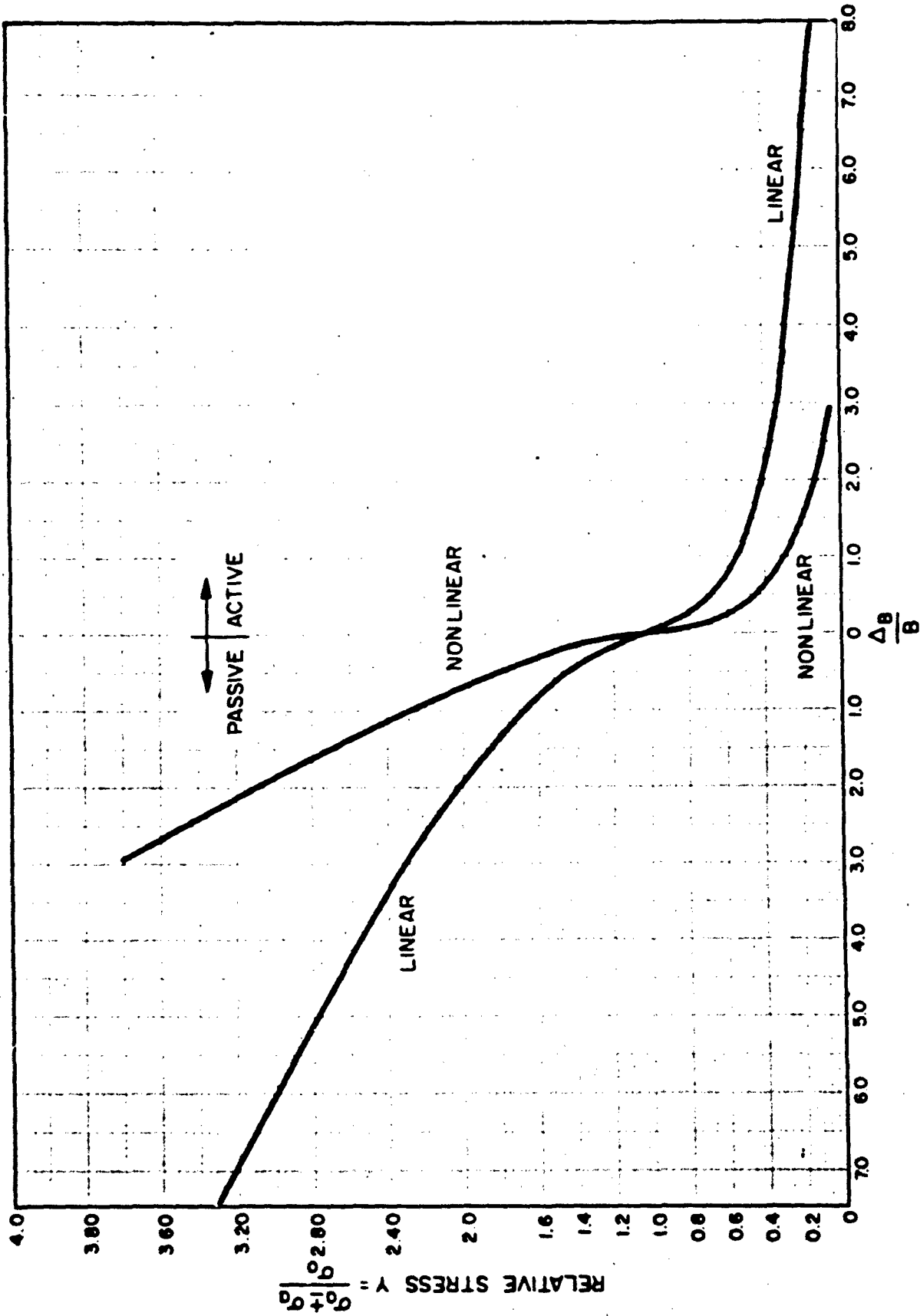


Fig. 36. Comparison Showing the Effect of Nonlinear Soil Conditions on the Relationship Between $\Delta B/B$ and Relative Stress (Y) for Constant $(A/\sigma_0)^{2/3} (J/1000)$ for the Active and Passive Cases

Section 7

COMPARISON OF THEORETICAL AND EXPERIMENTAL RESULTS

The real test of any theory is how well it fits experimental data, either in the laboratory or in the field. Predictions based on equations developed in the earlier parts of this report will be compared in this section with data obtained in the URS programs and with data presented in Refs. 10 and 11. Predictions of effects of structural length, compressibility, and differential displacements will be examined. With the exception of the structural length tests, the conditions covered are primarily confined to the deeply buried conditions* of soil-structure interaction, i.e., where the influence of interaction does not intersect the surface.

Excellent correlations are shown between the theory and the experimental results that were obtained from the studies of the effects of structural compressibility and of the differential displacement of a trap door. Meaningful correlations with the theory were not obtainable in the experimental investigation of the effects of structural length of rigid structures. However, since the theoretical relationships describing the effects of structural compressibility are simply extensions of those describing structure length, the lack of correlation is obviously the result of extraneous effects. In this case, it appears to be the influence of the surface, as will be discussed in a later section. The results of the structural-length study will be discussed first followed by discussions of those for the structural compressibility and for the trap door experiments.

STRUCTURAL LENGTH

Equations (27) and (69), derived for deeply buried rigid-structure conditions, are compared in Fig. 37 with the experimental data obtained

* Consideration of the shallow depth-of-burial conditions is undertaken where data are available and, in particular, where such considerations may account for a discrepancy between the predicted and the measured results.

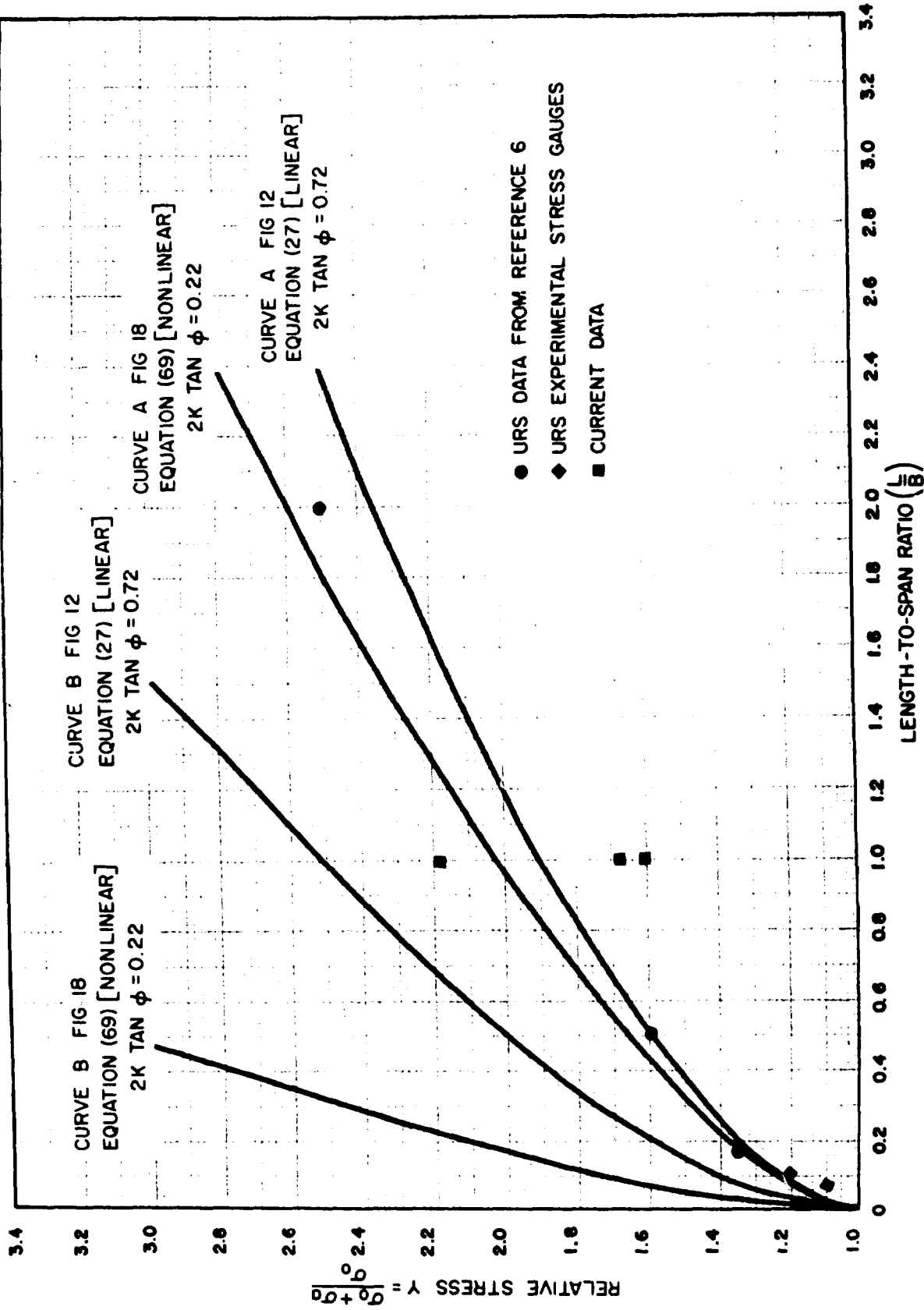


Fig. 37. Comparison of Experimental and Theoretical Results Indicating the Effect of Variations in Length-to-Span Ratio on the Load on the Structure

in the study reported in Ref. 6, with results obtained in the development of free-field stress gauges, and with the data taken in the experimental study encompassed by this contract. An examination of the data from Ref. 6 and the free-field stress gauges shows them to have been taken at the same actual depth of burial (3 in.), in similar soil conditions. Because, as will be discussed later, all the data appear to have been taken in a shallow depth-of-burial condition, the soil parameters used for the two "A" curves (Fig. 37) were arbitrarily chosen so as to bracket the data. Since the data do follow the general shape of the theoretical curves, they indicate that the theory is adequate to describe the behavior. However, the values of K and $\tan \phi$ used to compute both curves are less than the measured values of these parameters obtained in other laboratory tests. In fact, the "B" curves from Figs. 12 and 18 for the linear and nonlinear cases shown on Fig. 37 are obtained by means of the measured values.

The data obtained during this contract show a large range of values on either side of the curves which bound the other data. Although the tests were to have been conducted in the deeply buried condition, an examination of the data shows that this apparently was not true, since the load on the structure increased with an increase in depth of burial, which fact is indicative of shallow burial. The lower two points (A and B) represent a depth of burial of 5 in., i.e., a Z/B of $5/3$, while the upper point (C) represents a depth of burial of 8 in., i.e., a Z/B of $8/3$. Since the experimental program was a limited effort and its major purpose was to investigate the effects of compressibility, no further tests at greater depth were conducted. The assumption that these data were influenced by the surface conditions, which might account for the discrepancy of the K and $\tan \phi$ values required to fit the data, will be discussed further in the section on surface layer effects.

The only other data known which show the effect of structural length are those presented in a gauge study using the Goldbeck pressure cell; the results of this study are reported in Ref. 10. Since no soil data

were available, they were backfigured* from a single point on the experimental data curve. With these values, the linear and nonlinear curves on Fig. 38 were computed for various L/B values. Again, a reasonable correlation appears to exist.

STRUCTURAL COMPRESSIBILITY

Since Eqs. (35), (87), (61), and (97) were developed to account for the effect of structural compressibility in deeply buried conditions, the literature was searched for experimental results with which to compare the theory. Since none was found in which the soil and structural parameters were sufficiently controlled to make a comparison, URS undertook a limited experimental program.** The program consisted of testing an idealized structure 6 in. in diameter and 6 in. long (see Fig. 77, Appendix A). Two 1-in.-thick end plates containing a series of flush-mounted stress gauges, were separated by a replaceable thin-walled cylinder, which provided the uniform compressibility*** of the structure. The compressibility of the structure was measured by means of a linear variable differential transformer. The structure was buried 5 in. below the surface in 20-30 Ottawa sand placed at approximately 108 pcf in the URS Long Duration Dynamic Loader (LDDL).**** The sample surface was then uniformly loaded to 45 psi with a step pulse having a rise time of approximately 1 msec.*****

An examination of the development of the compressibility equations shows that one basic assumption was made in all cases; that is, that the

* To compute the $2K \tan \phi$ value at a point on the experimental curve, the L/B and Y values read for that point were substituted into Eqs. (27) and (69). Solving for $2K \tan \phi$ resulted in values of 0.72 for the linear and 0.22 for the nonlinear cases.

** A more detailed discussion of the experimental program is given in Appendix A.

*** By uniform compressibility is meant that the entire end-plate faces compress uniformly in the direction of loading.

**** A description of the LDDL is given in Ref. 6.

***** Although the loading was a dynamic load, comparisons were made between the equilibrium values and the static theoretical solutions.

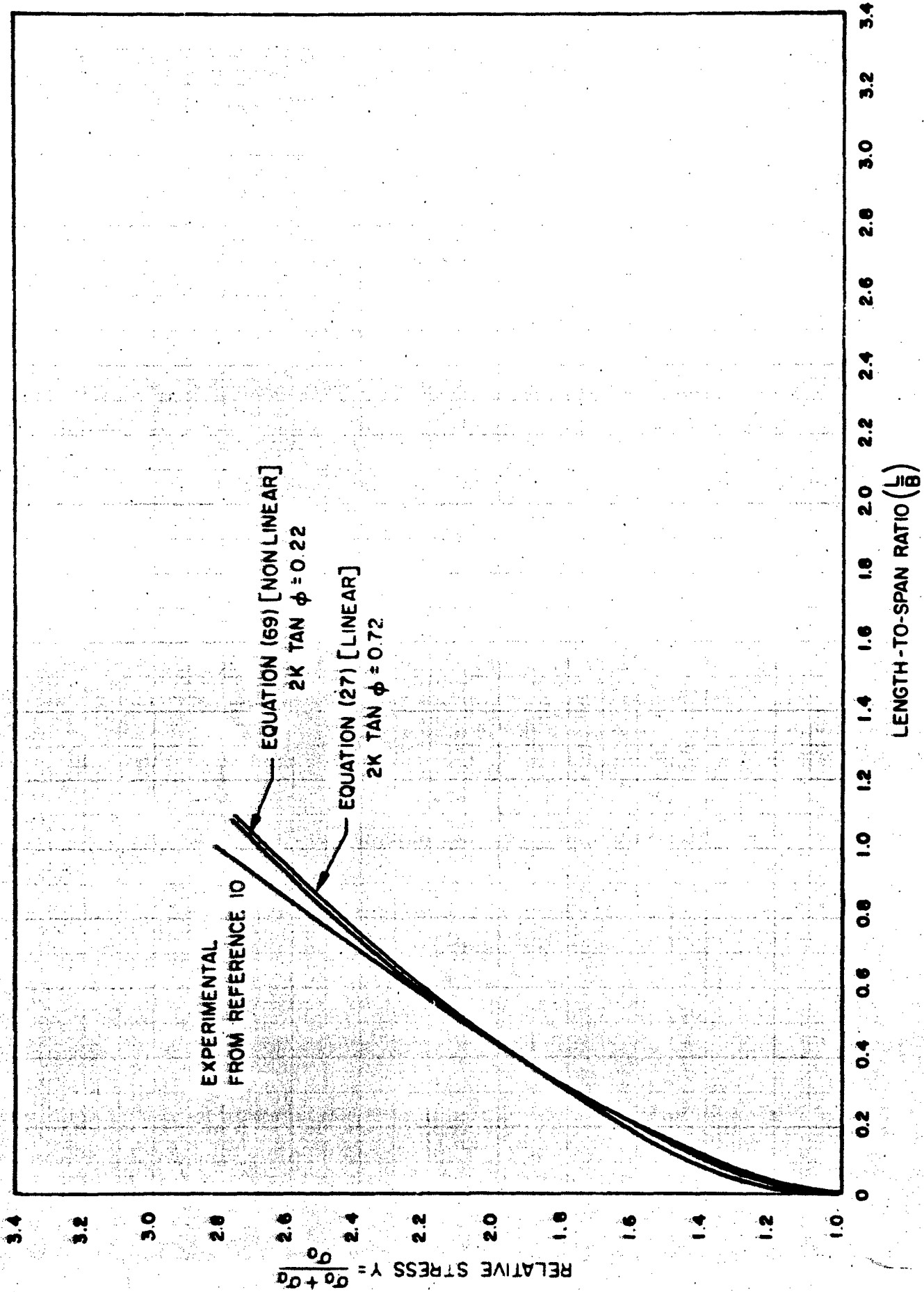


Fig. 38. Comparison of Theoretical Results with the Experimental Results From Experiments Employing the Calibrated Cell showing the effect of ϕ on the results.

entire load $\sigma_o + \sigma_a$ applied to the surface of the structure was transmitted to the soil beneath the structure, i.e., it was assumed that there were no effects of sidewall friction on the sides of the structure.

It was realized, however, that this condition was impractical to achieve experimentally, since in real soil conditions, it is only possible to reduce this friction, not to eliminate it. Attempts were made to reduce the sidewall friction and, in addition, an attempt was made to calculate the resulting value.

SIDEWALL FRICTION

Three methods of treatment were tried on the sidewalls of the structure in an attempt to reduce the friction: two continuous layers of 0.005-in.-thick teflon sheets over the entire length; two layers of 0.005-in.-thick teflon, the bottom layer continuous and the top layer in 1-in.-wide overlapping segments, and a grease layer covered with a thin rubber sheet. The effectiveness of these treatments in reducing the sidewall friction effects varied. The two continuous teflon sheets had the effect of appreciably reducing sidewall friction. However, the effect was intermittent. When the outer layer was segmented, the intermittent effect was overcome. The grease-and-rubber treatment had about the same effect as the segmented layer but was easier to use.

In order to take into account the effect of sidewall friction, it was assumed that a shear plane developed along the sides of the structure, i.e., that sidewall friction developed between the soil and the structure along the entire length of the structure. It was further assumed that the free-field stress conditions existed along that plane and that any change in ϕ' along the interface would not change the K value of the soil. The total force on the structure due to sidewall friction alone can be calculated by summing the incremental forces over the entire sidewall surface, i.e.,

$$\tau = (K \tan \phi' \sigma_o) (\pi^2 B^2 L) \quad (111)$$

or

$$= 4K \tan \phi' \sigma_o \pi B L \quad (111a)$$

where φ' is the friction angle* between the soil and the wall. In order to apply this effect as an average stress on the top surface of the structure, Eq. (111a) must be divided by the area of the end plate, i.e.,

$$\sigma_{\tau} = \frac{4K \tan \varphi' \sigma_o \pi B L}{\pi B^2} \quad (112)$$

Equation (112) then reduces to

$$\sigma_{\tau} = \frac{4K \tan \varphi' \sigma_o L}{B} \quad (113)$$

It can be seen that if the compressibility (effective modulus) of the structure is considered without regard to sidewall friction, it is related to the load and deformation in the following manner:

$$E_{ST} = \frac{\sigma_o + \sigma_a}{\Delta_{ST}} (2L) \quad (114)$$

where $\sigma_o + \sigma_a$ over the area is the force required to compress the structure an amount Δ_{ST} . If, on the other hand, sidewall friction is considered, it can be seen that the compressibility of the structure is still related to the load $\sigma_o + \sigma_a$ and the deformation Δ_{ST} in the same manner. However, the load applied to the upper surface must be $\sigma_o + \sigma_a + \sigma_{\tau}$, being resisted by the soil stress $\sigma_o + \sigma_a$ on the bottom surface plus the sidewall friction on the sides. Therefore, if the measured stress on the top surface is divided by the deformation, the effective modulus as computed by Eq. (115) appears greater than it really is, i.e., as computed by Eq. (114),

$$E_{ST} = \frac{\sigma_o + \sigma_a + \sigma_{\tau}}{\Delta_{ST}} (2L) \quad (115)$$

Therefore, σ_{τ} ** was subtracted from the measured stress before the structure modulus was computed for use in Eqs. (35) and (87). These values for

* When the friction between the soil and the wall is greater than the internal friction in the soil then the φ of the soil is used instead of φ' .

** The φ' values used in making this calculation were obtained from other tests at URS on the effects of sidewall friction in soil containers (Ref. 5).

structure modulus agreed very well with measured values for the structure in the unburied condition.

RESULTS

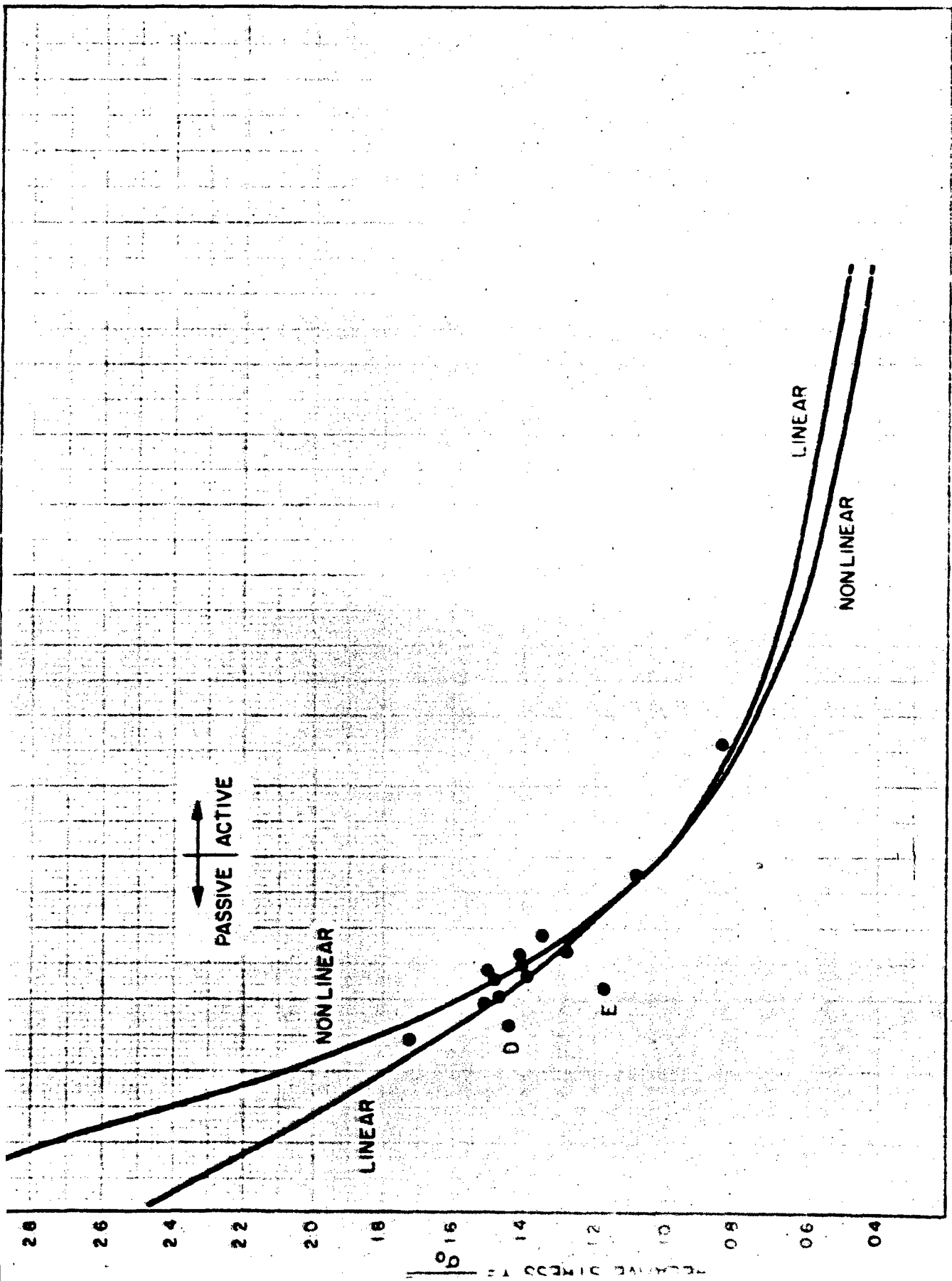
An examination of the data points obtained in this study for the deeply buried condition, and presented in Fig. 39 shows an excellent agreement with the theory. In plotting the data, the structure modulus E_{ST} was computed from the measured stress and displacement of the structure as described above. The soil modulus was obtained from the stress-strain curve (for the soil) developed under another URS program and reported in Ref. 3. The stress-strain curve is reproduced here as Fig. 40. Using these values for the soil and structural moduli, values of relative compressibility C_r were computed for each test* and plotted in Fig. 39 against the measured relative stress. Also plotted in this figure is the theoretical relationship for linear [Eqs. (35) and (61)] and the nonlinear [Eqs. (87) and (97)] soil conditions. The theoretical curves were computed by means of the K and $\tan \phi$ values measured in other laboratory tests. As can be seen, the measured data obtained in this program vary less than ± 10 percent from the theoretical curve for the nonlinear soil conditions.

Two of the points require further discussion. Points D and E fall off the theoretical curve, and although the cause was not identified, it was obviously related to some extraneous behavior, as evidenced by the measured stress and deflection time histories given in Fig. 41.**

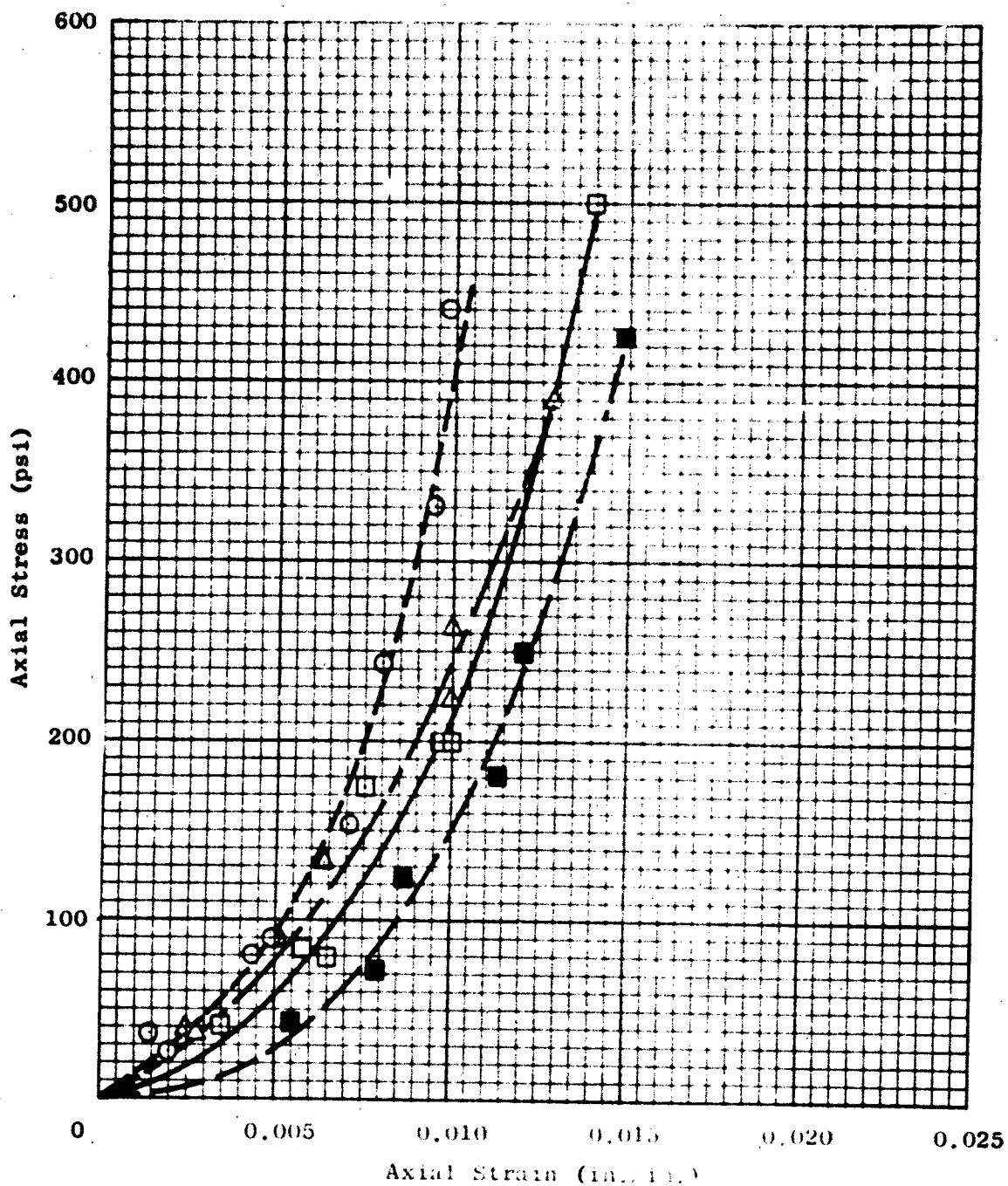
As can be seen from the data points given in Fig. 39, extreme difficulty was experienced in trying to fabricate a structure more compressible than the soil. This situation was true despite the fact that the

* All tests were first loading of the sample.

** The upper trace in Fig. 41a is a typical displacement-time curve for the tests whose results fall on the theoretical curve, while the upper trace in Fig. 41b is typical of the displacement-time trace for tests represented by points D and E. The lower traces in each figure are the stress-time history traces for one of the stress gauges on the upper face of the structure.



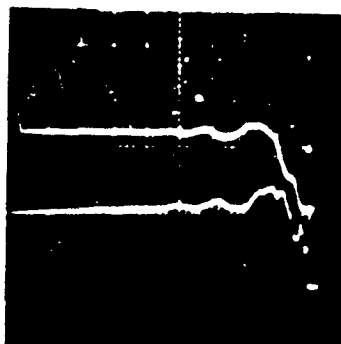
0013 013 10 20
0013 013 10 20



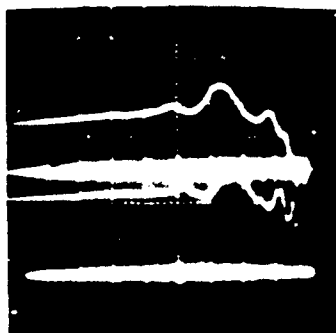
Legend:

- | | | |
|---|-------------------------|------------------------------------|
| □ | 20-30 Ottawa sand | $Y = 111.0 \text{ pci}$ (RD = 90%) |
| ■ | 20-30 Ottawa sand | $Y = 103.5 \text{ pci}$ (RD = 60%) |
| ○ | Cooks Bayou sand | $Y = 107.5 \text{ pci}$ (RD = 80%) |
| △ | Reid Bedford Model sand | $Y = 98.5 \text{ pci}$ (RD = 70%) |

Fig. 40. Stress-Strain Curves for Granular Media
(From Fig. 6, Ref. 3)



- (a) Upper Trace: Typical structure displacement-time history trace
Lower Trace: Typical stress gauge-time history trace



- (b) Upper Trace: Structure displacement-time history trace for points D and E
Lower Trace: Typical stress gauge-time history trace

Fig. 41. Structural Displacement, On-Structure Stress-Time Histories

sand was in a dense condition (approximately 85 percent relative density). Only one data point is presented for the circumstance in which the structure was more compressible, and that point represents the measurements just before the thin-walled cylinder separating the rigid end-plates buckled. However that point is in good agreement with the theoretical curve.

Two explanations have been postulated regarding the cause of the problem of fabricating a more compressible structure. First, if the structure has a response time* that is long compared to the rise time of the stress pulse,** then initially the load on the structure will be comparable to that resulting from a much stiffer structure. Therefore, in the case of a structure of high compressibility, i.e., one designed for large displacements under low relative stress, the stresses exceed those of the design, and the structure collapses. The second explanation has to do with the effect sidewall friction has on the effective modulus of the structure. Even though every effort was made to reduce its magnitude, it played an important part in the behavior as discussed above. In fact, in the case of the more compressible structure, where the relative stress is low, the average stress due to sidewall friction becomes large in proportion to the relative stress. Both of these behaviors could be very important in real structures as well.

DIFFERENTIAL DISPLACEMENT (Trap Door Experiments)

Passive Arching Case

As stated earlier, the basic theories developed in this report are founded on the principle of stress redistribution caused by differential displacement occurring between the soil and the structure. An examination of the trap door theory is therefore pertinent since it also involved differential displacement. The intent at this point is to compare experimental

* In these tests the structure had a response time of approximately 6 msec as compared to a rise time of the stress pulse of approximately 1.5 msec.

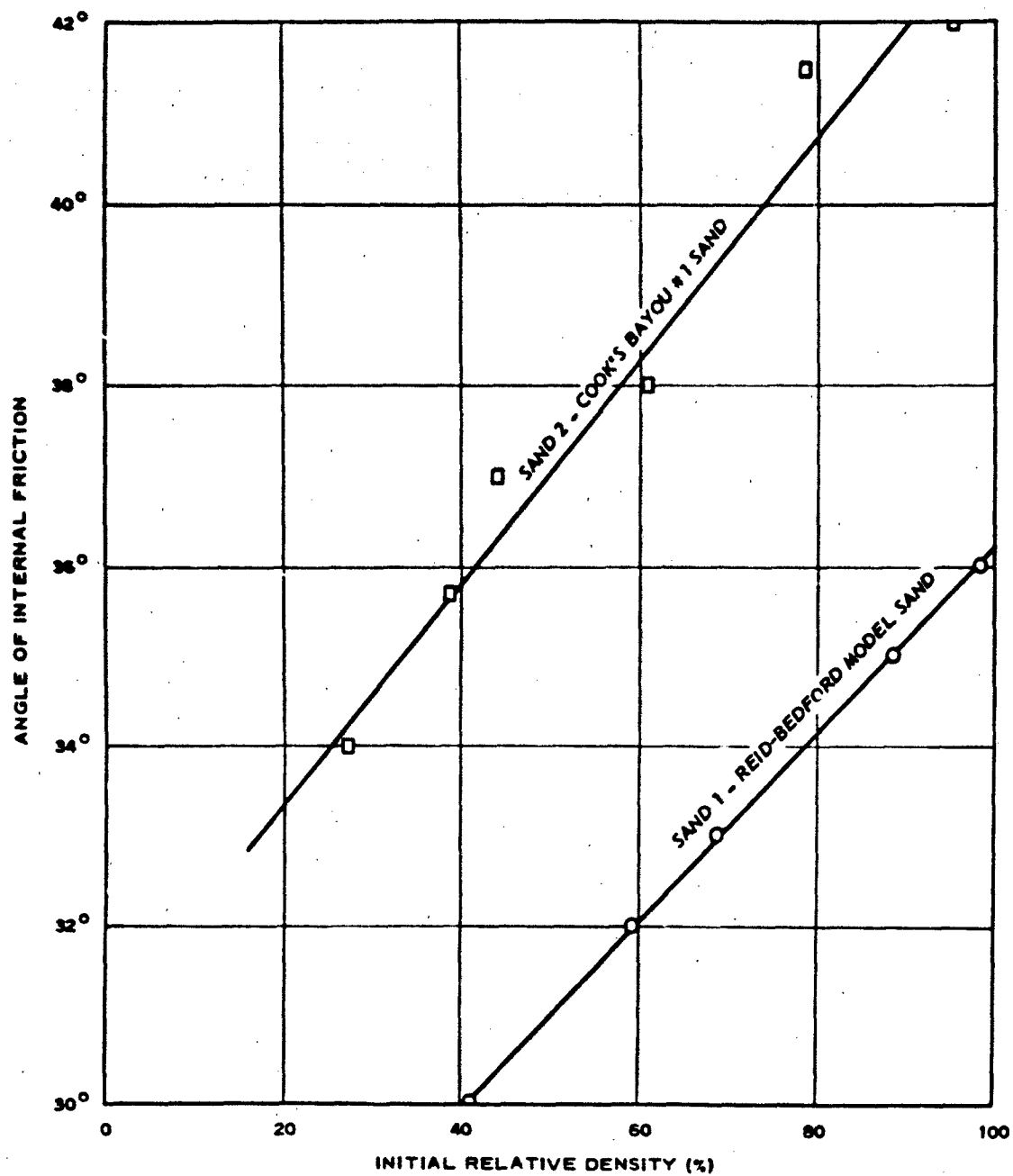
** Although comparisons were made between the static theory and equilibrium values, the loading was a dynamic one and therefore, this factor played a part in the observed behavior.

and theoretical results for a trap door experiment. A review of the literature revealed a well-documented experimental study of both active and passive trap door conditions (Ref. 11).

The test apparatus consisted of a 4-ft.-diameter cylindrical test chamber of variable height, with a specially constructed lower base provided with a flush-mounted-type trap door. An upper bonnet provided a means of applying static overpressure to the soil sample. The piston-type trap door was centrally located and was designed to provide a rigid plate parallel to the surface with a minimum vertical frictional resistance and tilting under the test load. The piston was mounted on a hydraulic jack which provided control of the vertical motion. During sand placement and assembly of the bonnet, and movement of the trap door relative to the bottom of the soil bin was carefully monitored. As needed during this operation as well as during subsequent application of the surface air overpressure, the jack was adjusted to maintain the top surface of the piston flush with the bottom of the soil bin. After the desired overpressure was reached, the jack was raised or lowered to induce active or passive arching in the sand. The total force on the piston was then recorded.

In addition, the soil conditions were well documented, making it possible to compare the theory previously presented* with the experimental results reported in Ref. 11. Two sands were tested; No. 1 was a clean, uniform, fine-grained dry sand referred to as Reid-Bedford Model sand; No. 2 was a clean, graded, medium-to-fine grained local dry sand referred to as Cooks Bayou No. 1. Figure 3.10 of Ref. 11 reproduced here as Fig. 42, shows the various properties of the two soils for a number of initial dry density conditions. Figures 43 and 44 show the stress-strain relationships for the two soils for various initial dry density conditions. The tests were conducted principally at 75 psi surface overpressure, however, a few were conducted at 40 psi and 110 psi. The initial density of No. 1 sand used in the active arching tests varied from 98.3 to 101.1 pcf (average of 100.0 pcf), while No. 2 sand varied from 104.2 to 108.4 pcf (average of 106.1 pcf). In the passive arching tests only No. 2 sand was used, and the initial density varied from 105.0 to 107.6 pcf (average of 105.9 pcf).

* See Section 6.



SAND 1	0.92	0.85	0.78	0.71	0.64	0.57
SAND 2	0.77	0.71	0.65	0.60	0.54	0.49
INITIAL VOID RATIO						
SAND 1	86.0	89.9	93.7	97.6	101.4	105.3
SAND 2	93.3	96.8	100.3	103.8	107.3	110.8
INITIAL DRY DENSITY (PCF)						

Fig. 42. The Relation Between Angle of Internal Friction and Density for the Sands Tested (From Fig. 3.10, Ref. 11)

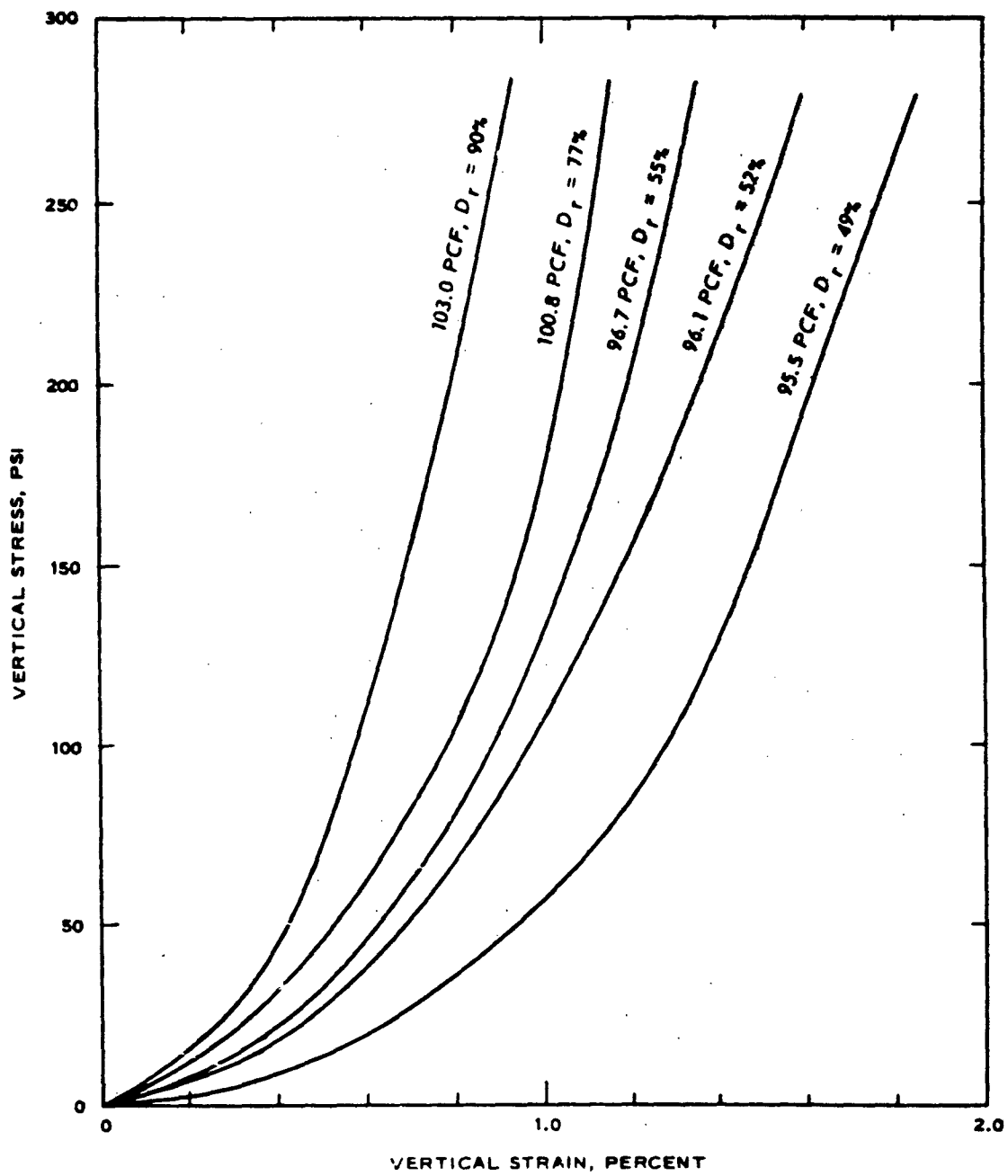


Fig. 43. Comparison of One-Dimensional Loading Curves for Sand 1 (From Fig. 3.12, Ref. 11)

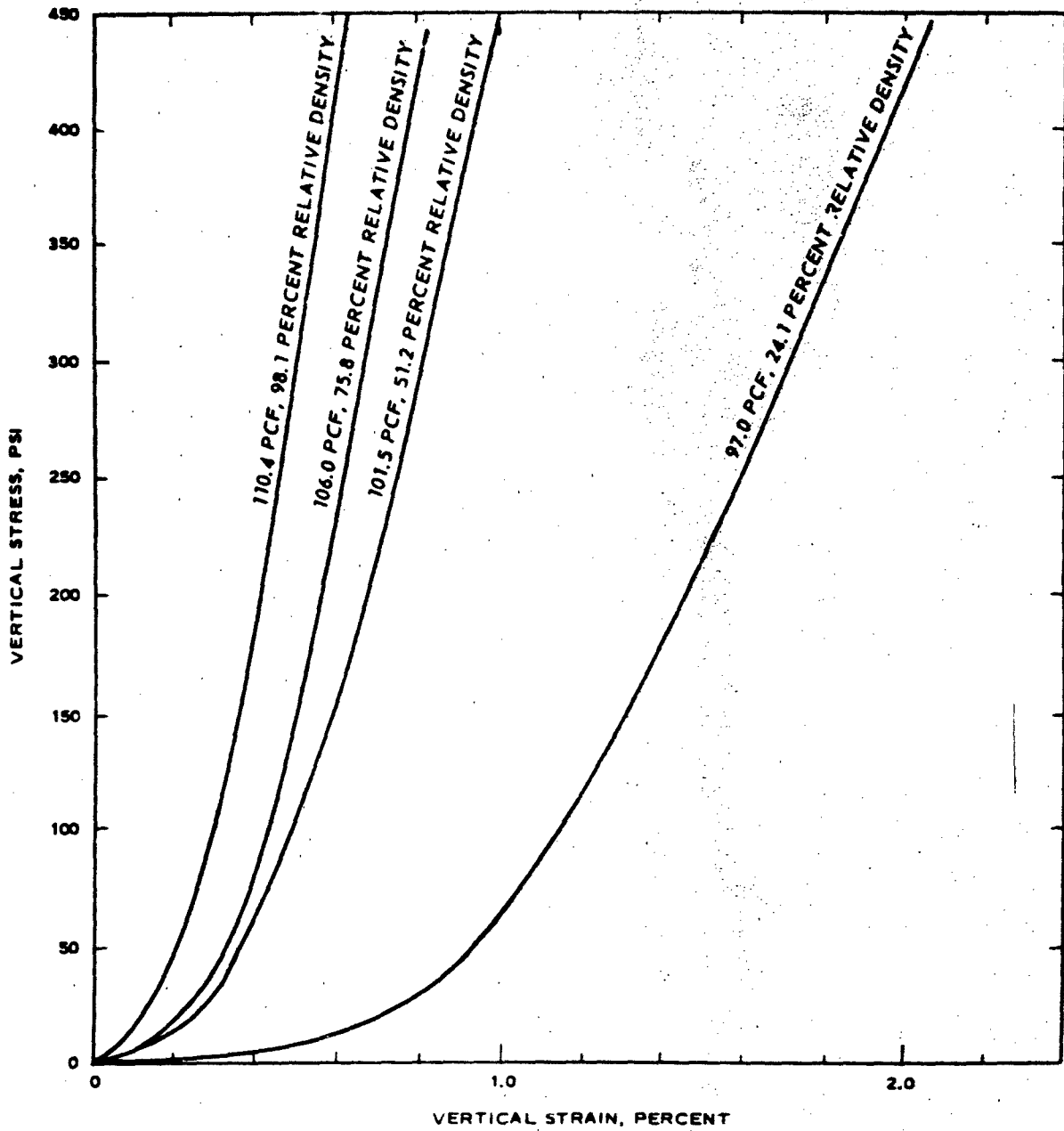


Fig. 44. Comparison of One-Dimensional Loading Curves for Sand 2
(From Fig. 3.15, Ref. 11)

In comparing the theoretical and experimental results, sand No. 2 will be considered first, since both active and passive arching tests were performed on this material. From Fig. 44 a strain value was read for the 75-psi stress level on a hypothetical curve representing an initial density of 105.9 pcf (the average value for the passive arching test). Using Eq. (62) below an A value was calculated

$$\sigma = Ae^{3/2} \quad (62)$$

From Fig. 42 an angle of internal friction of 40 deg was obtained for a density of 105.9 pcf.

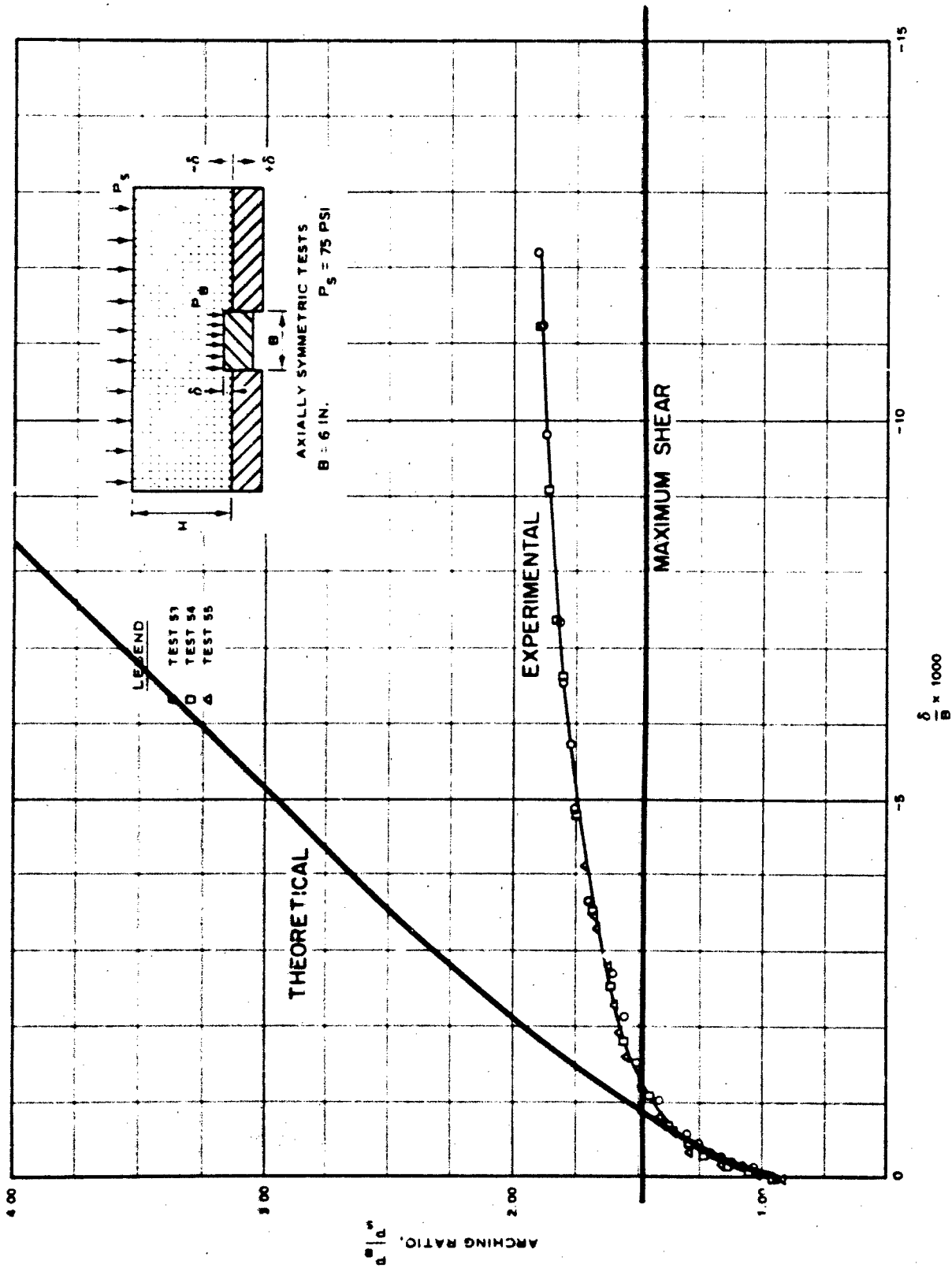
An examination of Eq. (105), which is for the passive arching case with nonlinear soil conditions, shows that the only other parameter required is K, the ratio of lateral to axial stress.

$$\frac{\Delta}{B} = \left(\frac{\sigma}{A}\right)^{2/3} \left(\frac{1}{2K \tan \phi}\right) \left(\frac{\sigma_o + \sigma_a}{\sigma_o}\right)^{2/3} - \left(\frac{1}{\frac{\sigma_o + \sigma_a}{\sigma_o}}\right)^{1/3} - \ln \frac{\sigma_o + \sigma_a}{\sigma_o} \quad (105)$$

The particular sands used in these tests were two on which URS had conducted one-dimensional compression tests for Waterways Experiment Station and on which K values were measured. Therefore, a K of 0.35* was used.

Using these soil parameters in Eq. (105) and correcting for the fact that at Δ/B equals zero, the arching ratio was not always 1.0, the theoretical curves in Figs. 45 through 52 were obtained. Equation (105) was written for the case where the depth of cover was greater than the zone of influence, i.e., deeply buried. Therefore, one would expect that since the zone of influence will increase with an increase in differential deformation, Δ/B , for a given depth of burial the theoretical curve of relative stress (Y) versus (Δ/B) would initially follow the experimental curve fairly closely as Δ/B increased. This would

* In addition if K is calculated from Jaky's equation $K = 1 - \sin \phi$, a value of 0.357 is obtained.



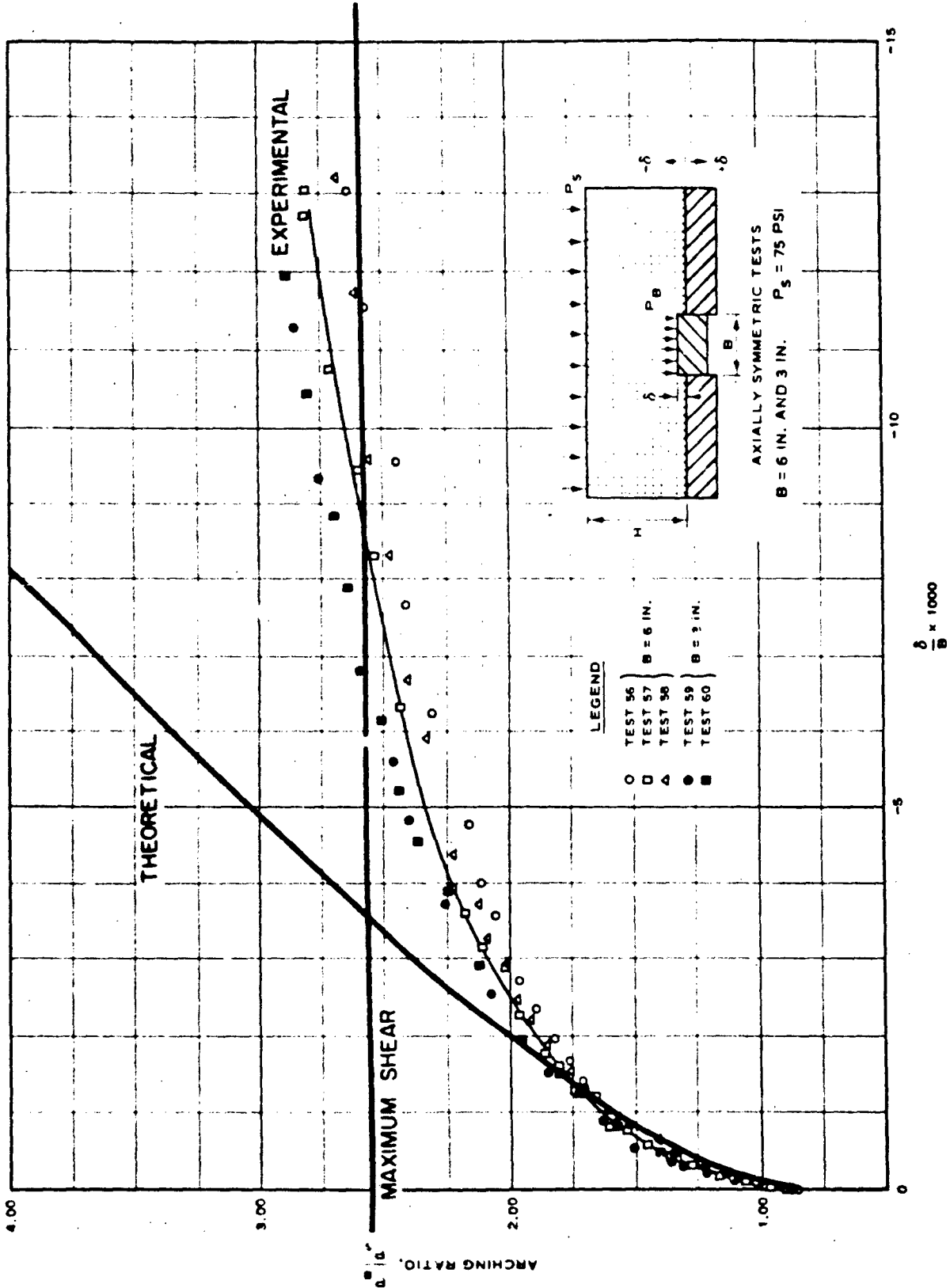


Fig. 46. Dimensionless Plot of Pressure vs Deflection for Passive Arching Tests With Sand 2, H/B = 2/3, P_s = 75 psi (From Fig. 4.19. Ref. 11)

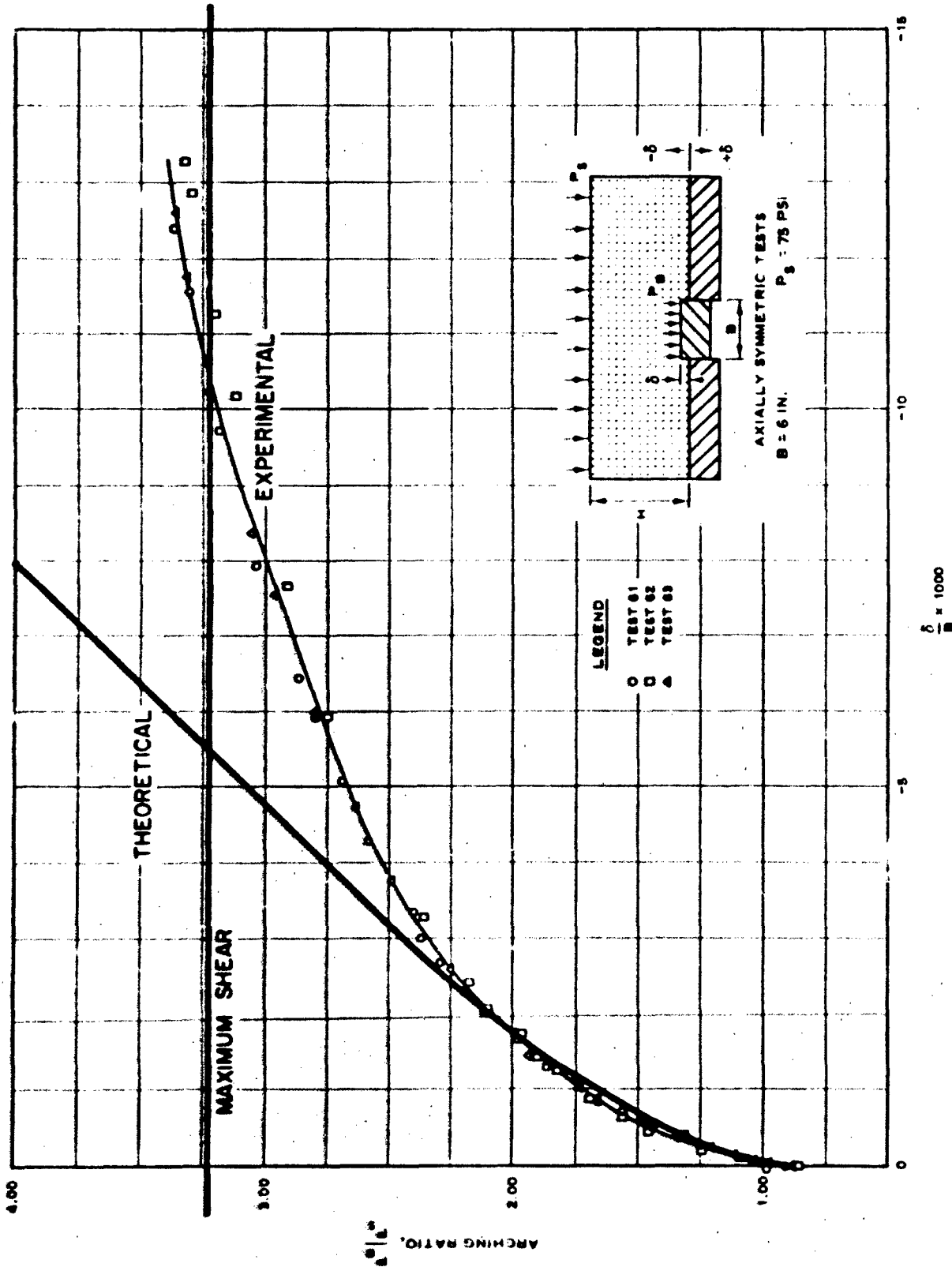


Fig. 47. Dimensionless Plot of Pressure vs Deflection for Passive Arching Tests With Sand 2, $H/B = 1$, $P_s = 75$ psi (From Fig. 4.20, Ref. 11)

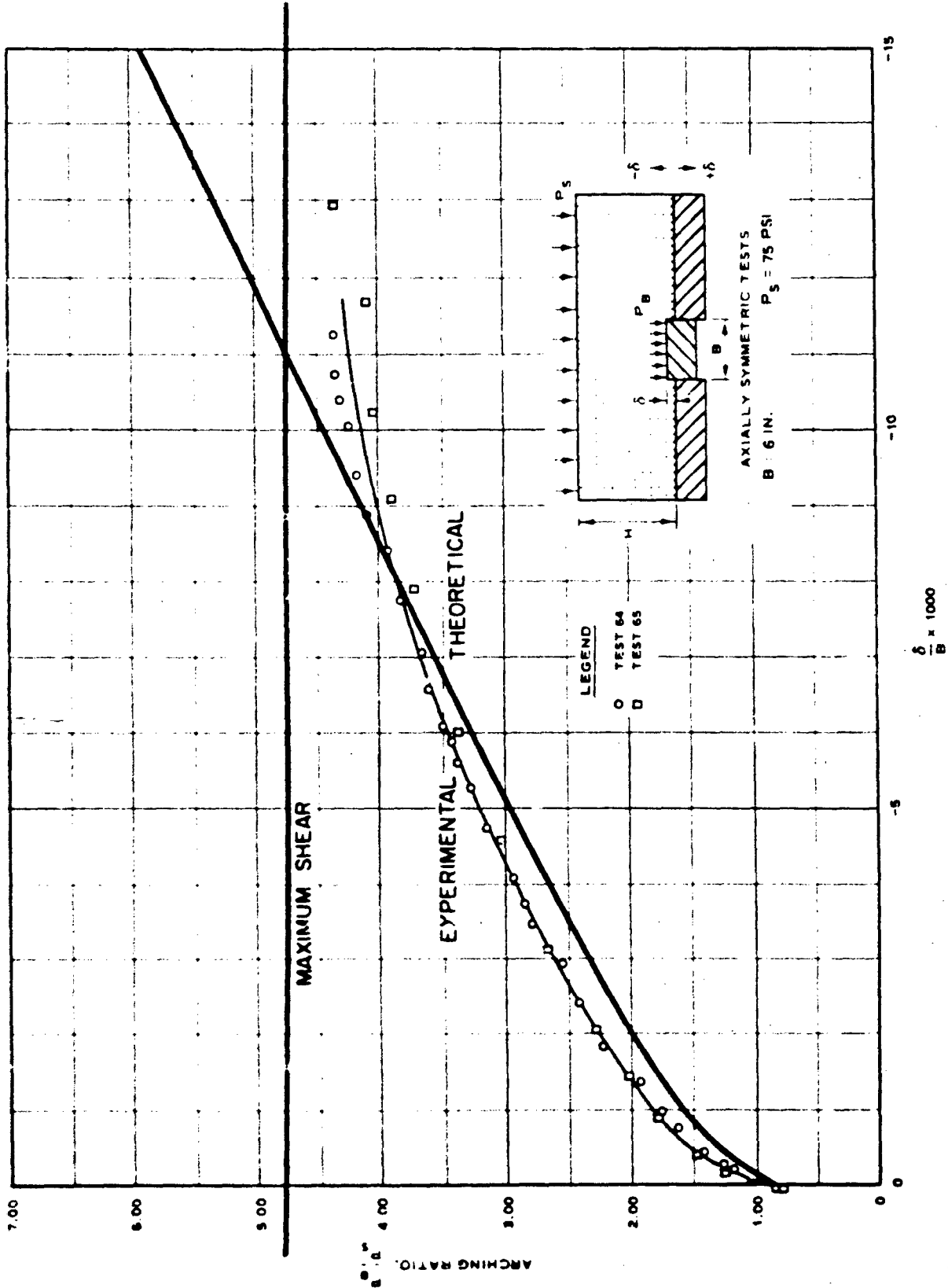
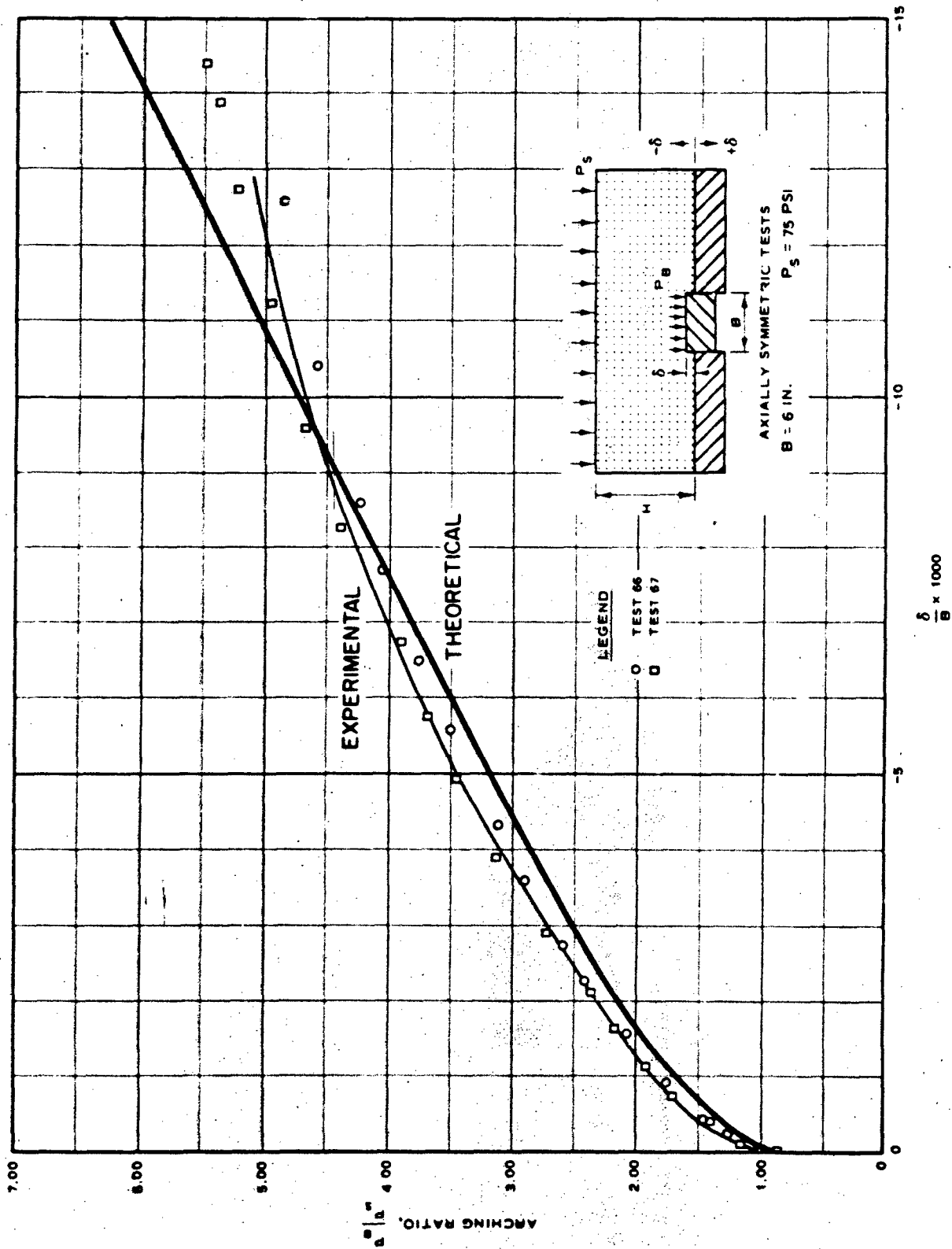


Fig. 48. Dimensionless Plot of Pressure vs Deflection for Passive Arching Tests With Sand 2, H/B = 1-1/3, P_c = 75 psi (From Fig. 4.21, Ref. 11)



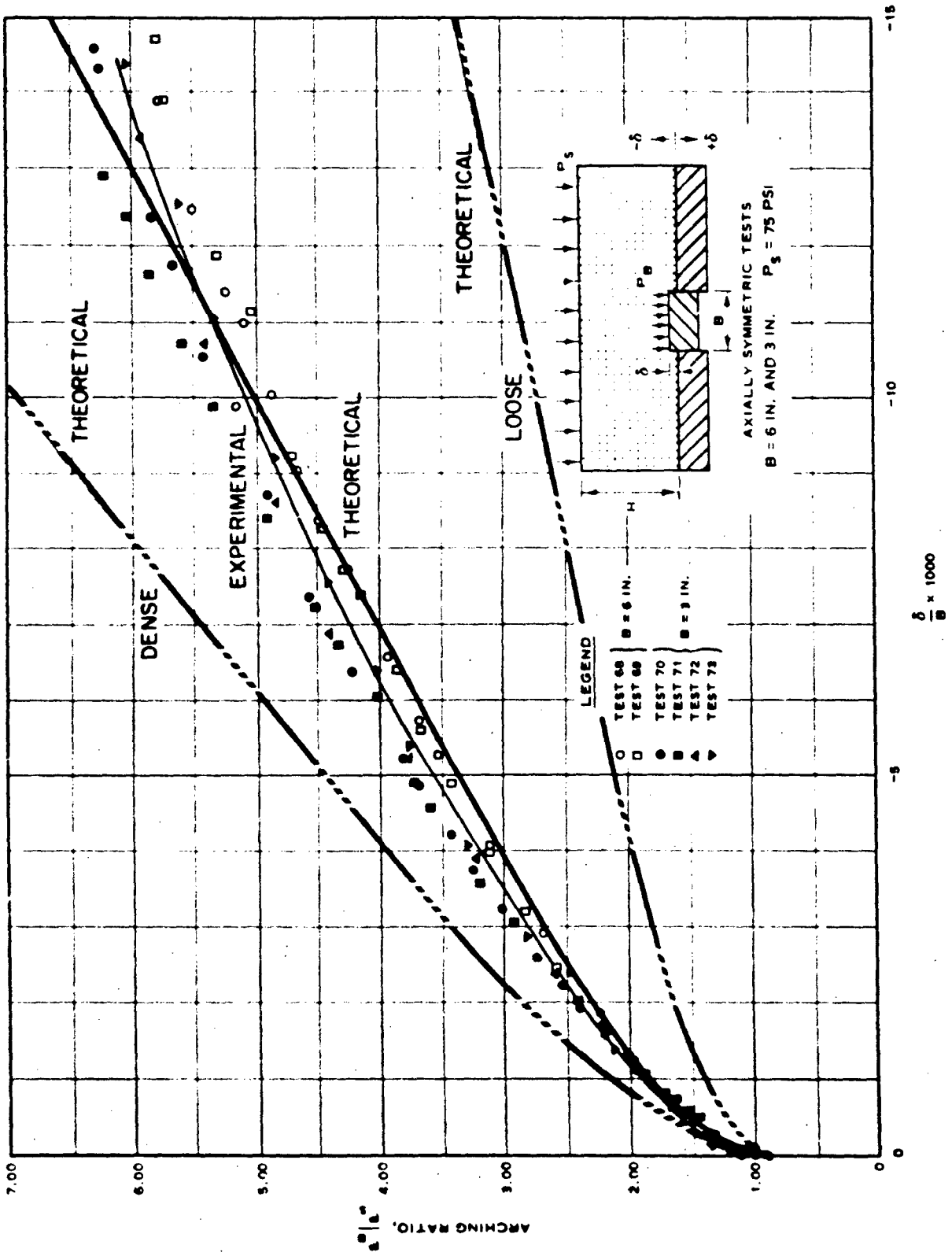


Fig. 50. Dimensionless Plot of Pressure vs Deflection for Passive Arching Tests with Sand 2, $H/B = 2$, $P_s = 75$ psi (From Fig. 4.23, Ref. 11)

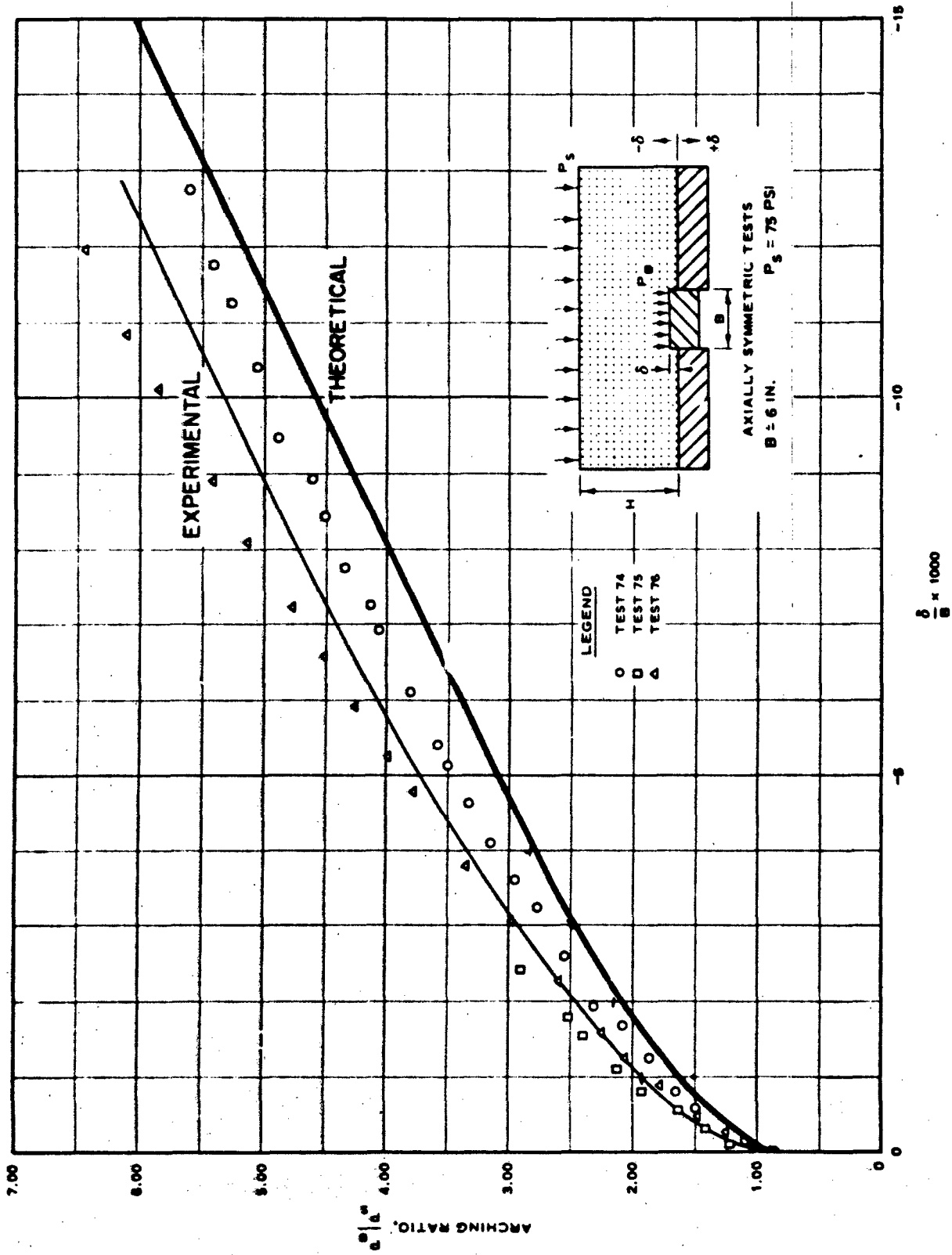


Fig. 51. Dimensionless Plot of Pressure vs Deflection for Passive Arching tests With Sand 2.

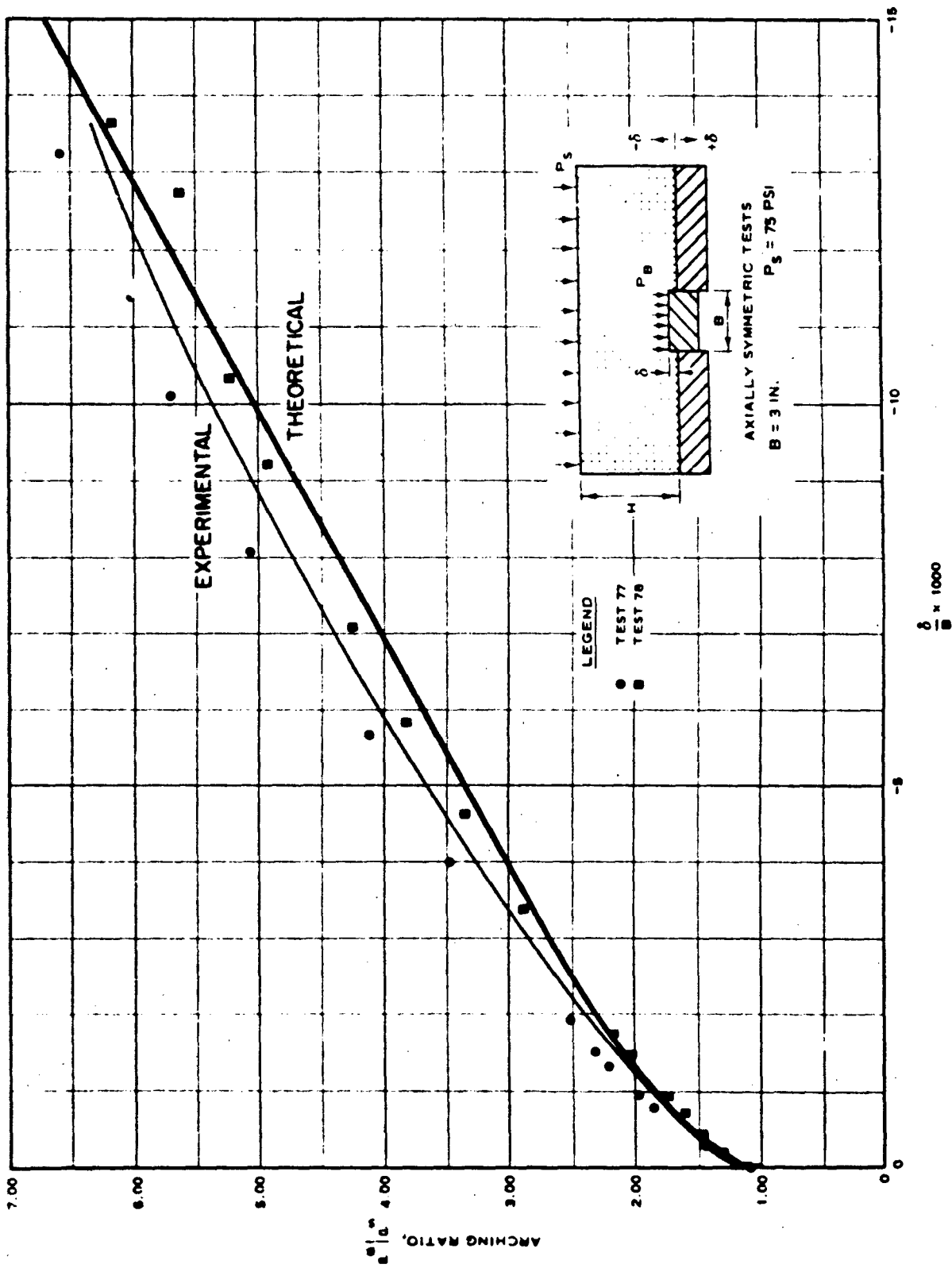


Fig. 52. Dimensionless Plot of Pressure vs Deflection for Passive Arching Tests With Sand 2, $H/B = 2-2/3$, $P_s = 75 \text{ psi}$ (From Fig. 4.25, Ref. 11)

continue until the zone of influence Z_1 equaled the depth of burial Z , at which point the relative stress (γ) would have reached a maximum and would not increase with additional Δ_B/B movements. The value of this maximum relative stress can be computed from Eq. (4a) since it represents the case where the maximum shear forces have been developed.

$$\sigma_v = qe^{2K \tan \phi Z/B} \quad (4a)$$

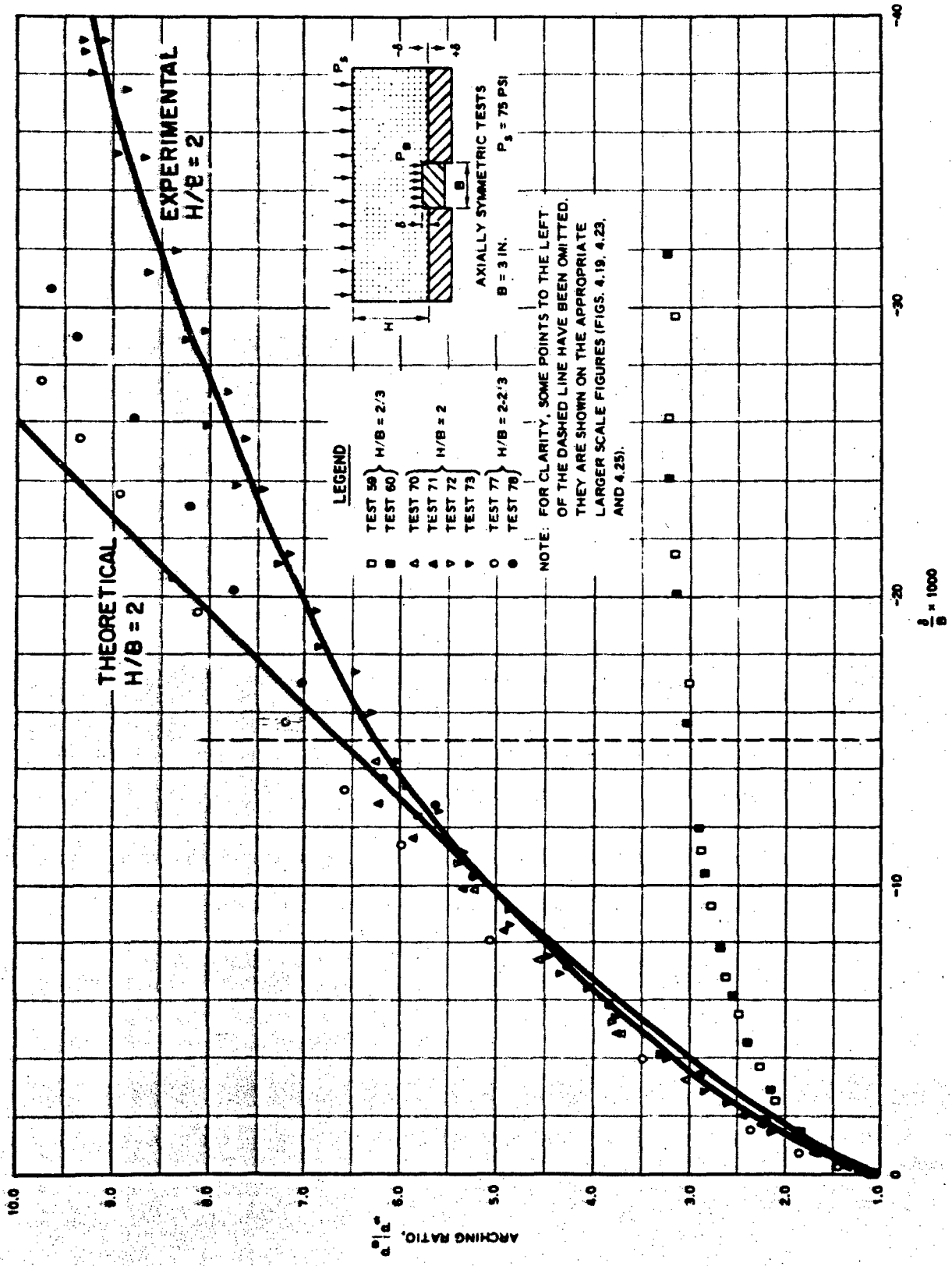
Values of the appropriate σ_v for the respective depth of burial (Z) are plotted in Figs. 45 through 48. They are not plotted in Figs. 49 through 52 since their magnitude exceeded the maximum value of the ordinate on the graph.

As can be seen from studying the figures, the theoretical curve does indeed follow the experimental curve at small differential displacements, and the greater the depth of burial, the longer it follows it as displacements increase, until (Figs. 50 through 52) the curves agree out to a Δ_B/B value of 15, the maximum value of the abscissa.

An examination of the shallow depths of burial shows that instead of the two curves following each other until the maximum value is reached, the experimental curve departs from the theoretical and becomes asymptotic at a value that actually exceeds the maximum shear value. These effects are attributed to surface soil conditions and will be discussed in a later section. The curves depart from each other in the same manner for the deeply buried conditions, however, the experimental curve becomes asymptotic to the maximum value as can be seen by examining Fig. 53 for the depth of burial H/B equal 2.

In order to give the reader an indication of the degree of agreement in terms of variation in soil conditions, the effects of extremes of initial density conditions have been plotted on Fig. 50. To obtain these curves, the A values were computed for the dense initial condition of 110.4 pcf and the loose initial condition of 97.0 pcf from the stress-strain curves in Fig. 44. ϕ values were obtained from Fig. 42 for the appropriate cases and K was calculated as before.

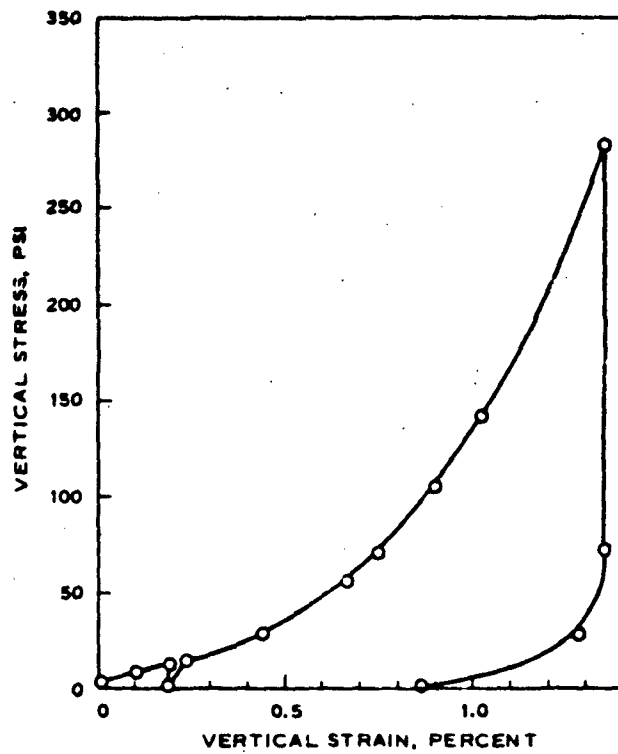
MAXIMUM SHEAR



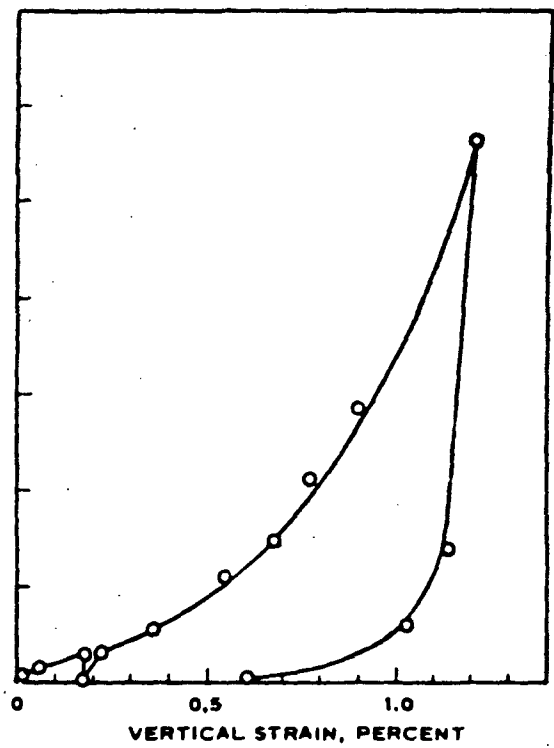
Active Arching Case

When a comparison was made for the active case on the assumption of the same A value as for the passive case, i.e., the same stress-strain curve, a poor fit was obtained. It was realized at that point that the test conditions were not compatible with that assumption. In the test setup, the overpressure was applied to the surface before any displacements of the piston were allowed. Therefore, the soil was fully compressed to the free-field stress level, and any movements of the trap door thereafter must of necessity be an unloading condition for the soil above the door. Since the soil is not elastic and has a different stress-strain curve for unloading, it was recognized that the unloading curve was the one to apply.

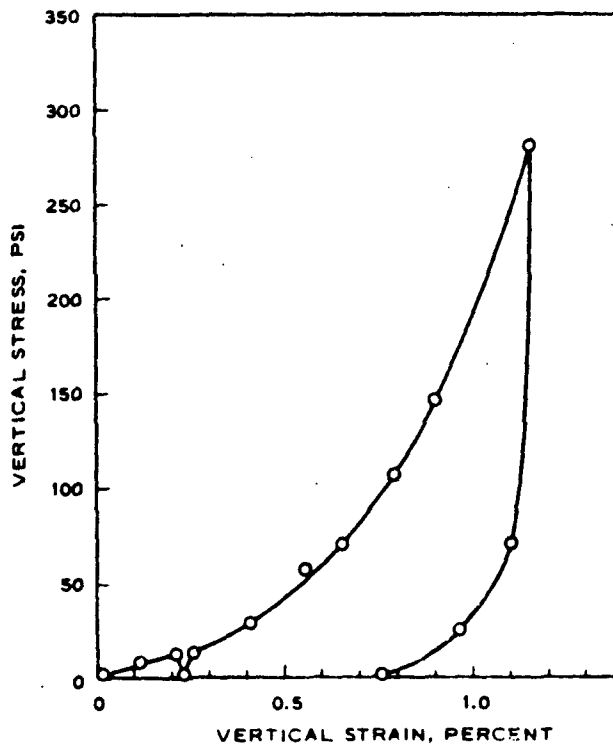
Fortunately, unloading curves had been obtained and were also presented in the reference. (They are reproduced here as Figs. 54 and 55 for sands No. 1 and No. 2, respectively.) Unfortunately, as can be seen from an examination of the graphs, they were for unloadings from much higher stress levels than those which were used in the arching tests. It was assumed, for the comparison of the experimental and theoretical, that the unloading curve from a lower stress level would in general be a parallel in construction to that from the higher level. Thus for this comparison, an unloading strain was taken from Fig. 55c for the appropriate stress level and an A value calculated from Eq. (62). This value was used with K and ϕ values determined previously. After correcting for the fact that the initial arching ratio was less than 1, i.e., normalizing for the loss caused by sidewall friction, the theoretical curves were computed and are plotted in Figs. 56 through 60. As was the case in the passive arching tests, one would expect, since the theory is for the deeply buried condition, that the fit would be good only for small displacement at shallow depths and should get better for larger displacements at greater depths. As can be seen by examining the figures as the depth of burial increases, the theoretical and experimental curves do come into closer agreement until, at depths of H/B of 2 and 4, they are in very close agreement. Early agreement between the experimental and theoretical curves isn't as good as in the passive case; however, several reasons may account for this. First is the fact that an approximate unloading curve had to be used



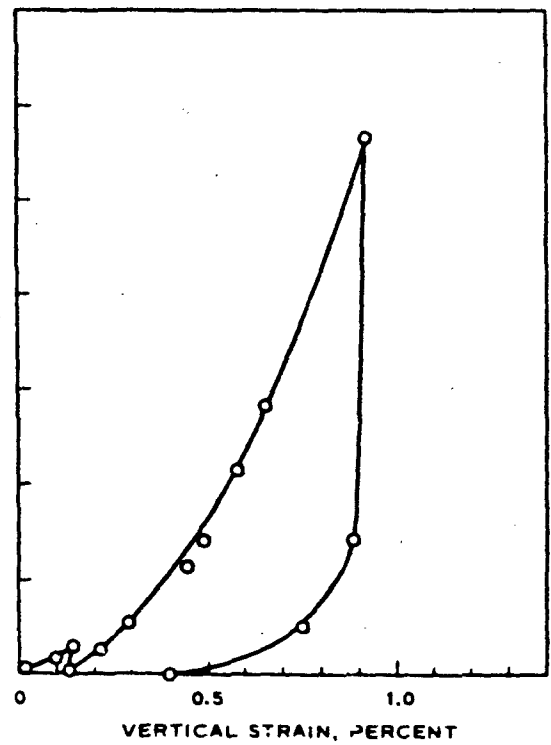
a. 96.7-PCF INITIAL DRY DENSITY
($D_r = 55\%$)



b. 99.6-PCF INITIAL DRY DENSITY
($D_r = 70\%$)



c. 100.8-PCF INITIAL DRY DENSITY
($D_r = 77\%$)



d. 103.0-PCF INITIAL DRY DENSITY
($D_r = 90\%$)

Fig. 54. One-Dimensional Compression Stress - Strain Curves for Sand 1
(From Fig. 3.11, Ref. 11)

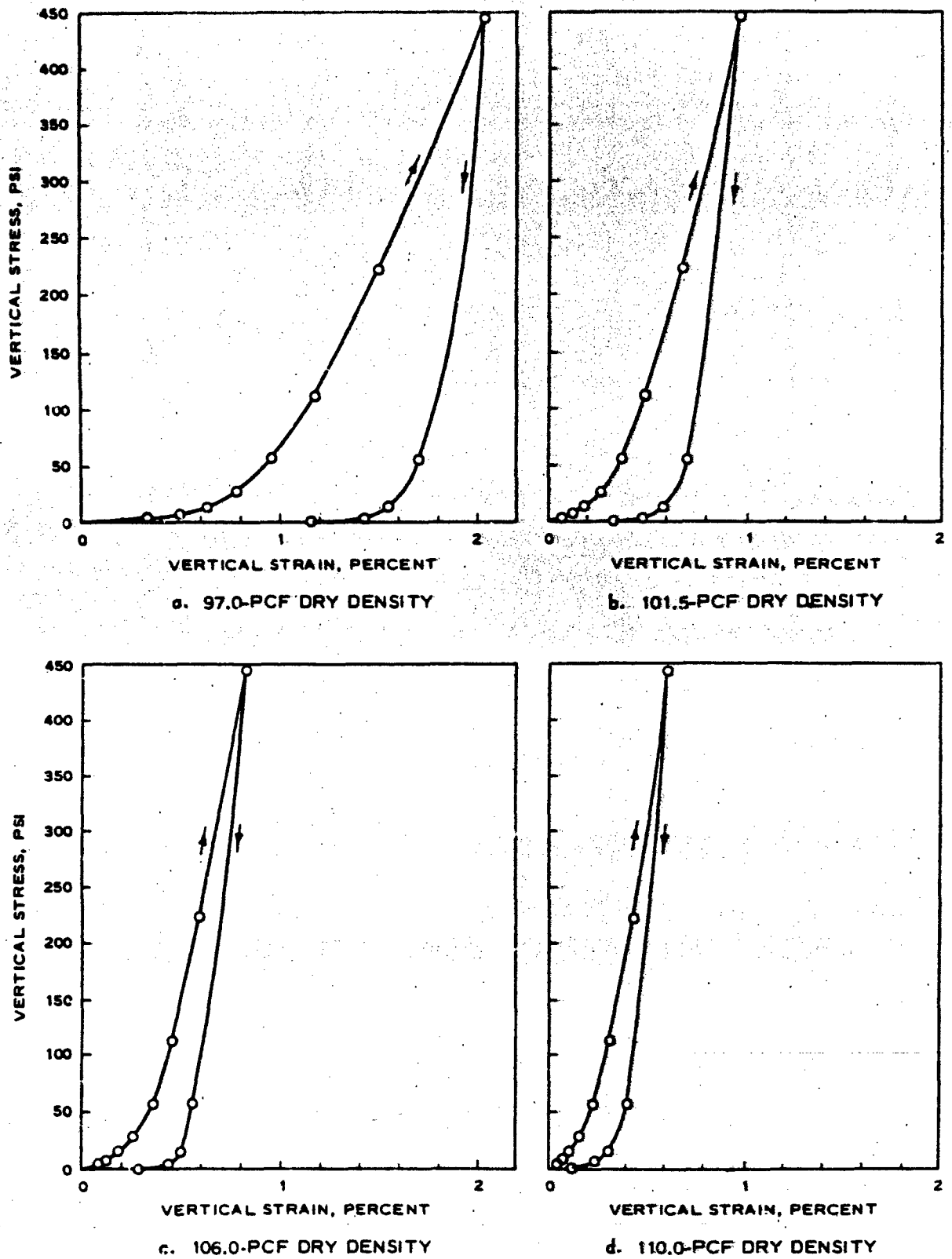


Fig. 55. One-Dimensional Compression Stress-Strain Curves for Sand 2 (From Fig. 3.14, Ref. 11)

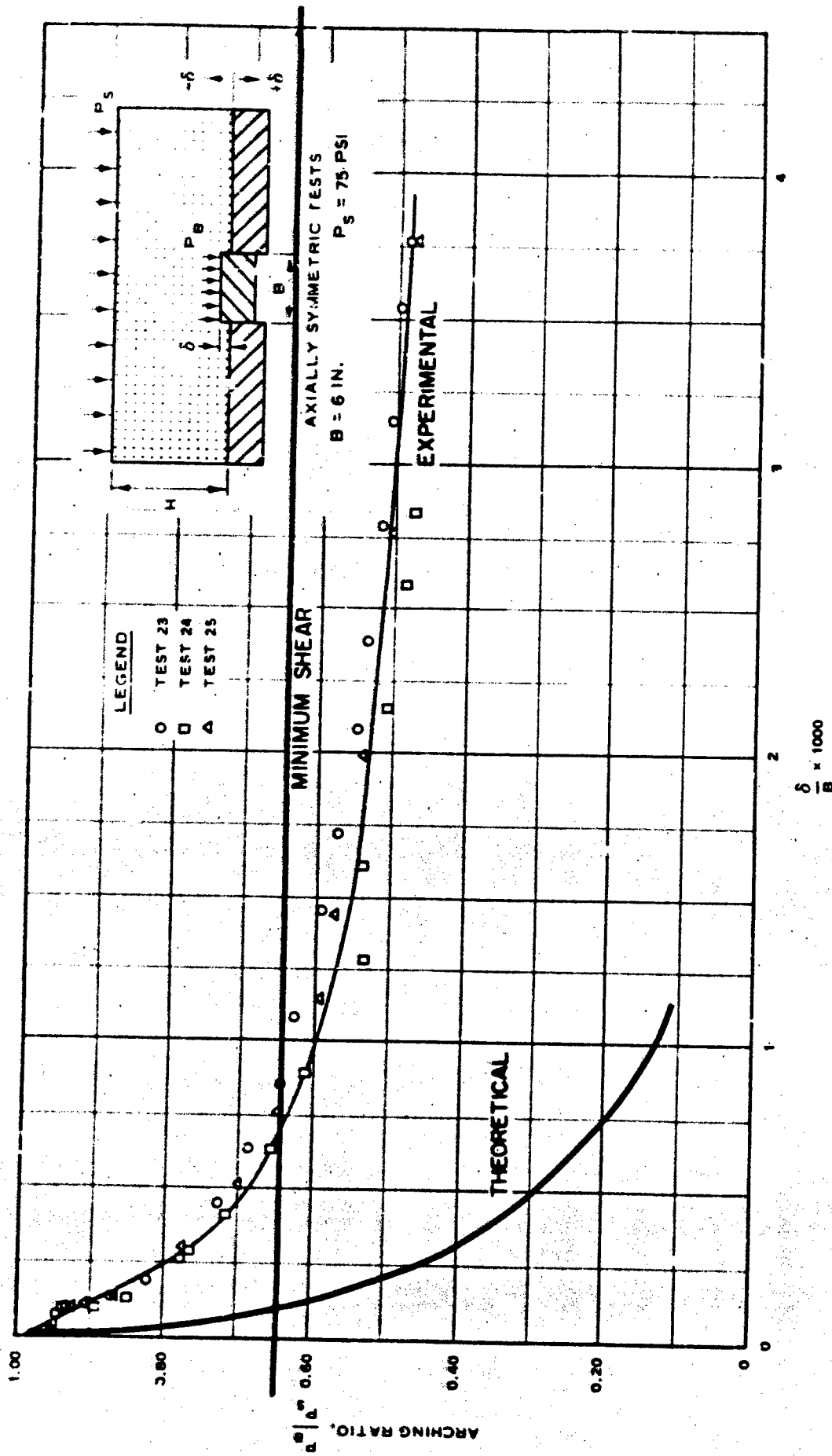


Fig. 56. Dimensionless Plot of Pressure vs Deflection for Active Arching Tests with Sand 2, $H/B = 1/3$, $P_s = 75 \text{ psi}$ (From Fig. 4.8, Ref. 11)

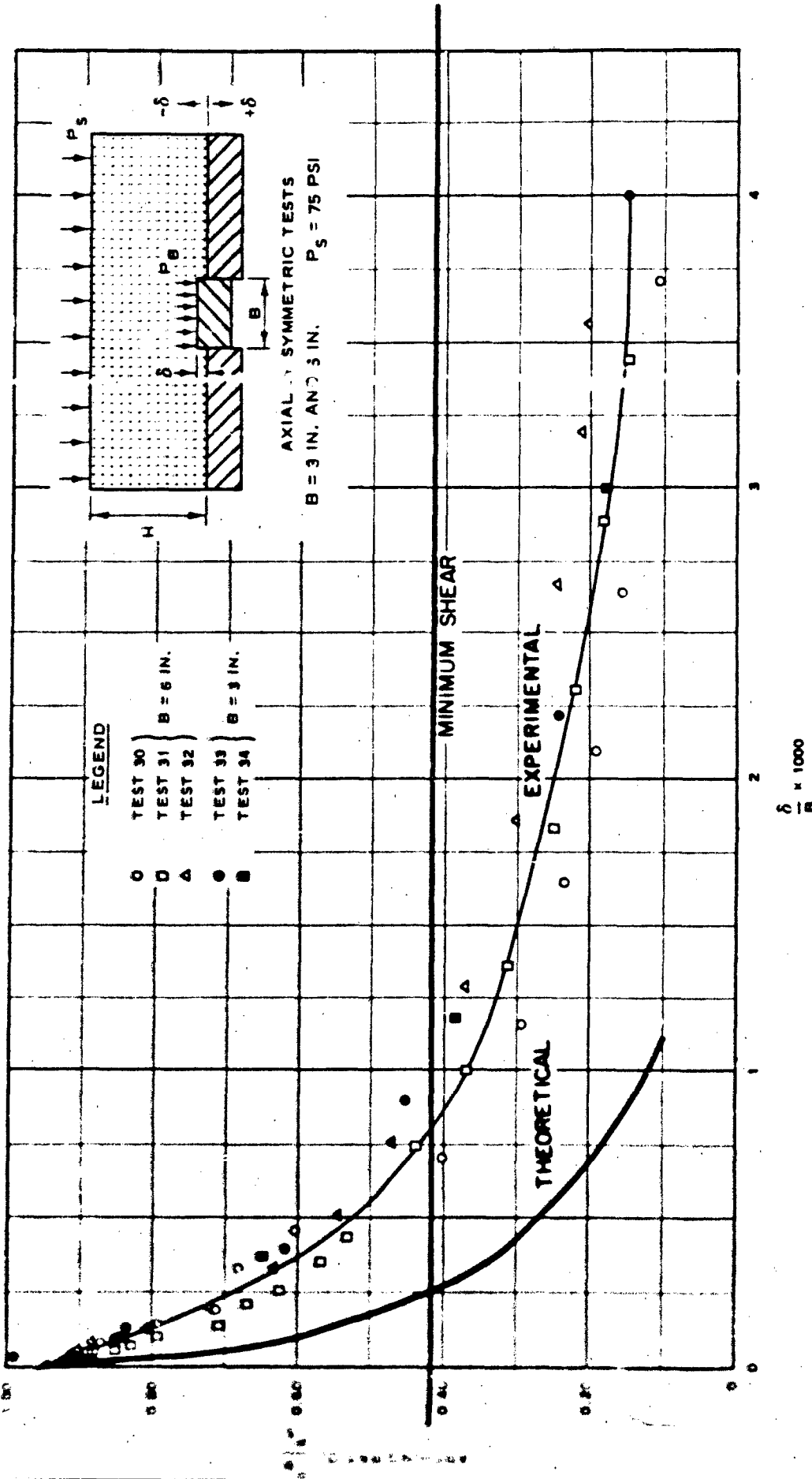


FIG. 57. Dimensionless Plot of Pressure vs Deflection for Active Arching Tests With Sand 2, $H/B = 2/3$, $P_s = 75$ psi (From Fig. 4.11, Ref. 11)

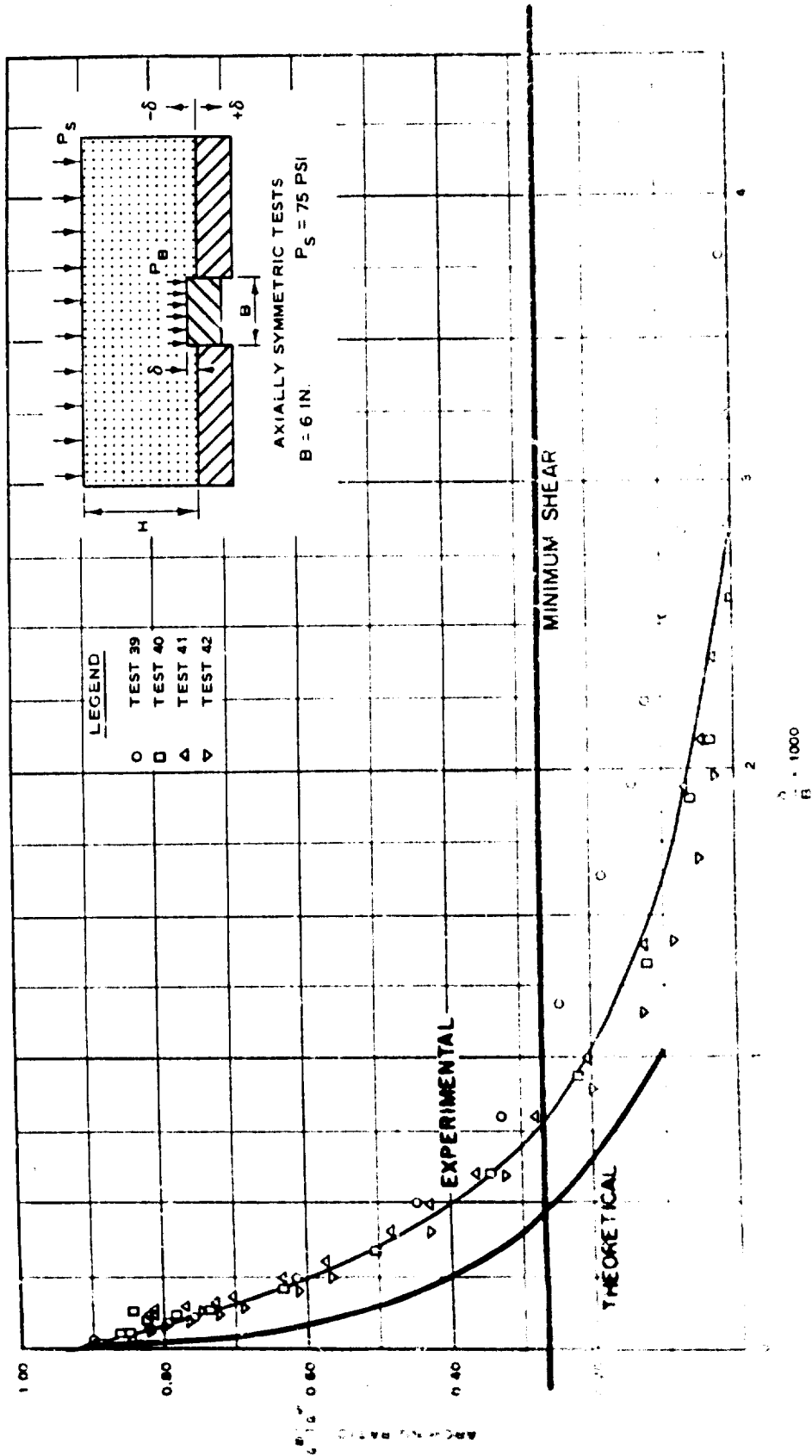


FIG. 38. Dimensionless Plot of Pressure vs Deflection, for Active Arcning Tests with Sand 2, $H/B = 1$, $P_S = 75 \text{ psi}$ (From Fig. 4.14, Ref. 11)

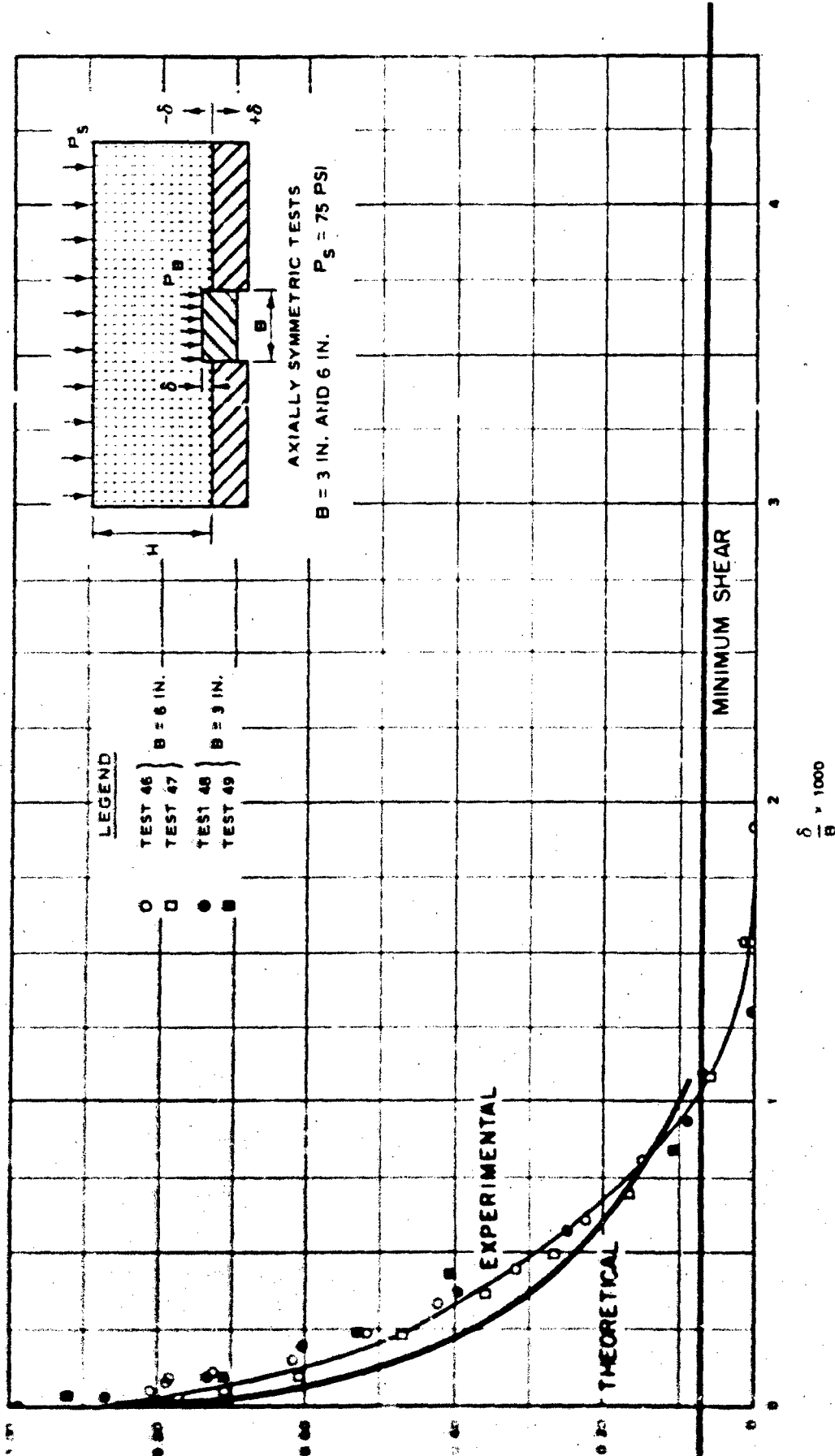


FIG. 59. Dimensionless Plot of Pressure vs Deflection for Active Arching Tests With Sand 2, $H/B = 2$, $P_s = 75$ psi (From Fig. 4.16, Ref. 11)

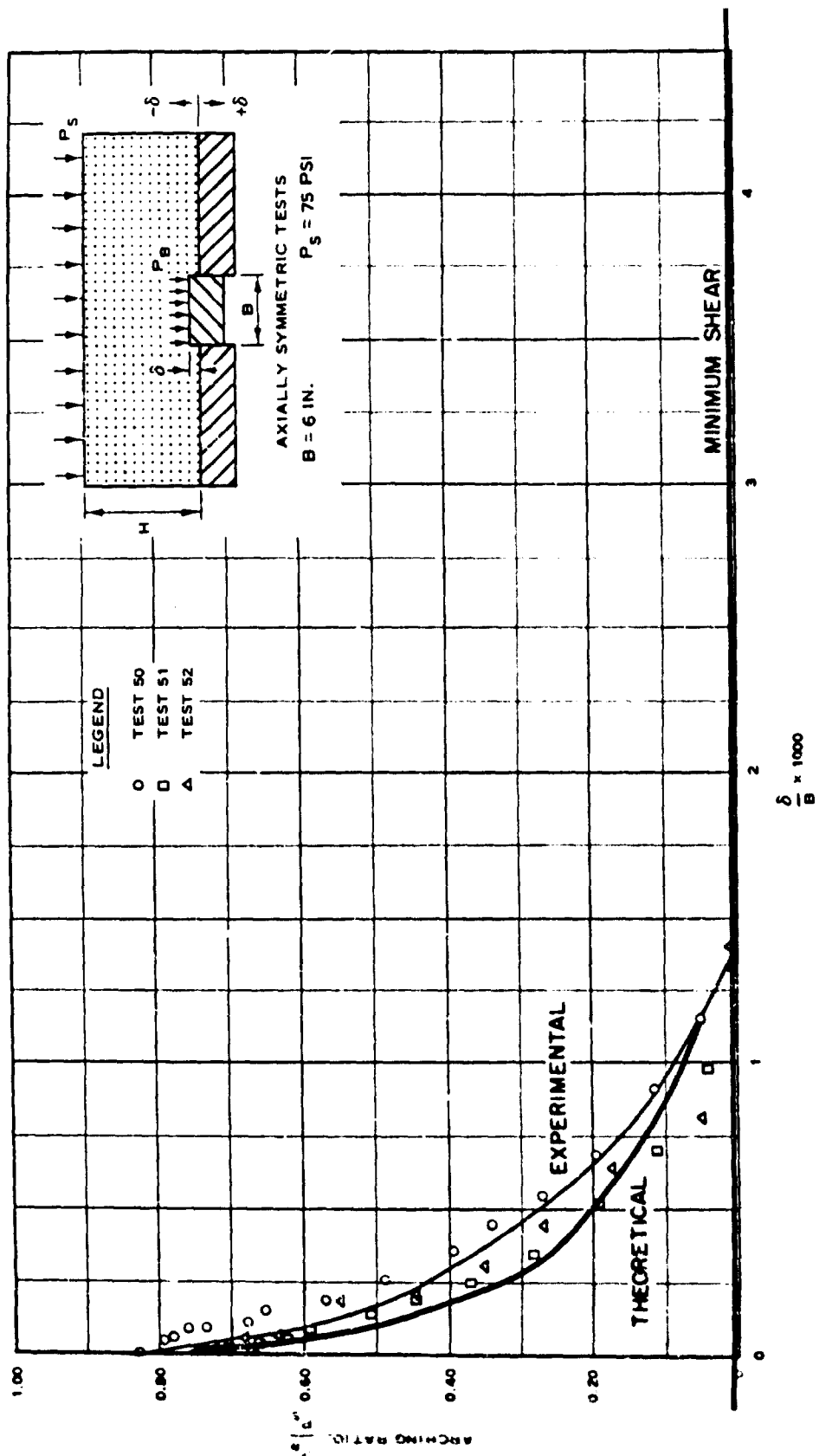


FIG. 60. Dimensionless Plot of Pressure vs Deflection for Active Arching Tests With Sand 2, $H/B = 4$, $P_s = 75 \text{ psi}$ (From Fig. 4.17, Ref. 11)

for the lower stress level. Second, the nonlinear relation of Eq. (62) is not so good a fit to the shape of the unloading curve as it was to the loading curve. Finally, the K value may not be appropriate throughout the entire range since on the unloading cycle, the ratio of lateral to axial stress has been observed to change, becoming larger at very low stresses at least in the dynamic case (Ref. 12).

The value of the minimum relative stress for each depth of burial was computed from Eq. (2a)

$$\sigma_v = qe^{-2K \tan \alpha Z/B} \quad (2a)$$

and is plotted on appropriate figures. Comparable to the passive case the experimental curve becomes asymptotic to a minimum value less than that predicted by Eq. (2a) at the shallow burials.

Figures 61 through 66 show that the same trends in correlation are in evidence regarding the theoretical and experimental results for the two other surface overpressure levels used.

A comparison between the theoretical and experimental active arching case for sand No. 1 is shown in Figs. 67 through 72. The same procedures as those used for sand No. 2 were used, i.e., employing soil parameters taken from Figs. 42 and 54c. As can be seen, the same good correlations exist. It should also be noted that a much better correlation exists between the theoretical and experimental minimum relative stress values.

Application of Differential Displacement Data

By referring to Figs. 7, 10, and 14, it can be seen that the arching forces are caused by differential displacement between plane of the face of the structure and that of the soil that was coincident with that plane before loading. It can be further seen that this displacement is related to all the soil and structural parameters, including the length of the structure. For shallow depths of burial, it has been shown that if the influence zone reaches the surface and the differential displacement has been more than necessary to

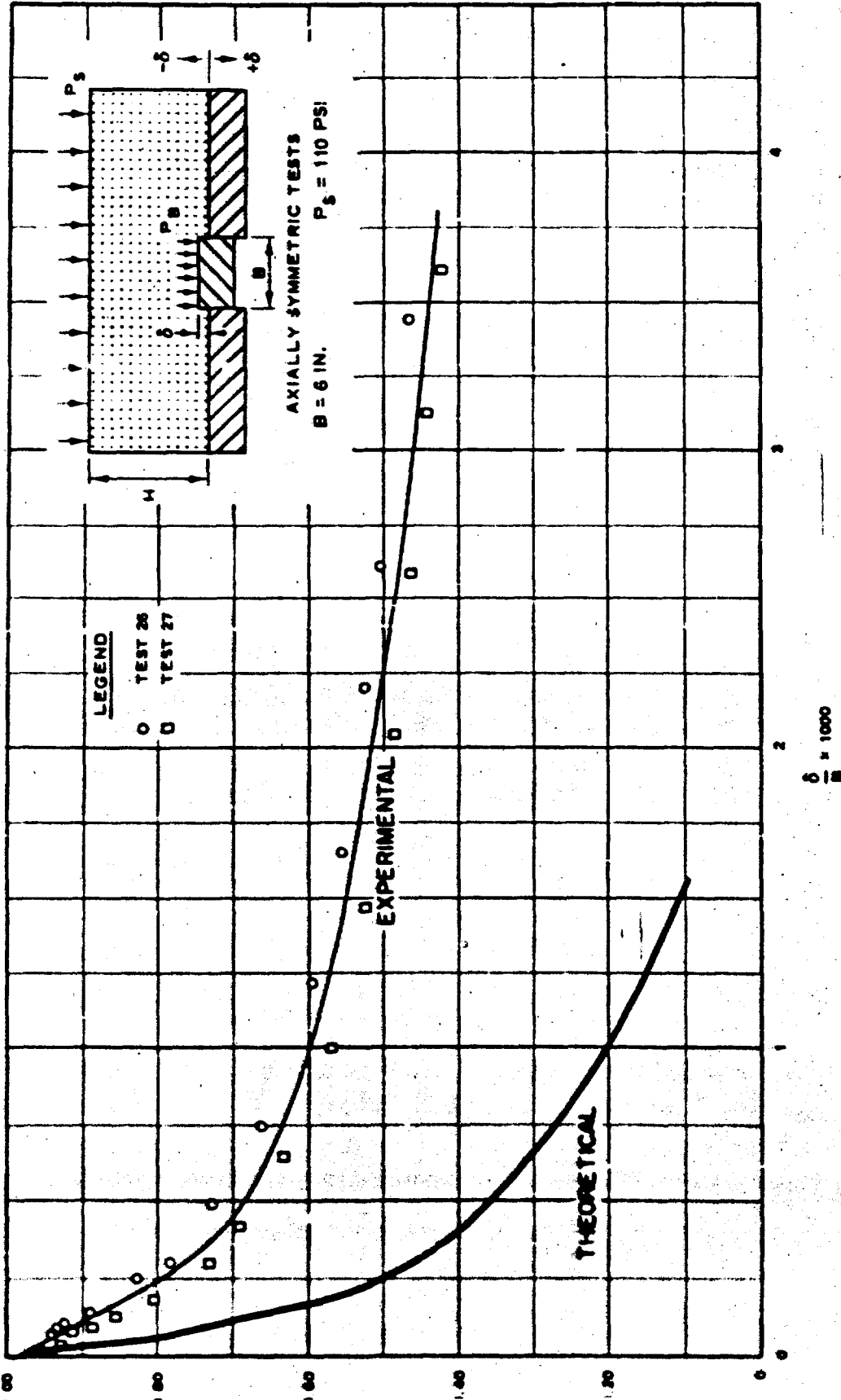
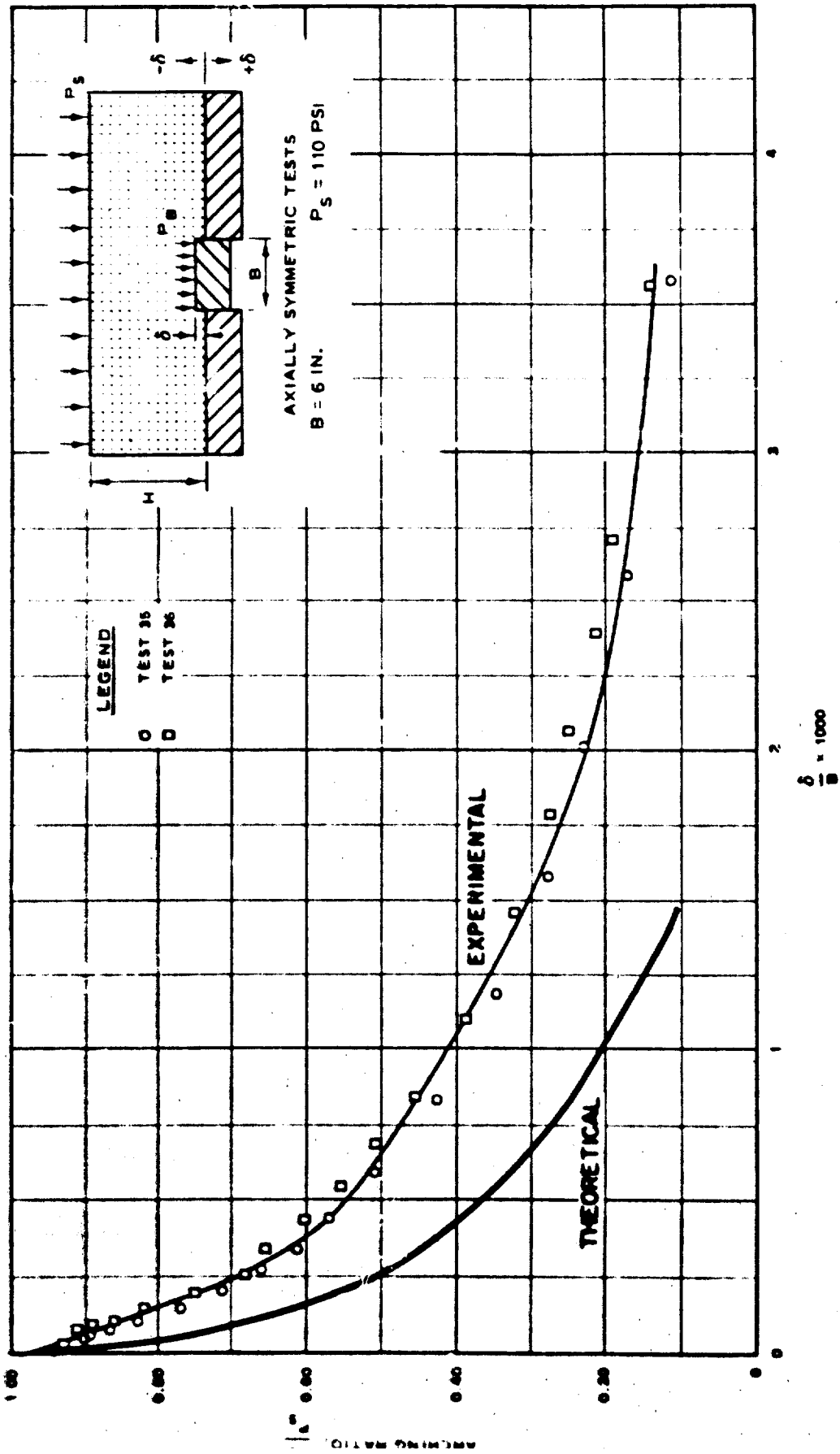


Fig. 61. Dimensionless Plot of Pressure vs Deflection for Active Arching Tests With Sand 2, $H/B = 1/3$, $P_s = 110 \text{ psi}$ (From Fig. 4.9, Ref. 11)



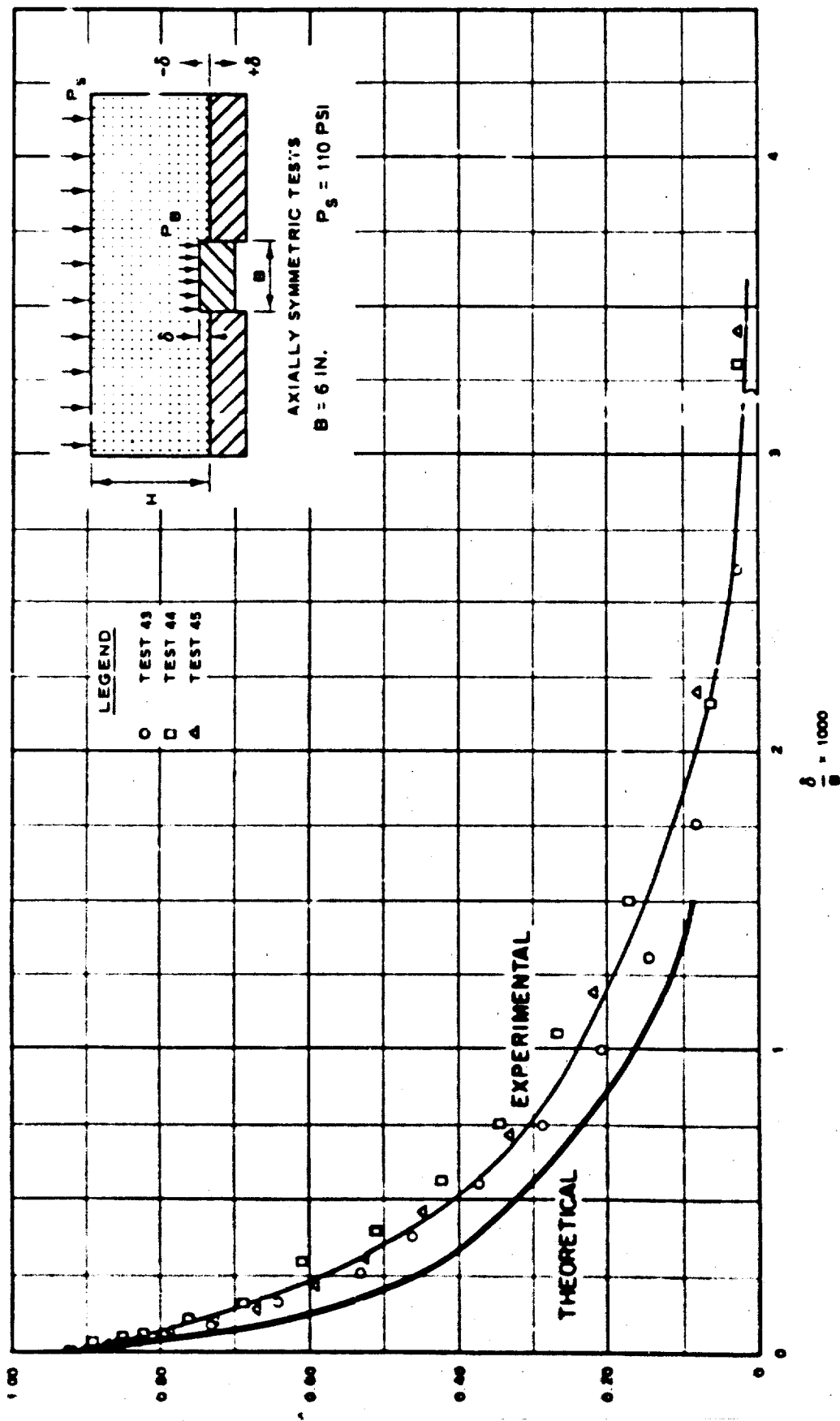


Fig. 63. Dimensionless Plot of Pressure vs Deflection for Active Arching Tests with Sand 2, $H/B = 1$, $P_s = 110 \text{ psi}$ (From Fig. 4.15, Ref. 11)

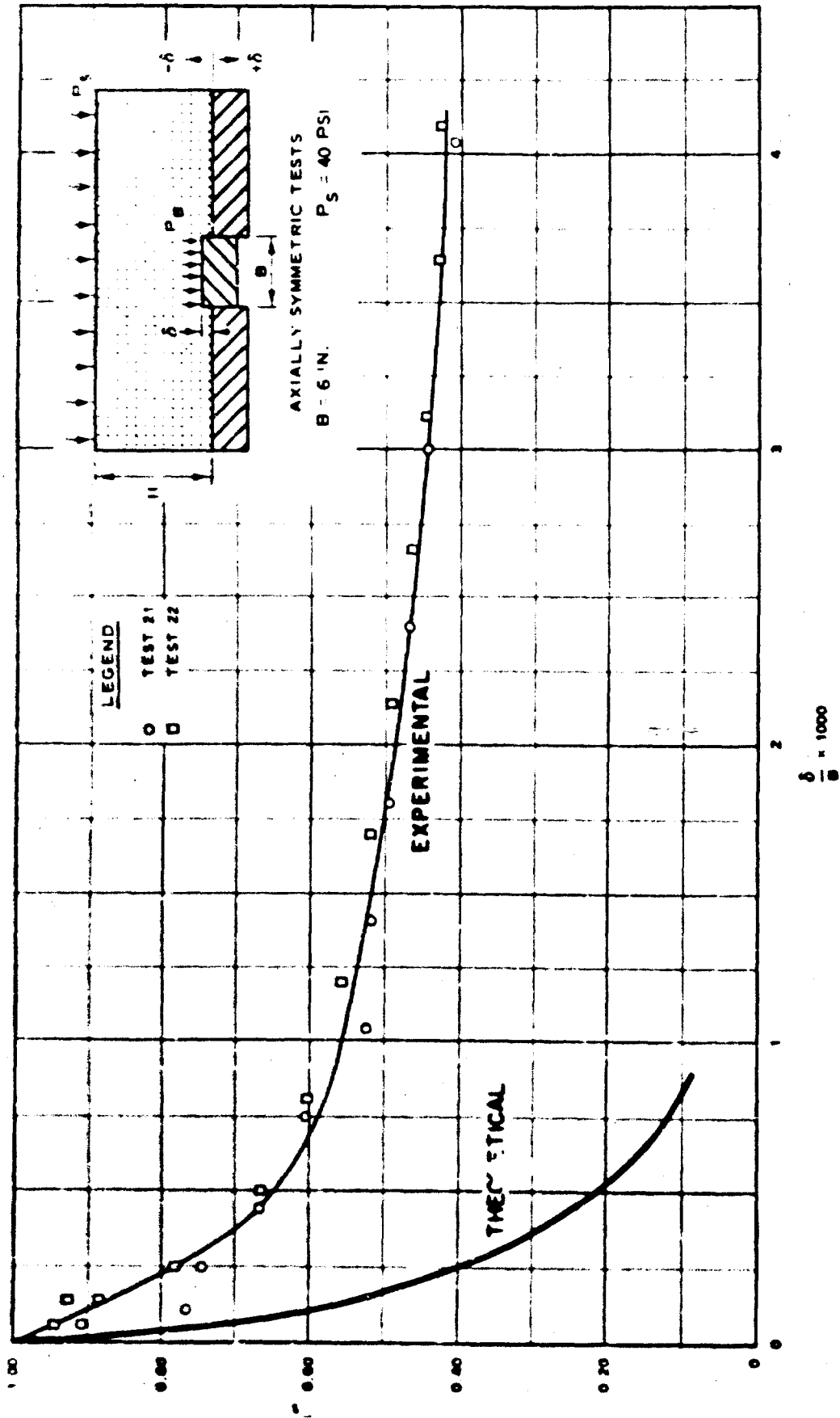


Fig. 64. Dimensionless Plot of Pressure vs Deflection for Active Arching Tests With Sand 2,

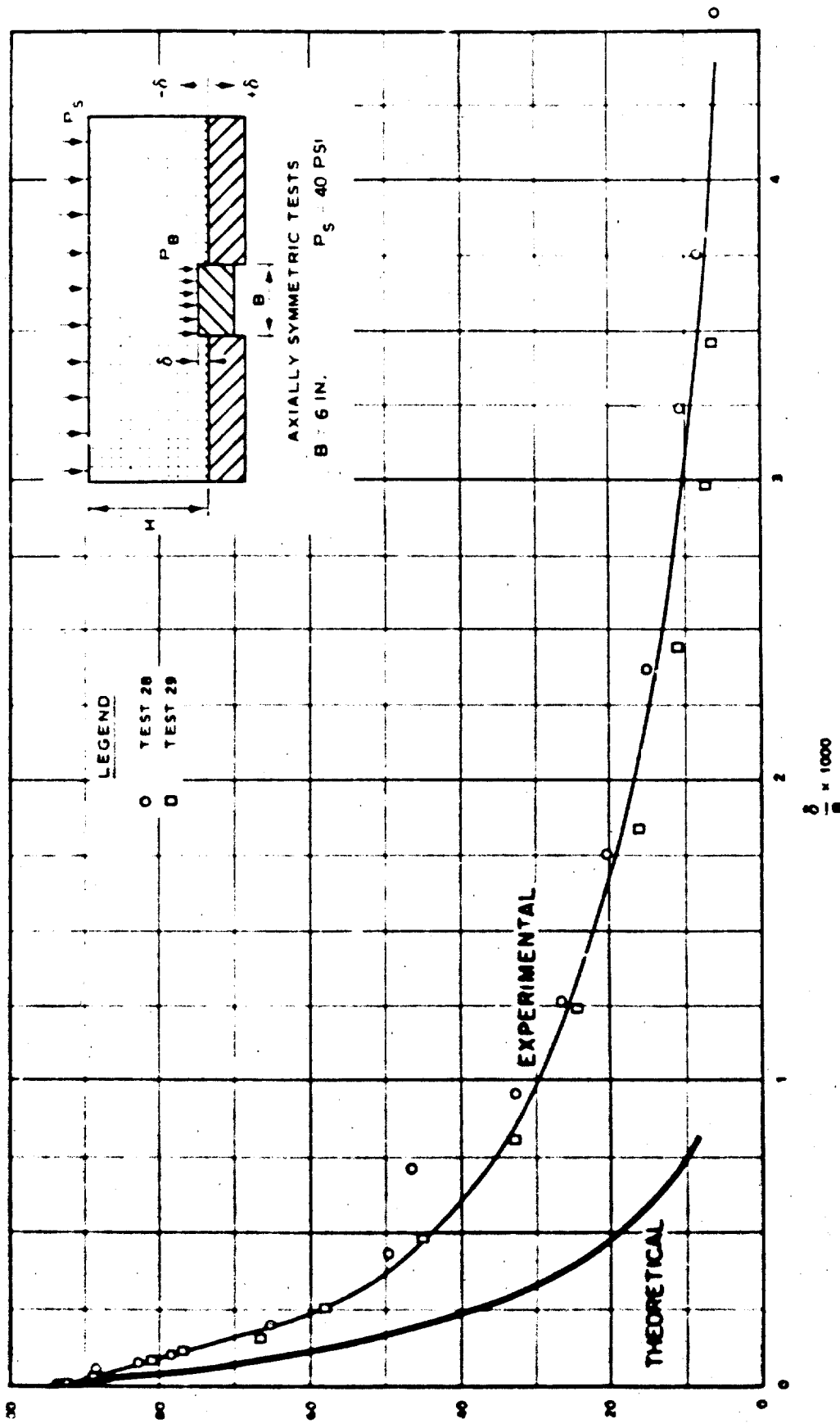


Fig. 65. Dimensionless Plot of Pressure vs Deflection for Active Arching Tests with Sand 2, $H/B = 2/3$, $P_s = 40 \text{ psi}$ (From Fig. 4.10, Ref. 11)

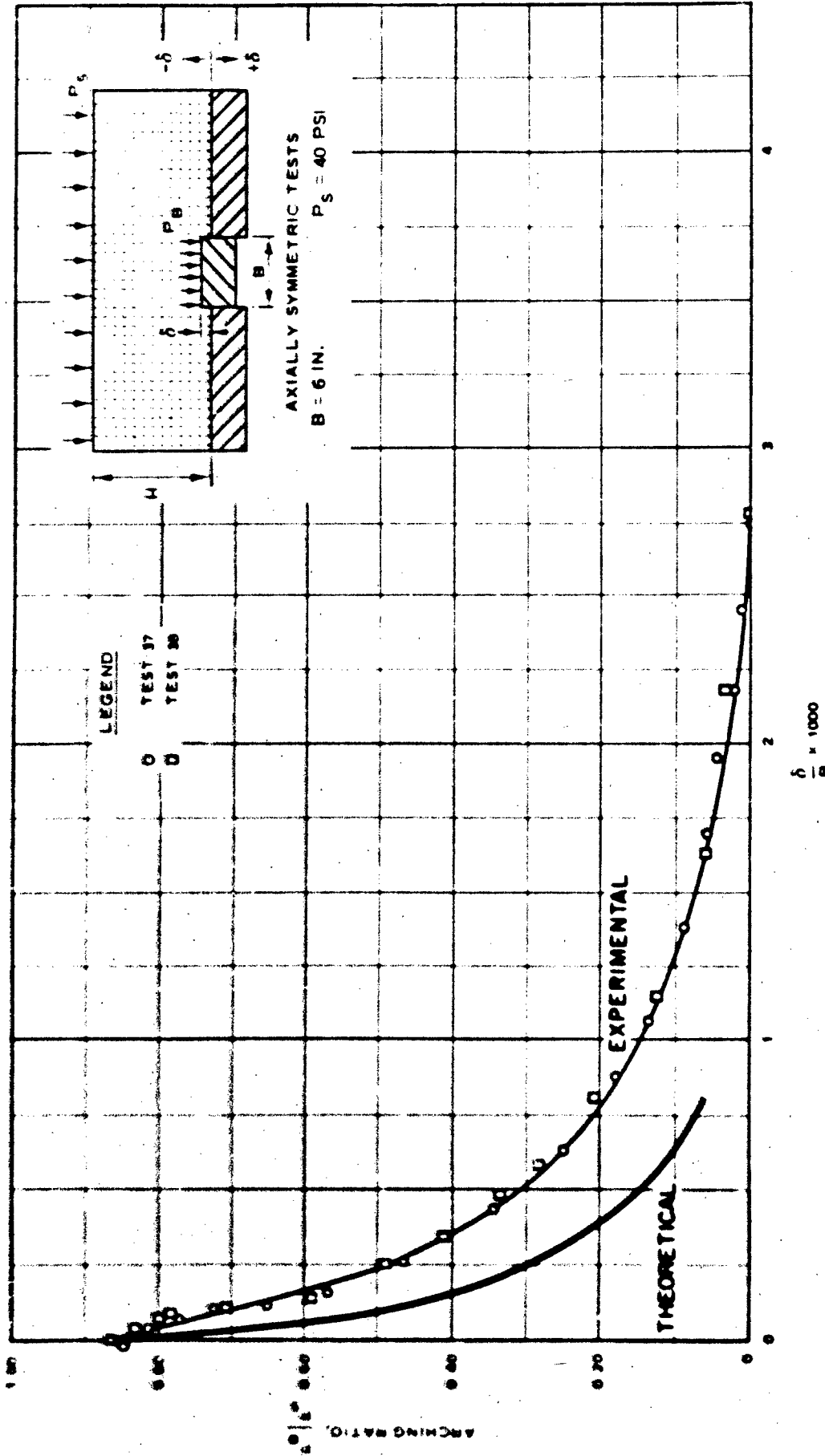


Fig. 66. Dimensionless Plot of Pressure vs Deflection for Active Arching Tests With Sand 2, $H/B = 1$, $P_B = 40 \text{ psi}$ (From Fig. 4.13, Ref. 11)

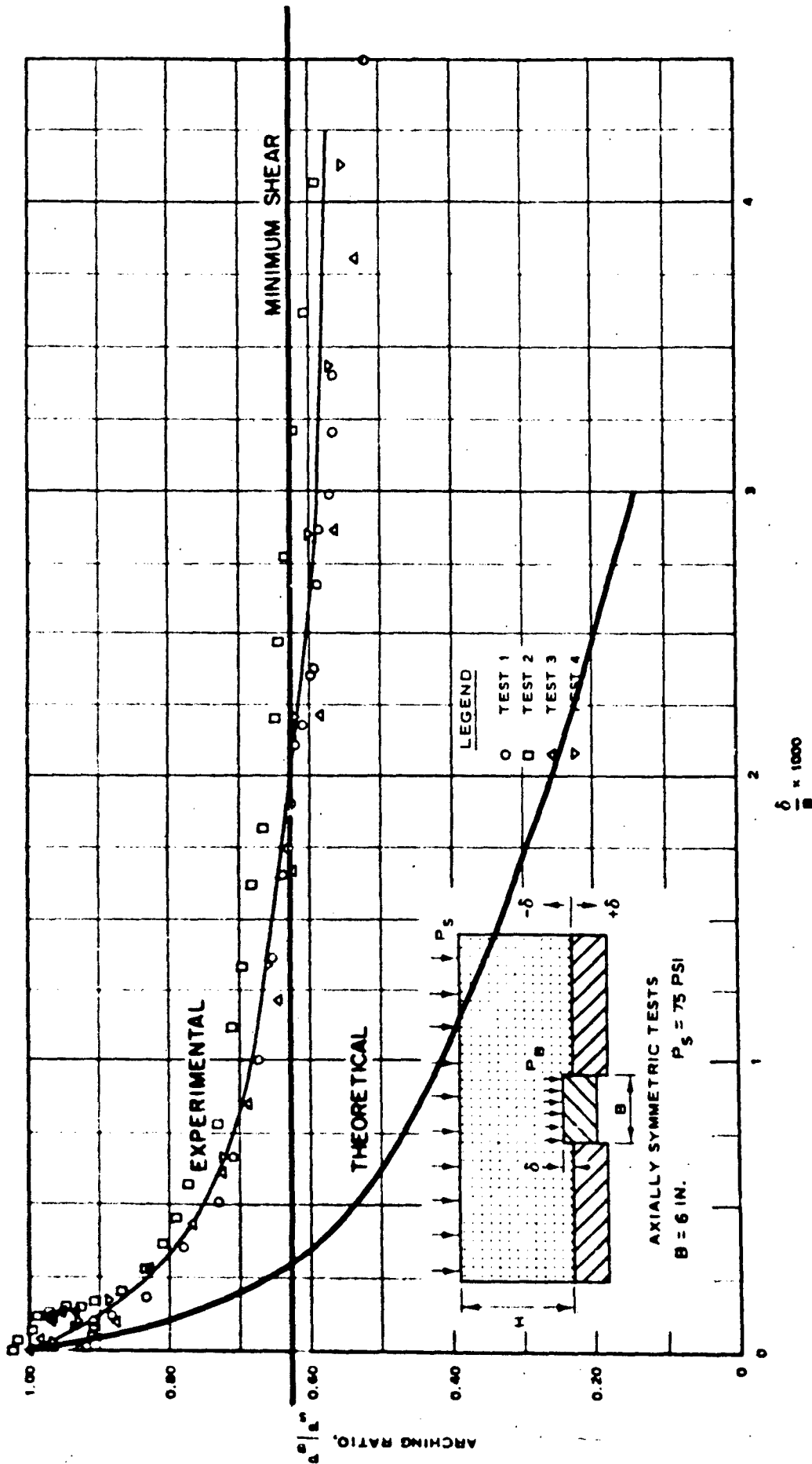


Fig. 67. Dimensionless Plot of Pressure vs Deflection for Active Arching Tests With Sand 1, $H/B = 1/3$, $P_s = 75$ psi (From Fig. 4.1, Ref. 11)

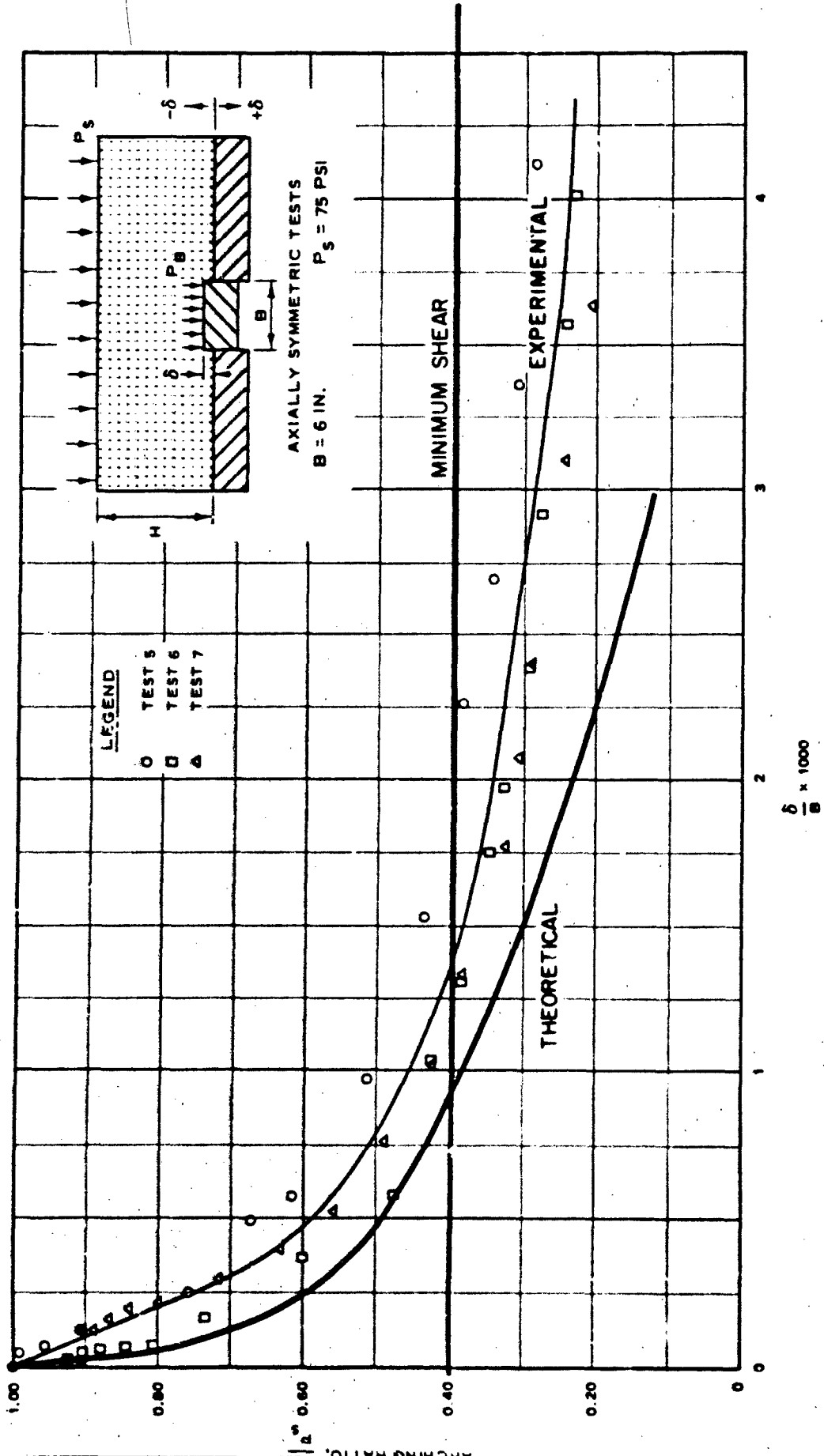


Fig. 68. Dimensionless Plot of Pressure vs Deflection for Active Arching Tests with Sand 1, $H/B = 2/3$, $P_s = 75 \text{ psi}$ (From Fig. 4.2, Ref. 11)

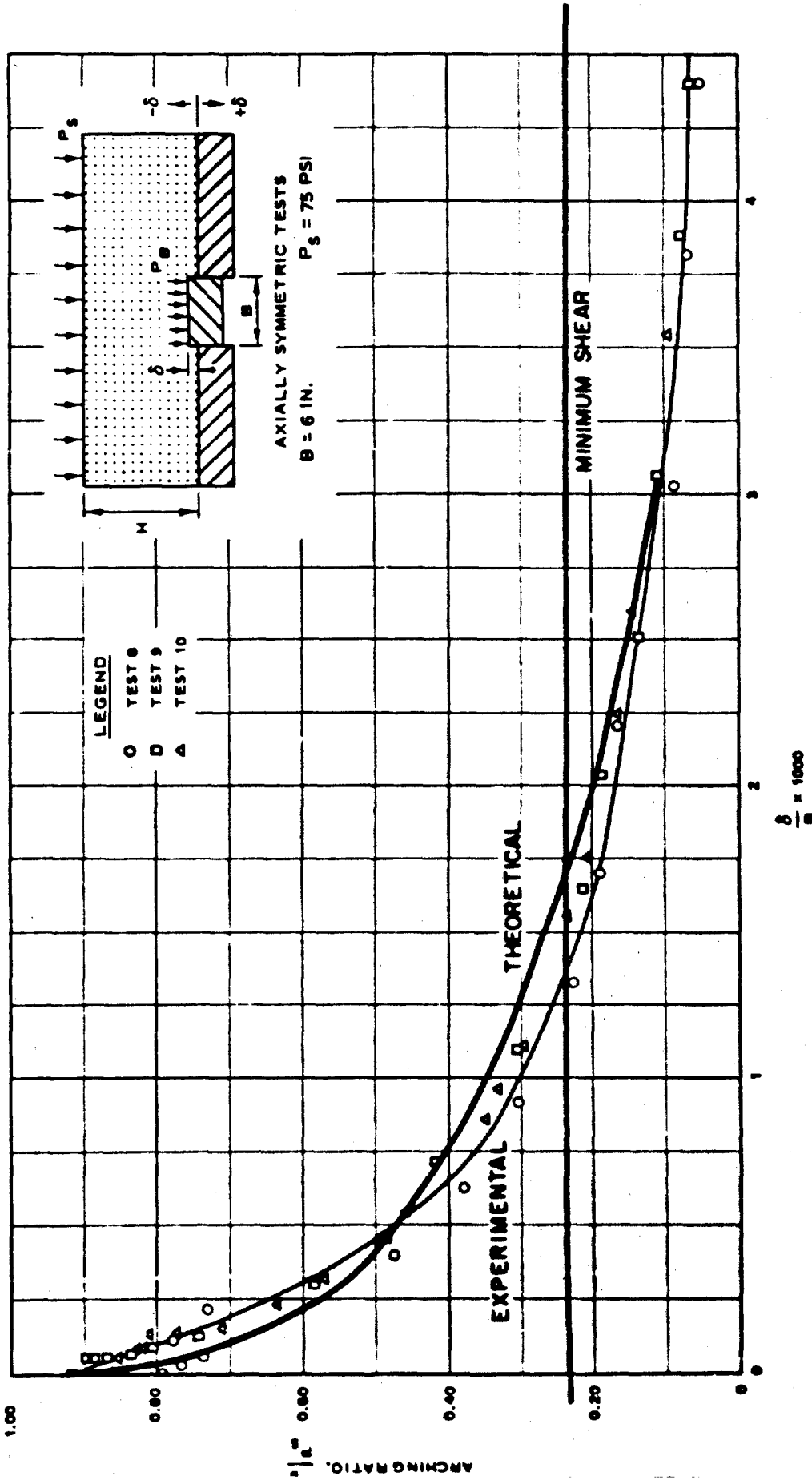


Fig. 62. Dimensionless Plot of Pressure vs Deflection for Active Arching Tests With Sand 1, $N/B = 1$, $P_s = 75 \text{ psi}$ (From Fig. 4.3, Ref. 11)

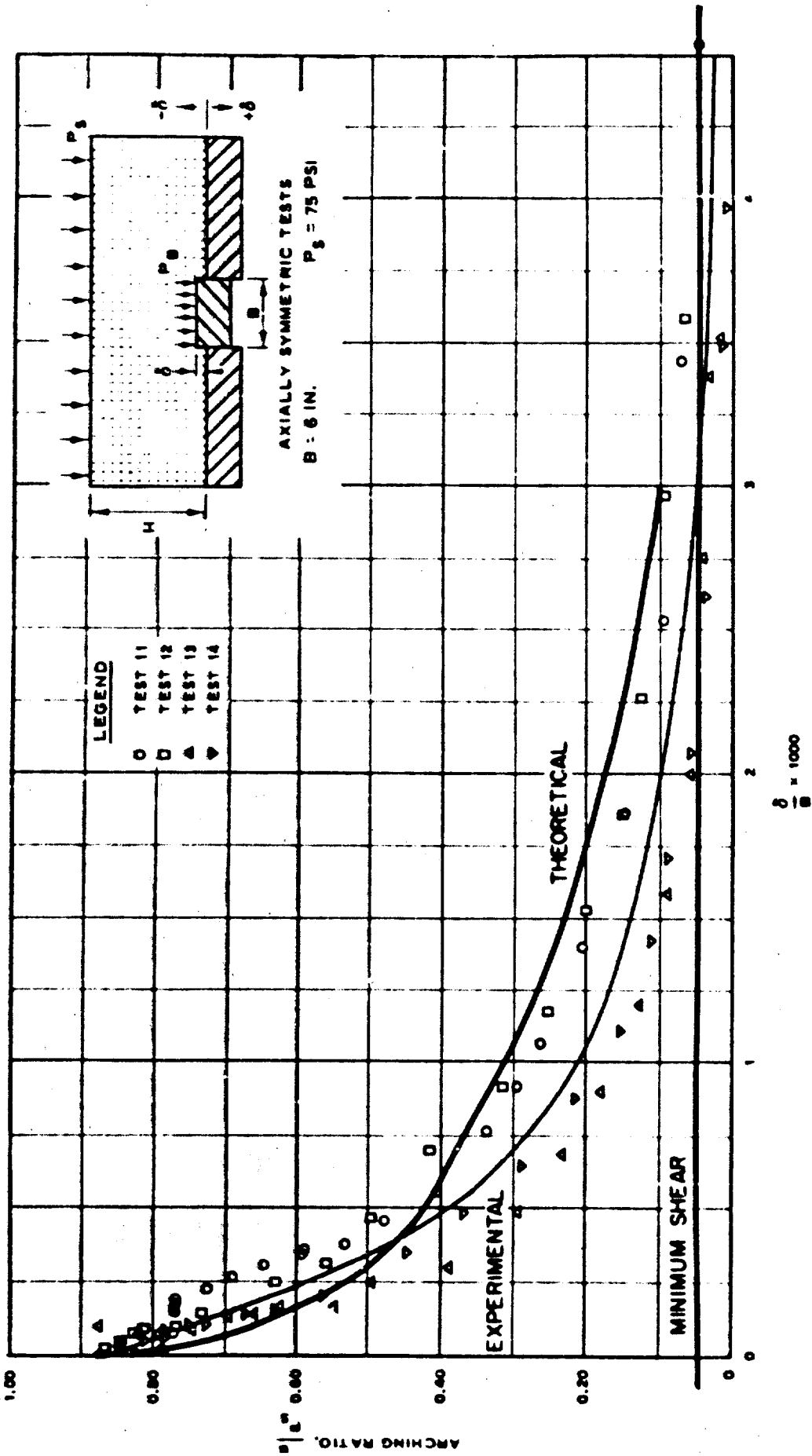


Fig. 70. Dimensionless Plot of Pressure vs Deflection for Active Arching Tests With Sand 1, $H/B = 2$, $P_s = 75 \text{ psi}$ (From Fig. 4.4, Ref. 11)

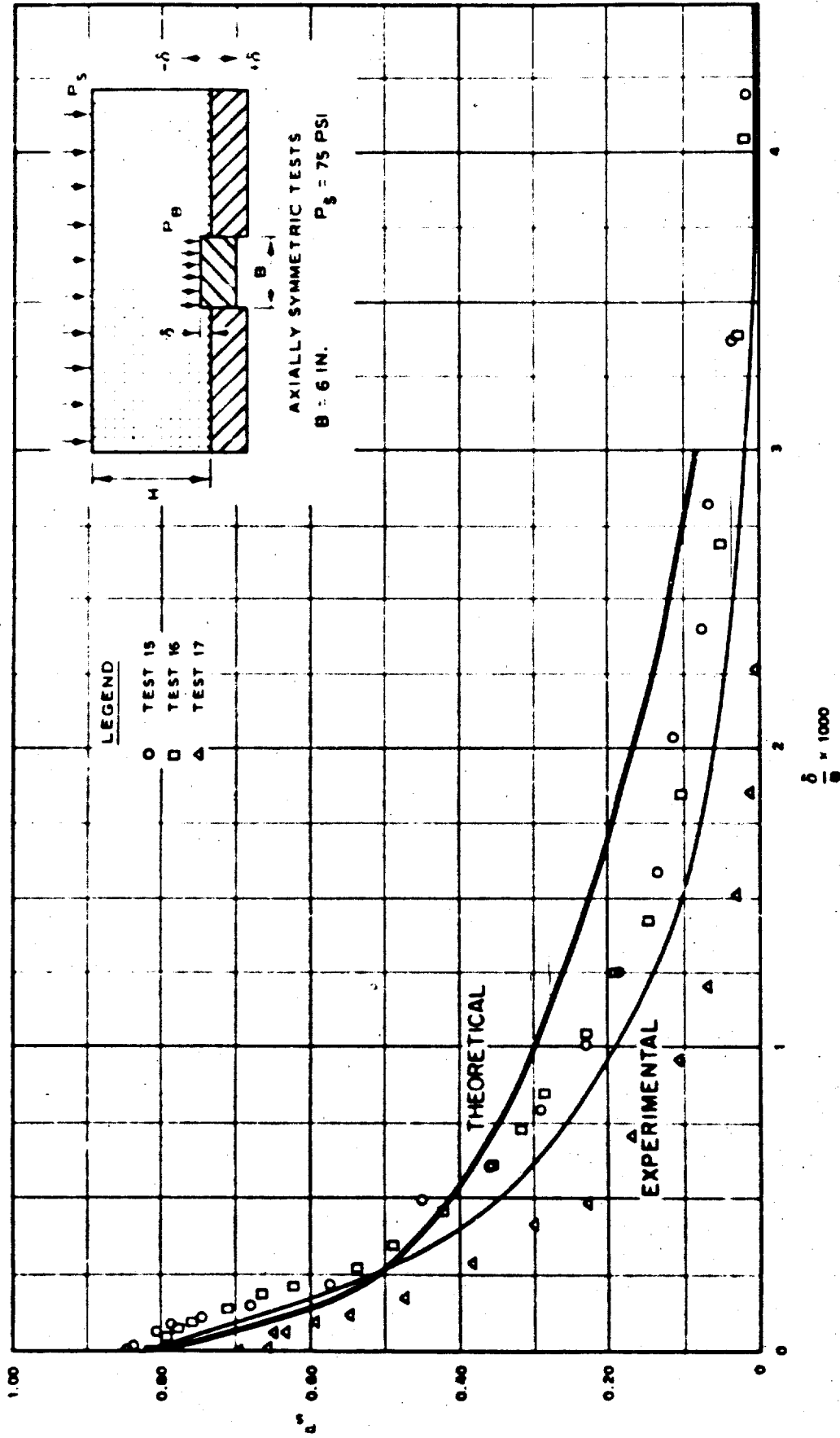


Fig. 71. Dimensionless Plot of Pressure vs Deflection for Active Arching Tests With Sand 1, $H/B = 4$, $P_s = 75$ psi (From Fig. 4.5, Ref. 11)

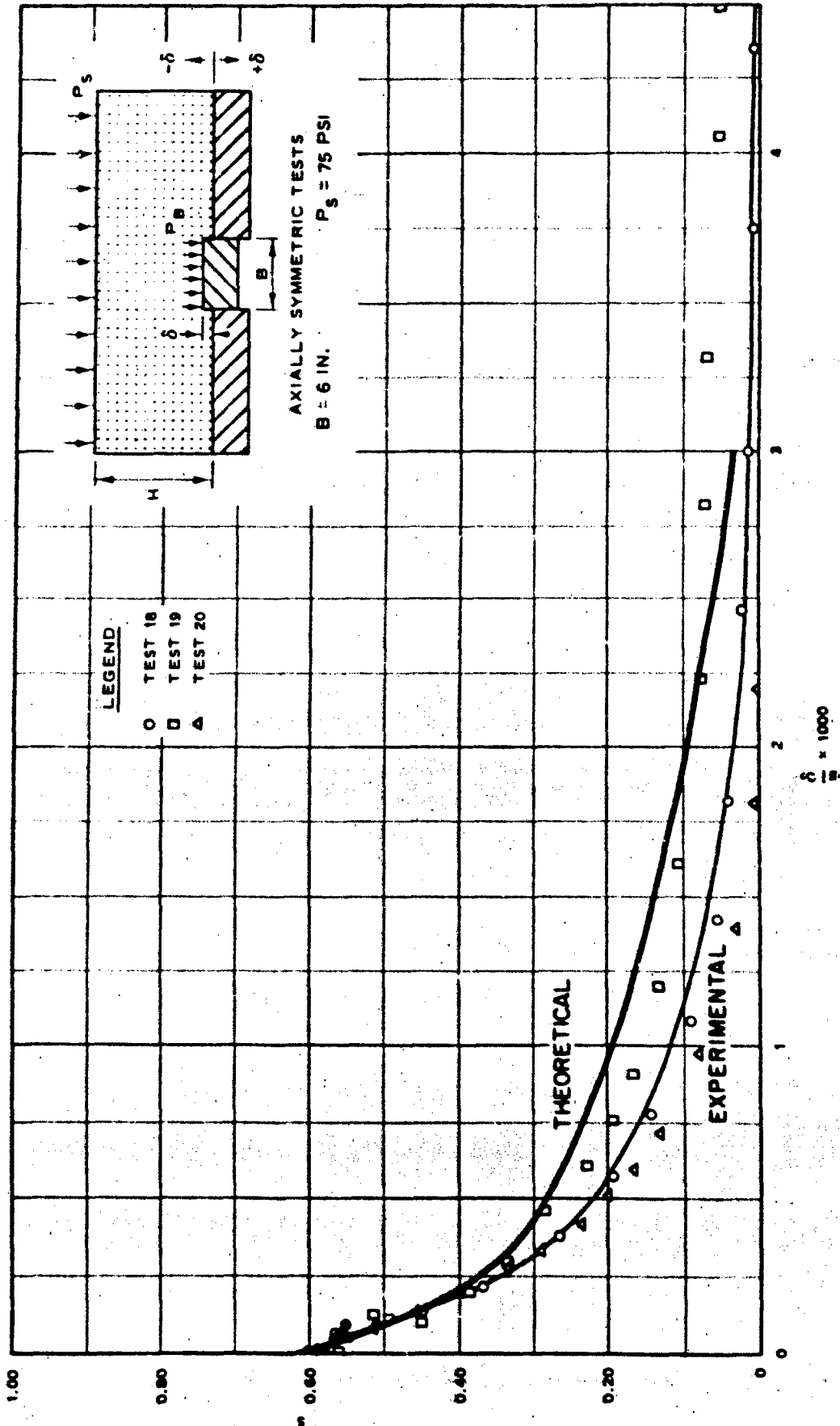


Fig. 72. Dimensionless Plot of Pressure vs Deflection for Active Arching Tests With Sand 1, $H/B = 6$, $P_s = 75 \text{ psi}$ (From Fig. 4.6, Ref. 11)

develop the maximum shear forces, then the load on the structure will increase exponentially with depth. For greater depths of burial, it has been shown that for a given set of soil and structure parameters, the total differential displacement available will be a constant and result in a constant overstress regardless of the depth of burial, provided the zone of influence doesn't intersect the surface. It can be hypothesized, therefore, in the case of the trap door experiments, that a given differential displacement is equivalent to a structure of given length and compressibility. All other parameters remaining constant, one might then examine the effect of depth of burial on the hypothetical structure by looking at the same value of differential displacement at all the various depths of burial. It should be possible then to plot curves similar to those in Fig. 5 by plotting constant differential displacement for various depths of burial, in the trap door experimental data.

It can be further reasoned that if differential displacement does control the zone of influence and total overstress, then one might consider that the various differential displacements represent a structure of given length, but each differential displacement is representative of a different compressibility. By plotting several such displacements as a function of depth a family of curves can be obtained indicating the effect of compressibility. As can be seen from a comparison of Fig. 5 with Fig. 73, a plot of such a family for sand No. 2 for the active and passive cases, such relationships appear to exist. Particular note should be taken that when the depth of burial becomes great enough the relative stress becomes a constant in both the active and passive cases. It should also be noted that although the theory suggests a sharp change in behavior between deep and shallow burial, it is a smoother transition probably due to surface layer soil conditions.

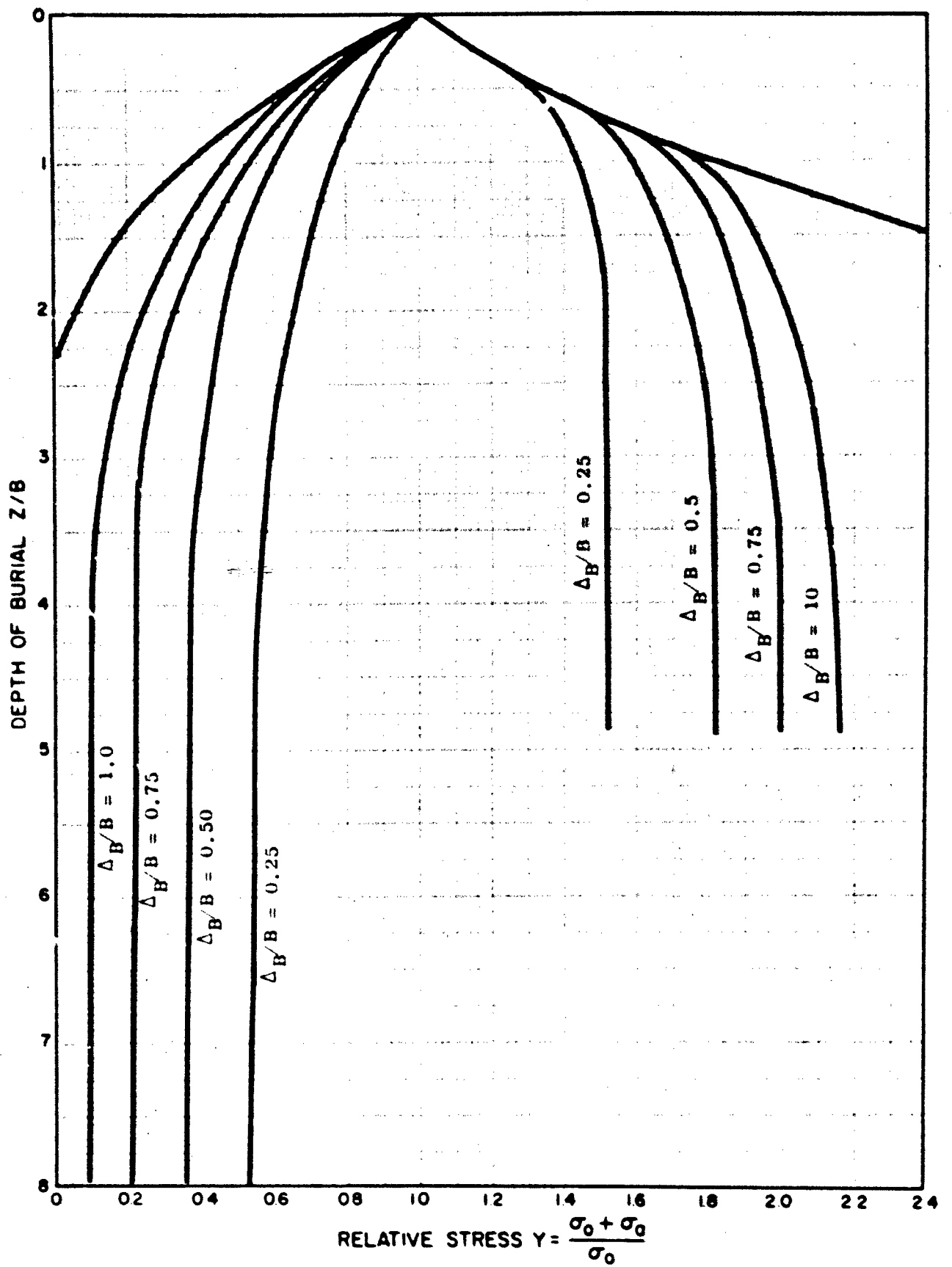


Fig. 73. Relationship Between Depth of Burial and Relative Stress for Various Δ_B/B Values

Section 8

EFFECTS OF SURFACE LAYERS

The surface layer 3 to 5 in. thick seems to possess different properties than the deeper layers. In real structures this is unimportant, but in the test of any shallow-buried small model-sized structures this could serve to confuse the investigation. Although shallow depth of burial was not a part of this study, certain observations worth noting were made.

First, as indicated, earlier tests at shallow depths of burial in both URS tests and those of Ref. 11 showed a departure between theory and experimental results. In the experimental program, the relative stress fell below the theoretical in the passive case and above in the active case, i.e., less arching occurred in each case for the shallow depths. A possible explanation might be that looser soil conditions probably exist in the surface layer than at greater depths. As support for this assumption, it can be shown that the fall off of the experimental from the theoretical follows the same shape as the low-density-condition theoretical curve plotted in Fig. 50.

The second effects are observed in the data reported in Ref. 11. At the shallow depths of burial in the passive case, the maximum relative stress measured is greater than theory would predict, while for the deeper depths it tends to agree. Similar results are found at shallow depths in the active case, i.e., the minimum relative stress measured is less than that predicted. Figure 74 shows a plot of the maximum relative stress vs depth of burial for various depths of burial. As can be seen, the experimental results show a higher relative stress in the surface layer than the theory predicts, but they become a closer fit at greater depths.

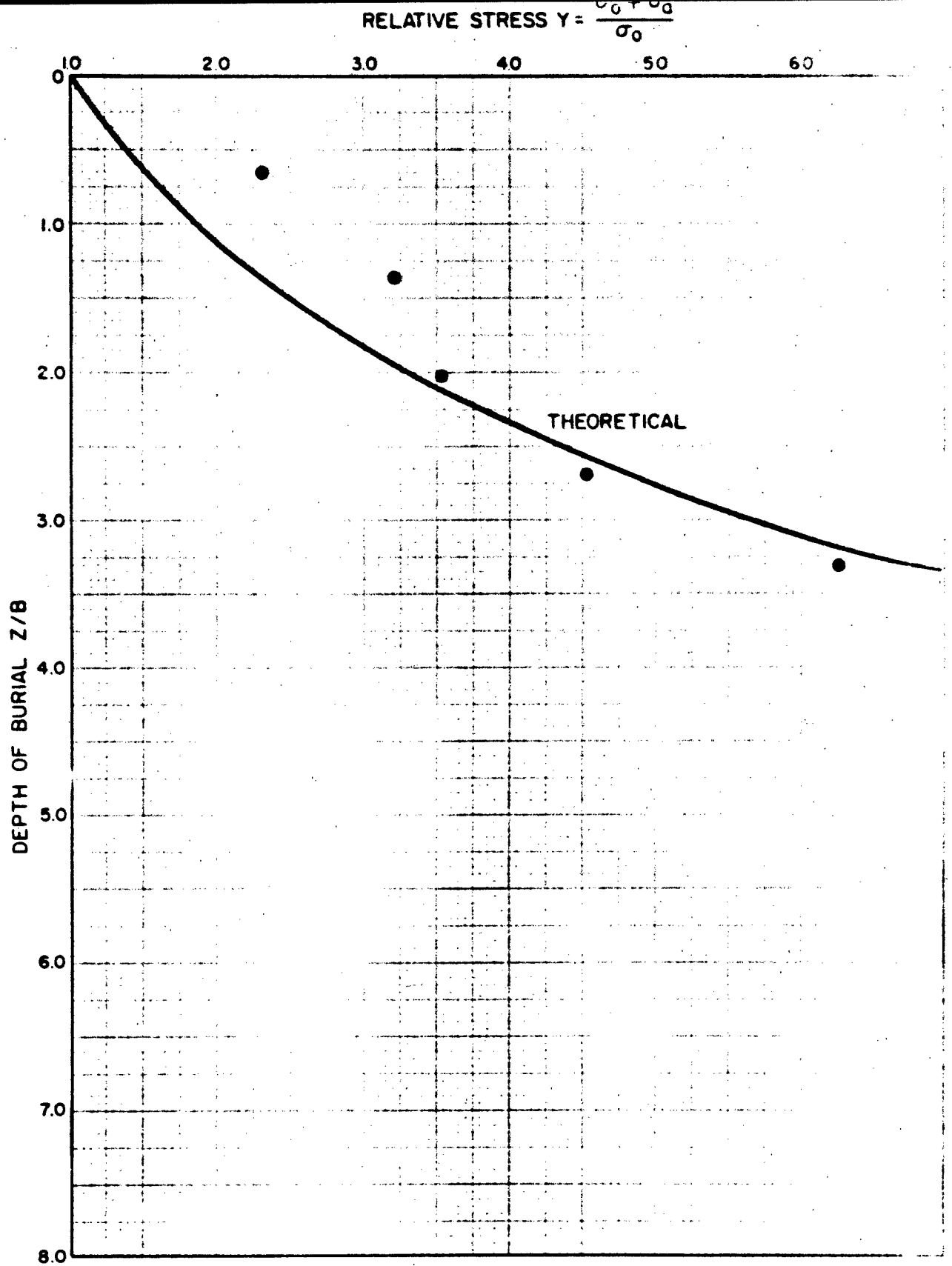


Fig. 74. Relationship of Maximum Relative Stress vs Depth of Burial Showing the Effects of Surface Layers

Section 9

CONCLUSIONS AND RECOMMENDATIONS

CONCLUSIONS

Based on the good correlations between the theory and the experimental results it can be concluded that the basic arching concept of soil-structure interaction involving shear planes is adequate to describe the behavior of small idealized structures. The concept also appears adequate to describe both active and passive conditions through a full range of compressibilities.

It is further concluded that real soil and structural parameters as measured separately in the laboratory can be used, together with the theory, to predict behavior, rather than assuming arbitrary soil parameters as has been done in the past. The soil parameters used in this study were the loading and unloading stress-strain curve, obtained from a constrained compression test; the angle of internal friction, obtained in the normal manner; and the ratio of lateral to axial stress, obtained from URS constrained compression tests*. The structural parameters used were the effective structural modulus, obtained from the in-place measurements**, and the structural geometry, i.e., the length and span.

From the correlation obtained by application of the theory to results of trap door experiments, conducted by other investigators, it appears that the interaction caused by the trap door motion and that caused by the relative compressibility of the soil and structure, on structures away from a boundary, are similar. It can also be concluded from an analysis of these results that in the active arching case the relationship between the loading rate and the response time of the structure will determine whether the loading or unloading portion of the soil stress-strain relationship is applicable and, therefore, the amount of arching that will occur. This results from the fact that if the structure responds during the rise time of the loading, then the arching will be governed by the loading portion of the stress-strain curve, since the soil will not have been compressed to the maximum stress before the motion

* This value can be calculated from the angle of internal friction by means of Jaky's equation.

** This value can be obtained from structural analysis also.

of the structure causes an unloading to occur. However, if the structure response is longer than the loading time, the soil will have been compressed to the maximum stress before unloading, and the arching will be controlled by the unloading portion of the stress-strain curve. The loading rate will, of course, be controlled by the relaxation effects* of the soil.

It has been concluded that surface layer effects, although not studied in detail, will have an influence on studies of shallow depths of burial for model-sized structures.

RECOMMENDATIONS

Since a good correlation seems to exist between the theory and the experimental results, the following recommendations are made:

1. That the theory be expanded to permit prediction of the distribution of stress across the face of the structure. (The results could be compared with existing experimental data.)
2. That the theory be expanded to include an investigation of the effects of dynamic arching.
3. That an experimental study be conducted to investigate more thoroughly structural compressibility in the active arching case.
4. That an experimental study be conducted to investigate more realistic structural shapes, such as those having arch and circular cross sections, to determine the influence of shape on stress distribution on the structure.
5. That an experimental study be conducted to investigate structural flexibility as distinguished from structure compressibility on stress distribution across the face of the structure.
6. That an experimental study be conducted to investigate further the causes of increased structural compressibility due to burial, i.e., sidewall friction, etc.

The above recommendations are not necessarily proposed as separate studies but may be combined or ordered in various manners, depending upon the immediate objective. These recommendations are, however, intended to outline what is felt are the major areas requiring investigation in order to develop the basic concepts presented herein to the point that they can be applied to real structural shapes and eventually to real structures.

* This subject is discussed in detail in Ref. 5.

Section 10

REFERENCES

1. Zaccor, J. V., "Dynamic Behavior of Granular Media," Proceedings of the Symposium on Soil-Structure Interaction, University of Arizona, Tucson, Arizona, Sep 1964, pp. 62 - 72
2. Zaccor, J. V., H. G. Mason, and D. F. Walter, "Concepts, Equipment and Techniques for the Study of the Dynamic Behavior of Soils," Report 1, Study of the Dynamic Stress-Strain and Wave-Propagation Characteristics of Soils, URS 637-24, Contract No. DA-22-079-eng-373, United Research Services for the U.S. Army Engineer Waterways Experiment Station, Vicksburg, Miss., Nov 1964
3. Durbin, W. L., "Correlation of Stress-Strain and Wave-Propagation Parameters in Shock-Loaded Dry Sands," Report 2, Study of the Dynamic Stress-Strain and Wave-Propagation Characteristics of Soils, URS 637-15, Contract No. DA-22-079-eng-373, Report No. 3-91, United Research Services for the U.S. Army Engineer Waterways Experiment Station, Vicksburg, Miss., Nov 1964
4. Durbin, W. L., "Measurements of Stress-Strain, Peak Particle Velocity, and Wave-Propagation Velocity in Three Sands," Report 3, Study of the Dynamic Stress-Strain and Wave-Propagation Characteristics of Soils, URS 637-23, Contract No. DA-22-079-eng-373, United Research Services for the U.S. Army Engineer Waterways Experiment Station, Vicksburg, Miss., Feb 1965
5. Zaccor, J. V., W. L. Durbin, N. R. Wallace, and H. G. Mason, "Concepts of Shock Behavior in a Granular Medium," Report 4, Study of the Dynamic Stress-Strain and Wave-Propagation Characteristics of Soils, URS 637-25, Contract No. DA-22-079-eng-373, United Research Services for the U.S. Army Engineer Waterways Experiment Station, Vicksburg, Miss., Mar 1965
6. Mason, H. G., O. H. Criner, R. Waissar, and N. R. Wallace, A Study of the Dynamic Soil-Structure Interaction Characteristics of Real Soil Media, AFSWC-TDR-63-3075, URS 621-13, United Research Services for the Air Force Weapons Laboratory, Kirtland Air Force Base, N.M., Dec 1963

7. Wiehle, C. K., "Review of Soil-Structure Interaction," Proceedings of the Symposium on Soil-Structure Interaction, University of Arizona, Tucson, Arizona, Sep 1964, pp. 239-245
8. Terzaghi, Karl, Theoretical Soil Mechanics, John Wiley and Sons, New York, 1943
9. Terzaghi, Karl, "Stress Distribution in Dry and in Saturated Sand Above a Yielding Trap-Door," Proceedings of the International Conference on Soil Mechanics and Foundation Engineering, Vol. I, No. Z-3, Harvard University, Cambridge, Mass., June 1936, pp. 307-311
10. U.S. Army Engineer Waterways Experiment Station, Soil Pressure Cell Investigation (Interim Report), Tech. Memo. No. 210-1, Vicksburg, Miss., 15 July 1944
11. McNulty, J. W., An Experimental Study of Arching in Sand, TR-1-674, Defense Atomic Support Agency for the U.S. Army Engineer Waterways Experiment Station, Vicksburg, Miss., May 1965
12. Zaccor, J. V. and N. R. Wallace, Techniques and Equipment for Determining Dynamic Properties of Soils, Final Report URS 155-30, DASA 1421, Contract No. DA-49-146-XZ-019, United Research Services for the Defense Atomic Support Agency, Washington, D.C., Nov 1963

Appendix A
URS EXPERIMENTAL PROGRAM

Since no experimental data were found in which the soil and structural parameters were sufficiently controlled to allow comparison with the theoretical relationships developed in the first part of this report, URS undertook a very limited program to provide enough data to enable a comparison to be made.

The basic objective of this experimental program was to find the effect on the static soil-structure interaction of changes in the ratio of soil modulus to structure modulus. Although the tests were conducted in the URS dynamic loader only data at equilibrium conditions were computed.* The approach used was to test a series of structures having a wide range of compressibilities in order to cover the passive and active arching cases. A 6-in.-diameter structure was chosen so that distribution of stress on the face could be measured and summed to obtain the total load. A 6-in. length was chosen so that sufficient passive arching forces would be developed to allow a reasonable resolution of the effects of structure compressibility on that arching force over the full range of compressibilities. The active arching forces would, of course, range from free-field stress to zero as the compressibility increased.

Structural load measurements were made with a series of piezoelectric stress gauges mounted in a spiral pattern in the rigid endwalls, as shown in Fig. 75. The spiral pattern is equivalent to a very close spacing along a diameter or radius and provides for stress distribution across the face of the structure. By applying the stress read by each gauge over the appropriate area of an annulus represented by the width of that gauge, the total load on the structure was calculated.

The structures were to be tested in a single soil, 20-30 Ottawa sand, placed at a constant relative density so that the compressibility of the

* Since the loader produces a step pulse which can be held for any desired duration, the equilibrium condition was considered to be equivalent to static conditions.

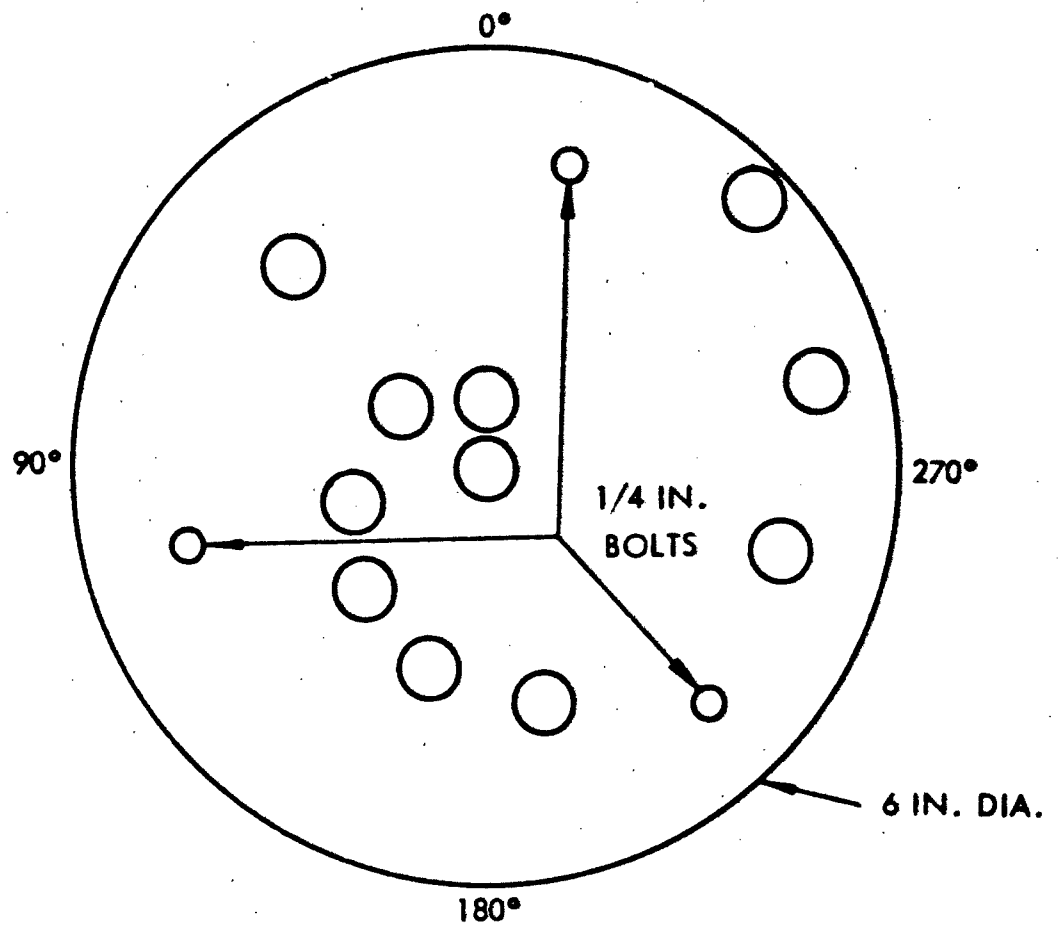


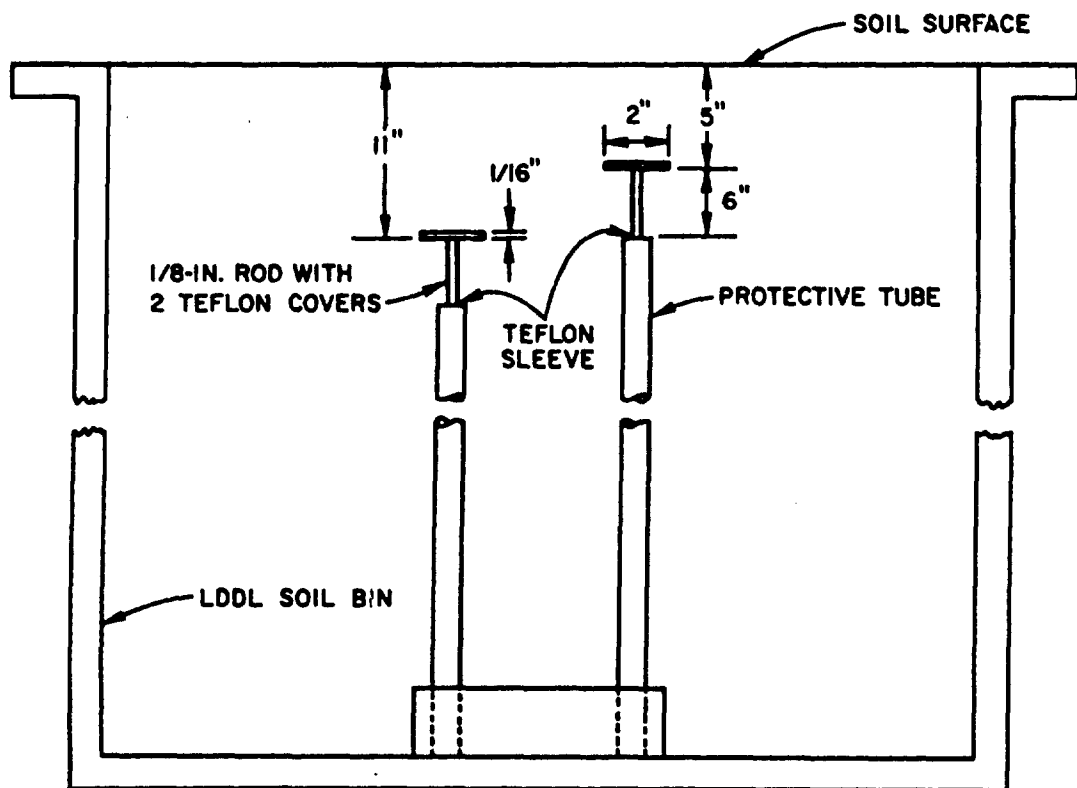
Fig. 75. Stress Gauge Pattern on Variable Compressibility Structure

soil would be a constant for all the tests. However, in efforts to obtain a structure compressible enough to provide active arching a second relative density for the soil was used.

In order to design the structures, it was necessary to ascertain the modulus of the soil for the anticipated test conditions. Since the soil used was the 20-30 Ottawa sand employed in other URS studies, the stress-strain curves obtained in those tests were used (see Fig. 40). A value of the modulus of the soil of approximately 9,000 psi was obtained for a soil density of 108 pcf.* As a further check the displacement was measured at two different positions within the soil mass. Since no known methods or instruments were available to measure the free-field strain of the soil over a gauge length of 6 in., it was necessary to devise a method for accomplishing the measurement. Two linear variable differential transformers (LVDT) were mounted in the bottom of the soil bin of the URS Long-Duration Dynamic Loader (LDDL) in such a fashion that they were isolated from the soil. A 1/8-in.-diameter rod was connected to the center probe of the LVDT and extended to an anchor plate embedded in the soil at the position at which the displacement was to be measured. The 1/8-in.-rod was protected from the friction of the soil, along its length, by running it through a 1/2-in.-diameter tube, which was terminated a short distance from the actual measuring zone in order that the effect of the rigid tube (soil-structure interaction) would not influence to an appreciable degree the soil in the area of the measurement. (See Fig. 76.) From the top of the tube to the anchor plate, the rod was covered with two layers of teflon tape to reduce the amount of friction on the rod over this length. The upper displacement measurement was taken at the depth of burial of the upper face of the structure, while the lower measurement was taken at the depth of burial of the lower face of the structure, such that the length over which the differential deformation was measured was 2L (the structure length, see Fig. 77). The soil modulus of deformation measured by this means was approximately 9,600 psi at 45-psi surface pressure.** This compares well with the value of approximately 9,000 psi computed from the stress-strain curve.

* 108 pcf was the density of the 20-30 Ottawa sand used in these interaction tests.

** To calculate the soil modulus, the free-field stress at the average depth was used.



Not to scale

Fig. 76. Soil Displacement Measuring System

As stated earlier the structural configuration selected was a cylinder, 6 in. in diameter, 6 in. long, with rigid endwalls (1-in.-thick aluminum plates), as shown in Figs. 75 and 77. To provide the wide range of overall compressibilities, the endwalls were connected with hollow cylinders of various compressibilities, as shown in Fig. 77. The variations in compressibilities were provided by a change in either the material or thickness of the cylinder. Three materials were used, aluminum, Plexiglas and Teflon. It was found in calibrating the finished cylinders that the Plexiglas and the Teflon had similar moduli; therefore, the more compressible structures (Teflon) were too stiff. After they had been machined thinner, it was found that the relative stress (overstress) was higher than was expected. An LVDT was installed in the structure to measure the compressibility between the two end plates. It was found that although sidewall friction on the sides of the structure had been reduced, the amount that was still present was sufficient to increase the effective stiffness. Even grease and a rubber membrane did not reduce it sufficiently. Again the wall thickness was reduced in an effort to create a structure more compressible than the soil. This structure collapsed under load. However, load-deformation values were obtained prior to collapse and are plotted in Fig. 39. In view of the effect that the rate of structural response has on determining which stress-strain curve is applicable, the reason for the collapse seems plausible. The structure has about a 6-msec response (to maximum deflection), as shown in Fig. 41, while the loading occurs in about 1.5 msec; therefore, the full load was probably applied to the structure before it had time to respond completely. Since the structure had been designed for high compressibility under low load, the structure collapsed under what were, apparently, the higher loads created by the slow structural response. The complexity of sidewall friction and wave propagation in the structure makes the calculation of the behavior difficult at this time.

The results of this limited experimental program are presented in Figs. 37 and 39 and are discussed in Section 7.

* To calculate the soil modulus, the free-field stress at the average depth was used.

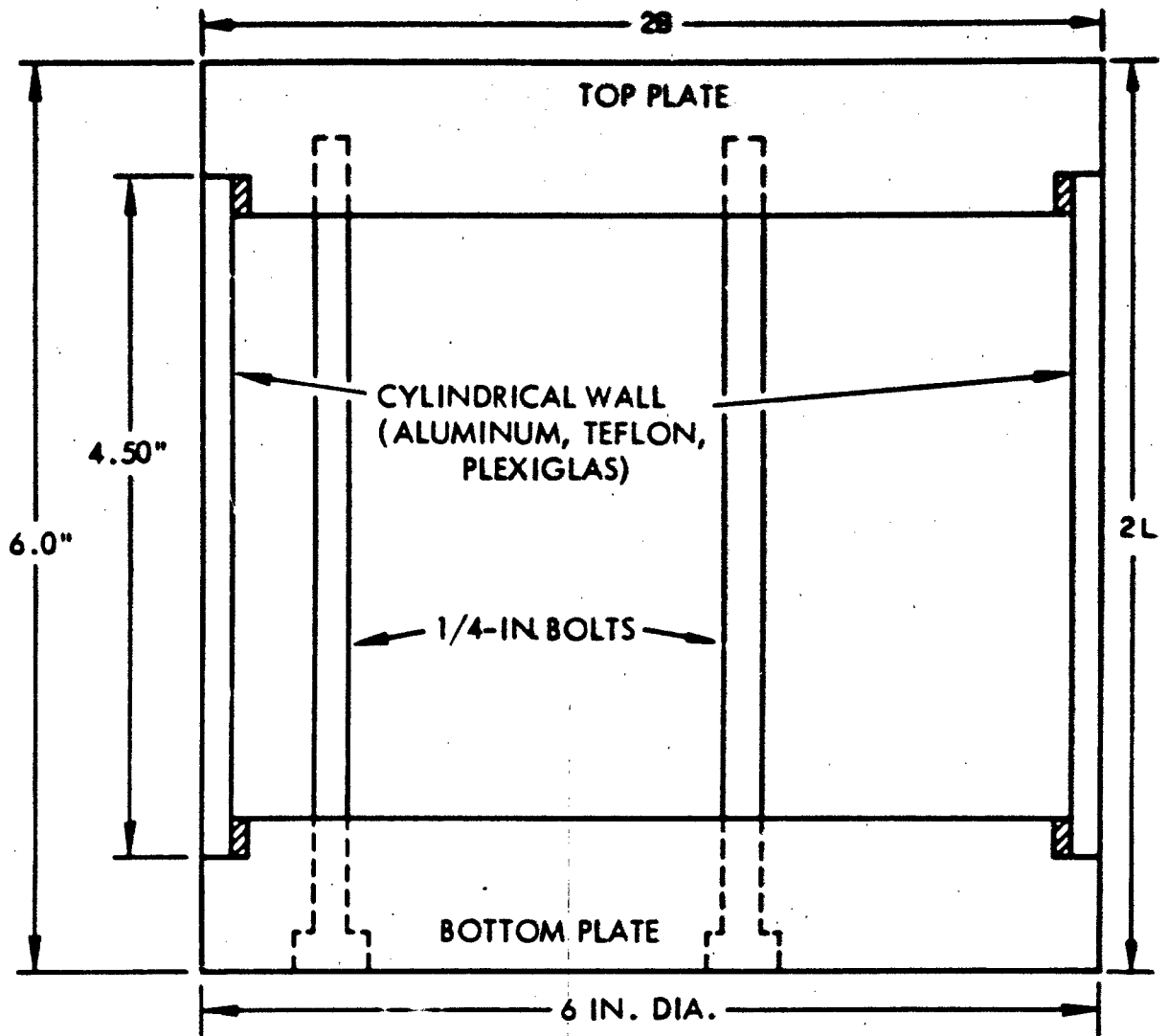


Fig. 77. Variable Compressibility Structure (Stress gauges are not shown)

UNCLASSIFIED
Security Classification

DOCUMENT CONTROL DATA - R&D		
<i>(Security classification of title, body of abstract and indexing annotation must be entered when the overall report is classified)</i>		
1 ORIGINATING ACTIVITY (Corporate author) URS Corporation 1811 Trousdale Drive Burlingame, California	2a REPORT SECURITY CLASSIFICATION UNCLASSIFIED	2b GROUP
3 REPORT TITLE Effects of Structural Compressibility on Active and Passive Arching in Soil-Structure Interaction		
4 DESCRIPTIVE NOTES (Type of report and inclusive dates) Final Report		
5 AUTHOR(S) (Last name, first name, initial) Harold G. Mason		
6 REPORT DATE November 1965	7a TOTAL NO OF PAGES 145	7b NO OF REFS 12
8a CONTRACT OR GRANT NO. DA-49-146-XZ-288	9a ORIGINATOR'S REPORT NUMBER(S) URS 645-8	
b. PROJECT NO. c d	9b OTHER REPORT NO(S) (Any other numbers that may be assigned this report) DASA 1718	
10 AVAILABILITY/LIMITATION NOTICES Qualified requesters may obtain copies of this report from DDC. This report has been approved for open publication by the Department of Defense.		
11 SUPPLEMENTARY NOTES	12 SPONSORING MILITARY ACTIVITY Defense Atomic Support Agency Washington, D.C.	
13 ABSTRACT This report describes a theoretical and experimental study of the effects of structural length and compressibility on soil-structure interaction, based on the applications of basic concepts of active and passive arching involving the development of shear planes in the soil. The basic theory of static active and passive arching is reviewed, and theoretical relationships describing the effect that structural geometry (length to span) has on the load on the structure, are developed. Equations are developed for passive and active arching for deeply buried idealized compressible cylindrical structures vertically oriented. Linear and nonlinear soil conditions are investigated. Equations are also derived to predict the load (on a trap door) resulting from differential strains occurring between the trap door and the bottom of the soil bin in the deeply buried condition. Both active and passive arching cases and linear and nonlinear soil conditions are considered. A limited experimental program was conducted to investigate the effects of the ratio of the soil to structural compressibility on the load on the structure. Good correlations are shown between the results of this study and the theoretical predictions employing soil parameters measured in normal laboratory soil tests. Similar correlations are also shown between the results of a trap door experimental study and the theoretical predictions. The relationship between rate of loading and the rate of structural response was shown to be a controlling factor in determining whether the loading or unloading stress-strain relationship governs the arching behavior.		

DD FORM 1473
1 JAN 64

UNCLASSIFIED
Security Classification

UNCLASSIFIED
Security Classification

14 KEY WORDS	LINK A		LINK B		LINK C	
	ROLE	WT	ROLE	WT	ROLE	WT
Soil - Structure Interaction						
Protective Structures						
Structure Compressibility						
Structure Geometry						
Underground Structures						
Blast Loading						
Nuclear Blast						
Shelters						

INSTRUCTIONS

1. **ORIGINATING ACTIVITY.** Enter the name and address of the contractor, subcontractor, grantee, Department of Defense activity or other organization (*corporate author*) issuing the report.
- 2a. **REPORT SECURITY CLASSIFICATION:** Enter the overall security classification of the report. Indicate whether "Restricted Data" is included. Marking is to be in accordance with appropriate security regulations.
- 2b. **GROUP:** Automatic downgrading is specified in DoD Directive 5200.10 and Armed Forces Industrial Manual. Enter the group number. Also, when applicable, show that optional markings have been used for Group 3 and Group 4 as authorized.
3. **REPORT TITLE:** Enter the complete report title in all capital letters. Titles in all cases should be unclassified. If a meaningful title cannot be selected without classification, show title classification in all capitals in parenthesis immediately following the title.
4. **DESCRIPTIVE NOTES:** If appropriate, enter the type of report, e.g., interim, progress, summary, annual, or final. Give the inclusive dates when a specific reporting period is covered.
5. **AUTHOR(S):** Enter the name(s) of author(s) as shown on or in the report. Enter last name, first name, middle initial. If military, show rank and branch of service. The name of the principal author is an absolute minimum requirement.
6. **REPORT DATE:** Enter the date of the report as day, month, year, or month, year. If more than one date appears on the report, use date of publication.
- 7a. **TOTAL NUMBER OF PAGES:** The total page count should follow normal pagination procedures, i.e., enter the number of pages containing information.
- 7b. **NUMBER OF REFERENCES:** Enter the total number of references cited in the report.
- 8a. **CONTRACT OR GRANT NUMBER:** If appropriate, enter the applicable number of the contract or grant under which the report was written.
- 8b, 8c, & 8d. **PROJECT NUMBER:** Enter the appropriate military department identification, such as project number, subproject number, system numbers, task number, etc.
- 9a. **ORIGINATOR'S REPORT NUMBER(S):** Enter the official report number by which the document will be identified and controlled by the originating activity. This number must be unique to this report.
- 9b. **OTHER REPORT NUMBER(S):** If the report has been assigned any other report numbers (*either by the originator or by the sponsor*), also enter this number(s).
10. **AVAILABILITY/LIMITATION NOTICES:** Enter any limitations on further dissemination of the report, other than those

imposed by security classification, using standard statements such as:

- (1) "Qualified requesters may obtain copies of this report from DDC."
- (2) "Foreign announcement and dissemination of this report by DDC is not authorized."
- (3) "U. S. Government agencies may obtain copies of this report directly from DDC. Other qualified DDC users shall request through _____."
- (4) "U. S. military agencies may obtain copies of this report directly from DDC. Other qualified users shall request through _____."
- (5) "All distribution of this report is controlled. Qualified DDC users shall request through _____."

If the report has been furnished to the Office of Technical Services, Department of Commerce, for sale to the public, indicate this fact and enter the price, if known.

11. **SUPPLEMENTARY NOTES:** Use for additional explanatory notes.
12. **SPONSORING MILITARY ACTIVITY:** Enter the name of the departmental project office or laboratory sponsoring (*paying for*) the research and development. Include address.
13. **ABSTRACT:** Enter an abstract giving a brief and factual summary of the document indicative of the report, even though it may also appear elsewhere in the body of the technical report. If additional space is required, a continuation sheet shall be attached.

It is highly desirable that the abstract of classified reports be unclassified. Each paragraph of the abstract shall end with an indication of the military security classification of the information in the paragraph, represented as (TS), (S), (C), or (U).

There is no limitation on the length of the abstract. However, the suggested length is from 150 to 225 words.

14. **KEY WORDS:** Key words are technically meaningful terms or short phrases that characterize a report and may be used as index entries for cataloging the report. Key words must be selected so that no security classification is required. Identifiers, such as equipment model designation, trade name, military project code name, geographic location, may be used as key words but will be followed by an indication of technical context. The assignment of links, rules, and weights is optional.